The Molecular Characterisation of TIMP3 Mutations Responsible for Sorsby's Fundus Dystrophy: is there a link to Age-related Macular Degeneration

Fatimah Abdulali A Alsaffar

A thesis submitted in part fulfilment of the requirement for Doctor philosophy degree in Molecular Medicine.

The University of Sheffield

Medical School

Department of Oncology & Metabolism

September 2016

Acknowledgment

All my praises and thanks are to Allah, my lord, for letting me through all the difficulties, finishing my degree and everything in my life. I am pleased to acknowledge researchers, colleagues, friends and others who have a major role throughout my PhD study. I would like to express my appreciation to everyone helped me in my research; however, I would like to especially mention and thank those who significantly assisted and supported me.

First of all, I would like to express my sincere gratitude to my supervisor Dr. Mike Barker who has been a tremendous mentor for me. Although my words will not be enough to express how grateful I am to my supervisor, I would like to thank him for his continuous support, patience, motivation, and immense knowledge. My supervisor guidance has helped me during the time of research and writing of this thesis. All his advice has been invaluable to both my research and future career.

I would like to thank my colleagues, the academic and technical staff at the medical school; in particular those who helped me over the years, Dr. Martin Nicklin, Dr. Russell Hughes, Dr. Simon Tazzyman, Dr. Ahmed Mujamammi and Mr. Mohammed Aldughaim. I would like also to thank my lovely friends and cousins whom I have shared so many excellent times.

Last but not the least, a special thanks to my family, words will be less than you deserve, my father and mother and my brothers. I thank them for all the sacrifices that they have made on my behalf, prayers, unconditional love and support throughout my research and writing my thesis. I would never have reached this stage without such a great family.

Abstract

Sorsby's fundus dystrophy (SFD) is a rare autosomal, dominantly inherited, degenerative disease of the retina that results in a loss of central vision in middle age. The disease is a single-gene disorder caused by specific mutations in the tissue inhibitor of metalloproteinase-3 (*TIMP3*) gene on chromosome 22. The SFD phenotype is very similar to age-related macular degeneration (AMD), a very common cause of blindness in the elderly. These phenotypic similarities include drusen, thickened Bruch's membrane, atrophy of choroid and photoreceptors and neovascularisation. While AMD is a multifactorial disorder that is not associated with mutations in *TIMP3,* increased levels of TIMP3 protein are observed in the retina of both diseases indicating TIMP3 could still play a role in this disease.

Although the disease mechanism responsible for the SFD phenotype is still uncertain, the evidence implies that the phenotype results from a toxic effect of the mutant TIMP3, rather than haploinsufficiency. At the start of this project, ten of the known mutations were localised to the coding sequence of exon 5 comprising most of the C-terminal domain of the molecule and demonstrated to result in dimeric TIMP3. There were also two exceptional mutations, including a mutation in exon 1 that encodes part of the N-terminal domain (Ser15Cys), and a splice site mutation caused by a single adenosine insertion at the intron4/exon5 junction. Recently, three additional mutations, including Tyr128Cys, Tyr154Cys and Tyr159Cys, were also identified in exon 5 but their effects on TIMP3 had not been examined. Thus, the consequences of these exceptional mutations and the newly identified C-terminus mutations on TIMP3 were still unknown.

We hypothesised that both SFD and ageing result in cross-linking of TIMP3 leading to formation of a toxic molecule that may play a role in both diseases. The initial aim of this project was to investigate the consequence of the *TIMP3* splice site mutation and these other recently described mutations on the TIMP3 protein. The second aim was to examine the effects of SFD mutation on a number of potential target molecules and downstream pathways. These included the interaction with tumour necrosis factor α converting enzyme (TACE) and its consequence for retinal pigment epithelial cell apoptosis; with vascular endothelial growth factor receptor 2 (VEGFR2) and its role in angiogenesis; with epidermal growth factor-containing fibulin-like extracellular matrix protein 1 (EFEMP1), mutations in which also cause an inherited retinopathy, and finally to examine potential activation of the receptor for advanced glycation end-products (RAGE).

This research project confirmed that all examined TIMP3 mutations expressed by human retinal cells formed dimers, including the novel splice site mutant, which resulted in the formation of several abnormally spliced truncated products. Dimerisation, therefore, almost certainly plays a crucial role in the SFD disease process.

Retinal pigment epithelial cells expressing these mutant proteins were more sensitive to Fas-induced apoptosis than those expressing the normal protein, although we were unable to confirm if this was mediated by increased avidity for TACE. Moreover, mutant TIMP3 proteins had a pro-inflammatory effect relative to the wild-type molecule, as determined by NF-κB activation, likely mediated by RAGE, although this still needs confirmation. Mutant proteins were, however, less effective at inhibiting VEGF-induced endothelial cell invasion than their wild-type counterpart, almost certainly due to decreased ability to inhibit VEGFR2, and this could explain the choroidal neovascularisation that accompanies SFD, despite the high levels of TIMP3 protein present in the retina. Mutations in TIMP3, responsible for SFD and in EFEMP1, responsible for Malattia Leventinese, did not appear to impair their mutual interaction and we speculate that increased deposition of TIMP3/EFEMP1 complexes are a common feature of SFD, Malattia Leventinese and age-related macular degeneration, and this may in turn lead to sequestration of complement factor H, a known binding partner for EFEMP1, impairing regulation of complement activation in the retina. If this proves to be the case, targeting the interaction between these three molecules may provide a novel therapeutic strategy for treating these currently intractable diseases.

Table of contents

List of figures

List of tables

List of abbreviations

a.a	Amino acid
ADAM	A disintegrin and metalloproteinase
ADAMTS	A disintegrin and metalloproteinase with thrombospondin-like motifs
aFGF/FGF1	Acidic fibroblast growth factor
AGE	Advanced-glycation end product
AMD	Age-related macular degeneration
APS	ammonium persulfate
Arg (R)	Arginine
ARPE19	A human retinal pigment epithelial cell line
α1-PI	Alpha 1-proteinase inhibitor
α2-M	Alpha 2 Macroglobulin
BCA	Bicinchoninic acid
bFGF/FGF2	Basic fibroblast growth factor
bp	Base pairs
BSA	Bovine serum albumine
BL	Burkitt's lymphoma cell
CAPS	N-cuclohexyl-3-aminopropanesulfonic acid
cDNA	complementary deoxyribonucleic acid
ChIMP3	Chicken TIMP3
CML	carboxy-methyl lysine
CMV	Cytomegalovirus
CNV	Choroidal neovascularisation

COMP	Cartilage oligomeric matrix protein
COOH-	Carboxyl group
COS-7	African green monkey kidney cells
CTGF	Connective tissue growth factor
Cys (C)	Cysteine
DEPC	Diethylpyrocarbonate
DMEM	Dulbecco's Modified Eagle Medium
DMEM/F12	Dulbecco's Modified Eagle Medium with Ham Nutrient F-12
DMSO	Dimethyl sulfoxide
DNA	Deoxyribonucleic acids
dNTP	Deoxy-nucleotide-triphosphate
DPBS	Dulbecco's phosphate-Buffered Saline
DTT	Dithioreitol
EBM-2	Endothelial Basal Medium 2
ECM	Extracellular matrix
ECs	Endothelial cells
EDTA	Ethylenediaminetetraacetic acid
EFEMP1	epithelial growth factor-containing fibulin-like extracellular matrix protein 1
EFG	Epidermal growth factor
ENSEMBL	A genome database browser
Fas-L	Fragment apoptosis stimulator ligand
FBS	Fetal bovine serum

FGF-2	fibroblast growth factor-2
FGFRs	fibroblast growth factor receptors
Fn	fibronectin
G-418	Geneticin
GAG	Glycosaminoglycan
GAPDH	Glyceraldehyde 3-phosphate dehydrogenase
HA	Hyaluronic acid
HB-EGF	heparin-binding epidermal growth factor like growth factor
HCl	Hydrochloric acid
HEK293T	Human embryonic kidney clone 293 with large T antigen
His (H)	Histidine
HIV	Human immunodeficiency virus
HRP	Horse radish peroxidase
HUVEC	Human umbilical vain endothelial cells
ICAM-1	Inter-cellular adhesion molecule 1
Ig	Immunoglobulin
IGFBP	Insulin-like growth factor-binding protein
Kb	kilobase pairs
kDa	Kilo Dalton
Kit-L	kit ligand
LB	Luria Bertani
LDL	Low density lipoprotein

Leu (L)	Leucine
Ln	Laminin
Lys (K)	Lysine
MAPK	Mitogen activated protein kinase
MCF10A	human breast epithelial cells
MCP-3	monocyte chemotactic protein-3
ML	Malattia Leventinese
MMP	Matrix metalloproteinase
mRNA	messenger ribonucleic acid
MT-	Membrane type
NaAc	Sodium acetate
NaCl	Sodium chloride
NaHCO3	Sodium bicarbonate
NaN3	Sodium azide
NaOH	Sodium Hydroxide
NEB	New England Biolabs
NF-κB	Nuclear factor-κB
NH2-	Amino group
NH4OH	Ammonium hydroxide
NP-40	Nonyl phenoxypolyethoxylethanol
ORF	open reading frame
P/S	Potassium Penicillin/Streptomycin sulphate

PAGE	polyacrylamide gel electrophoresis
PCR	polymerase chain reaction
PTD	photodynamic therapy
PEX	Haemopexin
PG	Proteoglycans
Phe (F)	Phenylalanine
PIGF	Placental growth factor
PMA	Phorbol 12-myristate 13-acetate
proIL-1β	Interleukin 1 beta
ProMMP	Inactive MMP
ProTGF-b	pro-transforming growth factor beta-b
PVDF	Polyvinylidene diflouride
RA	Rheumatoid arthritis
RAGE	Receptor for advanced glycation end-products
RANKL	Receptor activator for nuclear factor kB ligand
rhTIMP3	Recombinant human TIMP3
RPE	Retinal pigment epithelial
RNA	Ribonucleic acid
RNAi	RNA interference
rpm	Revolutions per minute
SDS	Sodium dodecyl sulphate
Ser (S)	Serine
shRNA	small hairpin RNA

siRNA	Small interfering RNA
SFD	Sorsby's Fundus Dystrophy
SNP	Single-nucleotide polymorphism
SP6	a promoter sequence for RNA polymerase
splT3.M	splice-site TIMP3 mutant construct
splT3.WT	splice-site TIMP3 wild-type construct
T7	a promoter sequence for T7 RNA polymerase
TACE	Tumour necrosis factor α-converting enzyme
TAE	Tri-acetate-ethylenediaminetetraacetic acid
TEMED	tetramethylenediamine
TGF	Transforming growth factor
TIMPs	Tissue inhibitors of metalloproteinases
TIMP3/T3	Tissue inhibitor of metalloproteinases 3
TK	Tyrosine kinase
T_m	Melting temperature
TNF	Tumour necrosis factor
TNF-R1	Tumour necrosis factor-1
TRAIL-R1	Tumour necrosis factor-related apoptosis-inducing ligand receptor-1
Trp (W)	Tryptophan
TSP	Thrombospondin
Tyr (Y)	Tyrosine
UCSC	University of California, Santa Cruz genome browser

uPA	Urokinase plasminogen activator.
UTR	Untranslated region
Val (V)	Valine
VEGF	Vascular endothelial growth factor
VEGFR2	Vascular endothelial growth factor receptor 2
VPE	Vascular permeability factor
vWF	von Willebrand factor
WT	Wild type
x g	Times gravity
X-gal	5-bromo-4-chloro-3-indoly-β-D-galactoside
α	Alpha
β	Beta
µm	Micrometre

Chapter 1: Introduction

1. Introduction

Tissue inhibitor of metalloproteinases 3 (TIMP3) is named for its ability to inhibit the matrix metalloproteinase (MMP) family of extracellular matrix (ECM) enzymes. However TIMP3 has a number of unique features that are not shared by the three other members of this family, including binding to the ECM and inhibition of vascular endothelial growth factor receptor 2 (VEGFR2). This complex functionality is reflected in the fact that specific mutations in TIMP3 give rise to Sorsby's fundus dystrophy (SFD), a dominantly inherited degenerative disease of the retina that leads to blindness, usually in middle-age. The functional consequences of these mutations, and the possible role of TIMP3 in other retinopathies is the topic of this thesis.

In order to begin to understand how these mutations may contribute to the disease phenotype, it is necessary to appreciate the complex nature of the ECM and the other molecules that TIMP3 interacts with in this environment and this will be the topic of the following sections. I will then discuss what is currently know about the role of TIMP3 in SFD and the potential role for TIMP3 in other retinopathies, specifically age-related macular degeneration and Malattia Leventinese (ML).

1.1 The extracellular matrix (ECM)

The extracellular matrix is a three-dimensional network of macromolecules that surrounds cells within tissues. The ECM constitutes a microenvironment, which provides a mechanical and structural support for tissues and cells (Hubmacher and Apte 2013, Kim *et al.* 2011, Mott and Werb 2004) but it is also an important repository of a vast array of growth factors and other potent molecules that play important roles in tissue development and homeostasis (Mouw *et al.* 2014). It is composed primarily of water and a complex mixture of insoluble macromolecules, primarily proteoglycans (PGs) and fibrous proteins such as collagen, elastin, laminins and fibronectins (Frantz *et al.* 2010, Ruoslahti *et al.* 1985).

1.1.1 ECM Components

1.1.1.1 Proteoglycans

Proteoglycans (PGs) are extracellular matrix macromolecules composed of a specific core protein with covalently attached glycosaminoglycan chains (Theocharis *et al.* 2010, Velasco *et al.* 2010). The glycosaminoglycans (GAGs) are linear and negatively charged polymers of

repeated disaccharide and classified into two types including sulphated and non-sulphated GAGs which can be present either on the cell surface or in the surrounding ECM (Velasco *et al.* 2010, Gandhi and Mancera 2008). Hyaluronic acid (HA) is the only entirely non-sulphated GAG, whereas there are many sulphated GAGs including chondroitin sulphate (CS), keratan sulphate (KS), dermatan sulphate (DS) and heparan sulphate (HS).

In nature, all these sulphated glycosaminoglycan chains are covalently bound to a core protein to form the proteoglycan. Proteoglycans are produced by all mammalian cells and categorised into three major groups depending on their location including extracellular secreted PGs, cell-surface associated PGs and soluble PGs present in ECM and serum (Theocharis *et al.* 2010, Gandhi and Mancera 2008). PGs include heparan sulphate proteoglycans (HSPGs) such as syndecans and glypicans, chondroitin sulphate proteoglycans (CSPGs) such as aggrecan and veriscan, and small leucine-rich repeats (SLRPs) such as decorin and biglycan (Mouw *et al.* 2014, Theocharis *et al.* 2010). They play a major role in a variety of physiological and pathological functions including cell growth and tissue maturation, organisation of the extracellular matrix, modulation of growth factor activity, development of the nervous system, regulation of cell signalling and growth and metastasis of tumour cells (Iozzo 1998, Perrimon and Bernfield 2001, Velasco *et al.* 2010). Their ability to bind water also plays an important role in maintaining tissue hydration in, for example, articular cartilage and the cornea.

1.1.1.2 Fibrous proteins

1.1.1.2.1 Collagens

Collagens are the major insoluble fibrous protein found in the ECM and the most abundant proteins in eukaryotes. Although there are at least 28 types of collagens reported in the literature (Kim *et al.* 2011), only three types including I, II and III constitute 90% of the collagen in the body. The 28 reported collagens have different sizes, structure and function but they have common characteristics. For instance, they are either trans-membrane or extracellular molecules and consist of three α-chains comprising two α1-chains and one α2-chain that form a triple helical structure that is a repetition of Gly-X-Y, with X or Y commonly being proline or hydroxyproline, respectively (Hubert *et al.* 2009, Mouw *et al.* 2014). It is well known that the primary function of collagens is to provide support and binding partners for other proteins in the ECM, but they are also involved in a diversity of biological processes such as neural development and tumourigenesis (Hubert *et al.* 2009).

1.1.1.2.2 Elastin

Elastin is the dominant extracellular matrix protein in vertebrate connective tissues; for example, arterial blood vessels, skin and lungs (Daamen *et al.* 2007, Keeley *et al.* 2002). It is synthesised by a variety of cells, such as fibroblasts, smooth muscle and endothelial cells, and secreted into the extracellular space as a soluble precursor named tropoelastin and subsequently undergoes specific post-translation modifications, and becomes a highly cross-linked molecule that binds to another molecules through lysines generating elastin fibres (Daamen *et al.* 2001, Daamen *et al.* 2007). Like collagens, elastin is a hydrophobic protein composed of uncommon amino acids including Gly, Val and Ala (around 75%), in which Gly account for 30% of the amino acids residues (Daamen *et al.* 2007, Vrhovski and Weiss 1998). Elastin plays an important role in supporting healthy cells and providing elastic tissues with the required resilience, allowing them to stretch and recoil (Almine *et al.* 2010).

1.1.2 ECM in the eye

All complex tissues such as cartilage, bones and teeth have their own specific ECM configuration and this is particularly apparent in the eye, which clearly contains some very specialised cell matrices in the cornea, lens and vitreous cavity, enabling light penetration through to the retina (Figure 1.1). The retina itself is an extremely complex structure containing several layers of highly specialised cell types (Figure 1.1). These structures are supported by ECM, which is particularly predominant in the basement membranes of the inner limiting membrane (ILM) that forms the innermost layer of the retina adjacent to the vitreous body and Bruch's membrane that separates the choroid from the retinal pigment epithelium. Bruch's membrane is of particular importance clinically as this structure is affected in age-related macular degeneration (AMD) and several other retinal diseases, including Sorsby's fundus dystrophy (SFD) and Malattia Leventinese (ML).

1.1.2.1 Bruch's membrane

Bruch's membrane (BM) is a unique thin layer of tissue in the eye, occupying the space between the retinal pigment epithelium and the choroid. The BM was originally named the lamina vitrea due to its glassy appearance; and later renamed after the German anatomist Carl Ludwig Wilhelm Bruch who first isolated and described the membrane in his doctoral thesis in 1844. In the past, it was considered to be a simple sheet of extracellular matrix; however it

is now known to play crucial roles in retinal function, ageing and retinal diseases. The BM is a pentalaminar structure consisting of five layers: the basement membrane of the RPE, inner collagenous layer, elastin layer, outer collagenous layer and the basement membrane of the choriocapillaris (Figure 1.1 B, Table 1.1). The pentalaminar membrane works as a single functional unit and is involved in the exchange of numerous biomolecules, nutrients, fluid, oxygen and waste products between its tissues and the general circulation. The properties of BM vary with factors such as genetics, age, environment, diseases and retinal location, and each human individual has unique BM properties affecting the development of normal vision and retinal disease. (Curcio and Johnson 2012, Booij *et al.* 2010)

Bruch's membrane undergoes significant structural and molecular age-related changes, and ageing is the strongest risk factor for developing AMD. However, those changes that have no direct clinical consequences and appear in the majority of individuals with time, are considered normal ageing. Currently, it is believed that AMD is a more severe form of the normal ageing process in RPE and Bruch's membrane. RPE cells are responsible for the synthesis of the structural elements of Bruch's membrane; for example, laminin, collagen type I and IV, metalloproteinases and their natural inhibitors (Alcazar *et al.* 2009, Nita *et al.* 2014). A high metabolic rate in RPE and photoreceptor cells; exposure to light and high local oxygen pressure lead to high levels of oxidative stress and participate in Bruch's membrane changes (Booij *et al.* 2010). A proteomic analysis of the Bruch's membrane and choroid from human post-mortem AMD patients was carried out by Yuan *et al.* (2010), who found that 99 out of 901 proteins had significantly altered levels of expression compared to controls. Among the elevated proteins were several complement proteins and complement-associated proteins, damage associated molecular pattern proteins (DAMPs), inflammatory response proteins and regulatory protein such as TIMP3 and α1-microglobulin (Crabb *et al.* 2002, Crabb 2014, Sparrow *et al.* 2012, Yuan *et al.* 2010).

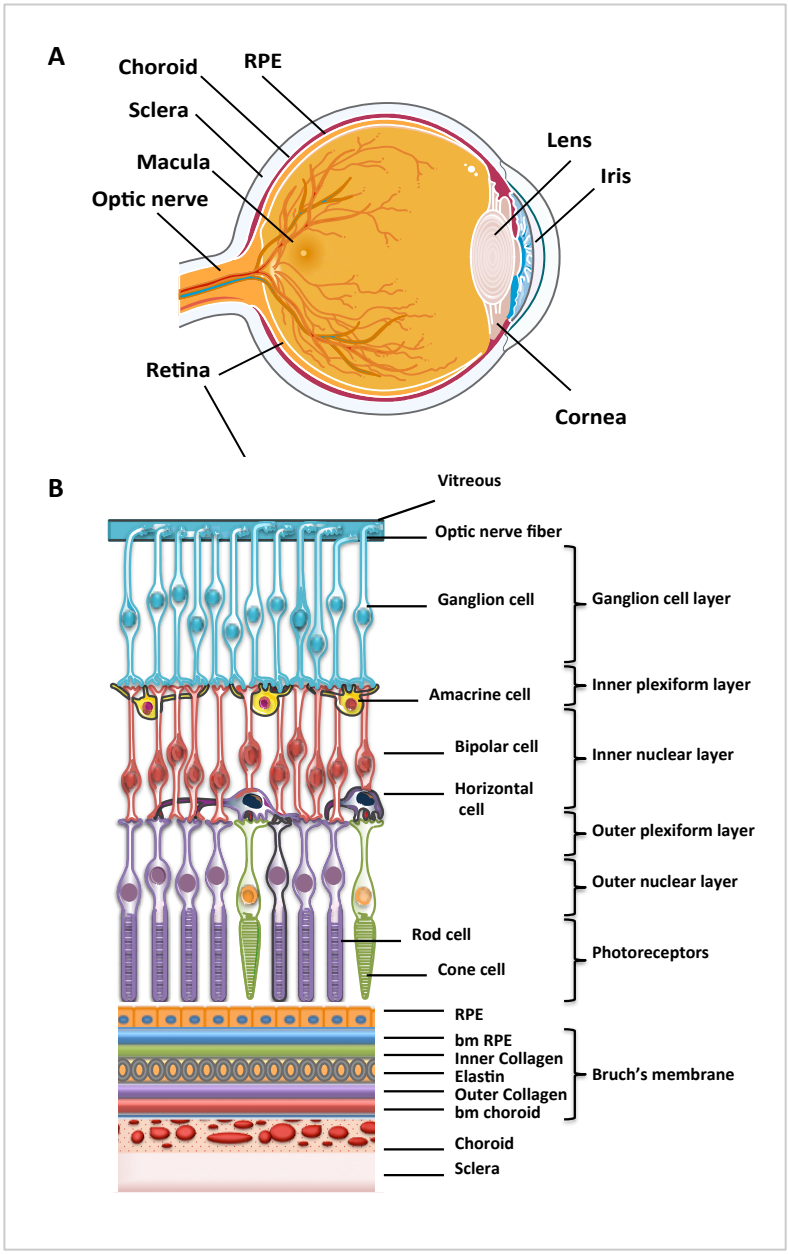

Figure 1.1: Illustration of different retinal layers in the human eye.

(A) Anatomy of the normal eye. (B) A cross-section slice of the retina demonstrating detailed layers. The retina layers were drawn using Servier medical art website (Available on http://www.servier.com/Powerpoint-image-bank).

Table 1.1: Protein components of regular human Bruch's membrane (BM).

PGs: proteoglycans; HSPGs: heparan sulphate proteoglycans; E/N: entactin/nidogen; LAM: laminin.

Retina Layers	Compositions
RPE basic membrane	Collagen IV & V, laminins, fibulins, PGs (HSPGs), E/N, LAM
Inner collagen layer	Collagen I, III & V, fibronectin, fibulins, HSPGs
Elastin layer	Elastin collagen VI, fibronectin, fibulins, HSPGs, TIMP3
Outer collagen layer	Collagen IV, V & VI, fibronectin, fibulins, HSPGs
Choriocapillaris basic membrane	Collage IV, V & VI, laminins, fibulins, PGs (HSPGs), E/N, LAM

1.1.3 Extracellular matrix function and degradation

As already documented, the ECM provides structural support, tensile strength and scaffolding for cells and tissues. Additionally it has diverse roles in most basic cell behaviour including proliferation, differentiation, adhesion, migration and apoptosis. Czyz and Wobus (2001); for example, demonstrated that the differentiation of embryonic stem cells is determined by various extracellular matrix components, while other studies showed that embryonic stem cells can be grown and differentiated into cells with retained fundamental characteristics on Matrigel, a commercial cell matrix material secreted by mouse sarcoma cells which contains various ECM components such as collagen VI, laminin-1 and growth factors as well as suitable growth medium (Guilak *et al.* 2009, Xu *et al.* 2001). The ECM also acts as a storage depot for cytokines, growth factors and chemokines that are released upon ECM degradation (Hubmacher and Apte 2013, Kleinman *et al.* 2003, Lu *et al.* 2011). Moreover cleavage of certain ECM components, such as collagen IV and laminin-5, exposes cryptic peptides that facilitate cell migration (Kessenbrock *et al.* 2010).

ECM degradation is an important mechanism that regulates cell differentiation and tissue remodelling in embryonic development, bone remodelling, angiogenesis and wound repair. For example, in angiogenesis endothelial cells respond to changes in ECM composition such

as cleavage of fibrillar type I collagen and show increased expression of integrins that mediate attachment to ECM components such as collagens and laminins (Seandel *et al.* 2001, Stupack and Cheresh 2002). In contrast, abnormalities in the ECM dynamic lead to pathological conditions such as tissue fibrosis and cancer. In cancer, for example, cleavage of ECM components by enzymes such as matrix metalloproteinases enables tumour growth, releases growth factors, facilitates angiogenesis and triggers endothelial to mesenchymal transition (EMT) promoting metastasis (Gialeli *et al.* 2011).

1.1.4 Proteinases in ECM degradation and remodelling

As the ECM contains a wide range of structurally and biochemically diverse components that undergo either degradation or modification processes during ECM remodelling, there are a large number of different proteinases to carry out these processes. Proteinases are classified into five main groups based on their chemical groups implicated in the hydrolysis of peptide bonds (Cawston and Young 2010). The five main proteinases groups include cysteine, aspartate, threonine, serine and metalloproteinases. Metalloproteinases including MMP (matrix metalloproteinases) and ADAM/ADAMTS (a disintegrin and metalloproteinases and a disintegrin and metalloproteinase with thrombospondin motifs, respectively) are considered the most significant extracellular enzymes in ECM remodelling (Cawston and Young 2010, Lu *et al.* 2011). Whilst serine proteinases such as cathepsin G and plasmin are extracellular proteinases working at neutral pH, cysteine, threonine and aspartate proteinases digest intracellular proteins at acidic pH (Cawston and Young 2010). However, some of the intracellular cysteine proteases, including cathepsins B and L, can be secreted and have the ability to digest ECM proteins (Burke *et al.* 2003, Guenette *et al.* 1994, Green and Lund 2005). The next section focuses on the extracellular metalloproteinases, specifically the MMP, ADAM and ADAMTS families, which are inhibited by TIMPs.

1.2 The metzincin superfamily

The metzincin proteinase superfamily are distinguished by containing a zinc ion and conserved methionine residue at their active site (Bode *et al.* 1993, Stocker *et al.* 1995) which comprises a conserved HEXXHXXGXXH...M amino acid sequence, where X can be any amino acid and the distance between the distal His and Met residues can vary. The Met residue forms a hydrophobic "seat" for the zinc ion which is chelated by the three His residues. The family comprises MMP (also known as matrixins), ADAM, ADAMTS (known

collectively as adamlysins), astacin and pappalysin families, with the first three families being by far the most abundant in the ECM and these will be considered in more detail in the following section.

1.2.1 Matrix metalloproteinases

To date, there are 23 different MMPs found in humans and most vertebrates (Lu *et al.* 2011, Bonnans *et al.* 2014), which share many common structures and functions. Confusingly human MMPs are numbered up to MMP28, which is largely a result of some being named before their sequences had been verified, resulting in some duplication. They have been categorised based on sequence similarities, domain organisation and substrate specificity (Table 1.2).

1.2.1.1 MMP structure

The mammalian MMPs share a common conserved structure that contains several domains including an autoinhibitory pro-domain, a catalytic domain, a flexible hinge motif and a haemopexin domain (Lu *et al.* 2011, Nagase and Woessner 1999, Page-McCaw *et al.* 2007) (Figure 1.2). The pro-domain at the N-terminus consists of a conserved cysteine residue coordinating to the zinc ion at the active site to inhibit catalysis. Destabilisation and cleavage of the pro-domain, usually by plasmin or other MMPs, uncovers the active site resulting in activation of the enzyme, a process known as the "cysteine switch". The catalytic domain comprises a conserved methionine and specific zinc binding amino acids sequence, three α-helices, five-stranded β-sheet and bridging loops. It also has calcium ions (two or three) and an extra zinc ion that provides structural stability required for enzymatic activity. The catalytic domain is linked to the haemopexin domain through a proline-rich linker peptide. The haemopexin domain is located at the C-terminus of MMP structure and contains a four-bladed β-propeller structure, each of which consists of an α-helix and four antiparallel β-strands, that function as a mediator for protein-protein interaction, which contributes to a variety of interactions such as enzyme activation, substrate recognition and protease localisation (Page-McCaw *et al.* 2007). However, MMP21 and 22 contain three different regions including cysteine-rich, proline-rich and IL-receptor like domains at their C-terminus instead of the haemopexin domain (Gururajan *et al.* 1998).

Table 1.2: Members of matrix metalloproteinases family.

Based on Lu et al. (2011), Shiomi et al. (2010) and Pant et al. (2010)

MMP member		Key Structure features	Substrates	
			ECM	Non-ECM
No	**Secreted-type MMP**			
1	MMP1 (Interstitial collagenase-1)	Haemopexin domain	Collagens type-I, -II, -III, -VII & X; entactin; gelatines; tenacsin; link protein; perlecan and aggrecan.	α1-antichymotrypsin; CTGF; IGFBP-2, -3 & -5; α1-PI; α2-M.
2	MMP8 (Neutrophil collagenase-2)	Haemopexin domain	Collagens type-I, -II & -III; aggrecan; gelatins and link protein.	α1-PI.
3	MMP13 (collagenase-3)	Haemopexin domain	Collagens type-I, II, III, IV, IX, X & XIV; osteonectin; perlecan; Fn; Ln; aggrecan and tenascin.	α1-antichymotrypsin; ProTGF-β; CTGF and MCP-3.
4	MMP2 (Gelatinase A)	Haemopexin & Fibronectin domain	Gelatins; elastin; link protein; aggrecan; Ln; elastin; Fn; collagens type-IV, -V, -VII, -X and -XI.	Galectin-3; IGFBP-5; FGF receptor I; proIL-1β; MCP-3; ProTGF-β; plasminogen.
5	MMP9 (Gelatinase B)	Haemopexin & Fibronectin domain	Gelatins; vitronectin; entactin; aggrecan; link protin; elastin; N-telopeptide of collagen I; Collagens type-III, -IV &-V.	Plasminogen; ProTGF-β; galectin-3; α1-PI; kit-L; IL-2 receptor α; IGFBP-3; ICAM-1; proIL-1β.
6	MMP3 (stromelysin-1)	Haemopexin domain	Type-III, IV, IX & X collagens; gelatins; tenascin; aggrecan; perlecan; decorin; link protein; Ln; Fn.	α1-antichymotrypsin; plasminogen; α1-PI; HBEGF; E-cadherin; α2-M; CTGF; uPA; proIL-1β; IGFBP-3; proMMP-1, 7, 8, 9 & 13.
7	MMP10 (stromelysin-2)	Haemopexin domain	Type-III, -IV & -V; Ln; Fn; link protein; aggrecan.	Pro-1, -8 & -10.
8	MMP11	Furin-activated	Aggrecan; Fn; gelatins;	α1-PI; IGFBP-1;

	(stromelysin-3)	secreted	Ln.	α2-M.
9	MMP-7 (Matrilysin-1)	Minimal domain (pro-domain & catalytic domain)	Collagen type-IV; gelatins; aggrecan; FN; link protein; tenascin; entatin; LN; decorin.	Fas-L; CTGF; HBEGF; RANKL; proα-defensin; IGFBP-3; proTNF-α; E-cadherin; plasminogen.
10	MMP-26 (Matrilysin-2)	Minimal domain (pro-domain & catalytic domain)	Fibrinogen; collagen type-IV; vitronectin; Fn; gelatins.	α1-PI; proMMP-9.
11	MMP28 (Epilysin)	Furin-activated secreted	Unknown.	Casein.
12	MMP12 (Metalloelastase)	Haemopexin domain	Aggrecan; collagen type-IV; Ln; Elastin; Fn; osteonectin; nidogen.	Apolipoprotein (a); plasminogen.
13	MMP19 (RASI-1)	Haemopexin domain	Collagen type-IV; Fn; aggrecan; Ln; gelatin; tenascin; COMP; nidogen.	IGFBP-3.
14	MMP20 (Enamelysin)	Haemopexin domain	Amelogenin; gelatin; COMP; aggrean.	Unknown.
15	MMP-21	Haemopexin domain	Unknown.	Unknown.
16	MMP27	Haemopexin domain	Unknown.	Unknown.
No	**Membrane-anchored MMP**			
17	MMP14 (MT1-MMP)	Type I Transmembrane domain	Type-I, -II & -III; aggrecan; Ln; Ln-5; gelatins; Fn; fibrin.	ProMMP-13; tissue transglutaminase; CD44; pro-MMP-2; MCP-3.
18	MMP15 (MT2-MMP)	Type I Transmembrane domain	Perlecan; nidogen; Fn; tenascin; aggrecan; Ln.	Tissue transglutaminease; proMMP-2.
19	MMP16 (MT3-MMP)	Type I Transmembrane domain	Fn; gelatins; type-III collagen.	Tissue transglutaminase; proMMP-2.
20	MMP24	Type I Transmembrane	PG.	ProMMP-2.

	(MT5-MMP)	domain		
21	MMP17 (MT4-MMP)	GPI-linked	Gelatins; fibrinogen.	Unknown.
22	MMP25 (MT6-MMP)	GPI-linked	Collagen type-IV; gelatin; fibrin; Ln; Fn.	ProMMP-2.
23	MMP23	Type II Transmembrane & Cysteine/Proline-rich IL-1 receptor like domain	Gelatin.	Unknown.

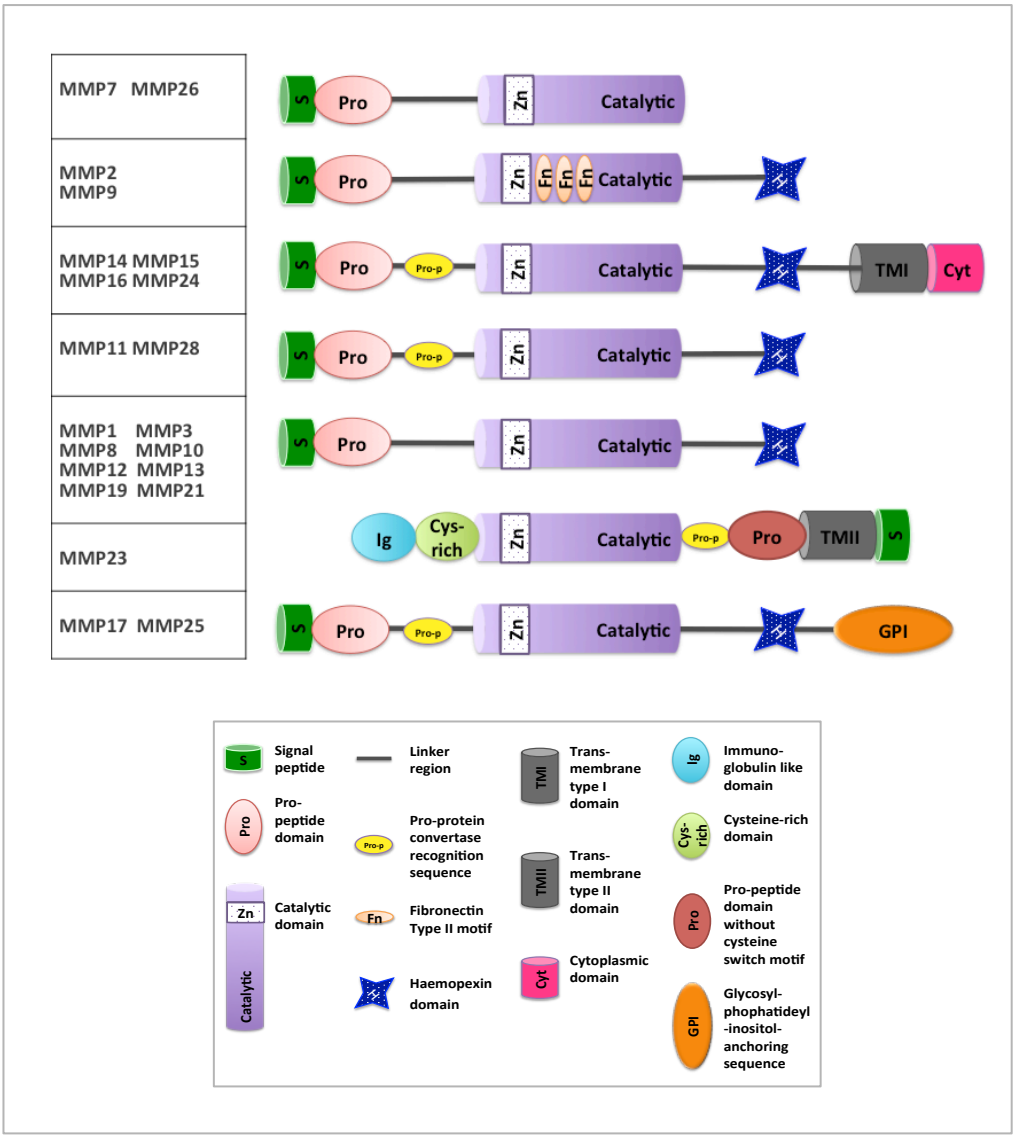

Figure 1.2: Domain structure of the metalloproteinases.

The figure illustrates domain arrangement of MMP family members based on Bonnans et al. (2014) and Khokha et al. (2013).

1.2.1.2 MMP functions

MMPs are produced as inactive zymogens that have a signal peptide allowing them to be either secreted to the extracellular space or anchored to the surface of the cell (Bonnans *et al.* 2014, Carmeliet *et al.* 1997, Fanjul-Fernandez *et al.* 2010). As already mentioned, most MMPs are activated by proteolytic cleavage of the pro-domain extracellularly. However, there are some exceptional MMPs regarding their presence in the extracellular space and activation. For example, a number of MMP family numbers were also found in the intracellular space such as MMP-1, MMP-2, MMP-11 and MMP-13 (Cuadrado *et al.* 2009, Limb *et al.* 2005, Luo *et al.* 2002). Also, MMP-11, MMP-21 and MMP-28 are intracellularly activated by furin-like protease and then secreted as active forms.

It is well known that MMPs function as ECM degradation enzymes; however, their proteolytic activities influence a variety of essential cellular and physiological processes. For instance, releasing cytokines and growth factors, cell adhesion, migration and proliferation, uterine and mammary involution, wound healing, bone development and angiogenesis (Fanjul-Fernandez *et al.* 2010, Page-McCaw *et al.* 2007, Rowe and Weiss 2008, Yamamoto *et al.* 2015). Numerous studies have shown that dysregulation of MMPs or their inhibitors result in a wide range of pathologies such as lung diseases, cardiovascular diseases, cancer, arthritis and different type of inflammatory diseases (Fanjul-Fernandez *et al.* 2010, Gaggar *et al.* 2011, Nagase and Woessner 1999).

1.2.1.3 MMP regulation

Under normal physiological conditions, MMPs activities are regulated at various levels including gene expression, precursor zymogen activation (the cysteine switch), binding to ECM components and specific inhibition (Tallant *et al.* 2010, Yamamoto *et al.* 2015). Although most MMPs are regulated transcriptionally and expressed in response to cytokines, hormones and growth factors, some are stored in inflammatory cell granules to restrict their action. Active MMPs are regulated by endogenous inhibitors such as α_2-macroglobulin (α_2M) for plasma associated MMPs and tissue inhibitors of metalloproteinases (TIMPs) for extracellular matrix MMPs (Brew and Nagase 2010, Yamamoto *et al.* 2015).

1.2.2 Adamalysins

In mammals adamalysins comprise two proteinase families, a disintegrin and metalloproteinase (ADAM) and a disintegrin and metalloproteinases with thrombospondin motif (ADAMTS) (Giebeler and Zigrino 2016).

1.2.2.1 ADAM and ADAMTS

ADAMs were originally also known as MDC proteins (metalloproteinase/disintegrin/cysteine-rich) (Giebeler and Zigrino 2016). To date 40 members of ADAM family have been identified in the mammalian genome, of which 22 *ADAM* genes have been described in humans (Table 1.3). In contrast to MMPs, only 12 of the human ADAMs encode proteolytically active proteins (Bode *et al.* 1993, Khokha *et al.* 2013, Reiss and Saftig 2009), with the remainder largely playing roles in cell adhesion via their disintegrin domains. On the other hand all of the known ADAMTS genes in mammalian genomes are proteolytically active and generally target proteoglycans. There are 19 known *ADAMTS* genes in humans, but these are named from 1 to 20 (Table 1.4), due to some, specifically *ADAMTS11* and *ADAMTS5,* being assigned to the same gene that encodes the protein aggrecanase-2 (Abbaszade *et al.* 1999, Hurskainen *et al.* 1999, Kelwick *et al.* 2015, Porter *et al.* 2005).

As their names suggest, ADAMs and ADAMTS share many structural features including metalloproteinases domain, pro-domain and disintegrin domain (Figure 1.3 & Figure 1.4). Despite the fact that they have common structural domains, there are also some significant differences, the most notable of these being ADAMs have transmembrane and cytoplasmic domains and are membrane bound molecules, although ADAM9 and ADAM12 have also been reported to have shorter, soluble variants (Gilpin *et al.* 1998, Hotoda *et al.* 2002), whereas ADAMTS proteinases lack a transmembrane domain but have varying numbers of thrombospondin-like repeats and are secreted proteinases (Lu *et al.* 2011).

Several ADAMs have the ability to cleave transmembrane protein ectodomains, releasing adhesion molecules, growth factor receptors and cytokines, giving then the name “sheddases”. The ADAMTS are secreted proteinases and include aggrecanases and pro-collagen-N-propeptidases that cleave matrix proteoglycans and collagens (Type I, II, and III), respectively (Bonnans *et al.* 2014, Kelwick *et al.* 2015). The disintegrin domain of the adamalysins is implicated in cell/cell cell/matrix interactions through binding integrins, while the Cys-rich domains bind to heparan sulphate proteoglycans.

ADAMs play important physiological roles in spermatogenesis, sperm-egg fusion, heart development, neurogenesis and morphogenesis in pancreas, kidney and lung. They have been also been implicated in playing pathological roles in diseases such as Alzheimer's, asthma, chronic inflammatory diseases, cancer, Duchenne muscular dystrophy and cone-rod dystrophy (Dreymueller *et al.* 2015, Giebeler and Zigrino 2016, van Goor *et al.* 2009). Similarly, ADAMTS plays an important role in a wide range of physiological processes; for instance, maintenance and development of tissues, extracellular matrix turnover, ovulation and blood coagulation. In addition, their dysregulation and mutations have been implicated in several pathologies such as arthritis, atherosclerosis, cancer, central nervous system disorders and thrombotic thrombocytopenic purpura (TTP) (Cal and Lopez-Otin 2015, Gottschall and Howell 2015, Kumar *et al.* 2012, Levy *et al.* 2001, Rocks *et al.* 2008).

Table 1.3: Members of the ADAM family.

Based on Reiss and Saftig (2009) and Shiomi et al. (2010).

Name of ADAM member	Alternative names	Proteolytic activity	Substrates	Potential functions in health and disease
ADAM1	Fertilin α, PH-30α	Pseudogene	Unknown	• Fertilisation; spermatogenesis
ADAM2	Fertilin β, PH-30β	Non-proteinase	Egg binding, sperm, fusion	• Similar to ADAM1
ADAM3	Cryitestin, CYRN, tMDC	Pseudogene	Unknown	• Similar to ADAM1
ADAM5	tMDC II	Pseudogene	Unknown	• Production and development of sperm
ADAM6	tMDC IV	Pseudogene	Unknown	• Similar to ADAM5
ADAM7	GP-83, EAP 1	Non-proteinase	Unknown	• Similar to ADAM5
ADAM8	MS2 (CD156)	Proteinase	proTNFα, CD23, RANKL	• Sheddase; fertilised egg implantation; neurogenesis • Inflammation; cancer.
ADAM9	MCMP, Meltrin-ϒ, MDC9	Proteinase	Fibronectin, gelatin, proHB-EGF, APP, TNF-p75 receptor	• Sheddase; organ development such as heart; pancreas and nervous tissue; cell migration • Alzheimer's disease; breast cancer
ADAM10	Kuzbanian, MDAM	Proteinase	Collagen type-IV, proTNFα, Fas-L, gelatin, IL6R and other	• Sheddase; development of pancreas and nervous tissue • Inflammation; Alzheimer's disease; cancer
ADAM 11	MDC	Non-proteinase	Unknown	• Tumour suppressor gene; breast cancer
ADAM 12	Meltrin-α, MLTNA, MLTN, MCMP	Proteinase	Gelatin, type-IV collagen, fibronectin, proHB-EGF and other	• Sheddase; fertilised egg implantation; adipogenesis; myogenesis • Breast cancer; cardiac hypertrophy and failure
ADAM15	Metargidin, AD56, CR II-7, MDC15	Proteinase	Gelatin, type-IV collagen	• Implantation of fertilised egg • Inflammatory bowel disease; atherosclerosis; cardiac hypertrophy and failure; glomerulonephritis; angiogenesis; cancer

ADAM17	TACE, cSVP	Proteinase	proTNFα, TNF-p75 receptor, proTGFα, L-selectin, IL6R and other	• Sheddase; neurogenesis; organ development including heart, lung, pancreas • Inflammation including arthritis, inflammatory bowel disease, and psoriasis; atherosclerosis; cardiac hypertrophy and failure; Alzheimer's disease; breast and pancreatic cancer; Glomerulonphritis
ADAM18	tMDC III, ADAM27	Non-proteinase	Unknown	• Spermatogenesis; fertilisation
ADAM19	FKSG34, Meltrin-β	Proteinase	RANKL, proneurgulin	• Sheddase; fertilisation and spermatogenesis; development of cardiovascular, kidney and neuron organs • Ventricular septal defect; valvular stenosis; brain cancer; glomerulonephritis; allograft nephropathy
ADAM20	P	Proteinase	Unknown	• Similar to ADAM18
ADAM21	ADAM31	Proteinase	Unknown	• Neurogenesis; sperm-egg fusion; Sperm formation
ADAM22	MDC2	Non-proteinase	Unknown	• Neurogenesis • Cancer
ADAM23	MDC3	Non-proteinase	Unknown	• Neurogenesis
ADAM28	e-MDC II, MDC-Ls, MDC-Lm	Proteinase	IGFBP-3, CD23, Myelin basic protein	• Spermatogenesis; Teeth development; Growth factor metabolism • Breast cancer
ADAM29	svph 1	Non-proteinase	Unknown	• Cancer and similar to ADAM20
ADAM30	Svph 4	Proteinase	Unknown	• Similar to ADAM20
ADAM32	AJ131563	Non-proteinase	Unknown	• Similar to ADAM20
ADAM33	-	Proteinase	Insulin B chain, APP, KL-1	• Lung development • Genetically implicated in bronchial asthma
ADAMEC1	-	Proteinase	Unknown	• Unknown

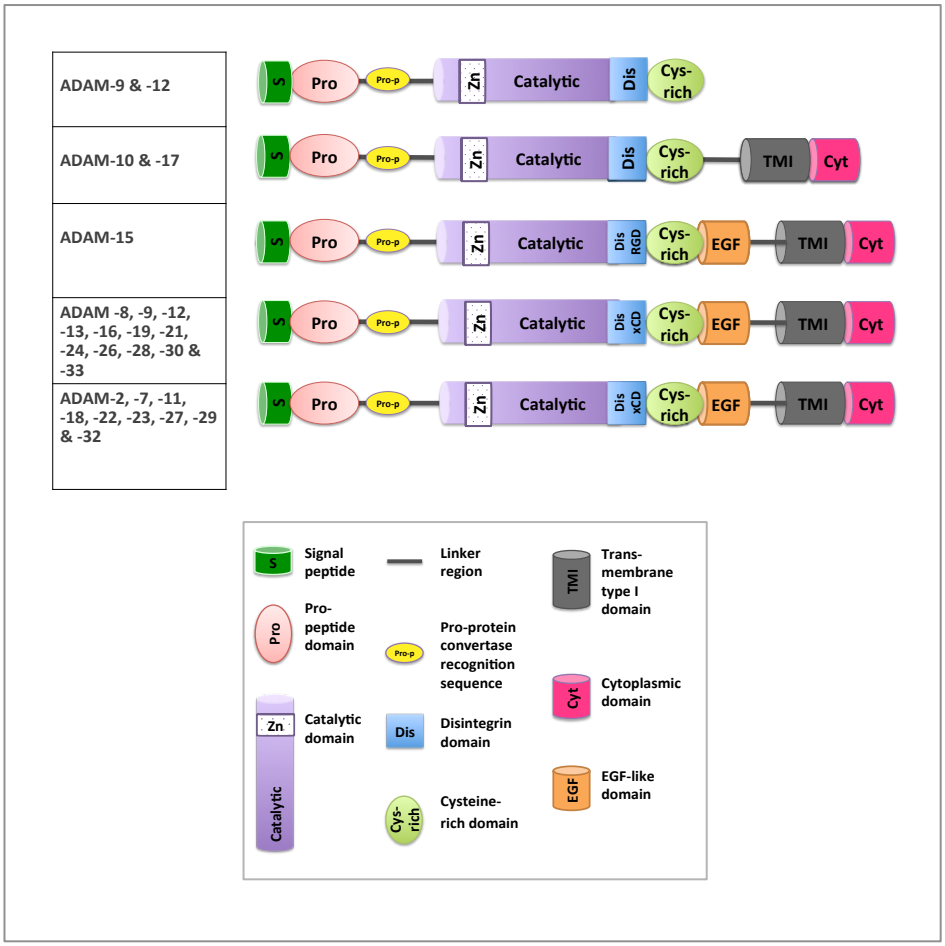

Figure 1.3: Structure of ADAM family members.

Demonstration of ADAM domain organisation was drawn according to Giebeler and Zigrino (2016) and Khokha et al. (2013). Dis-RGD: contains a RGD amino acid sequence, only ADAM15; Dis-xCD: contains a conserved consensus-binding motif.

Table 1.4: Members of ADAMTS family.

Based on Dubail and Apte (2015), Kelwick et al. (2015), Kumar et al. (2012) and van Goor et al. (2009).

ADAMTS members	Alternative names	Substrates	Function in health and disease
ADAMTS1	Aggrecanase-3, METH-1	Nidigen 1&2, aggrecan, versican	• Ovulation; implantation of fertilised egg; bone development • Anti-angiogenic, anti-tumorigenic and pro-tumorigenic
ADAMTS2	Procollagen N-proteinase, PCINP	Type-I, -II, -III & -V fibrillar procollagens	• Dermatosparaxis type VIIC, Ehlers-Danlos syndrome
ADAMTS3	KIAA0366	Biglycan, type-II fibrillar procollagens	• Unknown
ADAMTS4	KIAA0688, aggrecanase-1	Aggrecan, brevican, matrilin-3, versican	• Development of bone and adipose tissue • Brain cancer; Arthritis
ADAMTS5	ADAMTS11, aggrecanase-2, implantin	Aggrecan, brevican, neurocan, versican	• Implantation of fertilised egg; bone and adipose tissue formation • Brain cancer; anti-angiogenic and anti-tumorigenic; arthritis
ADAMTS6	-	-	• Unknown
ADAMTS7	-	COMP	• Coronary artery disease
ADAMTS8	METH-2	Aggrecan	• Unknown
ADAMTS9	KIAA1312	Versican, aggrecan	• Anti-angiogenic in cancer
ADAMTS10	-	Fibrillin-1	• Weill-Marchesani syndrome
ADAMTS12	-	COMP	• Asthma; Pro- and anti-tumorigenic
ADAMTS13	vWFCP	vWF	• Thrombotic thrombocytopenic purpura, congenital/upshaw-schulman syndrome
ADAMTS14	-	Type-I fibrillar procollagen	• Multiple sclerosis
ADAMTS15	-	Verican, aggrecan	• Anti-angiogenic; anti-tumorigenic; metastatic
ADAMTS16	-	Aggrecan	• Hypertension
ADAMTS17	LOC123271, FLJ32769	-	• Weill-Marchesani-like syndrome
ADAMTS18	HGNC:16662, ADAMTS21	Aggrecan	• Microcornea, myopic chorioretinal atrophy and telecanthus (MMCAT)
ADAMTS19	-	-	• Unknown
ADAMTS20	-	Versican	• Unknown

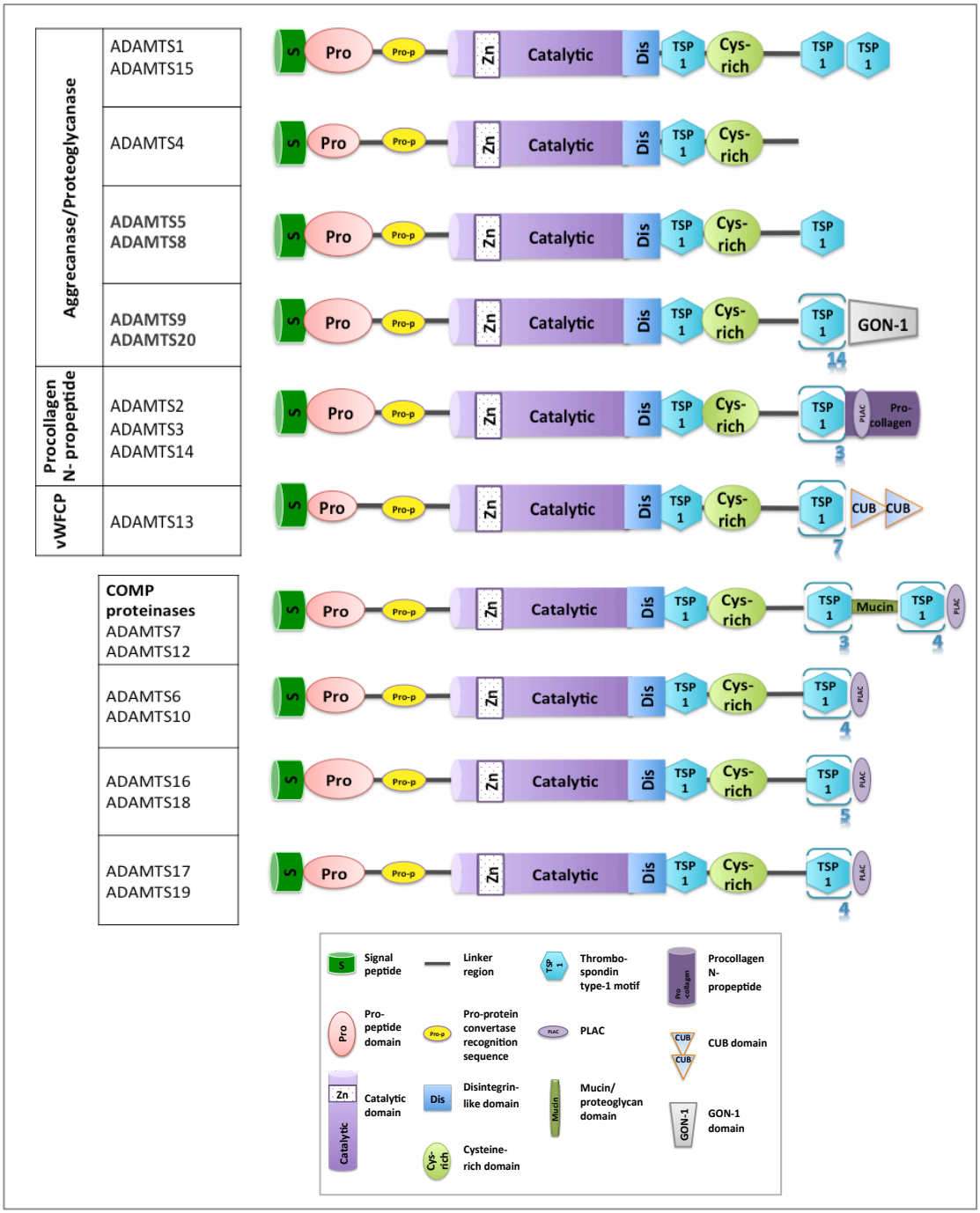

Figure 1.4: The ADAMTS family members.

Illustration of ADAMTS structure depending on their domain organisation into groups including aggrecanase/proteoglycanase, procollagen N-propeptidase, von wilbrand factor cleaving protease (ADAMTS13), and those cleaving cartilage oligomeric matrix protein (COMP), and those ADAMTS ungrouped. (Kelwick et al. 2015, Khokha et al. 2013, Kumar et al. 2012)

1.3 The TIMP Family

A variety of cell types, such as fibroblasts and macrophages, epithelial and endothelial cells, secrete small proteins termed tissue inhibitors of metalloproteinases (TIMPs) into the extracellular matrix. They are considered to be the major inhibitors of MMPs. TIMP1 was the first TIMP identified as a protein in human fibroblast culture medium and human serum and shown to inhibit collagenases (Bauer *et al.* 1975, Woolley *et al.* 1975). Three other TIMPs have been recognised in vertebrates and named TIMP2, TIMP3 and TIMP4. Genes for human TIMP1, TIMP2, TIMP3 and TIMP4 were mapped to the X-chromosome Xp11, 3-Xp11.23 by Willard *et al.* (1989), chromosome 17q25 by De Clerck *et al.* (1992), chromosome 22q12.1-q13.2 by Apte *et al.* (1994) and 3p25 by Olson *et al.* (1998), respectively.

1.3.1 TIMP structure

The four mammalian TIMPs have molecular weights between 21 to 29 kDa and comprise 184 to 195 amino acids excluding their signal sequences. Each TIMP contains 12 cysteine residues and two distinctive domains comprising the N-domain (about 125 amino acids) and the C-domain (about 65 amino acids), each of which is stabilised by three disulphide bonds. (Figure 1.5)

While all TIMPs have a similar three-dimensional structure, constrained by the six disulphide bonds and a shared ability to inhibit MMPs, sequence conservation between family members is fairly low with only about 40% identity (Brew and Nagase 2010) (Figure 1.6). In contrast, sequence conservation of each family member between species is very high, with TIMP3 being exceptional in this respect with, for example, human and chicken TIMP3 being 82% identical (Figure 1.7). The N-terminal domain of the TIMPs alone has been shown to be a completely active inhibitor of MMPs. In contrast, the C-terminal domain seems to give rise to the individual differences between TIMPs. For these reasons, each TIMP is believed to have a unique physiological role. (Li *et al.* 2005)

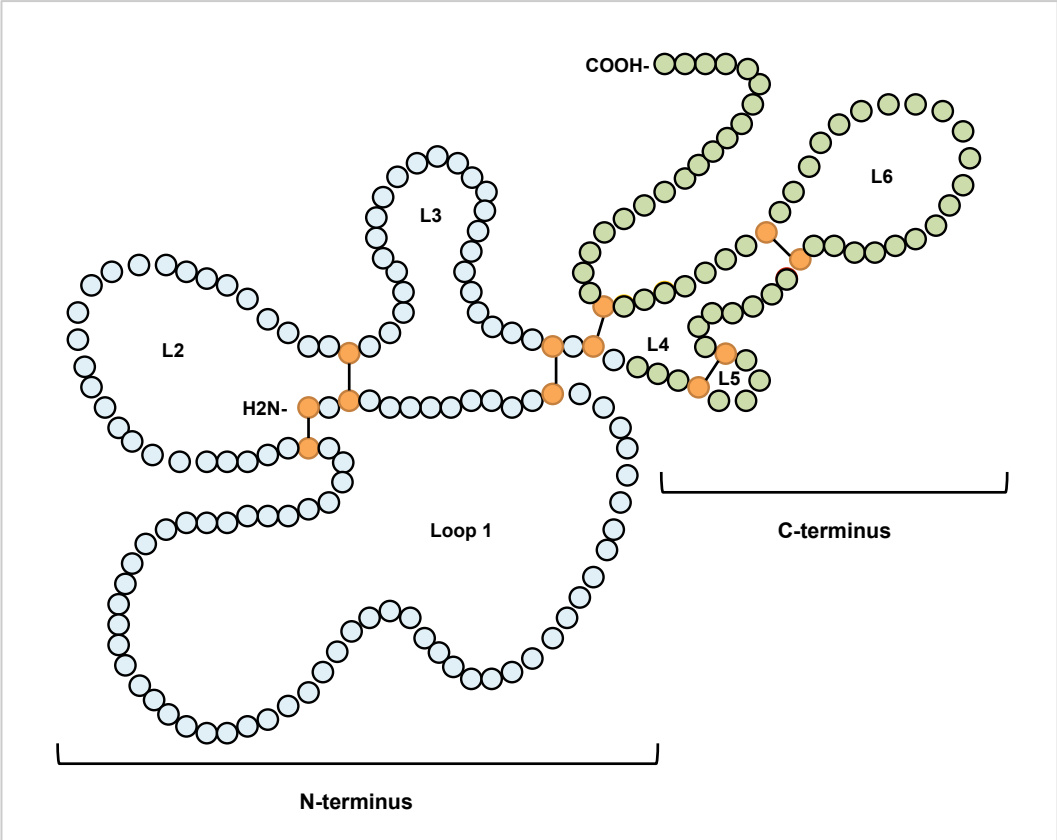

Figure 1.5: TIMP primary structure.

N-terminus is represented by pale blue circles including loop 1, 2 and 3 while the C-terminus is represented by pale green including loop 4, 5 and 6, and disulphide bonds are represented by orange.

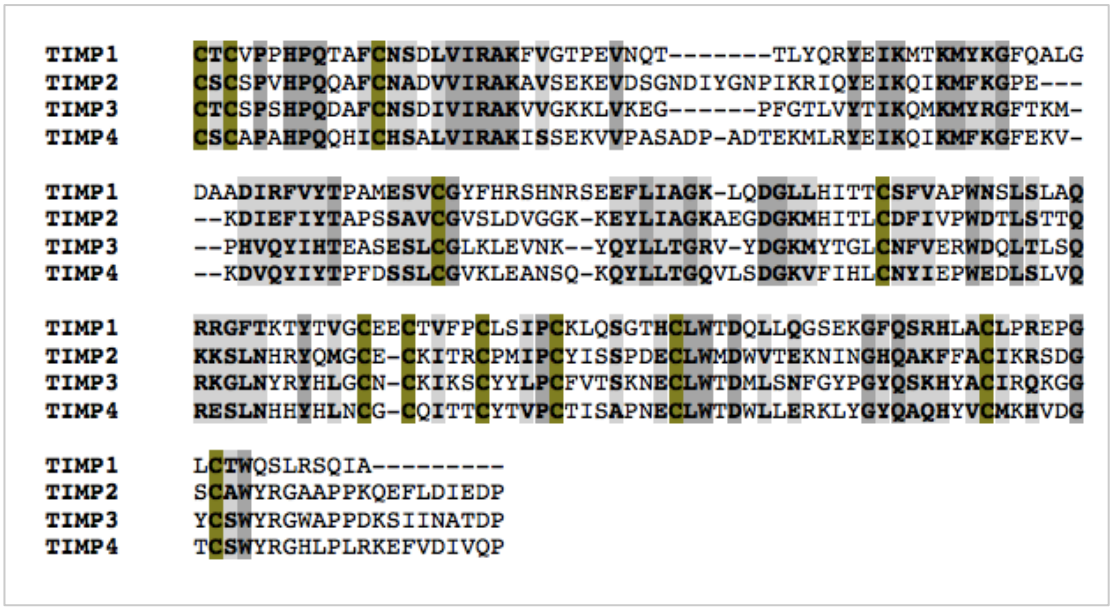

Figure 1.6: Multiple sequence alignment of human TIMP proteins.

Sequence alignment of human TIMP proteins in which the dark grey shaded letters refer to identical residues, pale grey to similar residues and the khaki coloured to cysteine residues.

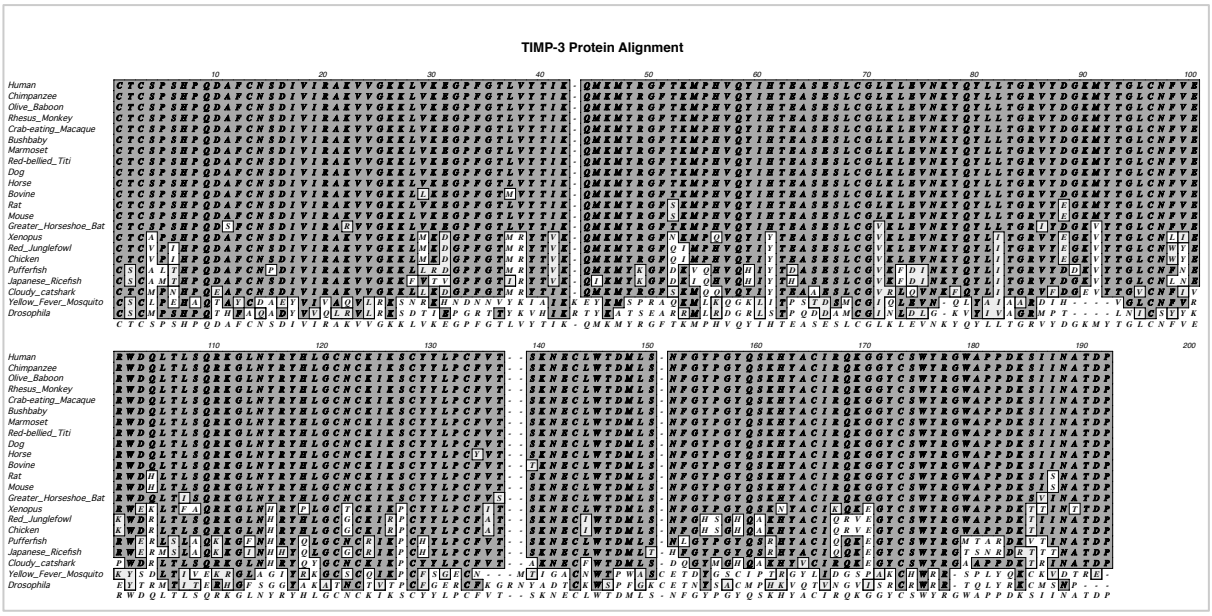

Figure 1.7: Alignment of TIMP3 protein sequence from various species.

Identical residues are highlighted in dark grey and similar residues in light grey. There is 100% identity between primate sequences, 96% identity between mammalian sequences and even 82% identity between human and chicken sequences.

1.3.2 TIMP function

TIMPs participate in numerous biological phenomena; for instance, cell proliferation, invasion and migration of cells, angiogenesis, apoptosis and synaptic plasticity, some of which are independent of their main inhibitory function against MMPs. (Olson *et al.* 1998, Stetler-Stevenson *et al.* 1992)

1.3.3 MMP inhibition

As described earlier, TIMPs are defined as natural inhibitors of MMPs. Most MMPs are inhibited by all TIMPs; however, different specificities and binding affinities have been noticed. For instance, MMP-3 and MMP-7 are weakly inhibited by TIMP-2 and -3 whereas TIMP-1 is a better inhibitor (Hamze *et al.* 2007). TIMPs inhibit MMPs through a 1:1 non-covalent binding at the active site. The binding involves the N-terminal Cys residue of the TIMP co-ordinating with the Zn^{2+} (Nagase *et al.* 2006) in a similar manner to the Cys residue of the pro-domain of the latent enzyme. Some TIMPs also have a broader inhibitory action that encompasses inhibition of ADAM and ADAMTS enzymes.

1.3.4 Cell growth promotion

Sequencing of TIMP1 cDNA revealed that it was identical to an erythropoietin potentiating factor sequence involved in erythroid progenitor cell proliferation (Brew and Nagase, 2010). TIMP1 also stimulates the growth of other cell types such as keratinocytes, chondrocytes and fibroblasts (Bertaux *et al.* 1991, Hayakawa 1994). TIMP2 has also been seen to have erythroid potentiating activity (Stetler-Stevenson *et al.* 1992) as well as promoting cell growth in many cell types including metanephric mesenchyme cells (Barasch *et al.* 1999, Hayakawa *et al.* 1994).

1.3.5 Cell growth inhibition

In contrast to the above, several studies suggest that both TIMP1 and TIMP2 are able to reduce the growth rate of some cells. For instance, Taube *et al.* (2006) showed that TIMP1 reduced the growth rate of human breast epithelial (MCF10A) cells via inducing cell cycle arrest at G1. In addition, TIMP2 was shown to have a suppressive effect on the mitogenic response to tyrosine kinase-type receptor growth factors through activation of adenylate cyclase and increase the level of intracellular cAMP (Hoegy *et al.* 2001).

1.3.6 Inhibition of angiogenesis

Angiogenesis (see section 1.4.1.4.1) requires the activity of MMPs to enable endothelial cell migration and vessel remodelling and so it is assumed that TIMPs will play a role in regulating this process. However TIMP2 and TIMP3 have also been shown to inhibit angiogenesis independently of their ability to inhibit these enzymes. For TIMP2 this appears to be mediated by interaction with α3β1 integrin (Seo *et al.* 2003). For TIMP3 it is mediated by direct binding to vascular endothelial growth factor receptor 2 (VEGFR2) (Qi *et al.* 2003) (see section 1.4.1.4).

1.4 TIMP3

The third member of the TIMP family was firstly identified in chicken and designated ChIMP3. Pavloff *et al.* (1992) described ChIMP3 cDNA as encoding a mature protein that consists of 212 amino acids with a molecular mass of 21 kDa, comprising a signal peptide (24 a.a) followed by 188 a.a. mature protein sequence. Whilst ChIMP2 was found in the media produced by chicken embryonic fibroblasts, ChIMP3 was observed as a component of the extracellular matrix. Mouse and human TIMP3 genes were subsequently cloned (Leco *et al.* 1994) and shown to display the same ECM binding ability.

The *TIMP3* gene maps to the long arm of chromosome 22, specifically to the q12.1-q13.2 region (Apte *et al.* 1994). The organisation of the human TIMP3 gene was described by Stohr *et al.* (1995) who reported that the gene is encoded by 5 exons, which span approximately 55 kb of human genomic DNA (now shown to be 61.3kb) and lacks a TATA box region. As a result of using alternative polyadenylation signals, the *TIMP3* gene gives rise to three different mRNAs encompassing 2.4, 2.8 and 5 kb transcripts but all with identical open reading frames. The *TIMP3* gene has a promoter region in which the first 112 bases were found to have the ability to give high basal level expression in growing cells. (Wick *et al.* 1995) (Figure 1.8)

The expression of murine TIMP3 mRNA was observed by Apte *et al.* (1994) in many tissues including the placenta, heart, kidney, liver and the brain, with the highest expression level in the placenta and the lowest level was in the brain. Human and mouse TIMP3 were expressed in mouse NSO myeloma cells and produced an *N*-glycosylated 27 kDa protein which was an efficient inhibitor of MMPs. In addition, Ruiz *et al.* (1996) showed that TIMP3 mRNA was expressed by human retinal pigment epithelium. A later study was conducted to investigate

the ocular site of TIMP3 expression using *in situ* hybridization of albino mouse eyes and showed that TIMP3 mRNA is only expressed in the RPE and the ciliary epithelium (Della *et al.* 1996).

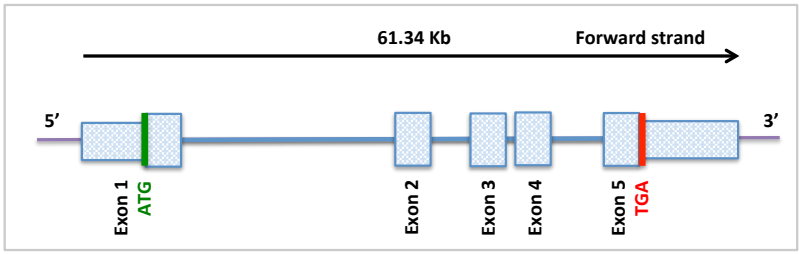

Figure 1.8: Gene structure of human TIMP3.

5' and 3' flanking regions are indicated by lilac lines, coding exons by solid coloured boxes, non-coding exons by narrow boxes and introns by solid lines in blue. Available from: http://www.ensembl.org/index.html *and based on (Stohr et al. 1995).*

1.4.1 Novel properties of TIMP3

As outlined in section 1.3.1, TIMP3 is extremely highly conserved across species and this probably reflects that it has been shown to engage in a number of interactions, in addition to MMP inhibition, and these will be discussed in more detail in the following sections.

1.4.1.1 Localisation to the ECM

TIMP1, TIMP2 and TIMP4 are all soluble proteins whereas TIMP3 is strongly bound to the ECM. Leco *et al.* (1994); for example, observed the expression of TIMP3 in the COS-1 cell line which gives rise to a 24 kDa protein that localised to the ECM.

Langton *et al.* (1998) investigated the functional domains of TIMP3 by expression in COS-7 cells. This showed that TIMP3, either in its unglycosylated (24 kDa) or glycosylated (27 kDa) forms, was completely localised to the ECM, whilst a carboxyl terminal domain deleted TIMP3 lost its ECM localisation properties. A chimeric TIMP containing the amino terminal domain of TIMP2 and the carboxyl terminal domain of TIMP3 showed ECM binding.

TIMP3 binds to heparin sulphate and sulphated glycosaminoglycans and it is likely that this characteristic is largely responsible for TIMP3 binding to the ECM (Yu *et al.* 2000). More recently, Lee *et al.* (2007) carried out a more detailed analysis of the interaction of TIMP3 with the ECM and found it to be mediated by residues in both the N-domain and the C-domain. The ECM binding motifs were identified as all basic amino acids, encompassing lysine residues at 26, 27, 30 and 76 of the N-terminal domain and arginine 163 and lysine 165 of the C-terminal domain. Mutation in these residues to glutamine or glutamate was shown to result in a soluble TIMP3 molecule lacking its ECM binding ability. These findings were supported by TIMP1 mutated to lysine at residues 26, 27, 30 or 76, which was seen to give rise to a TIMP1 molecule capable of ECM binding. (Lee *et al.* 2007)

1.4.1.2 Inhibition of ADAM/ADAMTS proteinases

Amongst the mammalian TIMPs, TIMP3 is a distinct member with a broader inhibitory action toward metalloproteinases. This inhibitory action encompasses members of the ADAM (a disintegrin-metalloproteinase) and ADAMTS (a disintegrin-metalloproteinases with thromospondin motifs) families. For example TIMP3 inhibits the sheddases, ADAM10 and ADAM17 (Amour *et al.* 1998, Amour *et al.* 2000) and is an effective inhibitor of ADAMTS 1, 2, 4 and 5 (Brew and Nagase 2010, Wang *et al.* 2006, Wayne *et al.* 2007). ADAMTS 4 and

5 are known as aggrecanases 1 and 2, respectively and appear to play a critical role in cartilage degradation in arthritis (Huang and Wu 2008, Tortorella *et al.* 1999).

TACE (ADAM17) was reported by Amour *et al.* (1998) as the first non-MMP metalloproteinase to be inhibited by TIMP3. The importance of TACE inhibition by TIMP3 is illustrated by TIMP3 knockout studies in which many of the symptoms result from increased activity of TACE and subsequently increased release of TNF-α. For example Mohammed *et al.* (2004) showed that mice lacking the *TIMP3* gene displayed chronic hepatic inflammation and Kassiri *et al.* (2005) demonstrated that T3 knockout mice developed dilated cardiomyopathy due to increased level of TNF-α. The crystal structure of TACE in complex with the N-domain of TIMP3 has been resolved to 2.3 Å, Wisniewska *et al.* (2008) demonstrating that the N-terminus of TIMP3, particularly Phe34, Leu94 and Leu67, binds to the hydrophobic surface of the TACE-catalytic domain. Xu *et al.* (2012) conducted a study to examine TACE activation and binding to TIMP3 and found that TACE is present on the cell surface in a dimeric form that favours the binding of TIMP3, thus maintaining it in an inactive state. Activation of the ERK/p38MAPK pathways resulted in a shift to monomeric-TACE and the dissociation of TIMP3 (Figure 1.9).

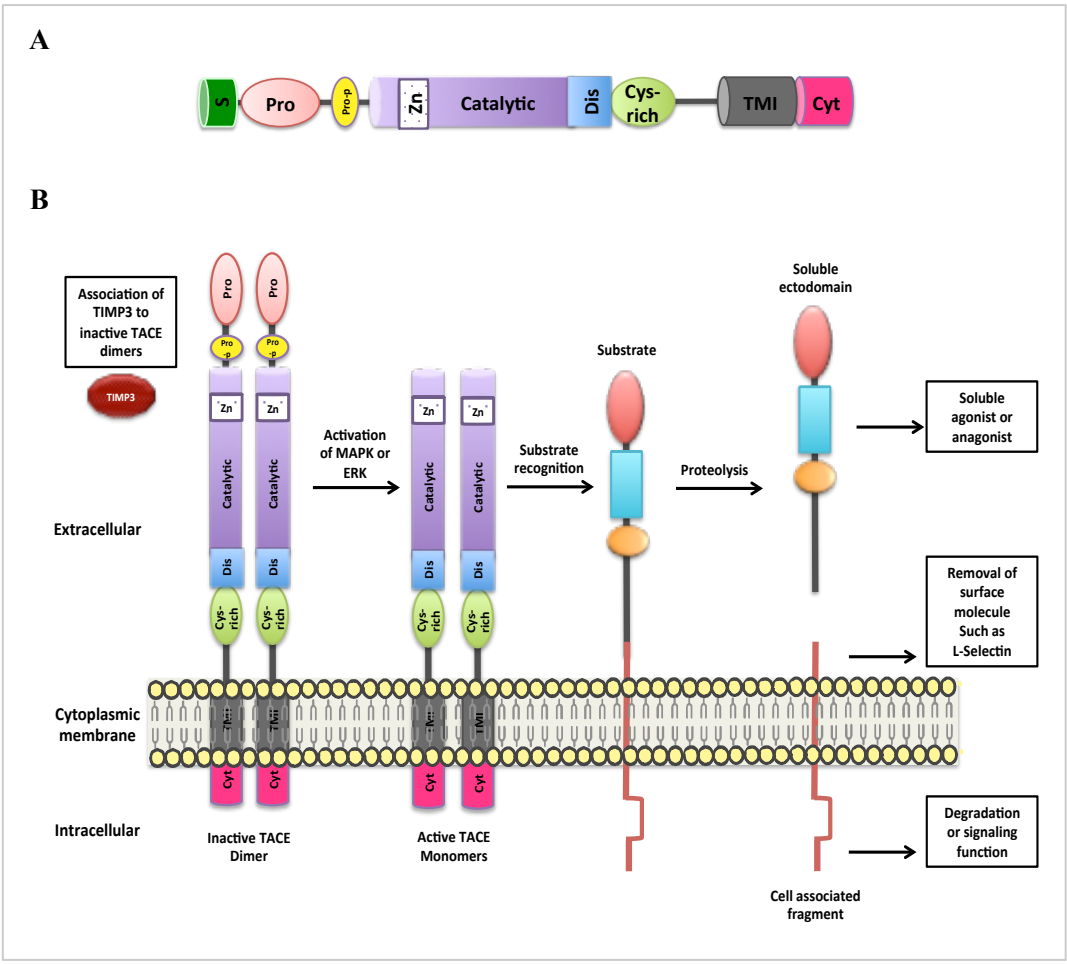

Figure 1.9: TACE domain organisation and activation.

(A) Domain organisation of TACE. S: Signal peptide (17 aa); Pro: pro-domain (196aa); Catalytic: catalytic domain (258aa); Dis; disintegrin domain (98aa); Cys-rich: cysteine-rich domain (98aa); TMI: transmembrane (23aa); Cyt: cytoplasmic domain (129aa). (B) Illustration of TACE activation. Upon activation of MAPK or ERK pathways, the balance between TACE dimer and monomer shift to monomer form, which is associated with increased TACE presentation on the cell surface and decrease TIMP3 interaction. Based on Dreymueller et al. (2015) and Xu et al. (2012).

1.4.1.3 Apoptosis

Several studies have demonstrated that apoptosis of various cell types, including cancer cell lines, is induced by increased expression of TIMP3. For example, TIMP3 overexpression was demonstrated to increase apoptosis of HeLa, HT1080 and MCF-7 cells (Baker *et al.* 1999) and retinal pigment epithelial cells (Majid *et al.* 2002).

Full length TIMP3 and N-terminal domain TIMP3 were found to promote apoptosis whereas a TIMP2-TIMP3 chimera that had the N-terminal domain of TIMP2 and the C-terminal domain of TIMP3 did not (Bond *et al.* 2002). It was concluded that the pro-apoptotic effect of TIMP3 is located in the three loops of the N-terminal domain of TIMP3 and that TIMP3 inhibition of metalloproteinases is associated with the induction of apoptosis. This appears to be due to increased inhibition to TACE leading to decreased shedding of death receptors such as TNF-RI (tumour necrosis factor receptor-1), FAS and TRAIL-RI (TNF-related apoptosis inducing ligand receptor-1) (Ahonen *et al.* 2003). Recently, however, Qi and Anand-Apte (2015) showed that overexpression of TIMP3 induced apoptosis in endothelial cells through an MMP- and caspase-independent mechanism.

In contrast to the evidence that over-expression of TIMP3 induces apoptosis, evidence from knockout mice suggests that TIMP3 inhibits apoptosis in the mammary gland (Fata *et al.* 2001) and this appears to be due to loss of TIMP3 resulting in increased shedding of TNFα, which plays a role in epithelial apoptosis (Hojilla *et al.* 2011).

1.4.1.4 Inhibition of VEGFR2

TIMP3 is unique among the TIMP family in specifically binding to vascular endothelial growth factor receptor-2 (VEGFR2) (Qi *et al.* 2003), resulting in inhibition of angiogenesis and this will be considered in more detail below.

1.4.1.4.1 Angiogenesis

Vasculogenesis is the *de novo* development of blood vessels that plays a vital role in embryonic vascular network formation. This is also accompanied by angiogenesis, the sprouting of capillaries from pre-existing vessels (Risau *et al.* 1988). While there is some evidence for vasculogenesis in adult tissues (D'Alessio *et al.* 2015), the new blood vessel

formation that occurs in adulthood, largely in the repair of injured tissue and the ovarian cycle, is primarily mediated by angiogenesis. Angiogenesis occurs in response to an initial stimulus such as ischemia, hypoxia and inflammation leading to upregulation of angiogenic stimuli.

A diverse group of proteins have been identified to regulate the different stages of angiogenesis. These proteins are classified into angiogenic stimulators, inhibitors and extracellular matrix-bound cytokines. Angiogenic stimulators include soluble growth factor such as vascular endothelial growth factor (VEGF) and fibroblast growth factor 1 (FGF-1, acidic) and fibroblast growth factor 2 (FGF-2, basic); the inhibitors (antiangiogenic) comprise pigment epithelium derived factor (PEDF), angiogenin, transforming growth factor β (TGF-β) and other small molecular weight molecules; and cytokines are also released by proteolysis and contribute to angiogenesis regulation. Among all these growth factors, VEGFs are considered the major mediators of angiogenesis and are described in more details in section 1.4.1.4.2. Deregulated angiogenesis plays a role in a number of disease processes, including retinopathies, haemangiomas, tumour growth and peripheral and myocardial ischemia (Dawson *et al.* 1999, Ferrara 1995, Patan 2000, Yoo and Kwon 2013).

1.4.1.4.1.1 Angiogenesis in retinopathies

In normal physiological conditions the blood vessels in the eye remain in a quiescent state, which is maintained by the balance between angiogenic and anti-angiogenic factors. In response to pathological conditions such as inflammation and hypoxia, angiogenic factors are activated and the balance may shift to angiogenesis. Ocular angiogenesis, the formation of new blood vessels from the existing vascular network in the eye is a major cause of severe vision loss and can occurs in different layers such as the cornea, choroid and retina. Choroidal neovascularisation (CNV) is exemplified by neovascular (wet or exudative) AMD and is also a common feature of SFD. The principle mediator of choroidal neovascularisation is VEGF.

1.4.1.4.2 VEGF

Vascular endothelial growth factors are essential for blood vessel formation in development and also for the growth of new vessels from existing vasculature. VEGFs are a family of six polypeptides including VEGF-A to -D (endogenous), VEGFE (viral) and PIGF, which

regulate the development of blood and lymphatic vessels. VEGFs are dimeric glycoproteins with a molecular weight of approximately 40 kDa. They were firstly discovered as vascular permeability factor.

Among the VEGF family, VEGF-A has been extensively studied due to its function in cell signalling, angiogenesis and cancer. VEGF-A was firstly described as the main player in angiogenesis (Ferrara and Henzel 1989, Keck *et al.* 1989, Senger *et al.* 1983). The VEGF-A gene is localised to the short arm of chromosome 6 consisting of 8 exons that are differentially spliced to give rise to multiple isoforms. These VEGF-A isoforms encode 12 polypeptides with variable amino acid length and numbers of heparin binding motifs that result in varying affinities for the ECM (Harper and Bates 2008, Nagy *et al.* 2007) (Figure 1.10). These 12 isoforms are further divided into two subfamilies termed pro-angiogenic and anti-angiogenic with isoforms designated with a b suffix, such as VEGF165b, being anti-angiogenic. However the actual existence of these anti-angiogenic isoforms *in vivo* has recently been questioned and may be an artefact of the detection method (Harris *et al.* 2012).

VEGF is expressed in several types of cell such as fibroblast, cancer cells, vascular endothelial and smooth muscle cells; and it regulates endothelial cell functions through auto and paracrine pathways (Barleon *et al.* 1997, Brogi *et al.* 1996, Chua *et al.* 1998, Lamalice *et al.* 2007). As outlined above, VEGF has been shown to play a role in several retinal diseases including age-related macular degeneration disease (AMD) and diabetic retinopathy. VEGF is expressed by various retinal cells, including retinal pigment epithelial cells, astrocytes and ganglion cells. (Penn *et al.* 2008)

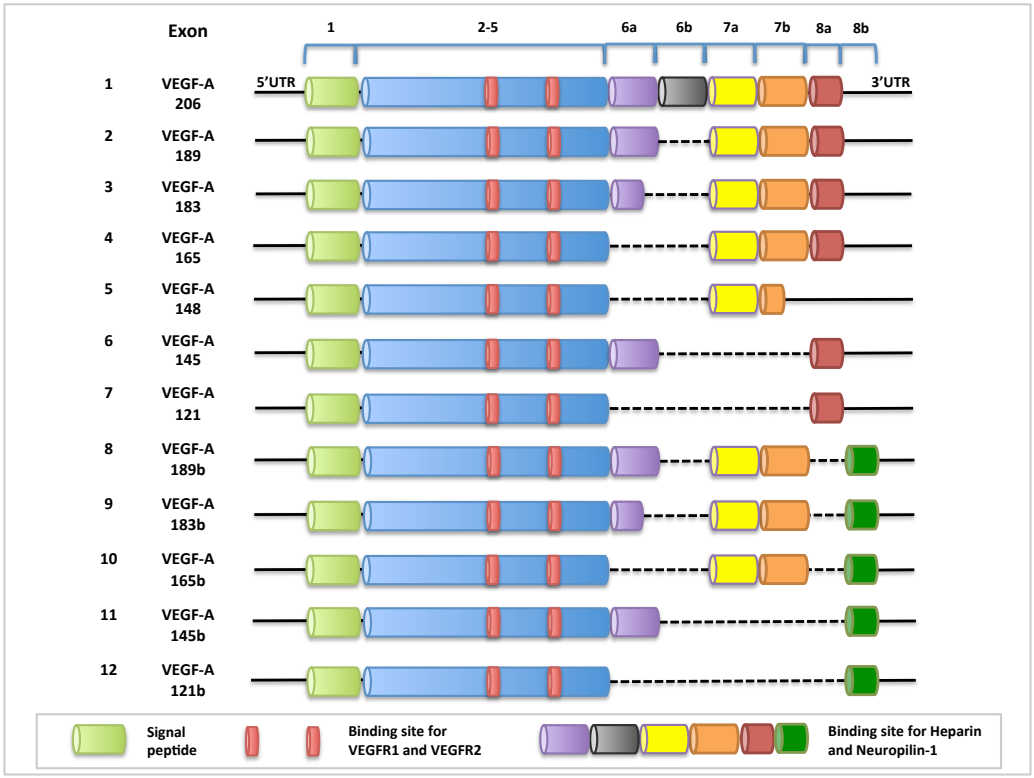

Figure 1.10: Protein isoforms of human vascular endothelial growth factor A (VEGF-A).

The figure illustrates VEGF-A family members divided into angiogenic (1-7) and anti-angiogenic (8-12) subfamilies. VEGF-A protein structures were drawn based on (Grunewald et al. 2010, Harper and Bates 2008, Penn et al. 2008).

1.4.1.4.3 VEGF receptor

While the effects of VEGF are mediated through several receptors including VEGFR1, 2 and 3 and neuropilins 1 and 2 (NRP-1, -2) (Grunewald *et al.* 2010), VEGFR2 is considered to be the major effector of VEGF-induced angiogenesis. Structurally, these receptors belong to the receptor tyrosine kinase family consisting of an extracellular domain that is arranged into seven immunoglobulin-like folds, a single transmembrane region, a juxtamembrane domain followed by split tyrosine kinase domain and cytoplasmic tail (Figure 1.11). The ligand-binding site is situated in the second and third immunoglobulin domains (Fuh *et al.* 1998, Leppanen *et al.* 2010). VEGF receptors are activated through ligand-induced dimerisation, which is associated with activation of the receptor kinase domains resulting in auto-phosphorylation. Auto-phosphorylation of the VEGFR2 leads to activation of several signalling pathways such as phosphoinositide-3 kinase (PI3K) and mitogen activated protein kinase (MAPK), and subsequently broad biological response in endothelial cells including proliferation, migration and cell survival. (Grunewald *et al.* 2010, Mac Gabhann and Popel 2007, Penn *et al.* 2008, Rahimi 2006)

Qi and colleagues (2003) showed that TIMP3 directly inhibited the binding of VEGF to its receptor (VEGFR2) and subsequently angiogenesis; the inhibition of TIMP3 was found to be independent of its MMP inhibitory action. Recent studies were carried out to localise TIMP3-sequence involved in VEGFR2 inhibition. Qi *et al.* (2013) showed that two short synthetic peptides, corresponding to TIMP3-loop-6 and TIMP3-tail region inhibited the interaction between VEGF and VEGFR2. Similarly, Chen *et al.* (2014) demonstrated that a peptide comprising loop-4 and loop-5 also inhibited VEGFR2. N-domain TIMP3 failed to inhibit VEGFR2 indicating that it is the carboxyl-domain of TIMP3 alone that is responsible for inhibiting the interaction between VEGF and VEGFR2.

As mentioned earlier TIMP3 is expressed in the RPE and it would seem this plays an important role in regulating neovascularisation of the retina. This is illustrated by the fact that eyes from knockout mice show abnormal vessel formation (Ebrahem *et al.* 2011, Janssen *et al.* 2008).

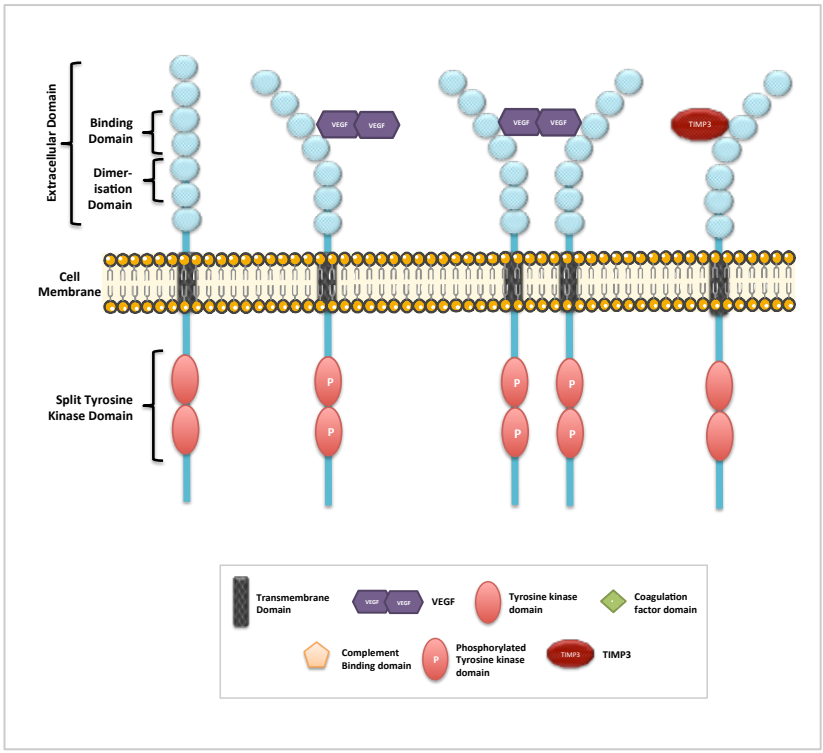

Figure 1.11: The VEGF receptors protein tyrosine kinases.

A schematic diagram illustrating the interaction of VEGF receptor with VEGF and TIMP3; VEGF receptor is activated by binding to its dimeric ligand VEGF and inhibited through binding to TIMP3. Based on figures from Nagy et al. (2007), Penn et al. (2008) and Grunewald et al. (2010).

1.4.1.5 TIMP3 and EFEMP1

The carboxyl-terminus of TIMP3 has been demonstrated to bind to epidermal growth factor fibulin-like extracellular matrix protein 1 (EFEMP1), which is also known as fibulin 3. EFEMP1 is a matrix glycoprotein and member of the fibulin protein family. A missense mutation (R345W) in the EGF domain of the *EFEMP1* gene causes a dominant retinal macular degeneration termed Malattia Leventinese (ML) with a phenotype that resembles that of age-related macular degeneration (AMD) and Sorsby's fundus dystrophy (SFD). This will be discussed in more details in section 1.5. (de Vega *et al.* 2009)

1.5 Sorsby's Fundus Dystrophy (SFD)

TIMP3 is unique among the TIMP family in being specifically associated with the retinal disease known as Sorsby's fundus dystrophy (SFD), which was firstly described in 1949 by (Sorsby and Mason 1949). SFD is defined as a rare autosomal dominantly inherited degenerative disease of the macula, which is the most sensitive part of the central retina, responsible for high-resolution colour vision. It is regarded as a single gene disorder caused by specific mutations in the *TIMP3* gene. It is considered as a late onset disorder that results in rapid loss of central vision; however, the age of onset ranges from the third to seventh decade amongst affected individuals (Brew and Nagase 2010, Gregory-Evans 2000). Surprisingly, considering the wide tissue distribution of TIMP3 and its role in regulating MMPs, SFD patients are otherwise healthy with a normal lifespan and no evidence for any disease other than in the eye (Li *et al.* 2005).

1.5.1 Retinal anatomy and SFD clinical manifestations

The retina comprises several layers including photoreceptors, the retinal pigment epithelium (RPE), Bruch's membrane and choroid. The RPE forms a single layer of cells and is responsible for transporting nutrients from the choroidal vascular bed to the photoreceptor cells via Bruch's multilayered basement membrane as well as removal of waste products in the opposite direction. (Figure 1.12 A) (Brew and Nagase 2010, Kolb 1995)

Histopathological analysis of retina from SFD patients shows increased deposition of extracellular waste products including proteins and lipids known as drusen, thickening in Bruch's membrane and atrophy of the photoreceptors, RPE and choroid, presumably as a result of a reduction in the transport of nutrients and metabolites from choroid to retinal

layers. This is usually accompanied by the growth of new blood vessels through Bruch's membrane resulting in haemorrhage and occasionally retinal detachment leading to total blindness. Most SFD individuals have a loss of central vision due to neovascularisation (wet-type macular degeneration); nevertheless, SFD can also be essentially an atrophic (dry-type) of macular degeneration. (Figure 1.12 B) (Brew and Nagase 2010)

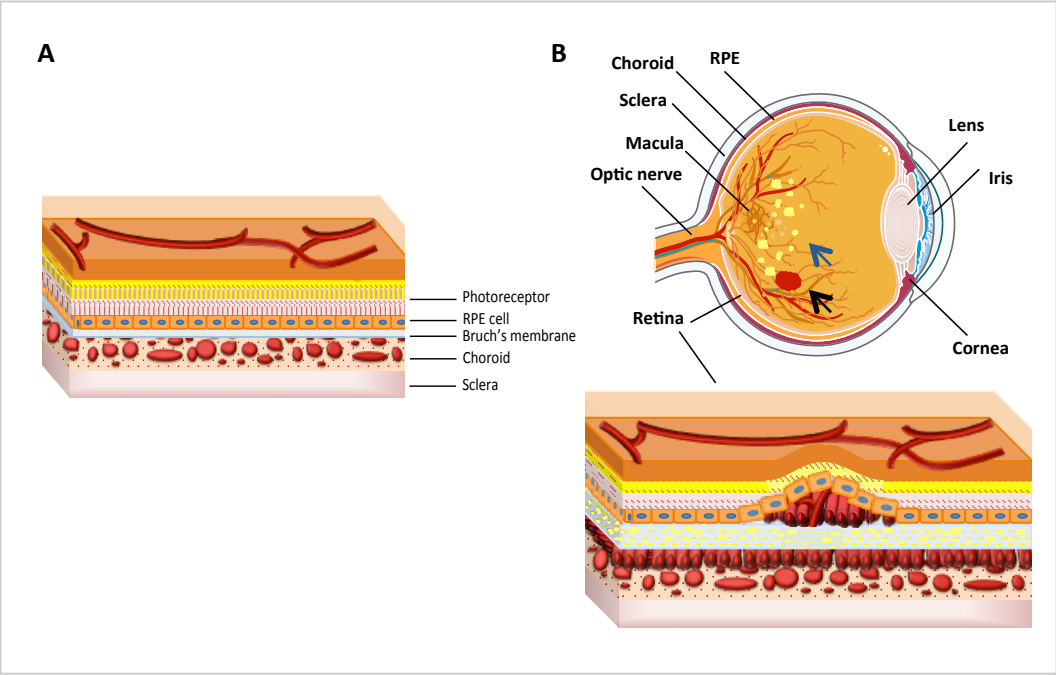

Figure 1.12: Structure of the retina and the SFD phenotype.

(A) Schematic diagram of normal human retina showing detailed layers. (B) Anatomy of SFD human retina demonstration drusen (navy arrow), choroidal neovascularisation, thickening in Bruch's membrane and Illustration of growing new blood vessels those disturb retinal layers resulting in haemorrhage (black arrow) and retinal detachment in later stage of SFD. The retina layers were drawn using Servier medical art website (available on http://www.servier.com/Powerpoint-image-bank).

1.5.2 SFD mutations

Currently, 15 different mutations have been shown to cause SFD. In the literature, these have largely been numbered by excluding the signal peptide sequence, however more recently described mutations have been numbered to include this causing some confusion. These are shown in Table 1.5 using both numbering methods to aid comparison. Figure 1.13 shows their position on the primary structure of TIMP3 excluding the signal sequence. Eleven of these mutations are missense mutations that change a residue to cysteine, with all except S15C (Figure 1.14) occurring in exon 5 that codes for most of the carboxyl-domain of TIMP3. Where examined, this additional cysteine has been shown to result in TIMP3 dimerisation. Moreover, there are two additional missense mutations in exon 5, E139K and H158R that do not change a residue to cysteine but do still result in TIMP3 dimerisation (Saihan *et al.* 2009, Mujamammi 2013), potentially by destabilising adjacent disulphide bonds. The nonsense mutation, E139X, results in deletion of most of the C-domain of TIMP3 but again results in TIMP3 dimerisation as a result of an unpaired cysteine residue (Langton *et al.* 2000). The other novel mutation is a splice site mutation that was discovered in two Japanese families by Tabata *et al.* (1998). Sequence analysis of the *TIMP3* gene revealed the presence of a single adenine insertion at the intron4/exon5 junction site that converts the acceptor site from CAG to CAAG. The effect of this mutation on TIMP3 mRNA or protein expression was not examined. While the consequence of such splice site mutations cannot be predicted, several possibilities were suggested by Li *et al.* (2005), encompassing exon skipping, intron retention and activation of a cryptic acceptor site (Figure 1.15). Although a splice site mutation can result in skipping of exons, in this case this is unlikely to yield a stable mRNA since exon 5 is the last exon of the *TIMP3* gene. Another possibility is that intron 4 retention could lead to expression of a mutant protein, possibly with an unpaired cysteine residue. Alternatively the activation of a cryptic acceptor site in exon 5 could also result in an abnormal protein, again with the possibility of aberrant disulphide bond formation.

Amongst different SFD families, the clinical presentation and age of onset vary depending on the type of mutation. For instance, individuals with the S156C mutation show symptoms in their third decade and have prominent neovascularisation in most affected individuals. In contrast the splice site mutation results in an exceptionally late onset form of SFD with a distinct phenotype including normal peripheral retina (Isashiki *et al.* 1999).

Table 1.5: List of identified TIMP3 mutations.

Mutation site (including signal peptide)	Age of SFD onset (decades)	Reference
S15C (S38C)	5	Schoenberger and Agarwal (2012)
Y128C (Y151C)	3	Gliem *et al.* (2015)
E139X (E162X)	3-4	Langton *et al.* (2000)
E139K (E162K)	5	Saihan *et al.* (2009)
Y154C (Y177C)	6	Gliem *et al.* (2015)
S156C (S179C)	2-3	Felbor *et al.* (1995)
H158R (H181R)	5-7	Lin *et al.* (2006)
Y159C (Y182C)	6	Fung *et al.* (2013)
G166C (G189C)	2-4	Felbor *et al.* (1997b)
G167C (G190C)	3-4	Jacobson *et al.* (1995)
Y168C (Y191C)	3-4	Felbor *et al.* (1996)
S170C (S193C)	4	Jacobson *et al.* (2002)
Y172C (Y195C)	**3-4**	Jacobson *et al.* (2002)
S181C (S204C)	**3-4**	Weber *et al.* (1994)
Intron4/Exon5 Splice site (CAG⇒CAAG)	**4-8**	Tabata *et al.* (1998)

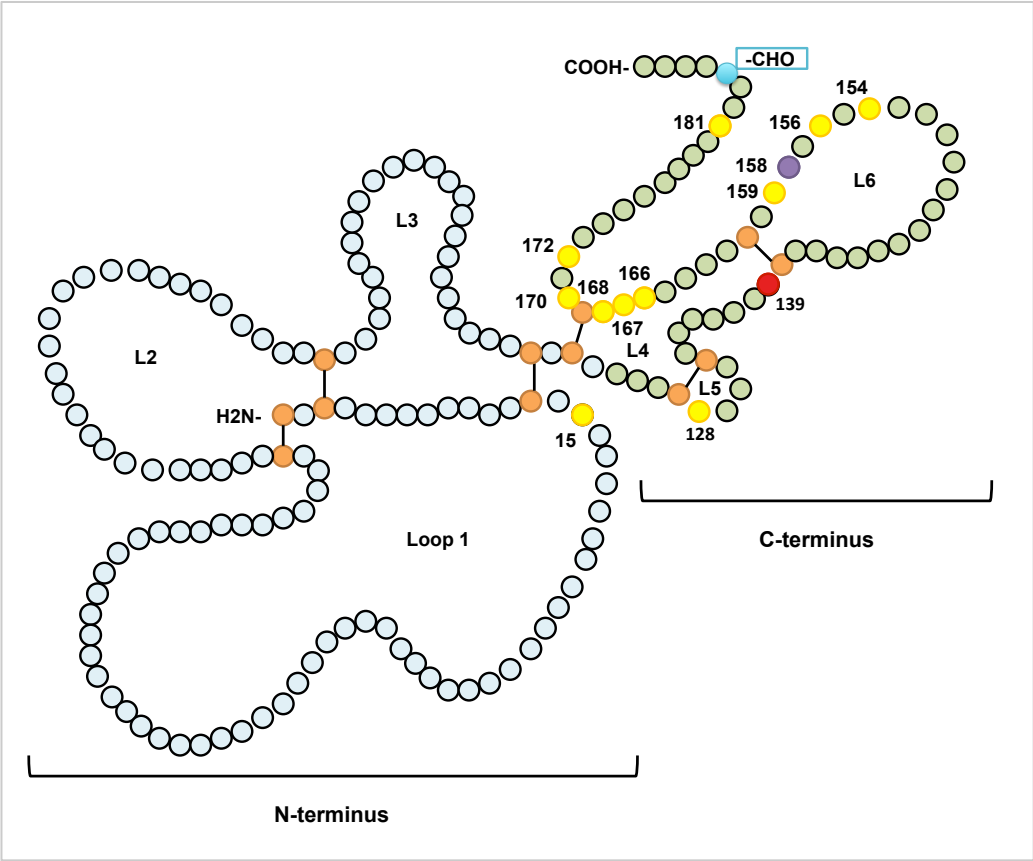

Figure 1.13: TIMP3 mutations shown to be responsible for SFD.

Yellow circles refer to those mutations changing to cysteine residues whereas the purple one refers to arginine. The red circle refers to the mutation changing to either lysine or premature stop codon.

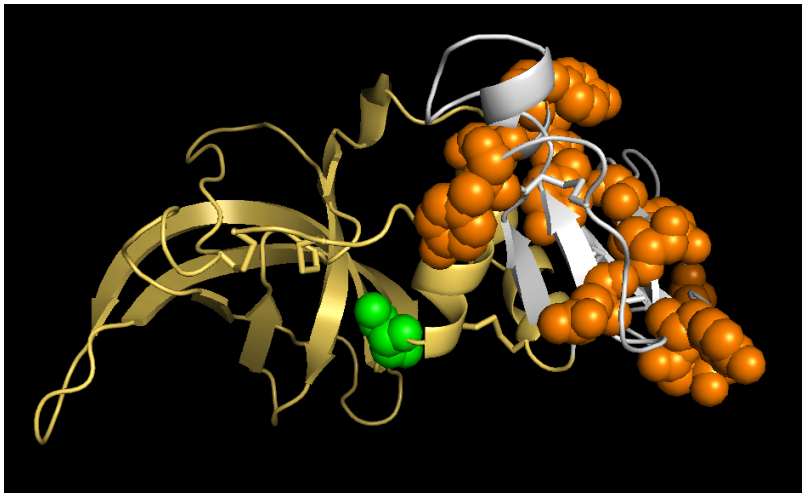

Figure 1.14: TIMP3 structure showing the position of the S15C mutation relative to all other SFD mutations.

The N-domain is coloured yellow and the C-domain grey with all known SFD mutations shown as orange spheres except for S15C, which is green. The TIMP3 structure was modelled using the Phyr2 Server (Kelley and Sternberg 2009) and then rendered using PyMol software.

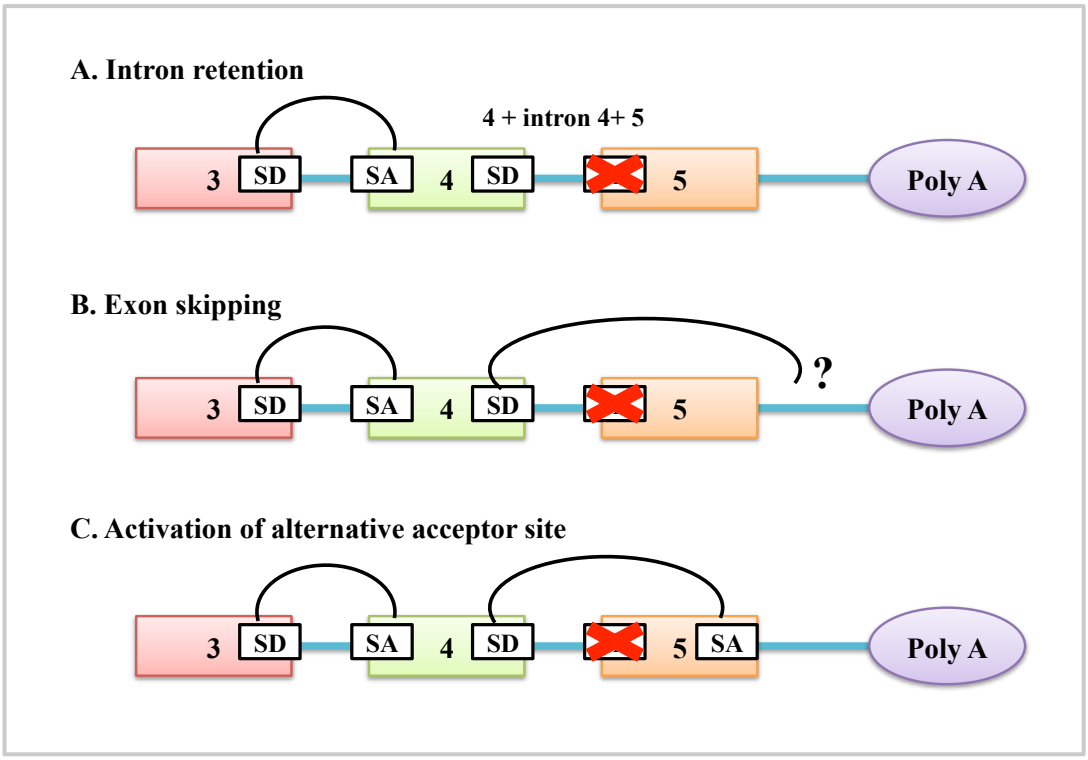

Figure 1.15: Possible effects of splice site mutation on TIMP3.

(A) Intron retention; (B) Exon Skipping; (C) Activation of cryptic acceptor site. SD: splice donor site and SA: splice acceptor site. The Red Cross refers to defective acceptor site.

1.5.3 Properties of SFD-TIMP3 protein

The biochemical properties of mutant TIMP3 protein, produced by different SFD mutations, have been studied by expression in various types of cell including the African green monkey kidney cell line (COS-7), baby hamster kidney cells (BHK) and the human RPE cell line (ARPE19). While the dimerisation of TIMP3 mentioned above was not reported in all cases, expression in RPE cells has always resulted in dimer formation, suggesting the different mutations all result in a common molecular phenotype and this would certainly explain the fact that the majority of mutations change a residue to cysteine.

Like most dominantly inherited diseases, it is believed that SFD is due to a toxic effect of the mutant protein rather than haploinsufficiency and this is supported by a number of reports. For instance, Langton and colleagues (1998) showed that mutant S181C-TIMP3 protein was expressed as a dimer that retained its ability to inhibit MMPs and still localise to the ECM.

Leco *et al.* (2001) showed that deletion of *TIMP3* in mice did not give rise to an SFD phenotype; conversely, these mice exhibited enlargement in the lungs due to an imbalance between MMPs and their inhibitors. However, *TIMP3* knock in mice carrying the S156C mutation developed abnormal changes in the Bruch's membrane similar to those in aged normal mice (Weber *et al.* 2002). Moreover the activity levels of ADAMTS4 and 5, TACE and aggrecan cleaving MMPs was unchanged in tissues from both heterozygous and homozygous S156C mice (Fogarasi *et al.* 2008), indicating S156C retains its ability to inhibit these enzymes. Additionally the same authors showed that recombinant S156C-TIMP3 had a comparable ability to inhibit the interaction between VEGFR2 and its ligand to the wild type molecule. However, it should be noted that the S156C-TIMP3 used in their experiments was expressed from bacteria and was monomeric and not dimeric as described in other studies. Furthermore, immunohistochemical analysis of eyes from an SFD patient with the S181C mutation showed an accumulation of TIMP3 in the retina, rather than its absence (Fariss *et al.* 1998) and this may be a result of SFD mutant TIMP3 dimers/multimers being resistant to turnover compared to the normal protein (Langton *et al.* 2005).

High level expression of TIMP3 has been shown to trigger apoptosis in RPE cells (Majid *et al.* 2002) with some evidence that SFD mutant TIMP3, including S156C, G167C, Y168C and S181C have an additional proapoptotic effect (Majid *et al.* 2002), and so accumulation of TIMP3 in SFD may play a role in choroidal and retinal atrophy by inducing apoptosis in these tissues.

While all the evidence indicates SFD is not due to haploinsufficiency, dominant mutations can also have what is termed a dominant negative or antimorphic effect. In this case the mutant protein has a toxic effect by having a deleterious effect on the wild-type protein expressed from the normal allele. However studies in mice indicate this is not the case in SFD as only the S156C/S156C homozygous mice have any detectable phenotype whereas the S156C/wild-type heterozygotes are asymptomatic (Weber *et al.* 2002).

1.6 Age-related macular degeneration (AMD)

Although SFD is extremely rare, its phenotype is very similar to the more severe (wet or exudative) form of age-related macular degeneration (AMD). AMD is a degenerative disease of the retina that affects older people and is the major cause of blindness in industrialised countries. In the UK alone over 500,000 people (2.4% of the population) were affected by this late stage form of the disease in 2012, and this is estimated to rise to approximately 700,000 cases by 2020 (Owen *et al.* 2012), which will have a significant impact on personal independence and the economy. As a result of the phenotypic similarities between SFD and AMD, it was suggested that TIMP3 might also play a role in the pathogenesis of AMD and this hypothesis was strengthened by the observation that the increased deposition of TIMP3 found in the eyes of SFD patients is also observed in the eyes of AMD patients (Kamei and Hollyfield 1999).

1.6.1 AMD clinical manifestations

Age-related macular degeneration is a chronic progressive retinal disorder and affects various retinal layers including the choroid, Bruch's membrane, RPE and photoreceptors; however, deregulation of metabolic processes in the RPE is considered to be the leading trigger of AMD due to the fact that these cells are responsible for synthesising all structural components of Bruch's membrane, particularly type-I and IV collagen, laminin and metalloproteinases and their natural tissue inhibitors.

AMD is associated with progressive visual impairment and occurs in two forms classified as dry or wet. Dry AMD is characterised by the formation of drusen, which are protein and lipid rich deposits under the retinal layers. A number of small drusen are considered part of the normal ageing process, however in dry AMD these increase in number and size and begin to affect central vision. Eventually these deposits result in atrophy of the RPE and photoreceptor layers (termed geographic atrophy) and can result in loss of central vision.

Approximately 15% of patients with dry AMD will go on to develop wet AMD, characterised by choroidal neovascularisation, haemorrhage, scarring and retinal detachment, which can result in sudden and severe loss of vision (Ferris *et al.* 2013, Nita *et al.* 2014, Saksens *et al.* 2014).

Despite these close similarities between SFD and AMD there are some pathological differences that distinguish SFD from AMD. In addition to dominant inheritance and age of onset, and these include differences in drusen composition, an early nyctalopia (poor night vision) and, in some cases, impaired peripheral vision (Gourier and Chong 2015).

1.6.2 Genetic studies and TIMP3 in AMD

Genetically, whilst SFD is a single gene disorder caused by mutations in *TIMP3*, AMD is considered to be a multi-factorial disease with both environmental and genetic risk factors and is not caused by changes to the coding sequence of *TIMP3* (Felbor *et al.* 1997a).

The strongest genetic risk factor found to be associated with AMD is a polymorphism (rs1061170) converting tyrosine-402 to histidine-402 in the gene that encodes complement factor H (CFH). The risk of developing AMD increases approximately 2.5 fold with one histidine at this position and up to 6 fold when histidine is present in both alleles in individuals of European decent (Edwards *et al.* 2005, Haines *et al.* 2005, Zareparsi *et al.* 2005). Complement factor H is an important regulator of the alternative pathway of complement and these data implicate complement activation as a key factor in AMD pathogenesis.

Despite the fact that high concentrations of TIMP3 are seen in the retina of both AMD and SFD patients (Fariss *et al.* 1998, Kamei and Hollyfield 1999), two genetic studies in 1997 failed to find a connection between *TIMP3* and AMD (De La Paz *et al.* 1997, Edwards *et al.* 2005). However more recently Kaur *et al.* (2010) reported the presence of strong association between two *TIMP3* intronic SNPs encompassing rs713685 and rs743751 and AMD, although the consequences, if any, on TIMP3 protein expression are unknown.

However the increased TIMP3 protein expression described in AMD is not associated with increased mRNA expression (Bailey *et al.* 2001) and could therefore be associated with a decreased turnover of TIMP3 as observed in SFD. This hypothesis was supported by examination of drusen from normal and AMD retinas by Crabb *et al.* (2002) who observed the presence of apparently cross-linked TIMP3 as a consequence of oxidative reactions.

Cross-linked TIMP3, either as a result of mutation or oxidation could, for example, have an increased avidity for TACE resulting in decrease shedding of death receptors and increased apoptosis.

An additional possibility is that TIMP3 cross-linking occurs as a result of advanced glycation end product (AGE) formation, a process that increases with age (Glenn and Stitt 2009). AGE products bind to pattern recognition receptors such as RAGE (receptor for AGE), which upon activation play a critical part in several inflammatory/degenerative diseases (Chuah *et al.* 2013). It is possible that the toxicity of SFD-TIMP3 might result from the fact that it also behaves as a RAGE ligand.

1.6.3 Advanced glycation end products (AGEs) and their receptor (RAGE)

Increased modification of lipids, DNA and free amino groups on proteins, is considered to be related to the ageing process. AGEs can be formed from a non-enzymatic reaction between reducing sugars or dicarbonyls and primary amino groups on proteins. (Glenn and Stitt 2009)

AGEs have been implicated as playing a role in several diseases, including Alzheimer's disease, and in diabetic complications where the high glucose levels result in increased AGE formation. The best-characterised AGE receptor is RAGE.

1.6.3.1 RAGE

The receptor of advanced glycation end products (RAGE) was firstly described as a binding partner of AGEs found on the surface of endothelial cells (Neeper *et al.* 1992, Schmidt *et al.* 1992). RAGE is a pattern recognition receptor that binds to a wide range of ligands including AGEs, S100 proteins, amyloid, β2-integrin-Mac-1, high mobility group box protein 1 and amophoterin (Chavakis *et al.* 2003, Hofmann *et al.* 1999, Taniguchi *et al.* 2003). The ligand-receptor binding initiates downstream pro-inflammatory signalling pathways involved in several illnesses including viral infection, Alzheimer disease, diabetic complications and cancer (Liliensiek *et al.* 2004, Sasahira *et al.* 2005, Wendt *et al.* 2003, van Zoelen *et al.* 2009). Activation of RAGE has also been shown to increase VEGF production by RPE cells (Ma *et al.* 2007).

1.6.3.1.1 RAGE structure

The human gene for RAGE is situated on chromosome 6 in the major histocompatibility complex class III region. The gene encompasses 11 exons encoding a 404 amino acid protein with a molecular weight between 45 and 55kDa depending on glycosylation. The expression of RAGE is detected in a variety of cell types such as endothelium, neural tissue, smooth muscle cells and cardiac myocytes; and tissue including kidney, heart, brain and liver (Brett *et al.* 1993). Structurally, RAGE is a member of the immunoglobulin superfamily that comprises a signal peptide at the amino-terminus, a variable-type immunoglobulin-like domain, two tandem constant-type immunoglobulin-like domains, a trans-membrane domain and an intracellular cytoplasmic tail (Neeper *et al.* 1992) (Figure 1.16).

Xie *et al.* (2008) showed that RAGE is present on the cell surface in oligomer form enabling recognition of multimeric AGE-modified proteins and more recently a study by Zong *et al.* (2010) demonstrated that RAGE-ligands such as AGEs and S100B initiated a process in which RAGE molecules form homodimers at the plasma membrane through their V-domain at the amino-terminus.

1.6.3.1.2 RAGE Activation

RAGE activation is achieved through ligand-receptor interaction in which most RAGE ligands, such as S100B and amyloid-β, are functional and have higher affinity in oligomer forms (Chaney *et al.* 2005, Ostendorp *et al.* 2007) (Figure 1.16A). This ligand-receptor binding results in phosphorylation of several transduction cascades such as phosphatidylinositol 3-kinase, mitogen-activated protein kinases (MAPK), Rac-1 and Cdc42, Jak/STAT (Janus kinase/signal transducer and activators of transcription) and the NF-κB pathway (Chuong *et al.* 2009, Hermani *et al.* 2006, Huttunen *et al.* 1999, Lander *et al.* 1997, Yeh *et al.* 2001, Wang *et al.* 2008). These pathways implicated RAGE in several cellular responses for instance migration, apoptosis, mobility, cancer and pro-inflammatory gene expression (Yan *et al.* 2009).

At least five alternatively spliced soluble variants of RAGE exist (sRAGE) that lack the transmembrane domain and these are thought to act as antagonists of the receptor. Chuong *et al.* (2009) demonstrated that the extracellular domain of RAGE inhibited nuclear translocation of NF-κB (p65 and p52) by S100A4 in human salivary gland cell lines. Moreover, when HEK293T cells were incubated primarily with soluble RAGE or RAGE-V-domain peptide prior to S100B treatment, RAGE dimerisation in response to S100B and the

following MAPK phosphorylation and NF-κB activation were inhibited (Zong *et al.* 2010) (Figure 1.16B).

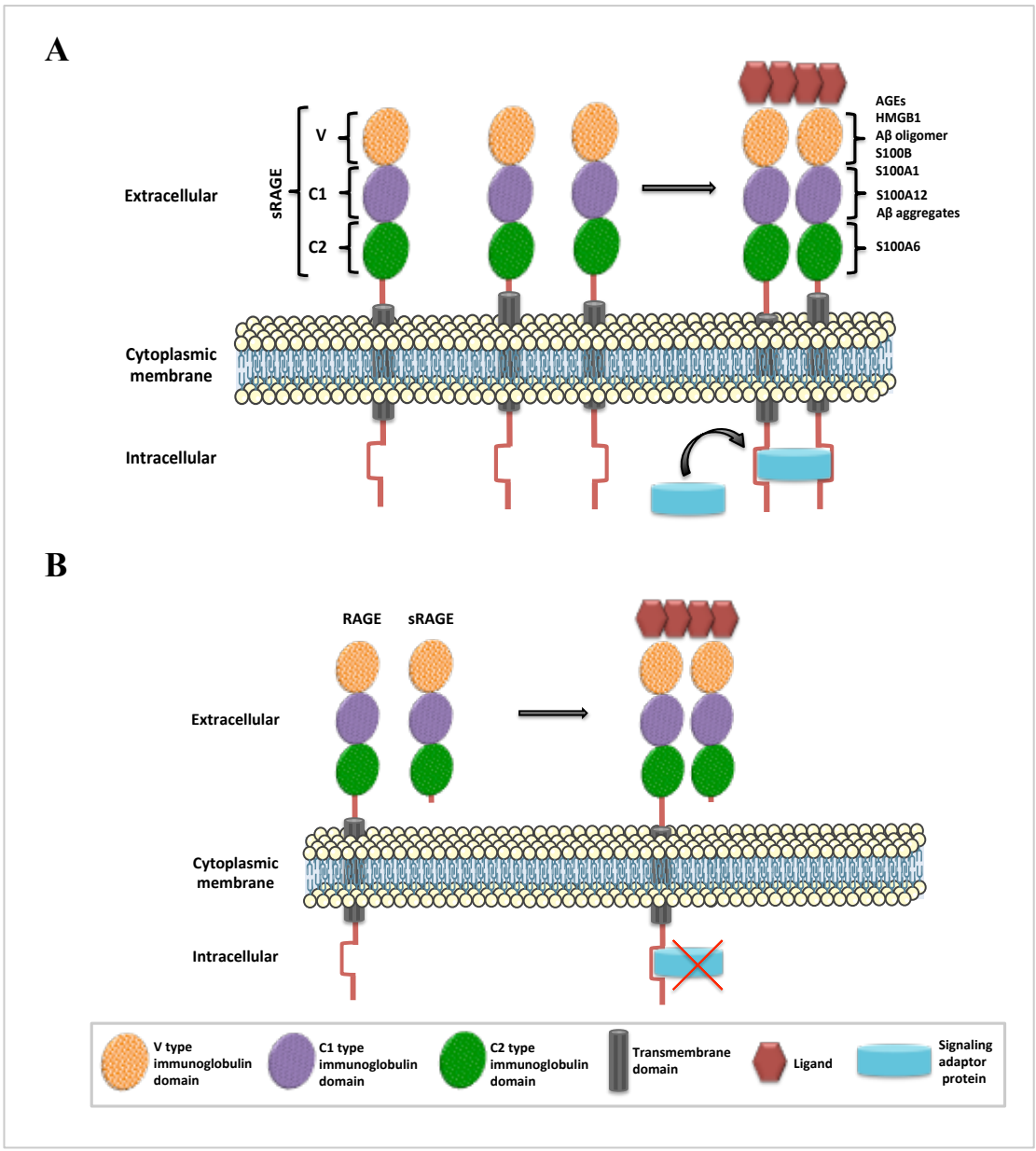

Figure 1.16: Schematic representation of AGE receptor.

(A) A model of RAGE activation by binding to its dimeric/oligomer ligands: RAGE-ligand binding stabilises RAGE-dimer enabling interaction with a signalling adaptor protein through the cytoplasmic region of the receptor and activating signal transductions. (B) A model of RAGE inhibition by sRAGE: RAGE binds to sRAGE that blocks the subsequent signal transduction. (Koch et al. 2010, Leclerc et al. 2007)

1.7 Malattia Leventinese

Malattia Leventinese (ML) is another rare autosomal dominantly inherited degenerative disease of the macula with an early onset. In contrast to SFD, ML is phenotypically much more similar to dry AMD with CNV being less common. The disease is characterised by a distinctive mosaic pattern of drusen, giving it the alternative name of Doyne's honeycomb retinal dystrophy (Querques *et al.* 2013). ML is caused by a missense mutation in exon 10 of epithelial growth factor-containing fibulin-like extracellular matrix protein 1 (EFEMP1) gene (also known as fibulin-3) converting an arginine at position 345 to tryptophan (R345W) (Zhang and Marmorstein 2010, Takeuchi *et al.* 2010, Zhang *et al.* 2014).

The gene of *EFEMP1* is situated on chromosome 2 and contains 11 exons that encoded a protein sequence with a molecular weight of 55kDa. The 493 amino acid protein encompasses signal peptide, a calcium binding epidermal growth factor (cbEGF) domain with a peptide insertion, five tandem unmodified cbEGF domains and a C-terminal fibulin domain (Figure 1.17) (Zhang and Marmorstein 2010).

Although EFEMP1 is widely expressed by endothelial and epithelial cells and in the brain, placenta, heart and eye (Timpl *et al.* 2003), its biological function is poorly understood. The *EFEMP1* sequence is highly conserved in mammals and expressed in bone and cartilage structures throughout development, suggesting a conserved fibulin-3 role in the skeletal system in vertebrates (Ehlermann *et al.* 2003).

Fibulin-3 is homologous to fibulin-5 that plays a significant role in regulating proliferation, invasion and migration of healthy and cancer cell lines. Like fibulin-5, fibulin-3 is also expressed in endothelial cells with its expression affecting their response to VEGF by inhibiting invasion, proliferation and angiogenic sprouting, inhibiting the expression and activity of metalloproteinases and stimulating the expression of tissue inhibitor of metalloproteinases. Fibulin-3 had the capacity to decrease tumour angiogenesis and growth (Albig *et al.* 2006). Recently, Lin *et al.* (2016) observed a reduction in MMP-2 and MMP-9 and oxidative stress in hypertensive vascular remodelling as a consequence of fibulin-3 and suggested that up-regulation of fibulin-3 might improve vascular health and thus decrease certain cardiovascular risk factors.

McLaughlin *et al.* (2007) found that mice lacking the EFEMP1 gene displayed decreased reproduction and early onset of ageing; however, these mice had no macular degeneration phenotype. This study indicates that the loss of EFEMP1 is not implicated in the pathological mechanism of mutant EFEMP1.

Marmorstein *et al.* (2002) demonstrated that the wild type EFEMP1 gene encodes a secreted protein (55 kDa) whereas mutant EFEMP1 encodes a poorly secreted misfolded protein that is also retained within the cells. ML mutant EFEMP1 protein accumulates in the RPE and between both the RPE and drusen. However, AMD eyes have also been found to contain accumulated EFEMP1 particularly overlying drusen formation. For this reason, it was concluded that the misfolding and accumulation of EFEMP1 might have a crucial part in the disease process of ML and AMD. Interestingly, EFEMP1 protein strongly binds to the C-terminal domain of TIMP3. Significantly, this finding was supported by examinations of ML and AMD eyes, which identified accumulation and overlapping expression of TIMP3 and EFEMP1 (Klenotic *et al.* 2004). Fu *et al.* (2007) showed co-localised deposits of EFEMP1 and TIMP3 between Bruch's membrane and the RPE in Efempl-R345W mice and, there was also evidence of complement activation at this site.

More recently, in addition to binding TIMP3, EFEMP1 has also been shown to be a binding partner for complement factor H (CFH) and colocalisation of CFH and fibulin-3 was observed in soft drusen from an AMD patient with the homozygous CFH polymorphism (Y402H) (Wyatt *et al.* 2013). This suggests that the interaction between TIMP3, EFEMP1 and CFH could contribute to the aetiology of SFD, ML and AMD.

Roybal *et al.* (2005) found that mutant EFEMP1 accumulated in the endoplasmic reticulum (ER) of ARPE19 cells. This accumulation resulted in activation of the unfolded protein response (UPR) signalling, elevation in VEGF expression and transcriptional stimulation of the VEGF promoter. Since the expression of ML mutant EFEMP1 cause ER stress and subsequently leads to RPE dysfunction and elevates the expressed VEGF, it may account for macular degeneration and choroidal neovascularisation (CNV).

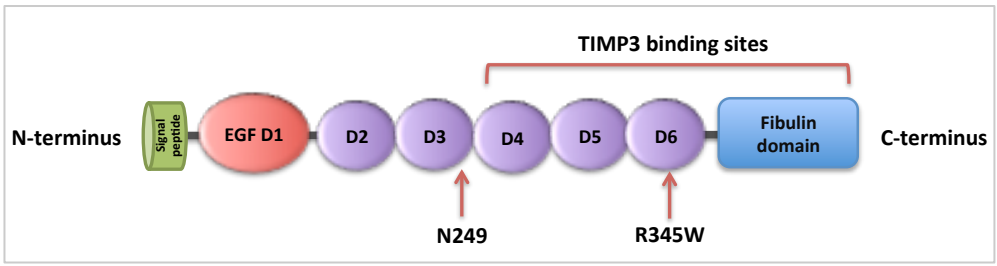

Figure 1.17: Domain structure of EFEMP1.

Demonstration of domain organisation of EFEMP1 as reviewed by Hulleman and Kelly (2015) & Zhang and Marmorstein (2010). The carboxyl-terminus of EFEMP1 (259-493) interacts with the carboxyl-terminus of TIMP3 particularly amino acid sequence between 105 and 188 (Klenotic et al. 2004). N249: N-glycosylation site at 249; R345W: a missense mutation at 345 converting arginine to tryptophan.

1.8 Therapeutic treatments for retinopathies

Treatment options for most retinopathies are limited and, at best, slow progression of the disease, rather than improve it. Nevertheless newer treatments, particularly the relatively recent availability of anti-VEGF therapies to treat CNV, have significantly improved the prognosis for patients with neovascular complications. Additionally the prospect for using gene therapy approaches to treat monogenetic disorders has greatly improved in recent years, and the retina, with its accessibility and immune-privileged status is one of the most promising targets for such treatments. Current and prospective treatment options will be considered in more detail in the following sections.

1.8.1 AMD treatments

As age-related macular degeneration is the leading cause of irreversible loss of vision in western countries, many medical therapies have been established including photodynamic therapy for subfoveal choroidal neovascularisation (CNV), argon laser photocoagulation of extrafoveal CNV, anti-vascular endothelial growth factor (anti-VEGF) agents, transpupillary thermotherapy, radiotherapy, surgery and dietary supplementation (Bylsma and Guymer 2005).

Newer AMD therapeutic approaches have attempted to target drusen formation and delay the occurrence of choroidal neovascularisation. AMD patients with multiple large soft drusen are at higher risk of developing serious AMD complications that can be prevented by reducing drusen with prophylactic laser treatment or targeting proteins involved in drusen formation. Drusen formation has been linked to inflammatory responses leading to up-regulating proteins such as toll-like receptor 4, apolipoprotein (APOE) and complement factors B, C3 and H (Crabb 2014). Amyloid β also localises within drusen and may play a role in their formation (Dentchev *et al.* 2003, Johnson *et al.* 2002). In a murine AMD model, amyloid β was detected in neovascular lesion and subretinal deposits and treatment with anti-amyloid β was shown to provide visual protection and prevent histopathological changes mimicking AMD (Ding *et al.* 2011).

Extensive evidence has demonstrated that VEGF plays a crucial role in neovascularisation of AMD and other eye diseases. Untreated neovascularisation can result in rapid vision loss, therefore VEGF has become a key target in the treatment of ocular neovascularisation.

Currently neovascular AMD is treated by intravitreal injection of either bevacizumab (trade name Avastin) or ranibizumab (trade name Lucentis), which are a humanised monoclonal antibody and a fragment of antibody, respectively, against VEGF. Bevacizumab was originally licenced for cancer treatment and ranibizumab for AMD. However, as the cost of bevacizumab is much lower than that of ranibizumab per patient, a number of clinical trails have compared the two drugs for AMD treatment and these have found comparable efficacy and safety between bevacizumab and ranibizumab for treatment of neovascular AMD (Solomon *et al.* 2016). Other studies have also shown that a regular monthly treatment with these drugs gives better results on visual acuity than as needed treatment (Chakravarthy *et al.* 2013).

In addition to targeting VEGF, Fovista is a novel new treatment for neovascular AMD that targets platelet-derived growth factor (anti-PDGF). PDGF receptors are highly expressed on pericytes. Pericytes are contractile cells that surround endothelial cells and play a critical role in angiogenesis and stabilisation of newly formed vessels. Fovista is being investigated in combination with anti-VEGF therapy such as ranibizumab. In phase two trails, Fovista and ranibizumab combination therapy showed superior efficacy in vision gain relative to ranibizumab alone (Cheung and Wong 2013, Jaffe *et al.* 2016).

While anti-VEGF therapies have proved very successful in treating CNV in wet AMD, they do not prevent the retinal atrophy that underlies dry AMD, and which affects many more patients. For this reason a number of alternative treatment modalities are being explored including anti-inflammatory agents, such as those targeting complement components (Yehoshua *et al.* 2014), and agents that target lipofuscin (Mata *et al.* 2013), or amyloid-β (Parsons *et al.* 2015). Oxidative stress, which is implicated in RPE damage, has also been targeted in a therapeutic/preventative approach by, for example, dietary supplementation (Chew *et al.* 2013).

1.8.2 SFD treatment

Although SFD is an inherited disorder, a few therapeutic approaches have been used help alleviate symptoms. The increased thickness in Bruch's membrane functions as a barrier decreasing transportation of nutrients, waste products and blood between choroid, RPE and photoreceptors. As a consequence of this impaired nutrient transport, some individuals affected with SFD have nyctalopia in the early stage of the disease that may result from severe deficiency in vitamin A level in the photoreceptors. Night blindness disappeared

within one week of high-dosage vitamin A treatment (oral administration) leading to improvements in photoreceptor function (Jacobson *et al.* 1995). However, treatment with high-dosage of vitamin A can also have harmful effect in the retina and other tissue and hence it has not become widely used.

Based on their success in AMD patients, most therapeutic interventions in SFD target the haemorrhage and neovascularisation that is a hallmark of the disease. Wong *et al.* (2003) reported that choroidal neovascularisation (CNV) in S181C-SFD patients is treatable by photodynamic therapy (PDT) and verteporfin. In contrast, Sivaprasad *et al.* (2008) found that argon laser therapy and PDT did not effectively treat CNV from S181C-SFD patients. Prager *et al.* (2007) demonstrated that systemic bevacizumab, anti-VEGF therapy, is an effective treatment for secondary CNV in SFD. Similarly intravitreal ranibizumab has proved very beneficial in treating CNV associated with SFD (Balaskas *et al.* 2013). However, treatments directed at CNV do not address the underlying atrophy and thus are only likely to delay loss of vision.

1.8.3 Malattia Leventinese treatment

Reported treatment for Malattia Leventinese is limited to those patients who develop CNV. Dantas *et al.* (2002) reported successful treatment of a 39-year-old Malattia Leventinese patient who developed choroidal neovascularisation with photodynamic therapy with verteporfin. More recently, bevacizumab has also been reported to have some efficacy in treating CNV in ML (Sohn *et al.* 2011).

1.8.4 Transplantation of retinal pigment epithelium

Changes in the RPE are thought to initiate the disease process in AMD and other retinopathies, such as SFD. Moreover these cells are essential for maintaining the photoreceptors, so that loss of the RPE inevitably results in atrophy of the photoreceptor layers. For this reason replacement of RPE should prevent degeneration of photoreceptors and subsequently restore visual function in these retinopathies. These cells are also attractive due to the fact that they are well studied, form a simple monolayer and can readily be grown and expanded in culture.

A number of approaches have been tested, including macular translocation (where the central photoreceptor layer is moved onto an area of healthy RPE), transplantation of RPE cells alone

or transplantation of a patch of RPE including Bruch's membrane and partial thickness choroid from a peripheral site to the macula. However, none of these techniques have proven as successful as initial animal experiments might have indicated, with various degrees of post-operative complications and RPE cell only transfers failing due to an inability of RPE cells to adhere to unhealthy Bruch's membrane (Alexander *et al.* 2015).

1.8.4.1 Stem cells transplantation

A more recent approach to restoring RPE function and preventing photoreceptor death is to use stem cells. Both human induced pluripotent stem cells (iPSCs) and human embryonic stem cells (hESCs) are capable of differentiating into RPE cells (Buchholz *et al.* 2009, Cho *et al.* 2012) and these are beginning to show promise in the clinic.

Schwartz *et al.* (2016), for example, reported findings of two studies at phase I/II trial involving 18 patients affected with AMD and Stargardt disease who underwent subretinal transplantation of hESCs-RPE. The results at 4 years follow up of the anatomical and functional level were encouraging as ≥ 50% of patient showed increased visual acuity, evidence suggesting potential cellular engraftment and no observation of adverse effect related to the cell therapy.

1.8.5 Gene therapy in retinal diseases

Clearly the ideal treatment for hereditary retinopathies would be to replace the defective gene itself, before irreversible damage occurs. While gene therapy has not generally lived up to early promise, treatment of retinopathies is one area where it has shown some success. This is largely because the eye possesses several unique characteristics that favour this approach. Primarily it comprises a small target that is readily accessible for gene delivery and subsequent *in vivo* assessment. It is also an immune-privileged tissue, making rejection of delivery vectors less likely. Additionally there are also a number of genetically well-defined animal models. Thus, retinal gene therapy has the potential to become a key therapeutic tool in treating inherited forms of blindness. (Alexander *et al.* 2007, Bennett *et al.* 2012, Borras 2003, Chaum and Hatton 2002, Naik *et al.* 2009)

After initial success in animal models, a number of clinical trials are now in progress for treating recessive retinal disorders. Probably the most advanced of these is for Leber's congenital amaurosis (LCA), caused by mutation in retinal pigment epithelium-specific 65-

kDa (RPE65) gene affecting the visual retinoid cycle, with early results demonstrating safety and some efficacy (Jacobson *et al.* 2012).

Treating recessive retinal disorders, such as LCA, simply requires transduction with a normal copy of the defective gene. However, treatment of dominantly inherited disorders, such as SFD, would be much more complex as it would require effective suppression of the toxic gene (by for example short interfering RNA - siRNA) without targeting the normal allele which is, at best, likely to be very difficult. Moreover even if it were possible, many dominant retinal diseases, such as SFD, can be caused by many different mutations, which would require a novel therapy for each one, making it a prohibitively expensive approach for treating rare disorders. One way this can be circumvented is to use an siRNA molecule to target all copies of the target gene, but then supplement the missing gene with a cDNA that is not susceptible to the siRNA molecule. This has now been successfully achieved in an animal model of autosomal dominant retinitis pigmentosa, which can be caused by over 150 different mutations in the rhodopsin gene (Millington-Ward *et al.* 2011).

While RNA interference is not a very efficient process and rarely results in complete suppression of the target mRNA in mammalian cells, gene editing using recent CRISPR/Cas9 (clustered regularly interspaced short palindromic repeat (CRISPR)-associated Cas9 nuclease technology - reviewed in Savic and Schwank (2016) is an extremely efficient method for deleting target genes, making treatment of dominantly inherited retinal disorders a much more likely prospect.

Gene therapy trials are not, however, limited to treating inherited retinopathies as gene therapy is also being explored as a way of delivering therapeutic molecules in AMD. This is intended to enable long-term drug delivery without the need for frequent and unpleasant intravitreal injections. For example an adeno-associated viral (AAV) vector is being used to deliver cDNA encoding soluble Fms- related tyrosine kinase-1 (sFLT-1), a naturally occurring inhibitor of VEGF (Rakoczy *et al.* 2015).

1.9 Project hypotheses and aims

The hypotheses of this project are:

1. that all TIMP3 mutations found in Sorsby's fundus dystrophy result in TIMP3 dimerisation
2. these TIMP3 dimers have a toxic effect on cells and trigger similar responses to those seen in age-related macular degeneration

The initial aim of the project is to confirm that the intron 4/exon 5 splice site mutation, N-domain mutation (Ser15Cys) and the newly identified C-domain mutations (Tyr128Cys, Tyr154Cys, Tyr159Cys), also result in TIMP3 multimerisation, which would provide overwhelming evidence that this is indeed the causative agent of the disease.

If this is the case, we then aim to examine the effect of mutant forms of TIMP3 on apoptosis, inflammation and choroidal neovascularisation, which are hallmarks of both SFD and wet age-related macular degeneration. We also aim to examine the effects of SFD mutations on the known interaction between TIMP3 and EFEMP1 as both molecules play a role in inherited retinopathies and have also been shown to accumulate in Bruch's membrane in age-related macular degeneration.

How the aims will be addressed

Dimerisation will be examined by expressing SFD TIMP3 cDNA constructs in retinal pigment epithelial cells followed by western blotting. However for the splice site mutation this will necessitate creating a synthetic TIMP3 gene construct that includes intron 4 and the whole of exon 5 and then examining the sequence of the mRNA products produced.

While very high level expression of TIMP3 and SFD TIMP3 have been reported to trigger ***apoptosis*** in a variety of cell types, we will determine whether mutant TIMP3 expressed *in situ* in the ECM increases the sensitivity of RPE cells to proapoptotic ligands by measuring casepase3/7 activation. We also aim to determine whether TIMP3 dimerisation alters its interaction with TACE, which is thought to play a role in TIMP3 mediated apoptosis by shedding death receptors. The ability of SFD mutants to bind to TACE will be determined by co-expression in HEK293T cells and then using a pull down assay, followed by western blotting.

The effect of TIMP3 mutation on ***EFEMP1 binding*** will also be investigated by pull-down assay in the same way.

TIMP3 potently inhibits ***angiogenesis*** through its ability to target VEGFR2. However, despite the fact that high levels of TIMP3 are found in both SFD and AMD eyes, angiogenesis is a hallmark of both diseases. We will examine the ability of vascular endothelial cells to invade through ECM containing either mutant or wild-type TIMP3 to determine if mutant TIMP3 is a less potent inhibitor of this process.

Inflammation plays an important role in AMD and this is also almost certainly the case for SFD. One way this is mediated in AMD is through activation of RAGE, which binds a number of products known to accumulate in Bruch's with age. As RAGE is a pattern recognition receptor, it is possible that TIMP3 dimerisation/multimerisation converts it into a RAGE ligand. We will assess the effect of mutant TIMP3 on RAGE mediated inflammation using an NFκB reporter assay.

Chapter 2: General materials and methods

2.1 Materials

2.1.1 General chemicals

All general chemicals were purchased from Sigma-Aldrich apart from those listed in the table below:

Chemicals	Catalogue number	Supplier
Acetic acid (glacial, 100%)	1000632500	Merck KGaA
Amersham Hyperfilm ECL 5x7''	28906835	GE Healthcare
Ammonium persulfate (APS)	17-1311-01	PlusOne
5-bromo-4-chloro-3-indolyl-β-D-galactoside (X-gal)	MB1001	Melford
Bromophenol blue water soluble	IC15250650	BDH
CAPS (transfer buffer)	BP321-500	Fisher BioReagents
Coomassie brilliant blue (R-250)	6104-59-2	Fisher BioReagents
Diethylpyrocarbonate (DEPC)	97062-650	BDH
Ethanol (96% vol)	BDH1158-4LP	BDH
Ethylenediaminetetraacetic acid (EDTA)	BDH9232-500G	BDH
Glycerol	G33-1	Fisher Scientific
Green cell tracker	C2925	Invitrogen
Hydrochloric acid (HCL)	15242380	Fisher Scientific
Hyper ladder ™ I	BIO-33053	Bioline Laboratory
IPTG	MB1008	Melford
Isopropanol (Propan-2-ol)	A416-1	Fisher Scientific
LB Agar High Salt Granulated	GL1706	Melford
LB Broth High Salt Granulated	GL1704	Melford
LIVE/DEAD® Fixable Blue Dead Cell Stain Kit, for UV excitation	L23105	Thermo Scientific
Methanol	BDH1135-4LP	BDH
TransBlot Turbo ™ Mini-size Nitrocellulose	1704158	Bio-Rad

Trypan Blue Dye	1450021	Bio-Rad
Novex Sharp Pre-Stained Protein Standard	LC5800	Fisher Scientific
Paper Developer	1757855	Ilford Multigrade
Phosphate buffered saline	BR0014	Oxoid
Precision Plus Protein ™ Dual Color Standard	1610374	Bio-Rad
Protease Inhibitor Cocktail Tablets	04693116001	Roche
PVDF Transfer Membrane, 0.45µm	88518	Thermo Scientific
Resolving Gel Buffer	1610798	Bio-Rad
Semi-skimmed Milk	-	Tesco
10% SDS Solution	1610416	Bio-Rad
Sodium acetate (NaAc) anhydrous	S2889	Sigma Aldrich
Sodium chloride (NaCl)	S0520	Melford
Gibco® Sodium pyruvate	11360070	Thermo Scientific
Stacking Gel Buffer	1610799	Bio-Rad
TransIT-LT1 Transfection Reagent	MIR 2300	Mirus
Tris-base	BP152-500	Fisher BioReagent
10X TRIS/GLYCINE/SDS (running buffer)	EC-870	Flowgen Bioscience
Triton® X-100	BP151-500	Fisher Scientific
Tween® 20	BP337-500	Fisher Scientific

2.1.2 Disposable labware

Labware	Supplier
0.2µm sterile filters	PALL, Life Science
0.2ml Single Thin Wall Tube	STAR LAB
7ml Bijou Container	STAR LAB
Carbon steel surgical blades	Swann-Morton Limited

Cell scraper 25cm	SARSTEDT
Chromatography paper, grade 3mm	WhatmanTM
Cryovials (Micro tube 2ml)	SARSTEDT
Detoxi-gel ™ Endotoxin Removing Columns, 5 x 1 ml	Thermo Scientific
Fluoroblock inserts	Falcon
96 well plate (black wall & clear bottom) and their lid	Greiner bio-one
Microfuge tubes (500, 1500 and 2000 µl)	Greiner bio-one
Corning® 96 well plates, opaque bottom	Sigma-Aldrich
Petri dishes (100mm)	Sterilin
Pipetting tips (20, 200 and 100µl)	STAR LAB
Sterile multi-well plates (6, 12, 24 and 96)	Costar
Sterile plastic pipettes (1, 5, 10 and 25 ml)	Costar
Sterile syringes (1, 5 and 10 ml)	BD Plastipak
Sterile tubes (15, 20 and 50 ml)	SARSTEDT
Tissue culture flasks (T25, T75 and T175)	Thermo
Tissue culture plates (60mm and 100mm)	Thermo

2.1.3 Antibiotics

Bacterial culture		**Mammalian tissue culture**	
Antibiotic	**Supplier**	**Antibiotic**	**Supplier**
Carbenicillin	Melford	Hygromycin B	Sigma-Aldrich
Kanamycin	Sigma-Aldrich	Geneticin	Gibco
-	-	Potassium Penicillin/Streptomycin Sulphate (P/S)	Gibco

2.1.4 Antibodies and recombinant protein

Antibody	Catalogue number	Supplier
Anti-Fas (human, activating) Monoclonal Antibody	05-201	Millipore
Anti-Tissue Inhibitor of Metalloproteinase-3, First Loop antibody produced in Rabbit	T7687	Sigma-Aldrich
Anti-TIMP3 antibody produced in Rabbit	SAB4502973	Sigma-Aldrich
Anti-V5 Mouse Monoclonal Antibody	R96025	Novex
PE Mouse Anti-Human CD309 (VEGFR-2)	560872	BD Pharmingen
PE Mouse IgG1, K Isotype Control	554680	BD Pharmingen
Polyclonal Swine Anti-Rabbit Immunoglobulins/HRP	P0399	DakoCytomation
Polyclonal Goat Anti-Mouse Immunoglobulins/HRP	P0447	DakoCytomation
TACE (D22H4) Rabbit Monoclonal Antibody	6978S	Cell signalling
TIMP3 (D74B10) Rabbit Monoclonal Antibody	5673S	Cell signalling
RAGE Rabbit Monoclonal Antibody	6697S	Cell signalling
Recombinant protein	**Catalogue number**	**Supplier**
Recombinant human TIMP3 (rhTIMP3)	973-TM-010	R&D System
Recombinant human vascular endothelial growth factor 165 (VEGF165)	100-20	Peprotech
S100B protein from bovine brain	S6677	Sigma-Aldrich

2.1.5 Cells and culture growth media

Cells	Growth Media	Supplier
α-Selected competent cells	-	Bioline
ARPE19 cells	DMEM:F12	ATCC
COS-7 cells	DMEM	ATCC
HEK293T cells	DMEM	ATCC
HUVEC	EBM2	Lonza
All mammalian cell culture growth media were ordered from Lonza.		

2.1.6 Enzymes

Enzyme	Catalogue number	Supplier
BamHI	R0136S	NEB
EcoRI	R0101S	NEB
EcoRV	R0195S	NEB
HindIII	R0104S	NEB
NheI	R0131S	NEB
NotI	R0189S	NEB
SacI	R0156S	NEB
Xbal	R0145S	NEB
XhoI	R0146S	NEB

2.1.7 Instrumentation

Instrument	Supplier
Autoclave	Rodwell
Cell Counting Slides for TC20 ™ Cell Counter	Bio-Rad
CO2 incubator	SANYO
Coulter Vi-Cell XR analyser	Beckman

3730 DNA sequencer	Applied Biosystem
DNA electrophoresis devices	Bio-Rad
FACSCalibur	BD Bioscience
Flow hood	Wolf labs
FLUOstar Galaxy plate reader	BMG labTech
Gel Doc ™ EZ system	Bio-Rad
Hypercassette™	Amersham Bio sciences
Inverted widefield fluorescence microscope LeicaDMI4000B	Leica
LSRII	BD Bioscience
Microscope Mini protean apparatus	Bio-Rad
Mini spin centrifuge	Eppendorf
NanoDrop spectrophotometer	Thermo Scientific
Orbital Shaker S01	STUART Science
SpectraMax 5Me microplate reader	Molecular devices
Trans-Blot ® Turbo ™ Transfer System	Bio-Rad
TC20 ™ Automated cell counter	Bio-Rad
Thermo cycler for PCR	G-STORM
Thermomixer 5437	Eppendorf
TL-100 ultracentrifuge	Beckman
UV transiluminator (model TX-312A)	Spectroline
Water bath	Fisherbrand
Water deioniser	NANOpure Diamond ™ Barnstead

2.1.8 Kits

Kit	Supplier
BCA Protein Assay Kit	Pierce
Cell Meter Caspase 3/7 Activity Apoptosis Assay Kit (Green Fluorescence)	Advancing Assay & Test Technologies

Dual luciferase reporter assay system	Promega
HaloTag ® Mammalian Pull-Down system	Promega
GenEluteTM Gel extraction Kit	Sigma-Aldrich
GenEluteTM HP Plasmid Miniprep Kit	Sigma-Aldrich
GenEluteTM Plasmid Midiprep Kit	Sigma-Aldrich
Luciferase assay system	Promega
LumiGLO Reverse Chemiluminescent Substrate Kit	KPL
Kit	**Supplier**
nanoScript reverse-transcriptase Kit	Primerdesign
Precision DNase Kit	.Primerdesign
Protein standard (liquid, 2mg protein/ml)	Sigma-Aldrich
QIAfilter Plasmid Maxi Kit	Qiagen
QIAfilter Plasmid Midi Kit	Qiagen
QuikChange II Site-directed Mutagenesis Kit	Agilent Technologies
TOPO cloning kit	Invitrogen

2.1.9 Primers

All oligonucleotide primers were commercially synthesised by Eurogentec or Eurofins MWG Operon; and were dissolved in the required volume of water to give a final concentration of 100µM and then stored at -20°C.

Primers for generating splice cDNA products	**Direction**	**Sequence**
Exon 1-4	Forward	5’ CGTCGTCCTCGAGAAGCTTACCATGACCCCTTGGCTCG GG 3’
	Reverse	5’ CTTGCAGTTACAACCCAG GTGATACCG 3’
Exon 5-SplT3.M.S1	Forward	5’ CGGTATCACCTGGGTTGTAACTGCAAGTTCATTCCACTT TAGG AAACAGAGCTGCC 3’
	Reverse	5’ GGCGGGCGGCCGCGCATCAGCTTCTGCTCACACTGCC3’
Exon 5-SplT3.M.S2	Forward	5’ CGGTATCACCTGGGTTGTAACTGCAAGAAACAGAGCTG CCAAT TGAAACAGAAG 3’

	Reverse	5’ GGCGGGCGGCCGCGCATCAGCTTCTGCTCACACTGCC3’
Exon 5-SplT3.M.S3	Forward	5’ CGTCGTCCTCGAGAAGCTTACCATGACCCCTTGGCTCG G G 3’
	Reverse	5’ CTCCTCGCGGCCGCTCAGGACAGCAGACTGGCTAAAGG GAA AG GCGGATGC TTGCAGTTACAACCCAGGT GATAC CG 3’
Exon 5-SplT3.M.S4	Forward	5’ CGTCGTCCTCGAGAAGCTTACCATGACCCCTTGGCTCG G G 3’
	Reverse	5’ CTCCTCGCGGCCGCTCACTTCTGGGTTTCAGGACAGCA GACTGG CTTGCAGTTACAACCCAGGTGATACCG 3’
Exon 5-SplT3.M.S5	Forward	5’ CGGAATATAAAATTCATAAATAACATGGAGGAAAACT TGCAG TTTACAACCCAGGTGATACCG 3’
	Reverse	5’ CTCCTCGCGGCCGCTTATGCAACATTACAAGACAATAT ACATTCACGGAATATAAAATTCATAAATAACATGGAGGA AA A CTTGC 3’
Primers for SFD-TIMP3 mutagenesis	**Direction**	**Sequence**
Ser15Cys	Forward	5’ CAGGACGCCTTCTGCAACTGCGACATCGTG 3’
	Reverse	5’ CACGATGCAGTTGCAGAAGGCGTCCTG 3’
Tyr128Cys	Forward	5’ CAAGATCAAGTCCTGCTGCTACCTTGCTTTG 3’
	Reverse	5’ CAAAGCAAGGCAGGTAGCAGCAGGACTTGATCTTG 3’
Tyr154Cys	Forward	5’ ATTTCGGTTACTGGCAGCCAGGGTAACCGAAAT 3’
	Reverse	5’ GTAGTGTTTGGACTGGCAGCCAGGGTAACCGAAAT 3’
Tyr159Cys	Forward	5’ GGCTACCAGTCCAAACACTGCGCCTGCATC 3’
	Reverse	5’ GATGCAGGCGCAGTGTTTGGACTGGTAGCC 3’
Primers for PCR (SplT3.M)	**Direction**	**Sequence**
PcDNA3	Forward	5’ CGACTCACTATAGGGAGA CCCAAGC 3’
Splice-TIMP3	Reverse	5’ CCACTTTACTGTTTAGAA TAAAGGACACAC 3’
Primers for sequencing splice constructs	**Direction**	**Sequence**
T3spl775-792	Forward	5’ AAGTGGTTTCAAGTGGGC 3’
T3spl1191-	Reverse	5’ CTACTGAGAGGACTTTTTCGTC 3’

1170r		
T3spl4878-4893	Forward	5’ TGGCTTCTGGCTACCTAAGG 3’
T3spl4576-4553r	Reverse	5’ AAGAGATGCCCAAAGGAGGAAGCG 3’
T3spl3576-3553r	Reverse	5’ TACTCTCTTCCCACTCTGCGGTTC 3’
T32167-2149r	Reverse	5’ TGCTTGCTGCCTTTGACTG 3’
T3spl3193-3214	Forward	5’ CAGTTGTAGGGTTTCTGTTGTG 3’
T3spl2275-2295	Forward	5’ AAGGAACTACAAGAGAGTCGG 3’
T3spl1575-1593	Forward	5’ AGTCCAAACACTACGCCTG 3’

2.1.10 Software

List of software	Version
CellquestPro	5.1
FinchTV	1.5.0
GraphPad Prism 6	6.0c
Image J	IJ1.46r
Image Lab	4.0.1 build 6
Macvector	14
Quantity One	4.6.3
Vi-CELL ^{TM} XR Cell Viability Analyzer	2.03

2.1.11 Vectors

List of vectors	Supplier
pcDNA3	Invitrogen
pcDNA3-KDEL-V5	Invitrogen
pcDNA3-HaloTag	Invitrogen
pcDNA3-SS-HaloTag	Invitrogen
PHTC HaloTag	Promega
pGL3-IL8-Luc	Promega
pGL3-Basic	Promega
pGL3-Control	Promega
pGL4-Luc2P/NF-$_K$B /Hygro	Promega

2.1.12 Web database/resources

Website	Purpose
Blast	Sequence alignment
ENSEMBL	Genome database browser
QuikChange	Mutational primer design
UCSC	Genome database browser

2.2 Methods

2.2.1 Molecular Biology Methods

2.2.1.1 DNA plasmid construction

2.2.1.1.1 End point Polymerase Chain Reaction (PCR)

The polymerase chain reaction is a common and cost-effective technique applied to amplify target segments of DNA. Briefly, the reaction is performed using a thermo cycler to process three essential steps including denaturation, annealing and extension. The first denaturation step consists of heating the reaction to a high temperature (typically 94°C) to separate the double stranded DNA template, while the annealing temperature (typically 55-65°C) allows hybridization of oligonucleotide primers to the single stranded DNA. Once annealed, strand extension is achieved at a slightly higher temperature (usually 72°C) to synthesise new double stranded DNA. Subsequently, the PCR results in exponential amplification of the target DNA fragments.

2.2.1.1.2 Overlapping Polymerase Chain Reaction

To synthesised cDNA splice variants identified from the Taq PCR products without any PCR errors, Phusion Hot Start Flex^{TM} 2x master mix (New England Biolabs) was used as instructed by the manufacturer. Using SplT3.M (3.3.1.2) maxiprep as DNA template, two amplification reactions were run separately to generate the exon 1 to 4 (E1-4) sequence of TIMP3 that is the same in all identified cDNA splice variants; and the novel exon 5 (E5) sequences using specific primers for each splice product. The primers were commercially synthesised to overlap about the novel splice acceptor sites (Figure 2.1).

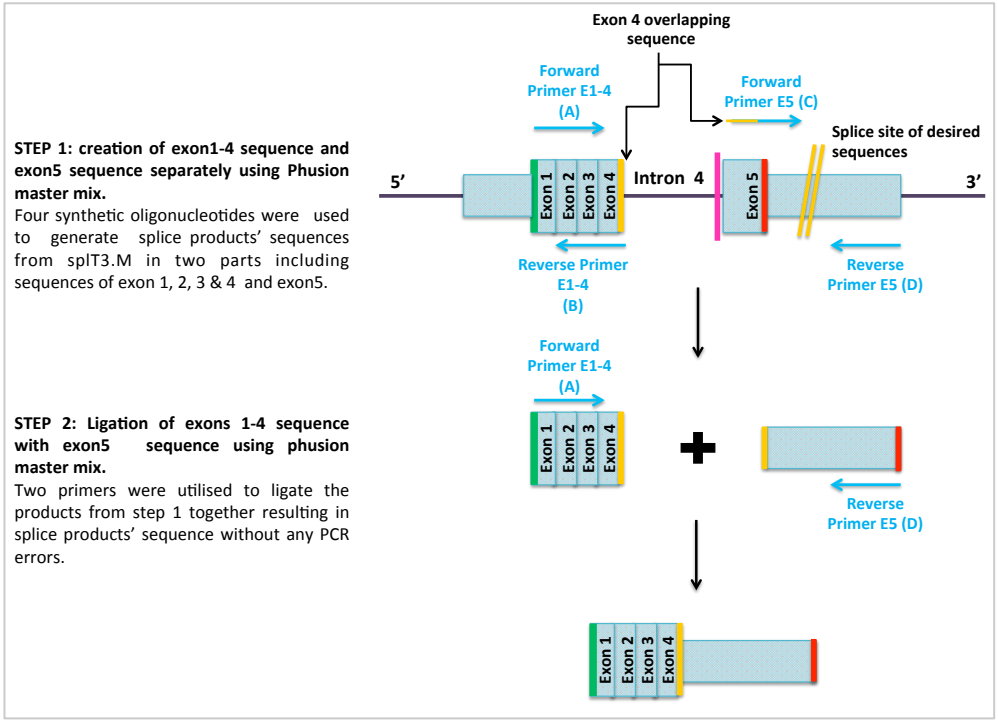

Figure 2.1: Overlapping PCR method to create cDNA of novel splice products.

2.2.1.1.3 Mutagenesis (QuikChange ™)

The QuikChange™ II Site-Directed Mutagenesis Kit facilitates the induction of genetic changes including substitution, insertion or deletion of single or multiple nucleotide bases in a specific DNA plasmid sequence. In brief, the mutagenesis process consists of three stages: synthesis of mutant strand, digestion of DNA template and transformation of competent cells.

The mutant strand DNA synthesis stage requires two completely overlapping oligonucleotide primers that are complementary to each strand at the mutation site but contain the desired mutation. Following denaturation of the plasmid template and annealing of the primers, strand extension using *Pfu*Ultra (High-Fidelity) DNA polymerase then copies the entire plasmid. The mutagenesis sample reaction was performed together with a control reaction. The control reaction contained the following: pWhitecript control plasmid (4.5kb), oligonucleotide control primers, dNTP mixture, 10x reaction buffer, water and *PfuUltra* HF DNA polymerase. The mutagenesis reaction was similar to the control reaction except that the DNA template was the normal TIMP3 construct and the primers were specific primers containing the desired mutation (see section 2.1.9). Both control and sample reactions were

amplified using a G-STORM 482 (GRI) thermal cycler. The thermo cycler was programmed according to mutagenesis protocol; this was 95°C for 30 seconds followed by 18 cycles that included: separation of dsDNA at 95°C for 30 seconds, annealing of the mutagenic primers at 55°C for 1 minute, and elongation at 68°C for 1minute/kb. This PCR stage results in nicked double stranded DNA plasmid carrying the desired mutation and the remaining parental DNA template.

In the second stage, the parental DNA plasmid template only is digested with *Dpn*I, which is a specific endonuclease for methylated and hemimethylated DNA. Therefore, the PCR products were endonuclease digested with *Dpn*I at 37°C for 60-90 minutes to digest the parental DNA template leaving the newly synthesised DNA intact. The final stage includes transforming the mutated plasmid into XL1-Blue supercompetent cells for nick repair and replication.

The QuikChange ™ II Site-Directed Mutagenesis kit was utilised in this project to create SFD-TIMP3 mutation constructs by substitution of specific single nucleotides in the wild-type *TIMP3* sequence.

2.2.1.2 Vector preparation

2.2.1.2.1 Restriction enzyme digestion

Restriction endonuclease digestion was used for both DNA cloning or confirming successful ligation of cDNA (restriction enzymes are listed in section 2.1.6). To clone a cDNA of interest into the desired plasmid, both cDNA and plasmid sequences were digested with the same restriction enzymes based on the manufacturer's protocol, in which the concentration of restriction enzymes was always less than 10% of the final reaction volume to avoid star activity (non-specific restriction). Where two enzymes had compatible reaction buffers, they were combined in a single digest. If the enzymes had incompatible reaction buffers, two separate digestions were performed, purifying the DNA between digests.

To quickly confirm successful ligation of DNA inserts into vectors, prior to sequencing, a restriction digest was often performed, followed by agarose gel electrophoresis.

2.2.1.2.2 Ligation reaction

Ligation reactions were performed to ligate inserts (cDNA of interest) into desired vectors. All ligation reactions were made using T4 DNA ligase in the supplied buffer (Promega, UK) in a total volume of 20µl. Generally 40ng of digested vector was used at a molar ratio of 3:1 (insert: vector), in which the amount of inserts was calculated as shown in the equation below:

ng of insert = (ng of vector * size of insert (Kb)) / size of vector (Kb) * molar ratio (3/1)

For each ligation reaction, a control reaction was also performed, containing vector only without any insert. Ligation and control reactions were incubated 2 hours at room temperature and then overnight at 4°C; and subsequently 5µl from each reaction was used to transform 50µl of α-select chemically competent cells.

2.2.1.3 Transforming α-Select Chemically competent cells

Transformation was performed using α-Select Chemically competent cells. These bacterial cells are derived from the *E*.coli K12 strain, and are comparable to the DH5α strain. They contain different genetic markers that allow efficient transformation including *lac*Z for blue/white colour screening and *end*A1 and *rec*A1 to improve the quality of plasmid DNA and minimise recombination, respectively. α-Select Bronze efficiency cells were used for routine sub-cloning and α-Select Gold efficiency cells used for recovering products following ligations.

Mutagenesis or ligation reaction products were transformed into α-Select cells according to the manufacturer's instructions. Cells were taken out of -80℃ and allowed to thaw on wet ice (50µl aliquot per reaction). 5µl of DNA reaction was added to the cells, which were then mixed gently by swirling and incubated on ice for 30 minutes. After that, cells were heated at 42℃ for 45 seconds and placed again on ice for 2 minutes. 450µl of sterile LB broth was then added to each tube and they were incubated at 37℃ for 60 minutes in an orbital shaker. Subsequently, transformed cells (50-100µl) were spread on LB agar plates containing appropriate selective antibiotics and incubated overnight at 37℃.

2.2.1.4 Small and large scale bacterial cell culture

In order to prepare small-scale (miniprep) bacterial cell cultures, single colonies were harvested from transformation LB agar plates and grown separately (one colony per culture) in 4ml of sterile LB broth that contained carbenicillin at a final concentration of 100µg/ml. The cultures were incubated overnight at 37℃ in a shaker at 250rpm.

After miniprep culture, large-scale bacterial cultures including midi and maxi prep were prepared by mixing 50µl or 150µl of miniprep culture with 50ml or 150ml of sterile LB broth containing 100µg/ml carbenicillin, respectively.

2.2.1.5 Plasmid DNA purification

To purify plasmid DNA from small-scale bacterial culture (miniprep), a GenElute ™ plasmid miniprep kit was used based on the manufacturer's instructions. Briefly, the kit is based on SDS/alkaline lysis, acetate precipitation of genomic DNA and protein; and then binding of the plasmid to a silica binding column followed by washing and elution in TE or water.

To extract the plasmid DNA from large-scale bacterial cultures, similarly, a GenElute ™ plasmid Midiprep kit was utilised to isolate the plasmid DNA from midiprep bacterial culture. Qiagen Maxiprep kits work on similar principles to the GenElute miniprep kits except the plasmid DNA is bound to an anion exchange resin instead of silica and is eluted using high salt buffer. Eluted DNA is then precipitated with isopropanol and washed with 70% ethanol to remove salts but also allow DNA sterilization, which is necessary for transfection of mammalian cells.

2.2.1.6 Nucleic acid quantification

Following the plasmid DNA isolation, the quality and quantity of plasmid DNA were measured using a NanoDrop spectrophotometer, in which a 260/280 ratio of 1.8 and 2.0 were regarded as highly pure for DNA and RNA, respectively.

2.2.1.7 Agarose gel electrophoresis

Agarose gels were prepared at 1-2% in 1XTAE buffer depending on the size of DNA to be separated. For 1% agarose gel, 0.6 of agarose was dissolved in 60ml 1XTAE buffer in a microwave oven and subsequently 3µl of ethidium bromide (from a 10mg/ml stock) was

added to give a final concentration of 0.5μg/ml. The agarose solution was poured into the casting plate with comb and allowed to set at room temperature.

In the meantime, the DNA samples were mixed with orange G loading dye (20% v/v) prior to loading in the agarose gel. The gel was placed in the gel tank filled with 1XTAE. The DNA marker and samples were loaded into the gel and allowed to run at a constant voltage of 80V. After that, the gel was visualised under UV light using Gel Doc ^{TM} EZ System and bands with the desired sizes were excised, when required.

2.2.1.8 DNA extraction from agarose gel

A GenElute Gel Extraction kit was used to purify separated DNA from agarose gel slices, according to manufacturer's protocol. In brief, excised gel slices were weighed and then melted in a ratio of 1:3 (w/v) of provided solubilisation buffer. Then DNA was extracted using a silica spin column and DNA elution in either the provided elution buffer or water.

2.2.1.9 DNA sequencing

In order to check the quality of all purified DNA plasmids and the absence of any induced PCR mutations, they were sequenced in the Medical School genomic core facility using an ABI capillary sequencer using specific sequencing primers that anneal before the desired region.

2.2.1.10 DNA precipitation

Plasmid DNA precipitation was performed to sterilise the purified DNA prior to transfection of mammalian cells. Briefly, 50μg of DNA eluted in 100μl elution buffer was mixed with 10% of 3M of sodium acetate (NaAc, pH 6). Each DNA sample was then mixed with two sample volumes of absolute ethanol and incubated on ice for 10 minutes. Samples were centrifuged for 10 minutes at maximum speed and 4°C. After that, the pellets were washed with 500μl of 70% Ethanol and centrifuged for 5 minutes. Finally pellets were air-dried inside a safety cabinet and re-suspended in sterile water at a concentration of 1μg/ml.

2.2.1.11 RNA isolation

To isolate total RNA from mammalian cells, TRI-reagent was used according to the manufacturer's protocol. The reagent is a monophase solution and contains phenol and guanidine thiocyanate. Briefly, the procedure is an improved single-step method that directly lyses cells in 1ml reagent per 10cm plate. The cell lysates were mixed by repeated pipetting to become homogenous and then incubated at room temperature for 5 minutes, following by vigorously mixing with 100µl of 1- bromo-3-chloropropane. The solution was incubated at room temperature for 2-15 min and then centrifuged at 12000g for 15 min at 4°C. The centrifugation separated the mixture into three layers encompassing: a red organic protein phase at the bottom of the tube, an interphase containing DNA in the middle and a colourless upper aqueous phase containing RNA (Figure 2.2). The RNA aqueous phase was transferred to a new tube and mixed with 500µl of 2-propanol to precipitate the RNA. The RNA mixtures were allowed to stand at room temperature for 5-10 min and subsequently centrifuged at 12000g for 10 min at 4°C. The RNA pellets were washed and mixed by vortexing with 70% ethanol and then centrifuged at 12000g for 5min at 4°C. The resulting pellets were air-dried for 5-10min and subsequently re-suspended in 50µl DEPC-treated water (diethyl pyrocarbonate). The quality and quantity of RNA was measured using a NanoDrop spectrophotometer as described in section 2.2.1.5. The purified RNA was stored at -80°C until use for cDNA synthesis.

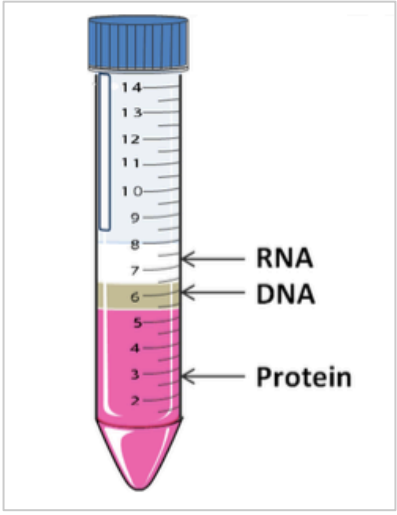

Figure 2.2: Separation of TRI-reagent.

The separation of TRI-reagent cell lysate into three layers encompassing red organic (protein), inter (DNA) and upper colourless phase (RNA). (Servier Medical Art used to prepare the figure, http://www.servier.co.uk/medical-art-gallery/)

2.2.1.12 Genomic DNA removal

The RNA extraction procedure should remove most of the genomic DNA; nevertheless, the Precision ™ DNase Kit was used to guarantee the purity of RNA. The kit was used according to the manufacturer's protocol prior to reverse transcription. In brief, 25µl of RNA samples were mixed with 2.5µl DNase enzyme in the supplied DNase reaction buffer and then incubated for 10 minutes at 30°C. After that, the DNase enzyme was inactivated by 5 minutes incubation at 55°C. RNA samples could be either used immediately or stored at -80°C.

2.2.1.13 Reverse transcription (RT)

In order to synthesise first strand cDNA from the isolated RNA, Precision Nanoscript ™ reverse transcription kit was applied according to manufacturer's protocol. The reaction was performed using specific oligonucleotide reverse primers in two stages including annealing and extension. The annealing stage was at 65°C for 5 minutes following by cooling on ice, and then an extension stage that included heating the reaction at 55°C for 20 minutes and

inactivation at 75°C for 15 minutes (detailed in Table 2.3). The synthesised cDNA was stored at -20°C until use.

Table 2.1: Reverse transcription reaction steps.

Annealing reaction components	
DNase-treated RNA (at 1µg/µl)	2µl
Oligonucleotide primers (at 10µM)	1µl
Nuclease free water	Up to 10µl
-	-
-	-
-	-

Extension reaction components	
nanoScript 10x buffer	2µl
dNTP mix (10µM)	1µl
DTT (100µM)	2µl
Nuclease free water	4µl
nanoScript enzyme	1µl
Annealing reaction	10µl

2.2.1.14 PCR purification

To purify PCR products from the reaction mixture, a GenElute ™ PCR clean up kit was utilised based on the manufacturer's protocol. Like the other GenElute kits, DNA is purified on a silica membrane in a spin column, then washed and eluted in either the provided elution buffer or water. The purified DNA can be either stored at -20°C or used immediately in other reactions such as TOPO cloning.

2.2.1.15 TOPO cloning

In order to clone purified Taq PCR products, the TOPO TA cloning kit was applied as described in the manufacturer's protocol. Briefly, the provided vector has a single 3' deoxythymidine (T) overhanging residue that allows efficient ligation to the 3'deoxyadenosine end of Taq PCR products. Additionally the ligating enzyme, topoisomerase I, is covalently bound at the 3' phosphate of the deoxythymidine overhang. This provides a highly efficient way of cloning very small amounts of PCR product, as further restriction and purification are unnecessary. The products of the TOPO reactions were used to transform chemically competent *E.coli* as described in section 2.2.1.2.3.

2.2.2 Mammalian cell culture methods

2.2.2.1 COS-7 cell line

African green monkey kidney cells (COS-7) are derived from the CV-1 cell line (Cercopithecus aethiops) by transformation with an origin defective mutant of SV40. They were used due to the fact that they express SV40 large T antigen, enabling vectors containing the SV40 origin of replication, such as pcDNA3, to replicate and transiently express high level of mRNA and protein.

2.2.2.2 ARPE19 cell line

ARPE19 is a human retinal pigment epithelial cell line derived from normal eyes (Dunn *et al.* 1996). The ARPE19 cell line was used in this project, as RPE cells are the primary source of TIMP3 in the retina.

2.2.2.3 HEK293T cell line

HEK is human embryonic kidney cell line derived from a healthy-aborted fetus. The cell line was firstly transformed with adenovirus in the 1970s and named HEK293 based on Frank Graham's 293rd experiment. Subsequently, HEK293 cell were transformed with the large T antigen of the SV40 virus that enable replication and amplification of vectors carrying SV40 origin.

2.2.2.4 HUVEC cell line

These are primary human umbilical vein endothelial cells (HUVEC) and derived from endothelium of veins from umbilical cord. HUVEC cells express VEGFR1 and VEGFR2 and are commonly used for pharmacological and physiological investigation, for instance, blood coagulation, fibrinolysis and angiogenesis. They were grown until 90% confluent in complete growth medium comprising Endothelial Basel Medium 2 (EBM2) and the supplied supplement at 37°C in 5% CO_2.

Serum starvation medium was used to examine endothelial cell signalling and function *in vitro* as complete growth medium contains VEGF and other growth factors that would interfere with signalling. Cells were grown to 90% confluence in complete growth medium and then washed twice with DPBS to guarantee complete removal of the complete growth medium. After that, cells were incubated in starving medium (0.5% FBS-EBM2) at 37°C in 5% CO_2 for 17-18 hours.

2.2.2.5 Cell culturing procedures

For routine culturing, when cells became 80-90% confluence they were passaged by trypsinisation. The medium was discarded from flasks and cells were washed in 5ml of DPBS (Dulbecco's phosphate buffered saline), which was discarded. Then 3ml of trypsin/EDTA was added to the cells and incubated at 37°C in 5% CO_2 for 8 minutes to remove cells from the surface of the flask. Cells detachment was checked under a microscope and, once complete, 7ml of complete growth medium was added to the cells to inactivate the trypsin-EDTA. Suspended cells were centrifuged at 400g for 5 minutes. The resulting pellet was re-suspended by addition of complete growth medium. Finally, the desired amount of cell re-suspension was seeded into a fresh tissue vessel containing complete growth medium.

Where functional assays required a specific number of cells, cells in suspension were counted using either Vi-CELL Cell Viability Analyser or TC20 Automated Cell Counter, and then the required numbers of cells were added to the desired tissue culture vessels.

2.2.2.6 Cell detachment using 10mM EDTA

Cells detachment using 10mM EDTA prepared in DPBS was performed instead of trypsin-EDTA, when cell membrane proteins and receptors required being intact for the subsequent assays. Cells were passaged as explained in section 2.2.2.5, except that cells were incubated in 10mM EDTA for 5-20 minutes at 37°C instead of using trypsin-EDTA.

2.2.2.7 Cell labelling

To label cells with CellTracker™ dye, cells at 90% confluence were rinsed twice with DPBS and then incubated at 37°C and 5% CO_2 in serum-free medium containing CellTracker™ Green dye at a concentration of 1:4000.

2.2.2.8 Cryopreservation of mammalian cell lines

Long-term preservation of cells is achieved using liquid nitrogen (-196°C). Cells were passaged as normal, however, cell pellets were re-suspended in a freezing medium composed of FBS (90%) and DMSO (10%). The re-suspension was put into cryopreservation vials (cryovials) and placed in a Mr Frosty box at -80°C for at least 24 hours to decrease the temperature gradually prior to transferring vials to a liquid nitrogen dewar.

For thawing cell lines, complete growth medium was warmed to 37°C prior to use. Cryovials were retrieved from liquid nitrogen and allowed to defrost at room temperature inside the laminar flow cabinet. Cells were mixed with complete medium and then centrifuged at 500g for 5 minutes to remove DMSO. The pellet was re-suspended in complete medium and grown in tissue culture vessels at 37°C and 5% CO_2.

2.2.2.9 Chemical transfection of cell lines using *Trans*IT-LT1 transfection reagent

In order to examine the mRNA/protein expression of the desired DNA plasmids, *Trans*IT-LT1 transfection reagent was used to transiently or stably transfect mammalian cells with the various DNA constructs. According to the manufacturer's instructions, transfection was conducted in the desired tissue culture vessels when cells became ≥80% confluent (Table 2.2). 24 hours prior to transfection, cells were seeded into the desired tissue culture vessels at a density of 0.8-3.0 $x10^5$ per well of a 6-well plate and incubated overnight in a 37°C, 5% CO_2 incubator. The following day cells were ~80% confluent and *Trans*IT-LT1 reagent and DNA complexes were prepared in sterile microcentrifuge tubes. Firstly, the serum free medium was mixed with plasmid DNA, and then *Trans*IT-LT1 reagent was added and mixed by gentle repeated pipetting. The complexes were incubated at room temperature for 15-30 minutes and then added drop-wise to different areas of the wells and rocked gently to ensure even distribution of TransIT-LT1: DNA complex and incubated at 37°C and 5% CO_2 for 24-48 hours prior to harvesting.

Whilst transiently transfected cells were harvested at 48 hours post-transfection, stably transfected cells were passaged and grown in 25cm flasks containing 5ml complete growth medium and selection antibiotic such as Geneticin at 500µg/ml. Then, growth medium was regularly replaced with fresh growth medium and antibiotic until cells became confluent.

Table 2.2: Required transfection conditions.

Culture vessels	**6-well plate**				**6cm dish**	**10cm dish**
Complete growth media (ml)	2.5				6	15.5
Serum-free medium (ml)	0.250				0.6	1.5
DNA (µl, stock concentration at 1µg/µl)	2.5				5.8	15
***Trans*IT-LT1 reagent:DNA ratio**	3:1	4:1	6:1	8:1	3:1	3:1
***Trans*IT-LT1 (µl)**	7.5	10	15	20	17.5	45

2.2.3 Protein analysis

2.2.3.1 Protein extraction

2.2.3.1.1 Cell lysis

In order to release cellular proteins and remove cell debris, mammalian cells were lysed in RIPA lysis buffer when needed. Briefly, cells were grown in 10cm diameter petri dishes in complete growth medium until they were 100% confluent. Then cells were washed twice in DPBS and scraped in 500µl of ice-cold RIPA lysis buffer. Cell lysates were transferred to a micro-centrifuge tube and a syringe with a 25-gauge needle was used to disrupt cell membranes and shear genomic DNA. Tubes were placed on ice for 30 minutes and mixed by vortexing every 15 minutes to complete solubilisation. To remove insoluble cell debris, a 10 minutes centrifugation was performed at 4°C and 21000 g. Clear cell lysates were pipetted into new micro-centrifuge tubes and stored at -80°C until use for protein assay and western blotting.

2.2.3.1.2 ECM preparation using hypotonic buffers

ECM was prepared from transiently transfected COS-7 cells two days post-transfection while it was prepared from stably transfected ARPE19 cells 10 days post seeding. Untransfected and transfected cells were lysed using hypotonic buffers and their ECM was prepared based on the method described by Fischer and Werb (1995). Cells were treated with three buffers including Hypo-buffer, NP40-hypo and 0.1% Deoxycholate to remove all cells, leaving behind the ECM. Briefly, cells in tissue vessels were sequentially washed (2-3 times) and incubated 2-10 min in the above-mentioned buffers. Then, plates were washed with water using a squeeze bottle and allowed to air-dry. Dried plates were stored inverted at 4°C until use. The ECM was then extracted for western blotting by scraping directly into 1X SDS sample buffer.

2.2.3.1.3 Cell removal using ammonium hydroxide

ARPE19 cells were lysed using ammonium hydroxide (NH_4OH) when ARPE19 basement membrane was required to be used for functional assays. ARPE19 cells were grown and maintained in tissue culture vessels for 10 days. The complete growth medium was discarded

and cells were incubated with 20mM NH_4OH for 5 minutes at room temperature to lyse cells and then the ECM/basement membrane was gently washed several times with DPBS ready for the subsequent assays.

2.2.3.2 Protein quantification

The Pierce BCA protein assay kit was used according to the manufacturer's protocol to determine the concentration of protein in ECM or cell lysates. The protocol briefly consists of two steps including formation of blue coloured complexes between copper sulphate solution and bicinchoninic acid (BCA) solution, and a second reaction between the preformed complex and test proteins. The second reaction products form a purple colour with a maximum absorbance at 562nm. Bovine serum albumin (BSA) was used to prepare six standard protein concentrations in the range (0-1mg/ml) with 1X sample buffer or lysis buffer depending on sample extraction method, and 25µl of sample was loaded into a well of a 96-well plate (three wells for each tested sample). Similarly 10µl of protein sample was mixed with 90µl 1X sample buffer and then pipetted into wells. A mixture of copper II sulphate and BCA was prepared at 1:50 ratio and added to each standard and sample (200µl/well). After addition of the BCA- copper sulphate solution, the 96 well plates were incubated at 37°C for 30min following by measuring the protein concentration in a Fusion plate reader at 570nm.

2.2.3.3 Sodium dodecyl sulphate polyacrylamide gel electrophoresis (SDS-PAGE)

2.2.3.3.1 Gel preparation and electrophoresis

10% polyacrylamide separating gels were prepared in a 1.5mm discontinuous mini gel system by mixing the reagents in Appendix 2. Firstly, the lower resolving gel layer was prepared and poured into the assembled plates. Water-saturated butanol (500ul per gel) was then added to the top of the gel to eliminate bubbles and to level the gel. After 1 hour at room temperature, the water-saturated butanol was discarded by washing with water and then excess water was removed using filter papers. Secondly, the upper stacking gel was prepared and poured onto the top of the resolving gel. A 1.5mm comb was immediately inserted in the assembled plate and then the gel allowed to set for 30 minutes.

Meanwhile, all protein samples were quantified with BCA to ensure equal amounts of protein were loaded/well and diluted by mixing with 2X sample buffer as necessary. Samples were

run at 120 volts for 15 minutes and then at 150 volts for 60 minutes or until the bromophenol blue dye reached the bottom of the resolving gel.

2.2.3.3.2 Protein transfer onto PVDF

A Bio-Rad mini-Protean 3 blotting apparatus was used to transfer separated protein samples from resolving gel onto polyvinylidene diflouride (PVDF) or nitrocellulose membrane. PVDF membrane was firstly soaked in methanol for 2 minutes and then in CAPS transfer buffer for 5 minutes, whereas nitrocellulose membrane was immediately soaked in CAPS transfer buffer. Then the gel, two foam pads and four filter papers were placed in the CAPS transfer buffer for 10 minutes. After that, they were prepared in a mini gel holder cassette and inserted into the Mini Trans-Blot apparatus in CAPS buffer or a cassette of the Trans-Blot Turbo ^{TM} transfer system as shown in Figure 2.3. The proteins transfer process was performed overnight at 4℃ and 60mA constant current (Mini TransBlot) or 10-30 minutes at 2.5A (Trans-Blot Turbo ^{TM}).

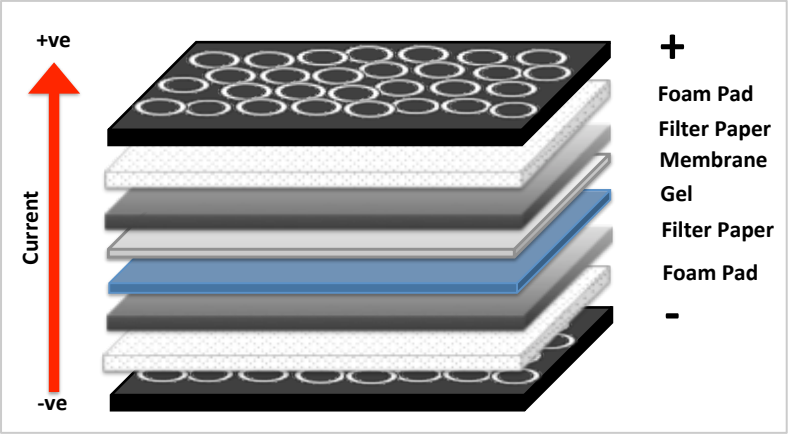

Figure 2.3: Illustration of prepared stack for protein transfer.

The diagram shows the organisation of different layers in protein transfer apparatus. (A) Layers arrangement inside the Mini Gel Holder Cassette for Mini Trans-Blot apparatus. For Trans-Blot ® Turbo Transfer System, the same arrangement was made but without the foam pads.

2.2.3.3.3 Blocking and probing of PVDF Membrane

To prevent non-specific binding of antibodies to the PVDF or nitrocellulose membranes, they were incubated in blocking buffer for 1-6 hours on a shaker at room temperature or overnight at 4℃.

The blocked membrane was incubated in the desired primary and secondary antibodies (Table 1.6) used at the optimal concentration (see results chapters) and diluted in blocking buffer. The membrane was initially incubated in the primary antibody overnight at 4℃ on a shaker. The membrane was then washed 4 times (10 minutes each) with 1X TBST to eliminate unbound antibodies.

Afterward, the membrane was incubated in polyclonal secondary antibody conjugated with horseradish peroxidase (HRP) for 1 hour at room temperature with gentle shaking. To remove unbound secondary antibodies, the membrane was washed 4 times (10 minutes each) with 1X TBST on a shaker.

Table 2.3: List of primary and secondary antibodies used in western blotting.

Primary Antibody	**Purpose of use**
Anti-Tissue Inhibitor of Metalloproteinase-3, First Loop antibody produced in Rabbit	A polyclonal antibody produced in rabbit and specifies to the first loop of human TIMP-3 (Amino-terminus of TIMP3), including wild type, all exon 5 SFD-mutant and splice site mutant TIMP3 proteins.
Anti-TIMP3 antibody produced in Rabbit	A polyclonal antibody, produced in rabbit, detects endogenous levels of full-length TIMP3 protein (Carboxyl-terminus of TIMP-3) such as wild type and exon 1 SFD-mutant TIMP3 proteins.
TIMP3 (D74B10) Rabbit Monoclonal Antibody	A monoclonal rabbit antibody corresponding to residues surrounding Lys 53, and used to detect the Amino-terminus of human TIMP3 including wild type and all exon 5 SFD-mutant and splice site mutant TIMP3 proteins.
Anti-V5 Mouse Monoclonal Antibody	A monoclonal antibody, produced in mouse, recognises protein with V5 epitope tag. For example, pcDNA3- WT-TIMP3-V5-KDEL and other -SFD mutants tagged with V5-KDEL.
Anti-HaloTag mouse monoclonal antibody	A monoclonal antibody, produced in mouse, recognises Halo-Tagged proteins, including pHTC, pHTC-WT.TIMP3, pHTC-S181C, pHTC-EFEMP1 (wild type and mutant), pcDNA3-SS-HaloTag and pcDNA3-SS-HaloTag-EFEMP1 (wild type and mutant).
TACE (D22H4) Rabbit monoclonal Antibody	A monoclonal antibody, produced in rabbit, reacts with endogenous levels of total TACE protein.
RAGE Rabbit Monoclonal Antibody	A monoclonal antibody, produced in rabbit, recognises endogenous levels of total RAGE protein.
Secondary Antibody	**Purpose of use**
Polyclonal Swine Anti-Rabbit Immunoglobulins/HRP	A horseradish peroxidase-conjugated polyclonal swine anti-rabbit antibody used to detect rabbit primary antibodies.
Polyclonal Goat Anti-Mouse Immunoglobulins/HRP	A horseradish peroxidase-conjugated polyclonal goat anti-mouse antibody used to detect mouse primary antibodies.

2.2.3.3.4 Detection of protein bands

A LumiGLO Reverse Chemiluminescent substrate kit was used to detect secondary antibodies based on the manufacturer's instructions. Briefly, the PVDF membrane was rinsed in 1X TBST and the excess wash buffer removed. The membrane was placed into a tray in

which bands should be placed upwards and then the substrate solution was added directly for 1 minute. Excess substrate was then removed and the membrane wrapped in a cling film. The wrapped membrane was then exposed to photographic film (Amersham Hyperfilm ECL) for a period of time between 1 second to 20 minutes. After exposure, the film was soaked in developing solution until the bands become clear then rinsed in tap water. Finally, the film was placed into fixing solution for 1-2 minutes, washed again in tap water and air-dried.

2.2.3.4 Caspase 3/7 activity apoptosis assay

To investigate the effect of WT.T3 and SFD-TIMP3 on ARPE19 cells apoptosis, Caspase 3/7 activity was measured as an indicator for cell apoptosis using Cell Meter ^{TM} Caspase 3/7 Activity Apoptosis Assay Kit according to manufacturer's protocol. In brief, un-transfected ARPE19 cells and ARPE19 cells stably transfected with TIMP3-constructs were plated in 2% FBS supplemented DMEM growth media in 96-well plates at $2x10^4$ cells per well and incubated at 37℃ and 5% CO_2. 24 hours post seeding, cells were treated with Camptothecin (20μM) or anti-Fas activating antibody (15-20μg/ml) for 24 hours at 37℃. Caspase 3/7 assay loading solution was added to treated cells at a 1:1 ratio (caspase solution: cell media) and incubated at room temperature covered from light for at least 1 hour. Fluorescence intensity was measured at an emission wavelength of 525nm and excitation wavelength of 490nm using the spectraMax plate reader.

2.2.3.5 Endothelial cell signalling and functional assays

2.2.3.5.1 Flow cytometry for VEGFR2 expression

In order to examine the influence of ECM proteins from ARPE19 cells transfected with wild-type and SFD-TIMP3 on VEGFR2 expression by vascular endothelial cells, the expression of the receptor was measured by flow cytometry.

Un-transfected and transfected ARPE19 cells were grown in 6 or 10cm tissue culture dishes for 10 days in complete growth media and selection antibiotic for transfected cells. Meanwhile, HUVEC were grown until they became 90% confluent and then incubated overnight in serum-starved media (0.5% FBS-EBM2). The following day, ARPE19-ECM was prepared using NH_4OH as described in section 2.2.4.1.3 and HUVEC were passaged as normal. Then, HUVEC were re-suspended in serum-starved medium and seeded at a density of $1\text{-}3x10^6$ per plate onto three different treatment groups including a negative control

without treatment, a positive control group containing VEGF (at 10ng/ml) and tested group with ARPE19-ECM. All treated HUVEC groups were incubated at 37℃ for 4-5 hours.

When treatment was completed, HUVEC were washed once with DPBS and detached by incubating in 10mM EDTA (prepared in DPBS) for 5-20 minutes at 37℃ (see 2.2.2.5-6). Cell pellets were re-suspended in 0.1% FBS-DPBS (110µl per sample) and then each sample was divided into micro-centrifuge tubes (50µl each), the first tube to be treated with PE (phycoerythrin) mouse anti-human CD309 (VEGFR2) and the second one for PE mouse IgG1, k isotype control. Tubes were mixed by gentle vortexing and then incubated for 15-30 minutes in a covered ice bucket to protect from light. HUVEC were washed once in 0.1% FBS-DPBS and centrifuged for 5 minutes at 127g and the second wash was with DPBS only. To check cell viability, cell pellets were re-suspended in 500µl DPBS and mixed with 0.5µl of LIVE/DEAD® Fixable Blue Dead Cell Stain Kit. Tubes were incubated for 30 minutes in a covered ice bucket. Subsequently cells were washed once in 1ml of DPBS and then re-suspended in 500µl of 1%PFA to fix stained cells, which could be either analysed immediately or stored at 4℃ protected from light for up to a week, prior to analysis by flow cytometry.

2.2.3.5.2 Migration assay

This assay was conducted to examine the effect of WT- and SFD-TIMP3 secreted in the ECM of transfected ARPE19 cells on the ability of HUVEC to invade/migrate through the matrix. HUVEC were grown in complete growth medium to reach 90% confluence and then serum starved overnight as described in section 2.2.2.4. CellTracker™ dye was then used to label HUVEC (section 2.1.9) that were seeded at a density of $50x10^3$ per insert onto ARPE19-ECM prepared using NH_4OH in the Falcon® HTS FluoroBlok™ Inserts (8µm pores) in serum starved medium. The FluoroBlok inserts were placed into wells of 24-well plates containing serum starved medium and VEGF at 10ng/ml. The HUVEC were incubated at 37 ℃ for 4-5 hours to allow cells to invade ARPE19-ECM and migrate to the lower chamber containing VEGF. Since the membrane of the inserts is opaque to fluorescent light, only cells that have migrated through the membrane are visible under the inverted fluorescent microscope or to the plate reader. After incubation the inserts were washed twice in DPBS and placed in fresh 24-well plates. The migrated cells in the inserts were fixed in 1% PFA prepared in DPBS and visualised immediately or stored at 4℃ for up to one week. The migrated cells were visualised using a fluorescent microscope at a final magnification of 200X (inverted widefield fluorescence microscope LeicaDMI4000B). The number of

migrated cells in the lower chamber was measured using a fluorescence plate reader at an excitation wavelength of 492nm and emission wavelength of 517nm.

2.2.3.6 Protein Pull down assay

To examine the interaction between EFEMP1 and TIMP3 proteins, a pull down assay was performed using HaloTag Mammalian Pull-Down and Labelling System kit and HEK293T cells. HEK293T cells were used for all pull down assays due to the fact that they are very highly transfectable cells and contain SV40 T-antigen allowing increased replication of vectors carrying SV40 region of replication. According to manufacturer's instructions, the pull-down assay was achieved in four stages including creating HaloTag fusion constructs, transfecting mammalian cells with HaloTag constructs, protein pull-down and detecting proteins bound to the HaloTag fusion proteins by western blotting.

2.2.3.6.1 Transfecting mammalian cells and cell lysate preparation

HaloTag-EFEMP1-pcDNA3 and TIMP3-pcDNA3 constructs were already available in our laboratory. HEK293T cells were transiently transfected with HaloTag-EFEMP1 and TIMP3-V5-KDEL constructs in 6-well plates (Section 2.2.3 & Table 2.2). 24 hours post transfection, transfected cells were washed with ice-cold DPBS and then harvested by gentle scraping in ice-cold DPBS followed by centrifugation at 4℃ for 5-10 minutes. Cell pellets were stored at -80℃ for at least 30 minutes before continuing with the cell lysis procedure. Thawed cells were re-suspended in 100µl mammalian lysis buffer provided in the kit and 2µl of 50x protease inhibitor cocktail and then incubated on ice for 5 minutes. Cell lysates were loaded onto QIAshredder columns to eliminate cell debris and shear genomic DNA and then the flow-through lysates were diluted with 100µl of 1X TBS buffer.

2.2.3.6.2 Protein Pull-Down protocol

HaloLink ^{TM} resin (25µl per cell lysate) was equilibrated by washing with 400µl of 1XTBS-NP40 wash buffer followed by 2 minutes centrifugation at 800g at room temperature. This was repeated three times. Diluted cell lysates were then added to HaloLink resin tubes and incubated at 4℃ overnight on a blood mixer. The following day, tubes were spun for 2 minutes at 800g and then washed 4 times with 1X TBS-NP40 wash buffer, briefly centrifuging after each wash. Protein samples were eluted in 25µl of SDS-Elution buffer at

95℃ for 10 minutes and subsequently centrifuged at 800g for 2 minutes. The supernatant was transferred to fresh micro-centrifuge tubes. In the final step, 10µl of supernatant was analysed by SDS-PAGE and western blotting (section 2.2.1.3 & 2.2.1.4).

2.2.3.7 RAGE signalling assays

Since RAGE-ligand binding is known to result in activation of the NF-$_K$B transcriptional pathway, NF-$_K$B firefly luciferase reporter vectors were used in conjunction with Promega's standard or dual luciferase reporter assay systems. The vectors comprised either the pGL4-*luc2P*/NF-$_K$B vector, which contains five copies of the NF-$_K$B response element, or the pGL3-IL8-Luc vector, which contains a 212bp section of the human interleukin 8 promoter sequence inserted into the pGL3-basic reporter vector. The IL8 promoter sequence contains a number of NF-$_K$B response elements, as well as additional transcription factor binding sites.

2.2.3.7.1 Dual luciferase reporter assay system

In order to investigate the effect of wild type- and SFD- TIMP3 on RAGE signalling, dual luciferase reporter assay was performed using ECM from both un-transfected and SFD-transfected cells. The Dual Luciferase reporter assay system was carried out according to the manufacturer's protocol. The assay enables distinct detection or both firefly and *Renilla* luciferase in the same sample. Cells are transfected with both the firefly reporter vector and a constitutively active *Renilla* vector. By determining the ratio of firefly to *Renilla* luciferase activity, rather than just total luciferase activity, it is possible to control for differences in transfection efficiencies that may occur between samples. The assay was divided into three stages involving transient co-transfection of mammalian cells, time course treatment of transfected cells and measurement of luminescence signals in cell lysates. Firstly, HEK293T cells were seeded into 6-well plates at a density of $5x10^5$ per well in 2% FBS-DMEM growth medium for 24 hours prior to transfection. The following day, cells were co-transfected with *Renilla* and firefly luciferase reporter vectors using *Trans*It-LT1 transfection reagent at ratio of 3:1 (*Trans*IT-LT1: DNA). Transfection of HEK293T cells was performed at two different vector ratios including 4:1 and 40:1 for experimental vector: co-reporter vector in four separate groups depending on the firefly vectors used (Table 2.4). Transfected HEK293T cells were then incubated at 37^{o}C and CO_2 for 24 hours. After transfection, 24-well plates were coated with S100B (10µg/ml), control-BSA or AGEs-BSA (200µg/ml) prepared in 0.05M bicarbonate buffer at 4^{o}C for 24 hours (500µl/well).

Table 2.4: Transfection group for dual luciferase reporter assay system.

Groups	Group 1	Group 2	Group 3	Group 4
***Renilla* luciferase**	pTK-*Ren*	pTK-*Ren*	pTK-*Ren*	pTK-*Ren*
Firefly luciferase	pGL3-Basic	pGL3-Control	pGL3-IL8-Luc	pNF-$_{K}$B -Luc

In the second stage, transfected HEK293T cells were washed once with DPBS and detached by incubating in 10mM EDTA prepared in DBPS at 37^{o}C and CO_2 for 5 minutes. Cells were collected in DPBS and centrifuged at 500 g at room temperature. The cell pellet was re-suspended in 2% FBS-DMEM growth media and counted. The transfected cells were then plated at a density of 40x10^{3} cells/well onto plates coated with the control proteins (S100B, normal BSA or AGE-BSA) or wells containing ECM from ARPE19 cells transfected with wild-type or SFD-mutant TIMP3. The plates were then incubated for 12, 24, 48 or 72 hours at 37^{o}C and 5% CO_2. Finally, following incubation and when cells were no more than 95% confluent, the growth medium was removed and the cells washed once with DPBS (500µl/well). 100µl of passive lysis buffer was dispensed into each well and then the plates incubated at room temperature for 15 minutes with gentle shaking. The cell lysates were transferred to a microcentrifuge tube and frozen at -80^{o}C or directly used in the reporter assay. For the luciferase reporter assay, 20µl of each of the cell lysates was transferred to an opaque 96-well plate and 30µl of luciferase assay reagent II (LAR II) added to each well. The mixture was mixed gently by repeated pipetting two to three times and the firefly luciferase activity was measured using a SpectraMax 5Me microplate reader. Then, 30µl of Stop & Glo® Reagent was mixed gently with each sample and the *Renilla* luciferase activity measured using the same microplate reader.

2.2.3.7.2 Luciferase assay system

To examine the influence of WT.T3 and SFD-TIMP3 on RAGE signalling and confirm the results of dual luciferase reporter assays, the Luciferase assay system was conducted based on manufacturer's protocol. Like the Dual luciferase reporter assay, the luciferase assay was divided into three stages encompassing transient transfection of mammalian cells, treatment of transfected cells and luminescence signal measurement in cell lysates.

Firstly, HEK293T cells were seeded into 24-well plate at a density of $4x10^4$ per well in 2% FBS-supplemented DMEM growth medium for 24 hours prior to transfection. The next day, cells were transfected with the desired DNA plasmids using *Trans*IT-LT1 transfection reagent. The transfection was performed with three DNAs encompassing pGL4-*luc2P*/NF-$_K$B, RAGE and pcDNA3-TIMP3 (WT/SFD mutant), and divided into four groups depending on the type of TIMP3 plasmids used per well (triplicate wells for each tested transfection TIMP3 DNA) (Table 2.5).

Secondly, 24 hours post-transfection, transfected cells were incubated for another 24 hours. Following 24 hours of treatment, all transfected cell groups were washed once with DPBS and the provided 1X lysis buffer was added directly to cells (110µl per well). The plate was gently rocked to ensure complete distribution by the lysis buffer and then cells were scraped and collected in a microcentrifuge tube. The cell lysate tubes were placed on ice for 5 minutes following by a short vortex and then centrifugation at 4°C and 12,000g for 2 minutes. The supernatant was transferred to a new tube which could be either stored at -80°C or immediately used to measure luminescence signals.

In the third stage, an opaque 96-well plate was utilised to prevent the luminescence from affecting adjacent wells. 20µl of cell lysate was added to each well of a 96-well plate and mixed carefully with 30µl of the luciferase assay reagent to prevent bubbles. The measurement of luminescence signals was performed using a SpectraMax 5Me microplate reader.

Table 2.5: Transfection groups for luciferase assay system.

Groups	Group 1	Group 2	Group 3	Group 4
DNA plasmid	pGL4-*luc2P*/NF-$_{K}$B	pGL4-*luc2P*/NF-$_{K}$B	pGL4-*luc2P*/NF-$_{K}$B	pGL4-*luc2P*/NF-$_{K}$B
	RAGE	RAGE	RAGE	RAGE
	WT.TIMP3	E139X-TIMP3	S181C-TIMP3	SplT3.Mutant

Chapter 3: Characterisation of TIMP3 mutant variants

3.1 Introduction

Many of the TIMP3 mutations have been examined and shown to result in TIMP3 dimers/multimers, decreased TIMP3 turnover and accumulation of TIMP3 in the ECM (Langton *et al.* 2005). Despite these biochemical characteristics, mutant TIMP3 protein is still a functional MMP inhibitor (Langton *et al.* 1998, Langton *et al.* 2005, Saihan *et al.* 2009). This strongly implicates TIMP3 dimerisation in the SFD phenotype. However, four missense mutations and a splice site mutation in the TIMP3 gene have also been reported to cause SFD, including a Ser15Cys in exon 1, Tyr128Cys, Tyr154Cys and Ty159Cys in exon 5, and a splice site mutation caused by a single adenosine insertion at the intron4/exon5 junction site (Fung *et al.* 2013, Gliem *et al.* 2015, Schoenberger and Agarwal 2012, Tabata *et al.* 1998). The effect of these four missense mutations on the TIMP3 protein has yet to be determined, however the splice site mutation was previously shown in our lab to give rise to several splice variant mRNA species and a protein with high molecular weight (Alsaffar 2011) when expressed in COS-7 cells. Nevertheless, this is quite an artificial non-human expression system mediated by episomally replicated vector and it was deemed important to examine the consequence of these mutations on TIMP3 protein produced by human retinal pigment epithelial cells, as these are the source of the protein in the retina. If any of these mutations failed to dimerise/multimerise it would cast great doubt on the hypothesis that this is a prerequisite for the disease process.

The hypothesis of this chapter is that TIMP3 dimerisation/multimerisation is a prerequisite for the SFD phenotype. Hence the initial aim is to confirm the common molecular characteristics of the Ser15Cys, Tyr128Cys, Tyr154Cys, Tyr159Cys and splice site mutations and, for the splice site mutation, to relate this to mRNA produced. SFD patients' samples were not available; therefore, this aim would be achieved by creating and expressing mutant gene constructs in retinal cells (ARPE19).

3.2 Methods

3.2.1 Creation of SFD-*TIMP3* gene constructs

3.2.1.1 Creation of S15C, Tyr128Cys, Tyr154Cys and Tyr159Cys

SFD-TIMP3 gene constructs encompassing S15C, Y128C, Y154C and Y159C were created using the QuikChange II site-Directed mutagenesis kit. The PCR mutagenesis reaction was applied as described in section 2.2.1.1.3 but using pcDNA3-WT-TIMP3-V5-KDEL as a DNA template instead of pcDNA3-WT-TIMP3 and primers listed in section 2.1.9. pcDNA3 is a mammalian expression vector that contains the cytomegalovirus (CMV) promoter upstream of a multiple cloning site for insertion of the cDNA of interest, together with antibiotic resistance markers. These resistances markers include ampicillin and neomycin allowing selection in bacterial and mammalian cells, respectively.

3.2.1.2 Creation of the splice site mutation construct

Synthetic TIMP3 gene constructs with and without the splice site mutation had previously been prepared in our laboratory. Briefly, an artificial TIMP3 gene was synthesised commercially by Eurofins MWG Operon, which contained a splice site mutation at the intron4/exon5 junction. Since the complete TIMP3 gene is very large (approximately 61kb), the construct omitted the first 3 introns that would not be expected to affect splicing at the intron4/exon5 site, reducing the overall size to 5.4kb. In order to reduce synthesis costs, the gene was synthesised in two parts. The first part of the gene, named T3spl1 (2.8kb in size), consisted of exons 1, 2, 3, 4, all of intron 4 and the coding region of exon 5 up to the natural EcoRI site in the untranslated region. The second part, named T3spl2 (2.6kb), contained the rest of untranslated region of exon 5 (Figure 3.1 & 3.2, Appendix 1). T3spl1 included XhoI, HindIII and EcoRV restriction sites at the 5' end and EcoRI and NotI sites at the 3' end, whilst the T3spl2 had SalI and EcoRI sites at the 5' end and NotI and EcoRV sites at the 3' end. Both synthesised parts (T3spl1 and T3spl2) were delivered in pBlueScript II SK (+), a cloning vector.

T3spl1 was subcloned into the pcDNA3 mammalian expression vector by restricting the cDNA and pcDNA3 vector with HindIII and NotI, followed by ligation, mini-preps and sequence verification (sections 2.2.1.2, 2.2.1.4 & 2.2.1.9). This construct was named T3spl1-M and contained the complete coding sequence but without the full exon 5 sequence. An equivalent wild-type gene construct was then made from this construct using the

Quikchange® Site-Directed mutagenesis kit with primers that removed the aberrant adenosine residue and named T3spl1-WT. Full length gene constructs were then made from these two clones by restricting them with EcoRI and NotI and ligating in similarly restricted T3spl2, excised from pBlueScript. Again mini-prep DNA was prepared and the sequence verified. These full-length gene constructs were named SplT3.WT and SplT3.M corresponding to wild type and mutant gene respectively.

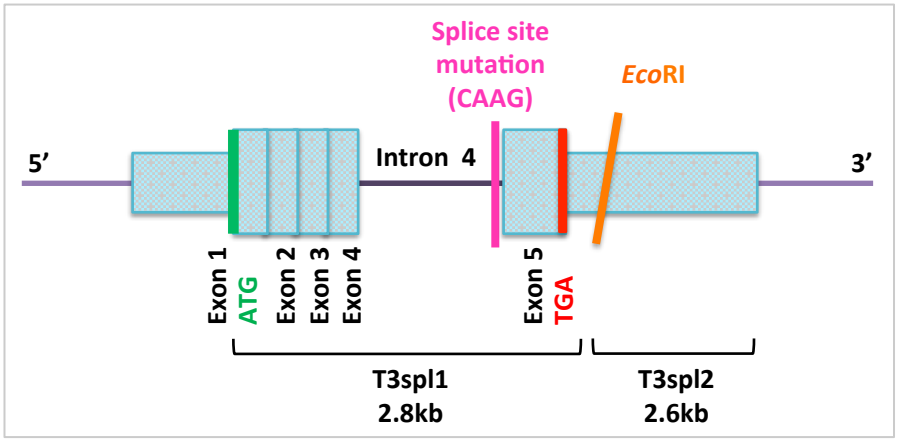

Figure 3.1: Synthetic TIMP3 gene containing the splice site mutation.

The wide pale blue boxes represent coding exons and narrow pale blue boxes represent non-coding exon sequence.

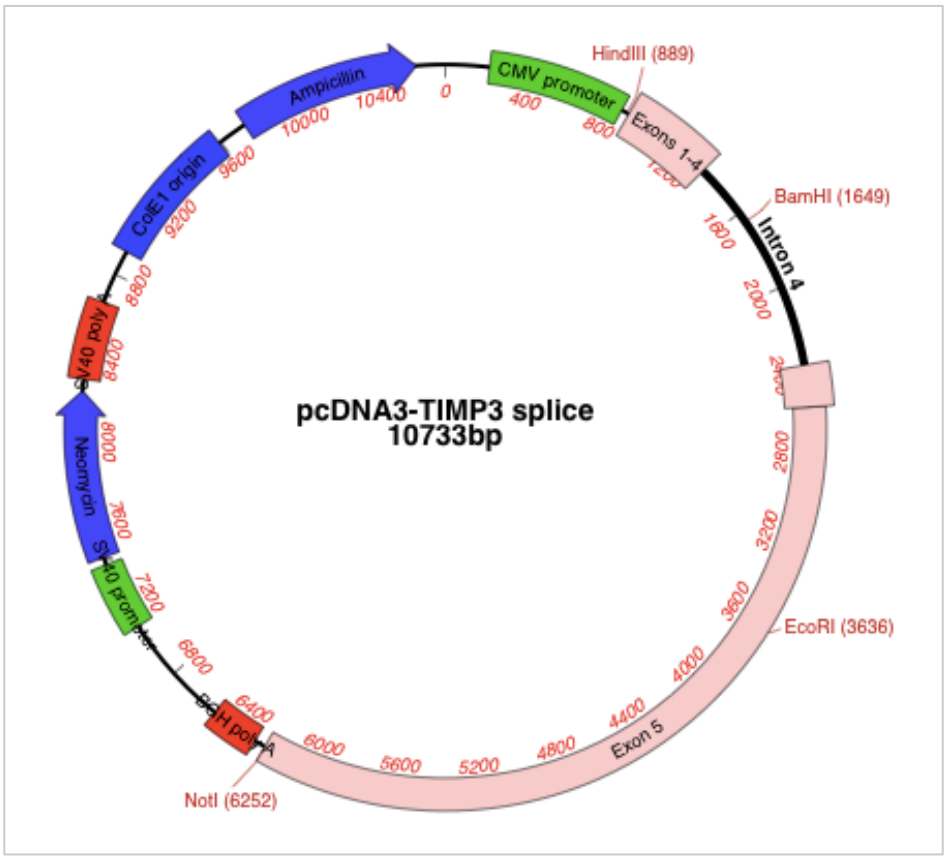

Figure 3.2: Synthetic TIMP3 gene construct map.

The vector map illustrates the structure of the pcDNA3-splice site-construct. The key features included TIMP3 exons (Exon 1-4 and Exon 5) shown in pink enclosing splice mutation in intron 4, unique restriction sites shown in red.

3.2.1.3 Transfection of mammalian cells

In order to examine expression of the S15C, Y128C, Y154C and Y159C -TIMP3 and the splice-site-TIMP3 mutations, TransIT-LT1 transfection reagent was used to transiently or stably transfect either COS-7 or ARPE19 cells respectively with the various DNA constructs. According to manufacturer's instruction, transfection was conducted as explained in section 2.2.2.9 in 10cm tissue culture dishes (COS-7 cells) or 6 well plates (ARPE19 cells) when the cells became 50-70% confluent. Following transfection, whole cell lysates and ECM proteins were prepared as described in sections 2.2.3.1.1 & 2.2.3.1.2 to analyse in western blotting using equal protein concentrations (sections 2.2.3.2 & 2.2.3.3).

3.2.2 cDNA synthesis for the splice site mutation

3.2.2.1 Amplification PCR

Polymerase chain reaction (PCR) was performed to amplify SplT3.WT and SplT3.M cDNAs using Taq DNA polymerase 2x Master Mix according to the manufacturer's protocol (section 2.2.1.1.1), and specific oligonucleotides primers (section 2.1.9, Table 3.1). The components of the PCR reaction were gently mixed and then briefly centrifuged to collect liquid to the bottom of the eppendorf. This reaction produced PCR products with 3'deoxyadenosine overhangs that allow direct cloning into TOPO TA cloning vectors according to the manufacturer's protocol explained in section 2.2.1.15.

Table 3.1: Taq polymerase amplification reaction.

Thermocycling condition
Initial denaturation: 95°C for 30sec 55°C for 1min 65°C for 2min
35 cycles: 94°C for 20sec 60°C for 1min 65°C for 2min
Final extension: 65°C for 10min
Store 10°C

3.2.3 Splice site-cDNA gene constructs

3.2.3.1 Creation of splice-site cDNA constructs

Phusion Hot Start Flex™ 2x master mix was used as described in section 2.2.1.1.2 and figure 2.1, to generate cDNA splice variants identified from the Taq PCR products, but without the errors that were apparent from the use of that enzyme.

Using the SplT3.M maxiprep as template DNA, two separate reactions amplified the sequence of exon 1 to 4 (E1-4) and novel exon 5 (E5) sequence of each splice product, using primers that overlapped about the novel splice acceptor sites (section 2.1.10 & 2.2.1.1.2). The PCR products of these first reactions were run on agarose gels and bands with the correct sizes purified and utilised in a second PCR reaction. Then, the second PCR products were ligated into pcDNA3 vector following by transformation of α-Selected Gold Competent cells and plasmid DNA isolation as described earlier in sections 2.2.1.3 & 2.2.1.5. Extracted DNA was sequenced using T7 forward primer to check its quality, and then used to transfect mammalian cells to test protein expression.

3.3 Results

3.3.1 Characterisation of TIMP3 missense mutations

3.3.1.1 S15C, Y128C, Y154C and Y159C TIMP3 cDNA construct creation and expression

SFD-TIMP3 gene constructs comprising S15C, Tyr128Cys, Tyr154Cys and Tyr159Cys were sequenced using T7 forward primer to confirm successful mutagenesis (Figure 3.3).

Western blotting of the whole cell lysates was performed to investigate whether the above-mentioned missense mutations would form dimeric TIMP3. Blots revealed that all cells, SFD-TIMP3 transfected, expressed a monomeric TIMP3 at 22kDa. In addition, a dimeric TIMP3 variant at ~48kDa was observed only in the non-reduced blot of SFD-TIMP3 transfected cells; upon reduction the 48kDa proteins disappeared and gave intense monomeric proteins at 22kDa (Figure 3.4).

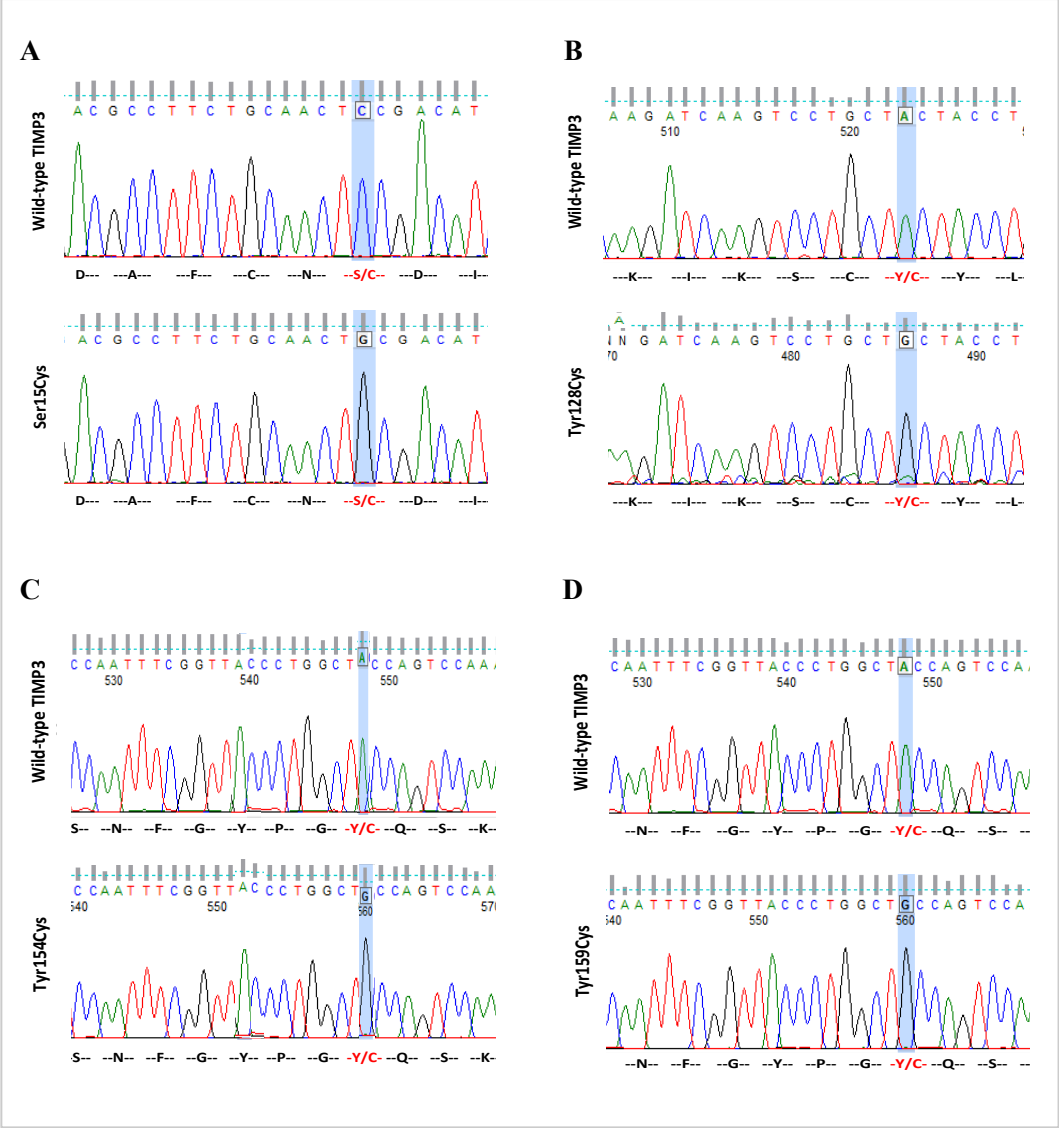

Figure 3.3: Automated sequencing SFD-TIMP3 mutant gene constructs.

The chromatograms illustrate part of sequencing data of exon 5 in Wild-type TIMP3 against SFD-TIMP3 including (A) Ser15Cys, (B) Tyr128Cys, (C) Tyr154Cys and (D) Tyr159Cys that have a single cytosine or adenine base substituted with a guanine base; and their corresponding protein sequences in which the substituted amino acids are shown in red font.

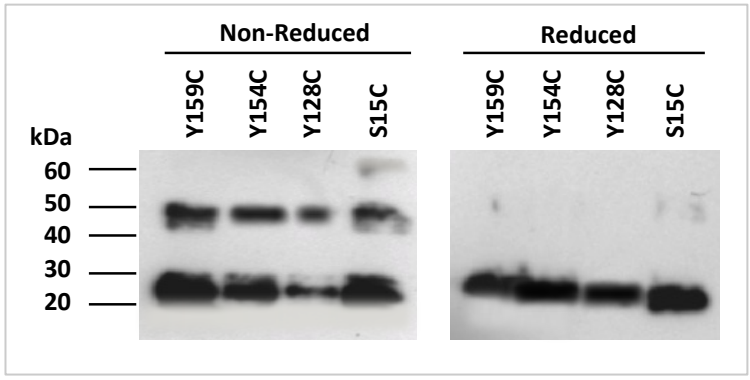

Figure 3.4: Western blotting of whole cell lysate from ARPE19 transfected with SFD-TIMP3 gene constructs.

The figures illustrate western blotting analysis of whole cell lysates from AREP19 cells transfected with the designated SFD-TIMP3 mutant proteins and probed with anti-V5 epitope tag monoclonal antibody. All transfected cells expressed a protein at approximately 22kDa, corresponding to monomeric TIMP3, and a higher molecular mass protein at approximately 50kDa, corresponding to TIMP3 dimer, on non-reduced gels. Upon reduction the 50kDa band reduced to 22kDa.

3.3.2 Characterisation of TIMP3 splice acceptor site mutation

3.3.2.1 Splice site gene construct creation and expression

Splice site WT and splice site mutant gene constructs were sequenced using nine sequencing primers that cover the whole splice construct sequence (primers listed in section 2.1.10) to confirm either the absence or presence of splice mutation and to check the quality of the rest of sequences (Figure 3.5).

Western blotting of ECM from ARPE19 cells revealed the presence of a level of endogenous TIMP3 at 22 and 28kDa that correspond to the previously reported unglycosylated and *N*-glycosylated TIMP3, respectively. ARPE19 cells transfected with WT-TIMP3 and splice-WT resulted in intense bands at 22kDa and 28kDa in both non-reduced and reduced gels compared to un-transfected cells. S181C-TIMP3 was used as a mutant positive control and was shown to express an additional band at 48kDa that reduced to 22kDa. In contrast the splice-mutant transfected cells gave rise to novel bands at approximately 15, 30 and 60kDa in non-reduced gels. Upon reduction the 30 and 60kDa bands disappeared and there was a concomitant increase in intensity in the 15kDa band, indicating that the 30 and 60kDa may be dimeric or multimeric forms, respectively (Figure 3.6).

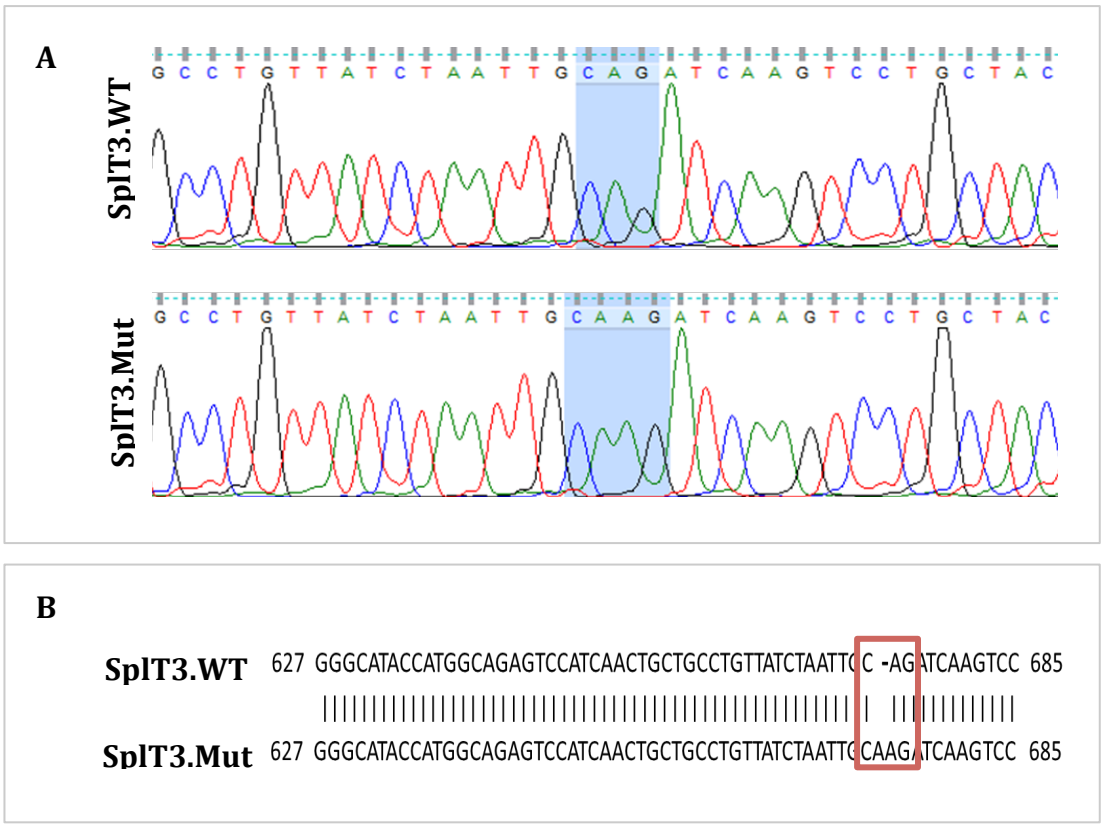

Figure 3.5: Atuomated sequencing of SpIT3 -WT and -Mutant gene constructs.

(A) The chromatograms illustrate part of sequencing data of intron 4/exon 5 in both SpIT3.WT and SpIT3.M; the mutant has a single adenosine base inserted at the intron 4/exon5 junction site. (B) Sequencing alignment of SpIT3.WT and SpIT3.Mutant shows the presence of the desired splice-site mutation, in red square, converting it from CAG to CAAG.

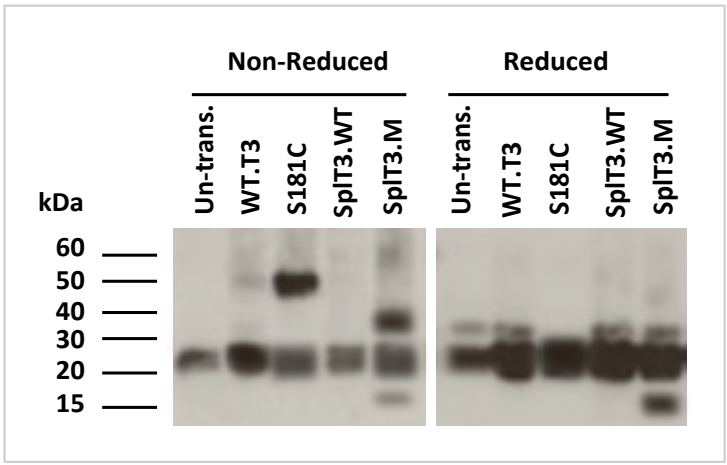

Figure 3.6: Western blotting of the ECM from ARPE19 transfected with SpIT3.WT and SpIT3.M gene constructs.

The figures demonstrate western blotting analysis of ECM from AREP19 cells either un-transfected or transfected with wild type TIMP3 (WT.T3), Ser181Cys (S181C) and SpIT3.WT and SpIT3.Mutant (SpIT3.M), probed with polyclonal anti-TIMP3 antibody. All cells showed endogenous TIMP3 at 22kDa, whereas S181C and SpIT3.M showed additional higher molecular weight proteins at 50kDa and 30 and 60kDa, which reduced to 22 and 15kDa, respectively.

3.3.2.2 Identification of the splice site cDNA products

In order to investigate mRNA transcripts from cells transfected with SplT3.WT and SplT3.Mutant constructs, total RNA was isolated and polymerase chain reaction (PCR) was performed to amplify SplT3.WT and SplT3.Mutant cDNA as described in sections 3.3.1.6.1-2 & 3.

A non-denaturing agarose gel was run to examine the quality of the extracted RNA (DNAse treated RNA samples); and showed two bands corresponding to large (28S) and small (18S) ribosomal RNA (rRNA) subunits that confirmed RNA integrity and lack of any significant genomic DNA contamination (Figure 3.7 A). N.B. the markers are a DNA ladder used in order to confirm proper running of the gel and cannot be used to determine the size of non-denatured RNA.

cDNAs were prepared from both ARPE19 and COS-7 transfected cells by reverse transcription and then amplified by PCR using Taq polymerase at an annealing temperature of 64.4°C using 5' primer that binds to the N-terminus of TIMP3 and a 3' primer that binds to the end of exon 5 just upstream of the polyadenylation site. The reactions were analysed on agarose gels which showed that SplT3.WT gave rise to one predominant product between 600-800bp and the SplT3.Mutant at least four bands at 1kb, 1.5kb, 2.5kb and 4kb (Figure 3.7 B & C). The PCR products from both wild type an mutant constructs were excised, and mutant PCR products were re-amplified using the same thermocycler conditions to increase the yield, shown in figure 3.10 D. All PCR products were then cloned into the TOPO vector to enable DNA sequencing.

Subsequently a 96 well plate of isolated miniprep plasmids was prepared for sequencing using a universal primer (T7 forward) that binds to the TOPO vector. Automated sequencing revealed the presence of a single WT product and five mis-splicing products with proper donor and splice acceptor sites. All the mutant products were shown to splice into exon 5 downstream of the normal acceptor site in non-coding regions (Figure 3.8 A & B). There were also some PCR products with non-consensus splice sites or only a short sequence of exon 5, which were presumed to be artefacts. The identified mutant splice products were translated and seen to give rise to five predicted novel C-terminal sequences S1, S2, S3, S4 and S5 (Figure 3.8 C & 3.9), several with potentially unpaired Cys residues. NB One of the Cys residues that forms part of the C-domain of TIMP3 is coded from exon 4 so that exon 5

sequences that lack a Cys residue would potentially also result in an unpaired Cys in the expressed protein.

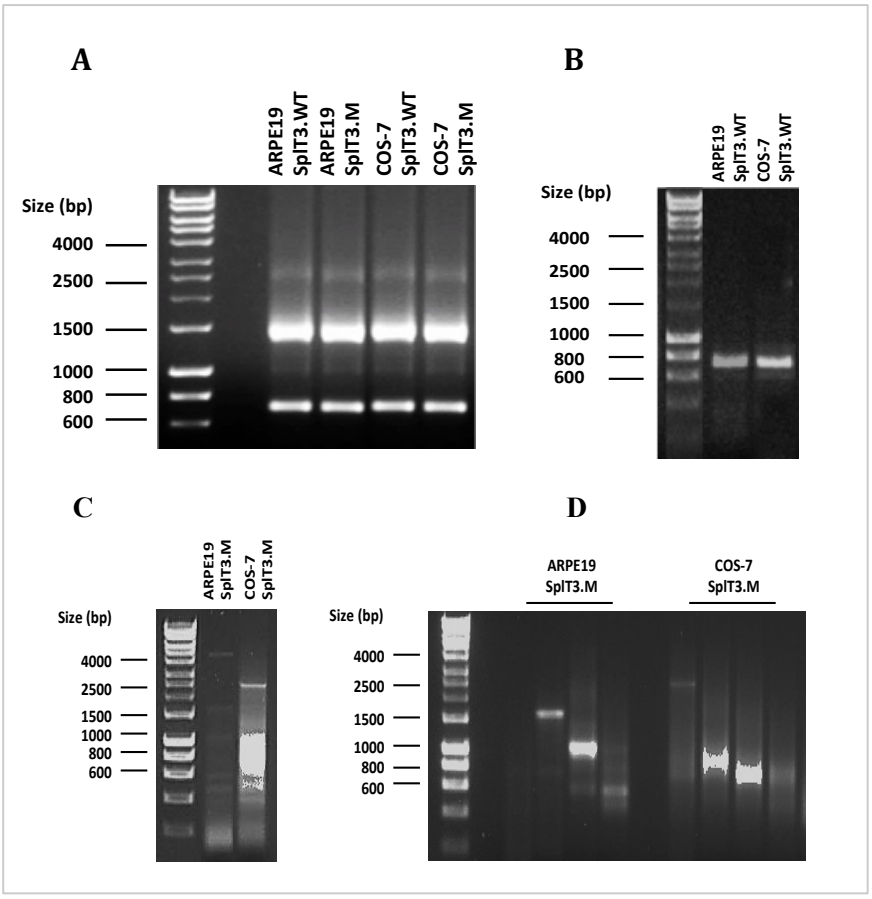

Figure 3.7: Agarose gel electrophoresis of splice site RNA and Taq PCR products.

(A) Non-denaturing agarose gel electrophoresis of RNA samples, the two bands correspond to the large and small rRNA subunits (28S and 18S, respectively) and confirm RNA integrity with no obvious genomic DNA contamination (both ARPE19 and COS-7 cells show identical bands). (B) & (C) Taq PCR products of wild type and mutant splice constructs, respectively. (D) Electrophoresis of repeat Taq PCR of mutant products in (C).

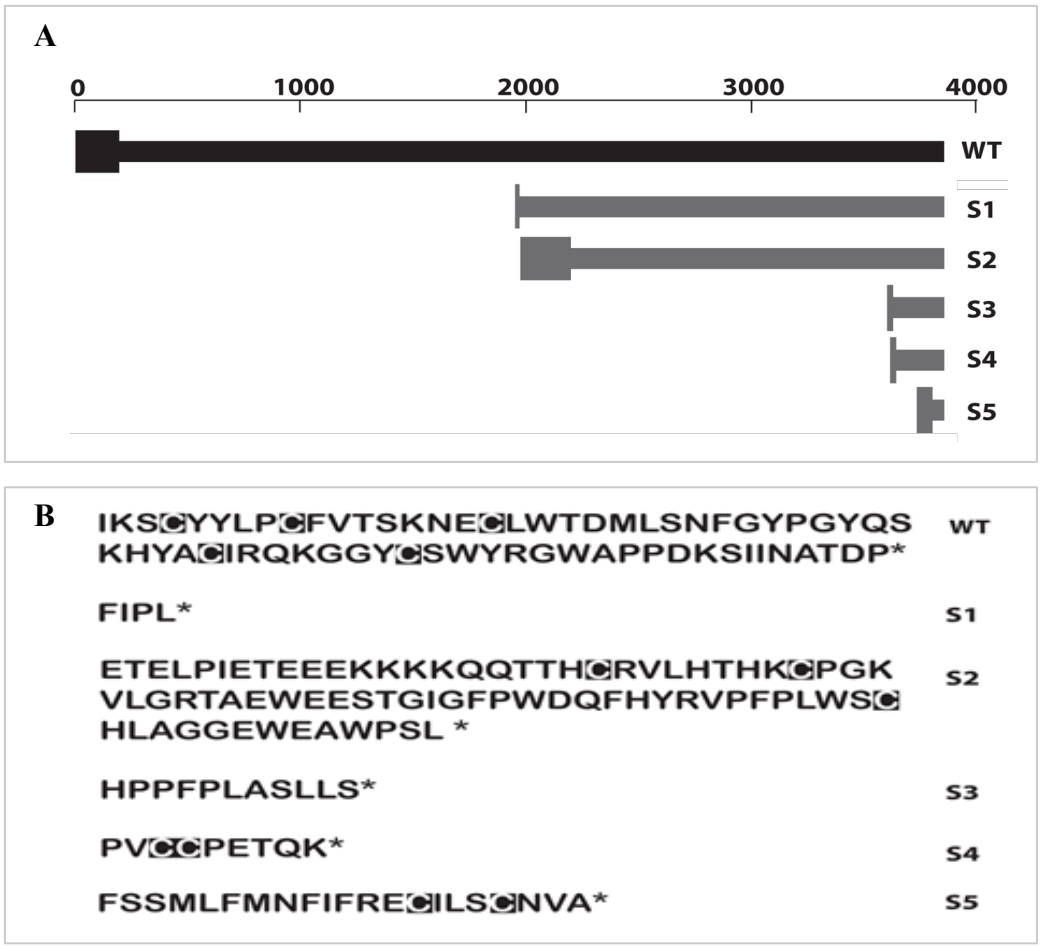

Figure 3.8: Identification of splice site cDNA products.

(A) Splicing sites of TOPO cloned PCR products identified using BLAT (UCSC genome browser), as shown above each PCR product has a splice acceptor site that differs from the normal site. All these new splice acceptor sites lie within the non-coding region of exon 5. (B) Protein sequence of splice cDNA products.

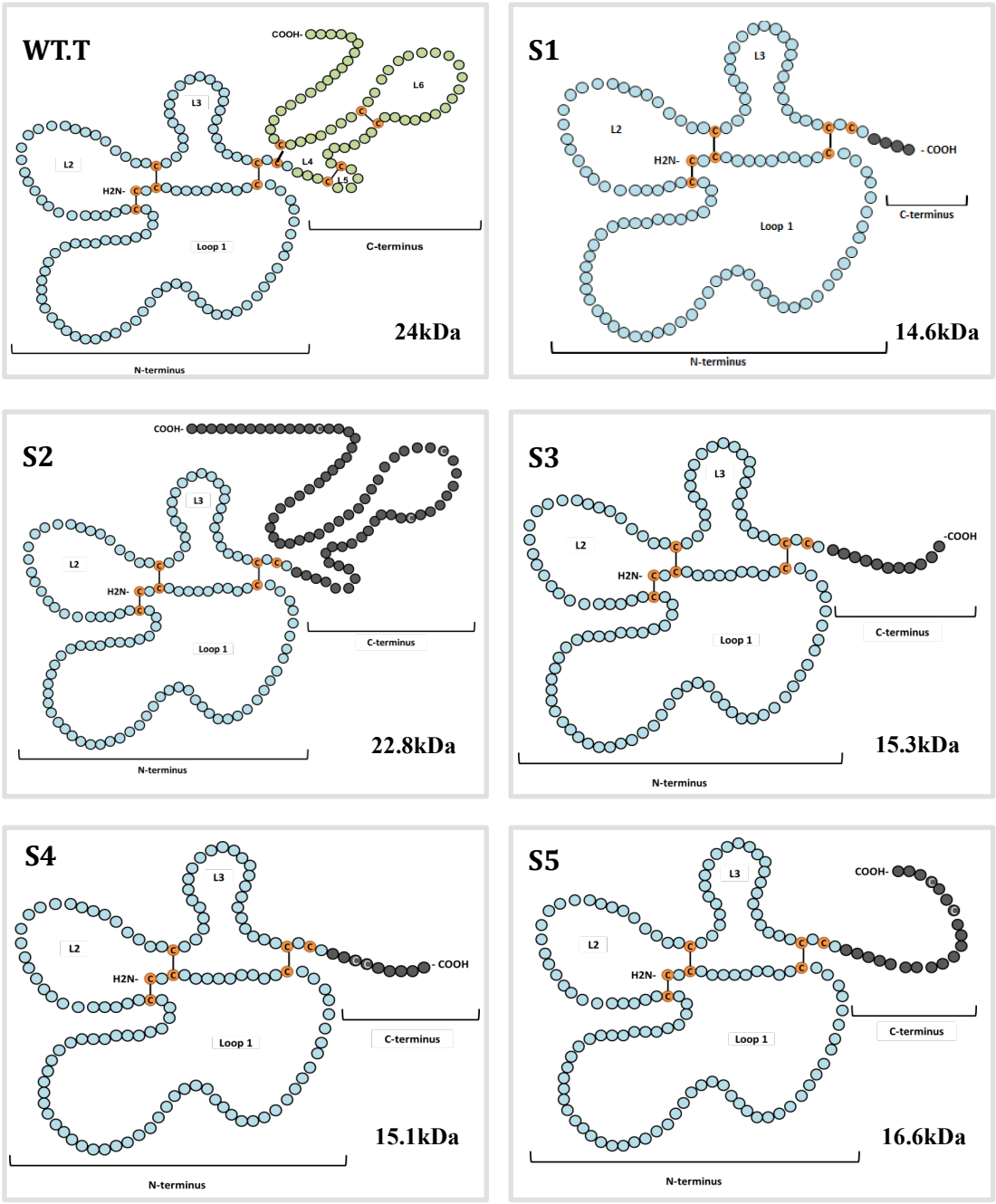

Figure 3.9: Illustration of the potential primary structures of the splice cDNA products.

Representation of amino acid composition of the splice site mutant products, including S1, S2, S3, S4 and S5, that spliced into the non-coding region of exon 5 resulting in potentially novel amino acid sequences (dark grey circles).

3.3.2.3 Creation of the splice site cDNA constructs and expression

All the splice mutant products identified from COS-7 and ARPE19, including S1, S2, S3, S4 and S5 (shown in Figure 3.9), were produced without any PCR errors using SplT3.M as template DNA and Phusion Hot Start Flex 2x master mix.

The created splice mutant products were purified, digested with *Hin*dIII and *Not*I; and then utilised in a ligation reaction with similarly cut pcDNA3 to give splice mutant product-constructs which were named SplT3.M.S1, SplT3.M.S2, SplT3.M.S3, SplT3.M.S4 and SplT3.M.S5. These five constructs were digested with *Hin*dIII and *Not*I to confirm the presence of the desired inserts and subsequently sequenced (Figure 3.10).

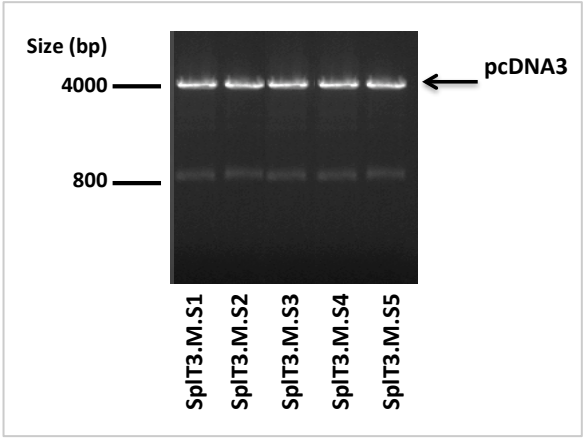

Figure 3.10: Splice cDNA gene constructs.

The figure demonstrates restriction digest of the splice constructs with HindIII and NotI to confirm the presence of splice created products. All splice constructs showed a product of approximately 800bp indicating the presence of the desired inserts.

Following creation of splice constructs, COS-7 and ARPE19 cells were transfected using TransIT-LT1 reagent with maxiprep plasmids of SplT3.WT, SplT3.M, SplT3.M.S1, SplT3.M.S2, SplT3.M.S3, SplT3.M.S4 and SplT3.M.S5 constructs (section 2.14). Whereas ECM proteins were prepared from COS-7 plates 72 hours post transfection, transfected ARPE19 cells were selected with Geneticin in 25cm^2 flasks until confluent, prior to seeding onto 10cm tissue culture plates for 10 days and then harvesting the ECM.

ECM proteins from both COS-7 and ARPE19 were isolated and quantified by BCA protein assay. Western blotting with anti-TIMP3 was performed using equal amounts of ECM proteins of SplT3.M.S1, S2, S3, S4 and S5 from either COS-7 or ARPE19, in which both cell lines exhibited similar results. All splice transfected cells showed a level of endogenous TIMP3 species at 22kDa corresponding to un-glycosylated TIMP3 on both non-reduced and reduced blots. However, only two splice cDNA products showed a high molecular mass species on non-reduced blots, SplT3.M.S1 and SplT3.M.S5. SplT3.M.S1 expressed additional species at approximately 30 and 60kDa in the non-reduced blot and upon reduction they disappeared and gave rise to a 15kDa protein which was considered to be the monomer form of a mutant protein. The other splice product, SplT3.M.S5 expressed two novel protein species at approximately 30 and 50kDa in the non-reduced blot; however only the 30kDa band completely disappeared on the reduced blot with the appearance of an ~15 kDa band (Figure 3.11 A & B).

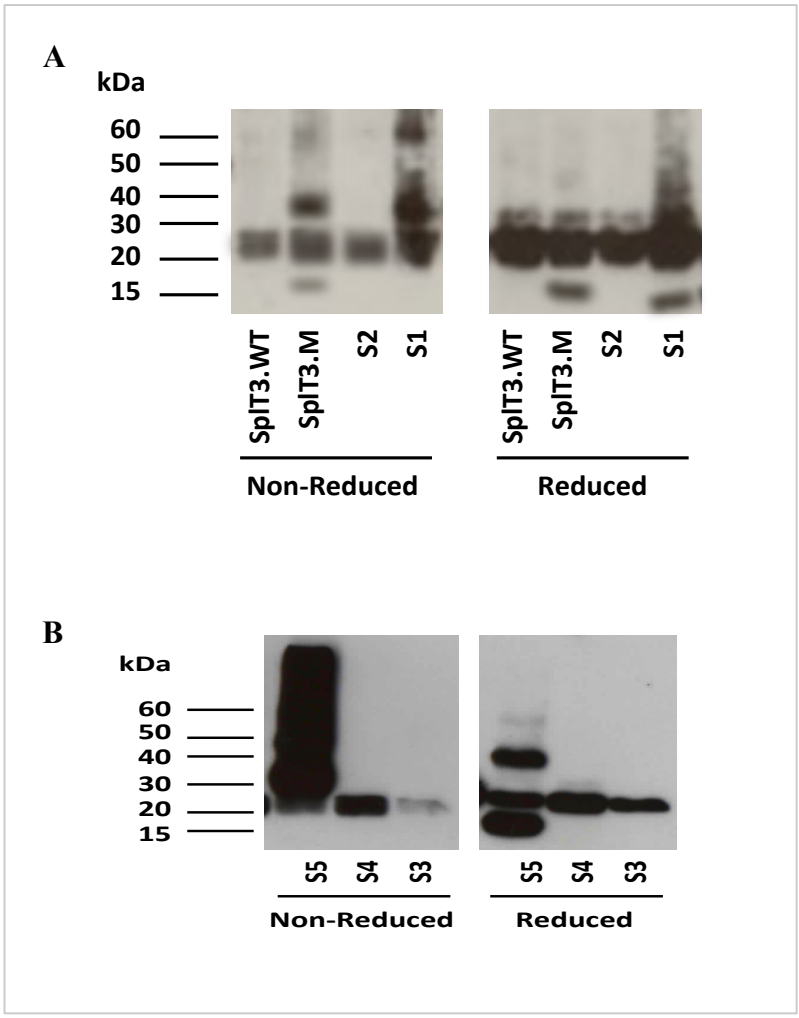

Figure 3.11: Western blotting of the ECM from ARPE19 transfected with splice cDNA gene constructs.

The figures demonstrate western blotting of ECM from AREP19 cells transfected with splice wild type TIMP3 (SpIT3.WT), splice mutant TIMP3 (SpIT3.M) and splice cDNA gene constructs including S1, S2, S3, S4 and S5, probed with polyclonal anti-TIMP3 antibody. All cells transfected with splice wild type and mutant TIMP3 constructs expressed endogenous level of TIMP3 at 22kDa. (A) S1 showed additional protein species at 30 and 60kDa that reduced to 15 and 22 kDa proteins and resemble the protein species from the original splice construct (SpIT3.M). (B) S5 also showed additional proteins species at 30 and 50kDa in non-reduced condition, and 15 and 50kDa under reduced condition.

3.4 Discussion

As outlined earlier, all of the SFD mutations examined to date had been demonstrated to result in TIMP3 dimerisation/multimerisation and retain their ability to inhibit MMPs but with impaired turnover in the ECM relative to the normal protein (Langton *et al.* 2000). This led to the hypothesis that accumulation of TIMP3 dimers/multimers is a causative factor in the disease. However, five TIMP3 SFD mutations have been identified but not examined for protein expression and dimer formation. Two of these are unusual mutations and include a mutation in the N-terminal domain (Ser15Cys) and a splice site mutation, caused by a single adenosine insertion at the intron4/exon5 acceptor site (CAG to CAAG) and could potentially challenge this hypothesis.

Here we confirm that all of the missense mutations that result in a change to a Cys residue do indeed appear to form dimers as non-reduced western blotting of the whole cell lysates from ARPE19 cells transfected with Tyr128Cys, Tyr154Cys, Tyr159Cys and Ser15Cys revealed anti-TIMP3 antibody-reactive bands at approximately 22kDa and 48kDa. In all cases the 48kDa band disappeared upon reduction, with a concomitant increase in intensity of the 22kDa band, strongly indicative of disulphide bonded TIMP3 dimer formation in all cases. In most cases the bands appeared as doublets indicative of glycosylated and non-glycosylated forms of the protein.

As outlines in Chapter 1, the effect of the splice site mutation is unpredictable, with possibilities including exon skipping, intron retention and activation of cryptic acceptor sites. Western blotting of the SplT3.M construct form ARPE19 cells gave rise to novel TIMP3 species at ~15, 30 and 60kDa in the non-reduced blot that were not present in the SplT3.WT control. The 30 and 60kDa species are likely disulphide bonded dimer/multimeric mutant protein because they appeared to be absent in the reduced blot, and the intensity of the 15kDa band increases, relative to the 22kDa TIMP3 band upon reduction. The presence of the 15kDa band in the non-reduced gel might be indicative of incomplete dimerisation of the mutant or it could be an additional cDNA product that was not identified, without any unpaired cysteine residues.

Sequencing of the various novel splice site products produced in either COS-7 cells or ARPE19 cells only showed evidence for mis-splicing into the non-coding region of exon 5 with the potential to translate into TIMP3 molecules with completely different C-domain

sequences compared to wild-type TIMP3 (Table 3.5, Figure 3.9). These novel C-domain sequences contain various numbers of Cys residues. Although all theoretical proteins could potentially result in TIMP3 dimerisation, S1, S3, S4 and S5 have an odd number of cysteine residues in the C-terminus. It is also possible that other splice mutant products might be present but were not successfully cloned.

Table 3.2: Analysis of splice cDNA mutant products.

cDNA product	SplT3.M. S1	SplT3.M. S2	SplT3.M. S3	SplT3.M. S4	SplT3.M. S5
Cell lines	COS-7	COS-7	ARPE19	COS-7 ARPE19	COS-7
Amino acid (w/o signal peptide)	127	197	134	132	143
Total number of Cys residues	7	10	7	9	9
Protein Size kDa	14.6	22.8	15.3	15.1	16.6
Dimer formation	Dimer	NO	NO	NO	Dimer

In order to determine whether any of the novel mRNA species cloned could actually produce TIMP3 protein dimers, constructs of splice mutant products S1, S2, S3, S4 and S5 were created and used to transfect COS-7 and ARPE19 cells. ECM from these cells was analysed by western blotting. Only two of the splice constructs, S1 and S5, gave rise to novel bands of the expected sizes for dimeric and monomeric forms of the protein on non-reduced and reduced gels respectively. S1 gave rise to novel bands at ~30 and 60kDa on the non-reduced blot and ~15kDa protein upon reduction, although the mobility of these bands did not seem to match the predominant novel dimers/monomers produced by the actual SplT3.M construct. In contrast S5 demonstrated novel bands at both 30 and 50kDa with some evidence for even higher MW products. This particular splice product potentially gives rise to a protein with three Cys residues in the C-domain, which could possibly concatermerize, resulting in

multimers of various sizes. Upon reduction at least some of the 50kDa band remained and the 30kDa band disappeared with a concomitant appearance of a novel 15kDa band but also a relative enhancement of the 22kDa band corresponding to wild-type TIMP3. The ~50kDa band could be a multimer form of the mutant protein that did not completely reduce to the 15kDa species or a heterodimer of mutant and wild-type TIMP3. The latter possibility is supported by the fact that the 22kDa band increases in intensity following reduction. None of the other identified splice products (S2, S3 and S4), showed any evidence of expression at their expected sizes. It is possible that these cDNA sequences failed to express stable mRNA or their protein products were rapidly degraded and this is highly likely for the long nonsense protein sequence on the end of S2, which would almost certainly elicit degradation by the proteasome so that no functional protein would be produced. While it is inconclusive whether any of the mis-spliced mRNA species cloned explain the predominant dimers seen with the SplT3.M gene construct, undoubtedly the splice mutation can give rise to mutant dimers in ARPE19 cells. Expression of dimers from the splice construct was much less pronounced than for the other mutant TIMP3 species examined here and this is not surprising as splicing at secondary splice acceptor sites is likely to be less efficient and not all of the mis-spliced sequences are likely to be expressed. This reduced expression of TIMP3 dimers from the splice site mutation may well explain the significantly later age of onset of the disease in the Japanese families (Tabata *et al.* 1998).

Interestingly, all the predicted proteins have exon 5 sequences that are completely different from normal TIMP3. This would almost certainly affect their ability to inhibit VEGFR2 since the inhibitory activity of TIMP3 toward VEGFR2 has been localised to the C-terminal domain. This may well explain the choroidal neovascularisation observed in SFD. It is also possible that dimerisation at the C-domain prevents or impairs VEGFR2 binding for all the other SFD mutant proteins, even though they retain an essentially normal C-domain.

Chapter 4: The effect of SFD-TIMP3 on TACE and apoptosis

4.1 Introduction

As discussed in Chapter 1, TIMP3 has been reported to be pro-apoptotic due to inhibition of TACE, resulting in decrease shedding of death receptors including FAS, TNF-RI (tumour necrosis factor receptor-1) and TRAIL-RI (TNF-related apoptosis inducing ligand receptor-1) (Ahonen *et al.* 2003, Bond *et al.* 2002).

It has previously been shown that over-expression of wild-type or SFD-mutant TIMP3 in primary RPE cells by transient transfection with naked vector or using adenovirus resulted in increased apoptosis and that there was an apparent increase in cell death/apoptosis with SFD-TIMP3 relative to the wild-type protein (Majid *et al.* 2002). However, this study did not examine whether these cells were more prone to apoptosis induced by specific receptors/ligands, nor propose a mechanism by which mutant SFD proteins may increase the apoptotic response.

More recently it has been shown that under basal conditions, TACE (ADAM17) is predominantly present on the cell surface as a homodimer that binds TIMP3, maintaining TACE in the inactive form. Phosphorylation of the cytoplasmic domain of TACE, via the ERK or p38 MPAK pathways, results in dissociation of the dimers into monomers and the dissociation of TIMP3, thus enabling activation of TACE (Xu *et al.*, 2012). This raises the question as to what effect SFD mutation-induced dimer formation may have on this process. This report did not ascertain whether one or two molecules of TIMP3 bind to the TACE dimers. However, if the latter is the case, it is possible that TIMP3 dimers stabilise the TACE dimers through the increased avidity of bivalent binding, resulting in an apparent increase in TACE inhibition and thus, apoptosis.

It is hypothesised, therefore, that TIMP3 dimers may stabilise this TACE dimerisation leading to decreased activation and thus increased apoptosis of retinal cells in SFD. To test this hypothesis, the expression of TACE in ARPE19 and TIMP3-transfected ARPE19 cells was initially examined by SDS-PAGE and western blotting. Then, the sensitivity of untransfected ARPE19 and ARPE19 stably transfected with SFD-TIMP3 constructs cells to anti-Fas activating antibody induced apoptosis was tested by measuring caspase 3/7 activity using caspase 3/7 activity apoptosis assay kit. Finally, the ability of SFD-TIMP3 to stabilise TACE dimers was investigated by pull down assay and western blotting.

4.2 Methods

4.2.1 Transfection of ARPE19 cells

To investigate the influence of wild type and SFD TIMP3 on TACE, ARPE19 cells were stably transfected with pcDNA3-WT.T3, -E139X, -S156C, -H158R and -S181C using *Trans*IT-LT transfection reagent (described in section 2.2.2.9).

Untransfected or stably transfected cells were then seeded onto 10cm tissue culture dishes at a density of $10x10^6$/plate to check for TIMP3 protein expression and, once confirmed, cells were prepared for the apoptosis assay.

4.2.2 TACE expression by SDS-PAGE and western blotting

To examine TACE expression in retinal cells, untransfected and SFD-TIMP3 transfected ARPE19 cells were seeded at a density of $10x10^6$ /plate in 10cm tissue culture petri dishes and grown until they reached 80-90% confluence. Then, all cells were collected and stored at -80°C until lysed in RIPA lysis buffer for analysing in SDS-PAGE (10% or 7.5%) and western blotting (sections 2.2.3.1.1 & 2.2.3.3).

TACE was detected by incubating PVDF membrane in primary antibody polyclonal rabbit anti-TACE antibody at 1:2000 dilution overnight at 4°C in a shaker; and subsequently in secondary antibody which was swine horseradish peroxidase-conjugated anti-rabbit antibody at 1:10000. Separated proteins were observed using chemiluminescent substrate.

4.2.3 Caspase 3/7 activity apoptosis assay

The effect of wild type and SFD-TIMP3 on ARPE19 cell apoptosis was examined by measuring caspase 3/7 activity using Cell Meter ^{TM} Caspase 3/7 Activity Apoptosis Assay Kit. The apoptosis assay was performed as instructed by the manufacturer and described earlier in section 2.2.3.4.

4.2.4 TACE pull down assay

To investigate whether endogenous TACE dimers can be stabilised by binding to SFD-TIMP3, HaloTag mammalian pull-down and labelling systems kit was used in a similar way to section 2.2.3.6.

HEK293T cells were transfected with pHTC-HaloTag vectors including empty pHTC vector (negative control), pHTC-WT-T3 and pHTC-S181C. The pHTC-HaloTag vector contains a multiple cloning site upstream of the HaloTag cDNA sequence. These are expressed under the CMV promoter and the vector also contains the neomycin resistance cassette, allowing constitutive stable expression of proteins bearing a C-terminal HaloTag in mammalian cells. A C-terminal HaloTag was used, as this was least likely to affect the MMP-inhibitory function (and presumably TACE binding) of TIMP3 that is mediated through the N-terminal domain.

The expression of TACE and HaloTag constructs in HEK293T cells was confirmed prior to proceeding with the TACE pull down assay. As described in section 2.2.3.6, TACE pull down was accomplished in four stages comprising constructing HaloTag fusion vectors, transfecting HEK293T cells with HaloTag vectors, pull down and detecting Halotag fusion proteins by immunoblotting against polyclonal anti-TACE.

pHTC-WT.T3-Halotag and pHTC-S181C-HaloTag constructs (previously prepared in my supervisor's laboratory) were used to transiently transfect HEK293T cells in 6-well plates (see section 2.2.2.9 & Table 2.2). At 24 hours post transfection, cells were treated with PMA (0-25nM) for 30 minutes at 37℃ and then cells were harvested and handled as described in sections 2.2.3.6.1 & 2.2.3.6.2.

Another approach was also performed to pull down TACE in similar way as explained above except that a water-soluble and reducible crosslinker, DTSSP (3,3-Dithiobis sulfosuccinimidyl propionate), was used after PMA treatment. In brief, transfected cells were treated with PMA for 30 minutes at 37℃ and then washed in PBS. The next step was to incubate cells in 1mM DTSSP at 4℃ for 60 minutes, in which the reaction was then stopped by adding 1M Tris (pH 7.5) at a final concentration between 10-20mM for 15 minutes at room temperature. Finally, cells were handled as described sections 2.2.3.6.1 & 2.2.3.6.2.

4.3 Results

4.3.1 TACE expression in ARPE19 cells

The anti-TACE antibody detected two distinct species between 100-150kDa in all cells, either untransfected or transfected with WT.T3, E139X or S181C, which may correspond to inactive and activated forms of the molecule (Xu *et al.* 2012). A very minor band was also observed at approximately 90kDa, which may correspond to degradation products of the above or non-specific interaction with other proteins (Figure 4.1).

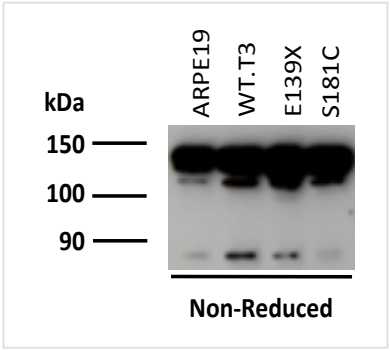

Figure 4.1: Western blot of TACE expression in ARPE19 cells.

Non-reduced western blot of cell lysates from untransfected ARPE19 cells or ARPE19 cells transfected with the pcDNA3-TIMP3 constructs indicated and probed using polyclonal anti-TACE antibody (1:2000).

4.3.2 Measuring Caspase 3/7 activity

To determine whether wild-type or SFD-TIMP3 increases the sensitivity of ARPE19 cells to induction of apoptosis, cells were stably transfected with WT.T3, E139X, S156C, H158R or S181C constructs, and analysed by western blotting to confirm TIMP3 expression and dimer formation in the SFD-TIMP3 transfectants. Cells were then treated with camptothecin (20μM) or anti-Fas activating antibody (at 10, 15 or 20 μg/ml) and caspase 3/7 activities from the cells measured using the Cell Meter Caspase 3/7 activity apoptosis assay kit (see section 2.2.3.5).

Initially caspase 3/7 activity was measured in complete growth medium. The first three experiments performed in complete growth medium showed insignificant differences between those cells expressing WT.T3 and those expressing SFD-TIMP3 for all treatments (Figure 4.2 A, B & C).

Subsequently the experiments were repeated but using serum depleted (2% FBS) "starvation" medium to grow and treat the cells. All untreated ARPE19 cell lines exhibited similar caspase 3/7 activities at 48 hours post seeding (Figure 4.3 A). At 24 hours, camptothecin treated cells exhibited increased caspase 3/7 activity compared to untreated cells; however SFD-TIMP3 transfected cells showed increased apoptosis relative to wild-type transfected cells and this was shown to be statistically significant for the E139X, S156C, H158R and S181C mutants (*P*-values: 0.0085, 0.0007, 0.0484 and 0.0016 respectively; Figure 4.3 B).

Similarly ARPE19 cells treated with anti-Fas for 24 hours also showed an apparent increase in caspase 3/7 activity in the SFD-mutant transfected cells relative to WT.T3 transfectants, although in this case this was only significant for the E139X and H158R mutants (Figure 4.3 C).

Taken together these data suggest that all of the SFD-mutants increase the sensitivity of ARPE19 cells to apoptotic induction, relative to wild-type TIMP3.

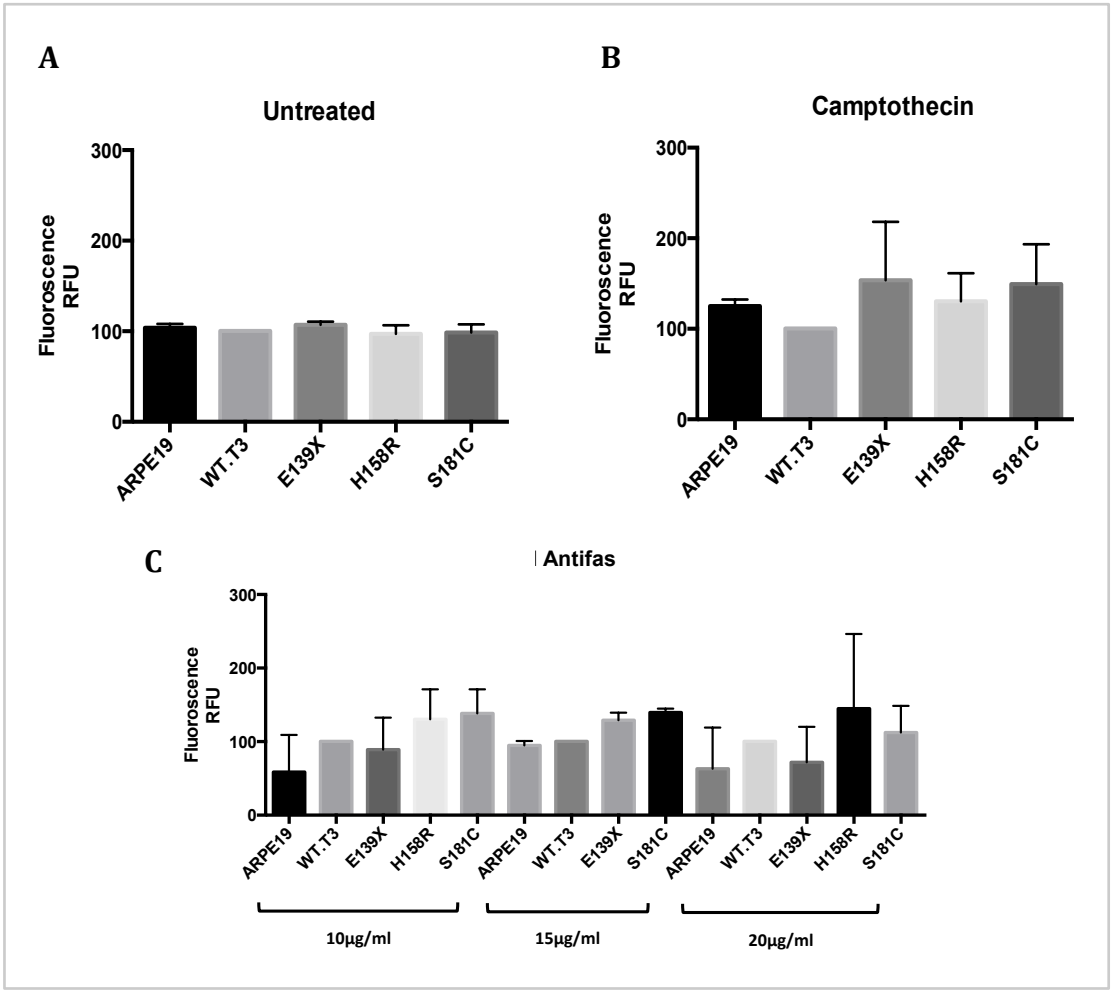

Figure 4.2:Caspase 3/7 activity in ARPE19 cells treated in complete growth medium.

Caspase 3/7 activity in: (A) untreated ARPE19 cells; (B) ARPE19 cells treated with camptothecin (20µM); (C) ARPE19 treated with anti-Fas activating antibody (at 10, 15 & 20 µg/ml). Data are means ± S.E. of triplicate experiments and analysed using one-way ANOVA.

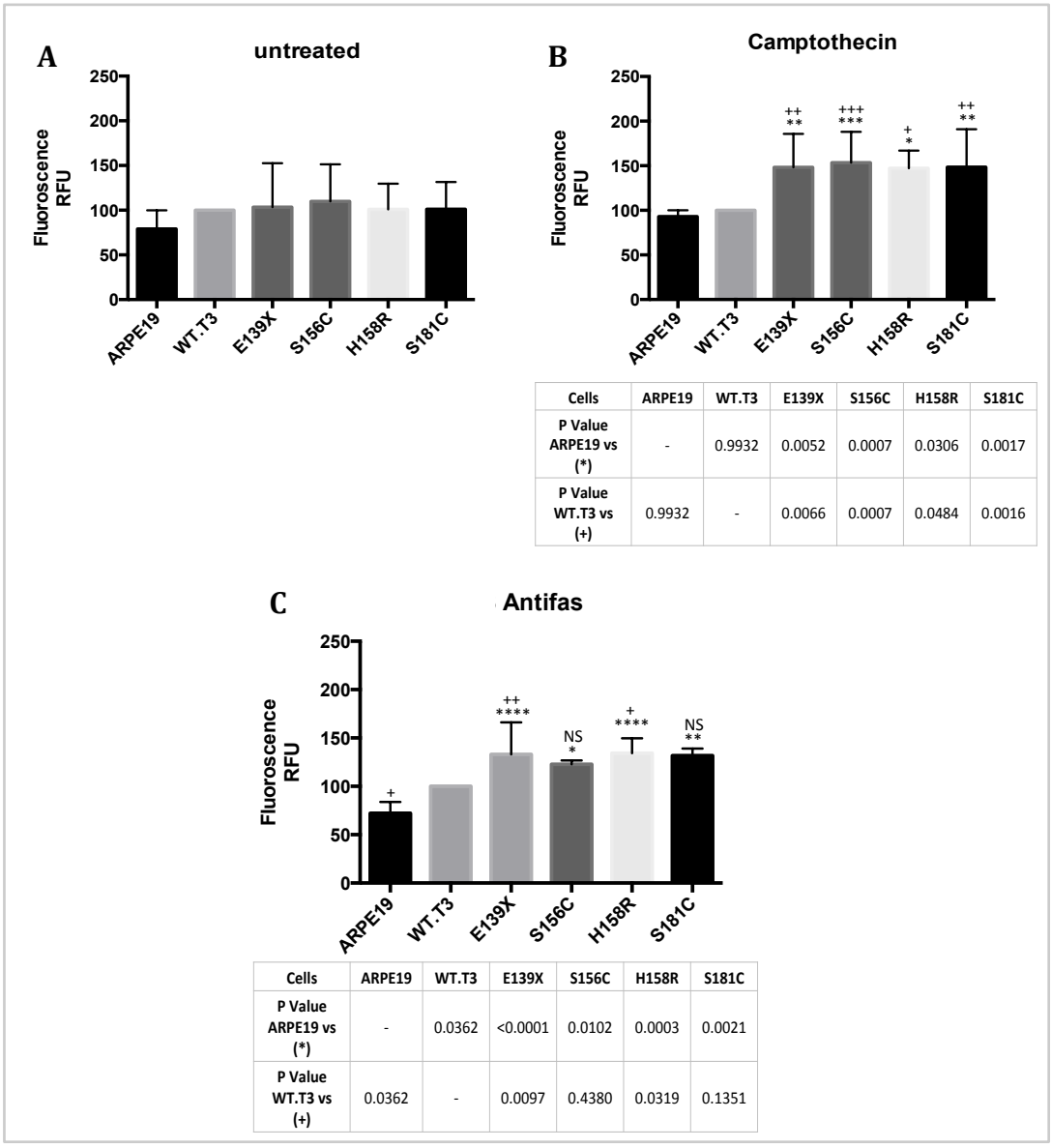

Cells	ARPE19	WT.T3	E139X	S156C	H158R	S181C
P Value ARPE19 vs (*)	-	0.9932	0.0052	0.0007	0.0306	0.0017
P Value WT.T3 vs (+)	0.9932	-	0.0066	0.0007	0.0484	0.0016

Cells	ARPE19	WT.T3	E139X	S156C	H158R	S181C
P Value ARPE19 vs (*)	-	0.0362	<0.0001	0.0102	0.0003	0.0021
P Value WT.T3 vs (+)	0.0362	-	0.0097	0.4380	0.0319	0.1351

Figure 4.3: Caspase 3/7 activity in ARPE19 cells treated in serum depleted (2% FBS) growth media.

Caspase 3/7 activity in: (A) untreated ARPE19 cells; (B) ARPE19 cells treated with camptothecin (20μM); (C) ARPE19 treated with anti-Fas activating antibody (at 15μg/ml). +/ Represents significant P-value, in graphs and tables, compared to untransfected and WT.T3 transfected ARPE19 cells, respectively. Data are presented as mean ± S.E. of three independent experiments and analysed using one-way ANOVA.*

4.3.3 TACE pull down assay

Immunoblotting confirmed the expression of endogenous TACE in HEK293T cells, revealing bands between 100-150 kDa (Figure 4.1 A).

In addition, HEK293T cells transfected with pHTC-HaloTag vectors including pHTC-vector, pHTC-WT.T3 and pHTC-S181C were also examined for TACE and TIMP3 expression. pHTC-HaloTag transfected cells expressed TACE identical to untransfected cells (Figure 4.4 A). Western blotting analysis of HEK293T cells transfected with WT.T3 and S181C showed TIMP3 species at ~60kDa in the reduced gel (corresponding to the TIMP3-HaloTag fusion protein); however, S181C also had an additional faint species at ~120 kDa, which might be resulted from in complete reduction of S181C-dimer form (Figure 4.4 B).

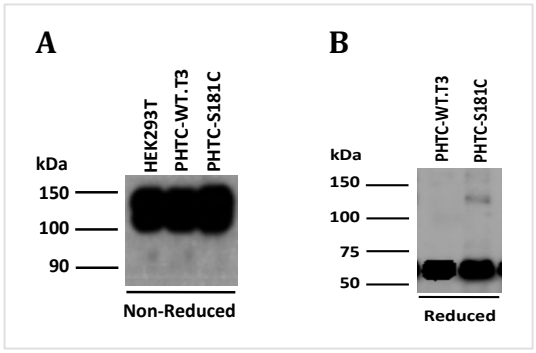

Figure 4.4: Western blotting of TACE and TIMP3 in HEK293T cells.

Cells were transfected with pHTC-WT.T3-HaloTag and pHTC-S181C-HaloTag in 6-well plates. (A) TACE: Cell lysates from untransfected HEK293T and transfected with HaloTag vectors were analysed in SDS-PAGE and western blotting (anti-TACE). (B) Western blotting of TIMP3 in HEK293T cells transfected with pHTC-WT.T3-Halotag and pHTC-S181C-HaloTag vectors (reduced, anti-HaloTag).

Since TACE-mediated ectodomain shedding is regulated by TIMP3, association between TIMP3 and TACE was examined using the HaloTag pull down system. HEK293T cells were transfected with pHTC-HaloTag vector, pHTC-WT.T3-HaloTag and pHTC-S181C-HaloTag and then treated with PMA (0-25nM) following by pull down as described in section 5.3.5.

It was anticipated that SFD-TIMP3 dimers may increase the stability of the interaction with TACE, relative to wild-type TIMP3 monomers, and this increase may be detected in an increased resistance to PMA-induced dissociation of the TACE/TIMP3 complex which may then be detected by pulling-down any TIMP3 associated TACE using the HaloTag on the TIMP3.

Western blotting analysis revealed the presence of TACE species between 100-150kDa corresponding to the previously reported inactive and activated forms in the cell lysates of all transfected cells whether untreated or PMA-treated (Figure 4.5). However pull down samples showed no TACE precipitation, indicating the absence of TACE-TIMP3 interaction.

The pull down assay was repeated using the reducible crosslinking agent, DTSSP, in an attempt to stabilise any potential TIMP3-TACE interactions. Immunoblotting analysis of reduced gels showed TACE at 100-150kDa in cell lysates and pull down supernatant in all samples either HaloTag vector or TIMP3-Halotag constructs but very faint bands were observed in some pull down eluate samples, however this was not restricted to any one HaloTag fusion protein species and may be contamination from other wells (Figure 4.6).

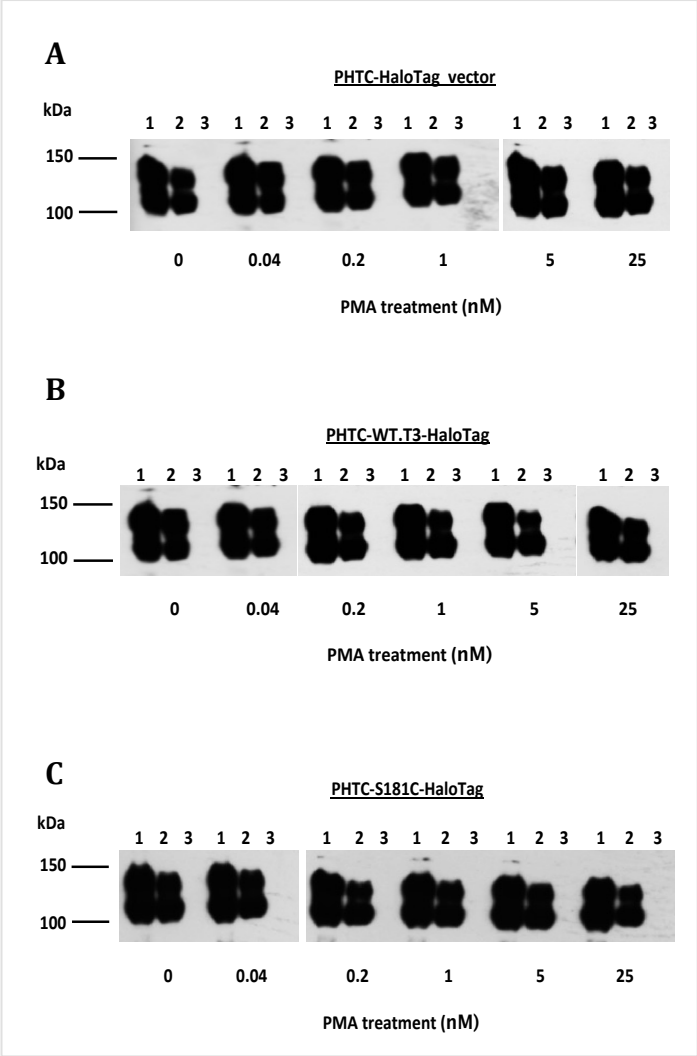

Figure 4.5: Western blotting analysis of TACE pull down in HEK293T cells.

HEK293T cells were transfected with empty pHTC-HaloTag vector, pHTC-WT.T3-HaloTag and pHTC-S181C-HaloTag and then treated with PMA (0-25nM). Cell lysates were analysed by non-reduced western blotting using anti-TACE polyclonal antibody. (A) Empty pHTC-HaloTag vector; (B) pHTC-WT.T3-HaloTag; (C) pHTC-S181C-HaloTag. (1) cell lysate; (2) pull down supernatant and (3) pull down eluate.

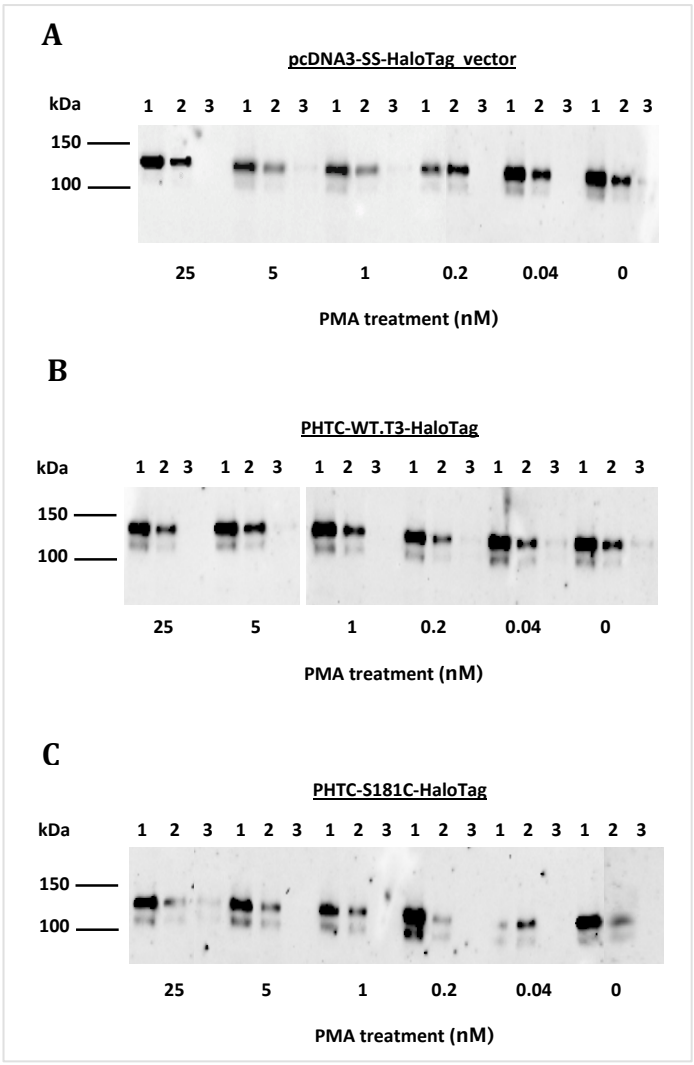

Figure 4.6: Western blotting analysis of TACE pull down in HEK293T cells following DTSSP cross-linking.

HEK293T cells transfected with HaloTag vectors were firstly treated with PMA (0-25nM) and then with DTSSP crosslinker (1mM). Cell Lysates were subjected to reduced western blotting using anti-TACE polyclonal antibody. (A) pcDNA3-SS-HaloTag vector (empty); (B) pHTC-WT.T3-HaloTag; (C) pHTC-S181C-HaloTag. (1) Diluted cell lysates; (2) pull down supernatant; (3) pull down eluate.

4.4 Discussion

While it has previously been shown that high level transient expression of TIMP3 directly induces apoptosis of RPE cells, and that SFD-mutant forms of TIMP3 seem to have an increased apoptotic effect (Majid *et al.* 2002), it was not known whether lower level stable expression of these molecules would have an effect on apoptosis. Clearly the production of ARPE19 cells stably expressing wild-type and SFD-TIMP3 proteins should select against directly pro-apoptotic levels of TIMP3. Nevertheless it is possible that lower level expression still increases the sensitivity of these cells to pro-apoptotic agents, which may be more relevant to the physiological situation.

Preliminary experiments, in which cells were grown in complete serum, failed to show any consistent differences in caspase activity between untransfected and TIMP3 transfected cells, with or without camptothecin or anti-Fas. However using serum deprived culture medium, clear differences became apparent and this may reflect an increased sensitivity to apoptosis in media containing lower concentrations of growth factors. Using this media, there did appear to be a slight increase in caspase activity in untreated cells transfected with either wild-type of SFD-TIMP3, although this was not significant. However treatment with either camptothecin or Fas activating antibody, revealed a significant difference in apoptosis between both untransfected and wild-type TIMP3 transfected cells and those transfected with all four different SFD mutant forms of TIMP3. While this did not reach significance for all mutants with both drugs, nevertheless it was significant for all mutants with at least one of the drugs. Camptothecin causes DNA damage by irreversibly binding to the topoisomerase I/DNA complex, resulting in apoptosis. The anti-Fas antibody is a surrogate for membrane bound Fas ligand and activates Fas receptor (CD95), also triggering apoptosis.

Effects of TIMP3 on Fas-induced apoptosis can readily be explained by TACE inhibition and decreased shedding of death receptors (Ahonen *et al.* 2003). The effects of TIMP3 on camptothecin-induced apoptosis probably reflects the fact that this drug increases the cells' sensitivity to naturally occurring apoptotic ligands present in the media or on other cells, which transduce their effects through death receptors on the cell surface.

We then went on to explore one possible mechanism by which SFD mutant forms of TIMP3 may result in increased sensitivity to Fas activating antibody, that being by stabilising the dimeric, inactive form of TACE (Xu *et al.* 2012), which would potentially result in increased expression of Fas receptor on the cell surface. This was done by attempting to pull-down

TIMP3/TACE complexes using HaloTagged wild-type or SFD mutant TIMP3. In this case transient transfection of HEK293T cells was used as these cells had previously been reported to express TACE (Endres *et al.* 2003), transfect readily, and also should yield high-level protein expression from vectors containing the SV40 origin of replication (as pHTC-HaloTag does), due to the presence of the SV40 large T antigen. Western blotting confirmed that these cells express high levels of endogenous TACE protein, with the anti-TACE antibody detecting two particularly strong bands between 100-150kDa; and that the TIMP3 and SFD-TIMP3 HaloTagged fusion proteins are expressed as monomer and dimer respectively.

Despite this, the HaloTagged wild-type or SFD mutant TIMP3 proteins failed to pull down any TACE protein, even in the absence of PMA or when DTSSP reducible crosslinker was used. There are a number of reasons why this may be the case, for example the HaloTag may interfere with TIMP3 binding to TACE. While the tag was placed on the C-terminus to avoid interfering with the proteinase binding site, the fact that TIMP3 only appears to bind to TACE dimers (Xu *et al.* 2012) may indicate that a second site on the TIMP3 molecule is also involved, which could be masked by the HaloTag. While it is possible that solubilisation of the TACE in the lysis buffer results in dissociation of TIMP3, the DTSSP cross-linker should have prevented this. Had time permitted, the former may have been addressed using a smaller tag, such as the haemagglutinin- (HA-) or Myc-tags.

An alternative or additional explanation for the increased pro-apoptotic effect of SFD-TIMP3, relative to wild-type, might be that the mutant protein has been shown to have an increased resistance to degradation (Langton *et al.* 2005) and so accumulates in the ECM, resulting in increased TACE inhibition. This may not be particularly apparent in these experiments as HEK293T cells do not produce a great deal of ECM and the caspase 3/7 activity was measured 2 days post-seeding so there would probably be relatively low levels of TIMP3 relative to TACE, which was highly expressed on these cells. To tackle this issue, the extracellular matrices from cells transfected with wild type or SFD-mutant TIMP3 could be used as treatment for un-transfected ARPE19 cells to see if the higher levels of TIMP3 present in this matrix have a pro-apoptotic effect. Nevertheless, the finding of this chapter suggested that retinal cells expressing mutant TIMP3 are more susceptible to pro-apoptotic ligands than those expressing the normal molecule and this could play a role in the geographic atrophy of SFD.

Chapter 5: The effect of SFD-TIMP3 on VEGFR2

5.1 Introduction

As discussed in Chapter 1, TIMP3 is a potent inhibitor of VEGFR2 (Qi *et al.* 2003) and this activity is likely to be a key reason for its expression by RPE cells in the retina where it probably plays a vital role in preventing vascularisation of the photoreceptor layer. As choroidal neovascularization is a common feature of SFD, it seemed likely that TIMP3 dimerisation may be affecting the interaction of the molecule with VEGFR2. It is possible that CNV is entirely a result of Bruch's membrane thickening, triggering increased VEGF expression. However this raises the question as to why the increased expression of TIMP3 observed in SFD (Fariss *et al.* 1998) fails to prevent this.

Previous work in our laboratory and elsewhere (Chen *et al.* 2014) (Qi *et al.* 2013) (Mujamammi 2013) has demonstrated that the majority of VEGFR2 binding residues of TIMP3 are localised in the C-terminal domain, where the vast majority of the mutations also lie. Based on these observations TIMP3 dimerisation may impair or prevent TIMP3 binding to VEGFR2. Alternatively it is possible that TIMP3 dimers mimic the dimeric VEGF ligand, which activates the receptor by dimerisation. While it has been reported that wild-type and S156C TIMP3 are equally potent at inhibiting VEGF binding to VEGFR2 (Fogarasi *et al.* 2008), these experiments utilised S156C TIMP3 expressed from bacteria and the molecule was almost completely monomeric, with wild-type and mutant forms appearing identical on non-reduced SDS-PAGE gels.

Preliminary data from our laboratory (Mujamammi 2013) indicated that at least two of the SFD mutants, H158R and S181C, did indeed show a reduced ability to inhibit VEGF-mediated invasion of endothelial cells in vitro; however whether this is more widely applicable to other SFD mutants and the precise mechanism of the inhibition were unknown. Moreover, it has been reported that the S156C mutant form of TIMP3 induces angiogenesis by increasing the surface expression of VEGFR2 (Qi *et al.* 2009). This latter possibility could potentially explain the increased invasiveness of endothelial cells, rather than a decreased ability to inhibit VEGFR2.

The hypothesis of this chapter is that all SFD-TIMP3 mutants have a decreased ability to inhibit VEGF-mediated angiogenesis, either through upregulation of and/or decreased inhibition of VEGFR2. This would be examined using two techniques: flow cytometry to test cell surface expression of VEGFR2, and endothelial cell migration to investigate TIMP3 inhibition.

5.2 Methods

Ideally the binding characteristics of mutant forms of TIMP3 would be determined using purified proteins. However, previous experience from our laboratory and elsewhere has shown this to be extremely difficult, precluding this as a realistic method for comparing several different mutants. While TIMP3 has been successfully purified from bacteria, as mentioned above, the protein then fails to dimerise.

Human umbilical vein endothelial cells (HUVEC) were used in this chapter due to fact that they are one of the few cell types, readily available, known to express VEGFR2. However, these primary cells transfect poorly making it very difficult to introduce TIMP3 mutant constructs into the same cells. Moreover, the primary source of TIMP3 in the retina appears to be the RPE rather than the choroid (Della *et al.* 1996). For these reasons, as mentioned above, we have previously assayed the inhibitory effect of two SFD mutants using an endothelial invasion assay in which HUVEC cells are allowed to invade through ECM from TIMP3-transfected ARPE19 cells in response to VEGF. The aim here was to repeat this for several different SFD mutants but also to determine the effect of this ECM on VEGFR2 expression.

5.2.1 The effect of SFD-TIMP3 proteins expressed *in situ* on HUVEC VEGFR2 expression

ARPE19 cells were stably transfected with WT.T3 or S15C, E139X, E139K, S156C, H158R or S181C SFD mutants as described (section 2.2.2.9) and maintained in their complete growth medium (section 2.2.2.2). ARPE19-ECM was prepared using ammonium hydroxide lysis (section 2.2.3.1.3) for flow cytometry for VEGFR2 expression (sections 2.2.2.4, 2.2.2.6 & 2.2.3.5.1) and for western blotting for TIMP3 protein expression (section 2.2.3.3).

5.2.2 The effect of SFD-TIMP3 proteins expressed *in situ* on VEGF-induced HUVEC invasion/migration

The invasion assay was carried out as described in section 2.2.3.5.2 using ECM (section 2.2.3.1.3) from ARPE19 cells, either untransfected or transfected with WT.T3, S15C, E139X,

E139K, S156C, H158R or S181C TIMP3 in FluoroBlock ™ inserts in complete growth medium. To perform migration assay (section 2.2.3.5.2), ARPE19 basement membrane was then prepared using ammonium hydroxide lysis buffer (section 2.2.3.1.3). To confirm SFD-TIMP3 expression, the same cell lines were simultaneously grown in plates and their ECM prepared by ammonium hydroxide lysis to analyse in western blotting (section 2.2.3.1.3).

5.3 Results

5.3.1 Western blotting of ARPE19 cell lines used in flow cytometry and migration assays

Western blotting was performed alongside the flow cytometry and migration assays, which confirmed the expression of TIMP3 protein as well as SFD-TIMP3 dimers (Figure 5.1).

When comparing the untransfected cells to those transfected with the SFD mutants on the non-reduced blot it is apparent that the majority of the mutant protein is expressed in dimeric/multimeric form. Upon reduction there was a concomitant increase in the monomeric form that was, while somewhat varied, comparable to that seen with the wild-type protein.

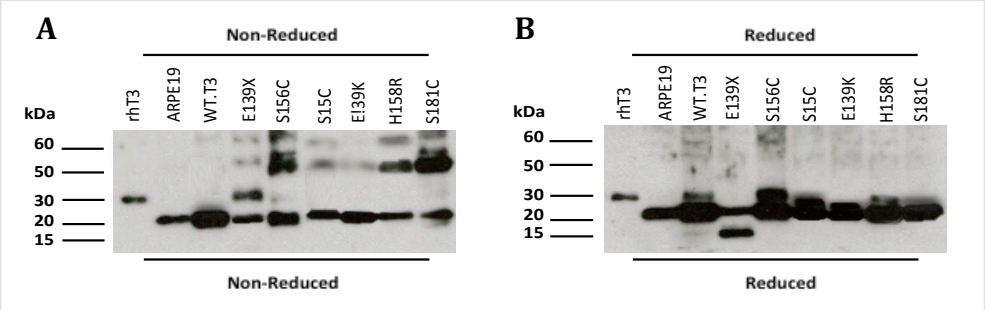

Figure 5.1:Western blotting of TIMP3 expression by ARPE19 cell lines used in flow cytometry and migration assay.

Western blots of cell matrix from ARPE19 cells transfected with SFD-TIMP3 confirmed the expression of TIMP3 protein and the presence of dimeric/oligomeric SFD-TIMP3. (A) Non-reduced and (B) reduced samples.

5.3.2 The effect of SFD-TIMP3 mutants on VEGFR2 expression in HUVEC

HUVEC cells were allowed to grow for 5 hours (the length of time cells were incubated with the ECM in the invasion assays) on ECM from untransfected or WT.T3, S15C, E139X, E139K, S156C, H158R or S181C transfected ARPE19 cells as described in (section 2.2.3.6.1). None of the mutant transfected cells showed a significant difference in VEGFR2 expression, relative to wild-type TIMP3 transfected cells, nor was there any significant difference between untransfected and transfected cells, indicating that incubation of HUVEC cells with ECM containing SFD-TIMP3 mutants does not significantly affect the expression of VEGFR2 in these cells. HUVEC treated with VEGF did show a small but significant decrease in VEGFR2 expression (Figure 5.2 & 5.3), relative to untreated cells.

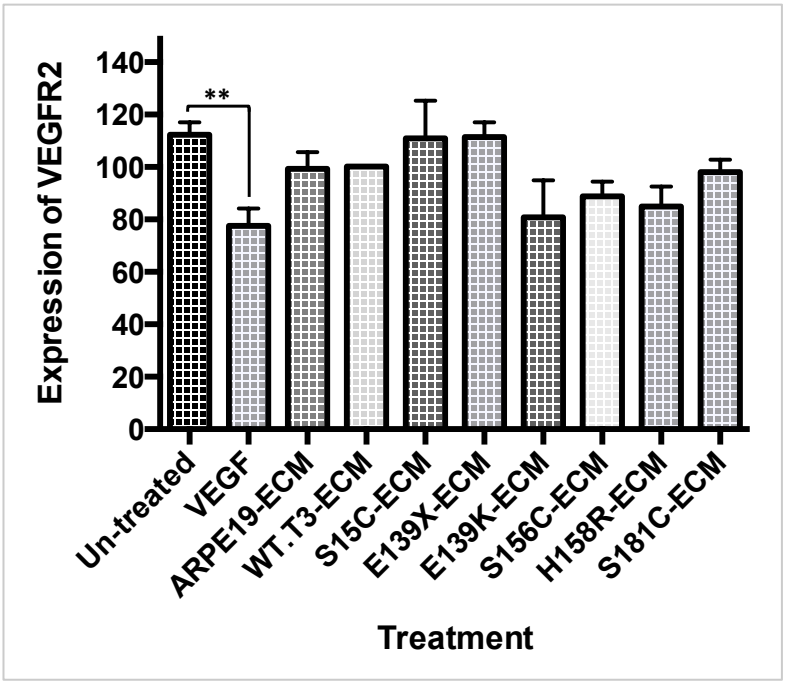

Figure 5.2: Expression of VEGFR2 on HUVEC treated with VEGF or ECM from transfected ARPE19 cells.

Flow cytometric determination of VEGFR2 expression on HUVEC treated with VEGF or ARPE19 cell ECM from untransfected, wild type TIMP3 (WT.T3) or the specified SFD-TIMP3 mutant transfected cells. The Y axis shows percentage VEGFR2 expression, relative to cells treated with ECM from wild-type TIMP3 ARPE19 cells. None of these differences were significant; although VEGF-treatment did significantly, decrease VEGFR2 expression, relative to untreated HUVEC (p-value = 0.0031). Data are representative of triplicate experiments (as means ± S.E) and analysed one-way ANOVA.

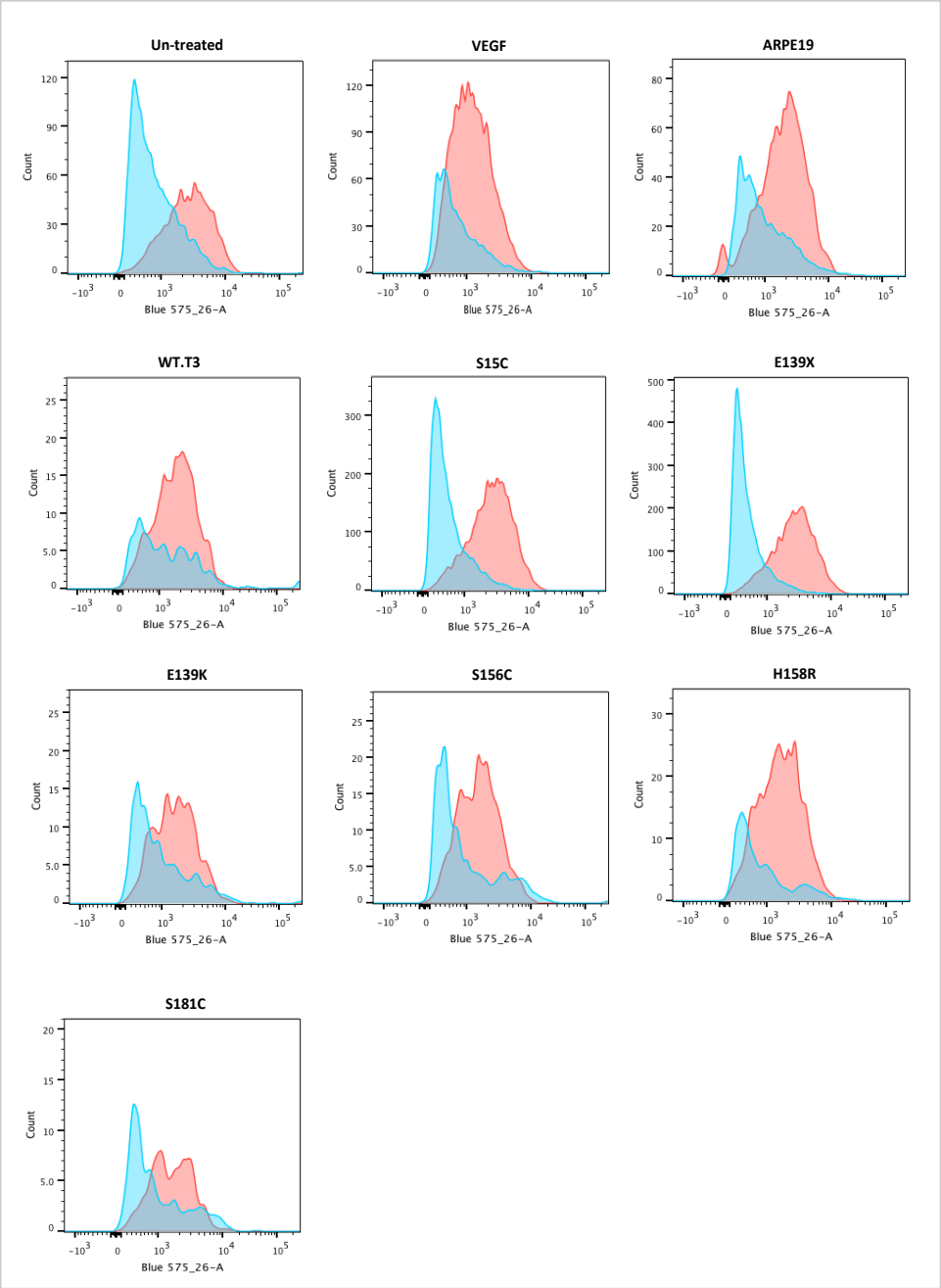

Figure 5.3: Flow cytometric analysis of VEGFR2 expression on HUVEC cells.

Representative graphs showing binding of Phycoerthrin mouse anti-human VEGFR2 (red) relative to IgG κ isotype control (blue) on HUVEC cells following the specified treatments.

5.3.3 The effect of SFD-TIMP3 mutants on HUVEC migration

The cell matrix from cells transfected with wild type TIMP3 inhibited HUVEC migration by approximately 60% compared to the cell matrix from untransfected cells (Figure 5.4). On the other hand, ECM from SFD-TIMP3 transfected cells showed less inhibition than that from wild type TIMP3 that was approximately 30% compared to untransfected cells.

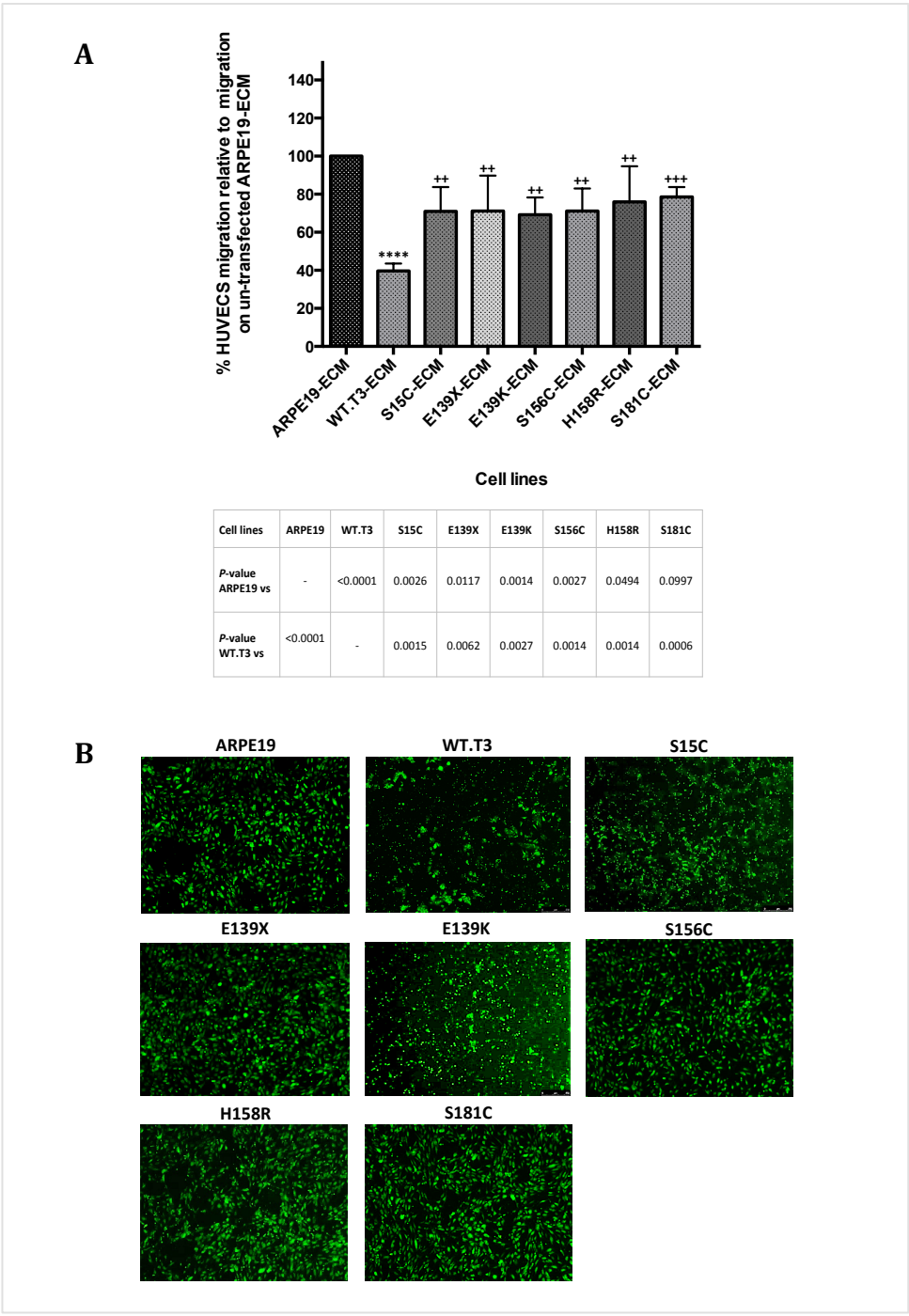

Cell lines	ARPE19	WT.T3	S15C	E139X	E139K	S156C	H158R	S181C
P-value ARPE19 vs	-	<0.0001	0.0026	0.0117	0.0014	0.0027	0.0494	0.0997
P-value WT.T3 vs	<0.0001	-	0.0015	0.0062	0.0027	0.0014	0.0014	0.0006

Figure 5.4: Migration of HUVEC through cell matrix of ARPE19 cell lines.

(A) Represents the percentage of HUVEC cells migrating to the underside of FluoroBlok inserts compared to those cells migrated through untransfected ARPE19-ECM (B) Representative micrographs of the migrated HUVEC cells. P-value is shown as a variable number of asterisks and relative to un-transfected; ++++ relative to WT.T3 in the graph and in the table below the graph. Data are as means ± S.E of three experiments and analysed using one-way ANOVA.

5.4 Discussion

As outlined earlier, CNV is a common feature of SFD and the fact that TIMP3 mutations in SFD almost exclusively affect the C-terminal domain, which has also been implicated in VEGFR2 binding, indicates that these mutations may affect the TIMP3/VEGFR2 interaction. Moreover, earlier work in our laboratory indicated that His158Arg and Ser181Cys TIMP3 show reduced inhibition of endothelial cell invasion relative to the wild-type molecule (Mujamammi 2013). However it has also been reported that the S156C mutation up regulates VEGFR2 expression on endothelial cells (Qi *et al.* 2009) and this could offer an alternative explanation for the increased invasion of the endothelial cells in these experiments.

In this chapter we have demonstrated that several other SFD mutants, namely S15C, E139X, E139K and S156C, also appear to have a reduced ability to inhibit endothelial cell invasion through ECM containing these proteins. Expression of the mutant proteins by the ARPE19 cells, determined by western blotting, was somewhat variable, but not sufficient to explain the differences in invasion seen between wild-type and mutant proteins. This was particularly apparent for the S156C mutant where expression was, if anything, higher than for the wild-type (Figure 5.1).

Flow cytometric analysis of VEGFR2 expression showed no significant difference in VEGFR2 expression between cells incubated on ECM containing wild-type or mutant forms of the protein (Figure 5.2). This suggests that upregulation of VEGFR2 on the HUVEC by the mutant proteins, including S156C, is not the explanation for the increased invasion seen on the ECM containing mutant TIMP3, even for S156C. This supports the notion that TIMP3 dimerisation inhibits the ability of the molecule to bind to VEGFR2 and could help to explain the CNV seen in this disease, despite high levels of TIMP3 in Bruch's.

The data presented by Qi *et al.* (2009), indicate that over-expression of S156C TIMP3 in porcine aortic endothelial (PAE) cells increases expression of VEGFR2 on the cell surface, and also VEGFR2 expression is upregulated in the eyes of $Timp3^{S156C/S156C}$ mice. While it might be argued that over-expression of the protein in this system is very artificial, and that RPE cells, rather than vascular endothelial cells, appear to be the main source of TIMP3 in Bruch's (Della *et al.* 1996), the increased expression in transgenic mice is more difficult to dismiss (although the A3 anti-VEGFR2 antibody used in these experiments has been shown to cross-react with other molecules (Smith *et al.* 2010).

While, in our assay, increased VEGFR2 expression does not appear to be the explanation for the enhanced invasion seen with mutant TIMP3, it may play a role in some cells. Another possibility is that VEGF itself maintains the expression of VEGFR2 on the cell surface. Wild-type TIMP3 would inhibit this effect, potentially decreasing VEGFR2 on the cell surface, whereas mutant TIMP3, which does not inhibit the receptor, would not do so and could give rise to the perceived increase in VEGFR2. However in our case VEGF did not increase VEGFR2 expression on the HUVEC cells (Figure 5.2) but appeared to slightly decrease it. This may be a cell type specific effect and account for the differences between the HUVEC used here and the PAE cells used by Qi *et al.* (2009).

Taken together the data shown in this chapter indicate that SFD mutation-induced dimerisation of TIMP3 appears to impair its ability to inhibit VEGFR2. However this may only be shown conclusively if it becomes possible to purify sufficient quantities of the dimeric protein to carry out receptor binding assays.

Chapter 6: Investigating the interaction of TIMP3 with EFEMP1

6.1 Introduction

As outlined in Chapter 1, Malattia Leventinese (ML), like SFD, is a rare autosomal dominant retinal dystrophy that leads to irreversible visual loss, usually in middle age. The disease is caused by a single mutation in the gene *EFEMP1* (converting arginine at 345 to tryptophan) (Stone *et al.* 1999). Like SFD and AMD, ML is characterised by the presence of extracellular deposits (drusen) between the retinal pigment epithelium (RPE) and Bruch's membrane, although in this case these form a characteristic honeycomb pattern and neovascularisation is rare.

EFEMP1 and TIMP3 have been shown to accumulate in the eyes of patients with both ML and AMD (Klenotic *et al.* 2004). *Efemp1*$^{R345W/R345W}$ mice also show deposits of EFEMP1 and TIMP3 as well as evidence of complement activation in the RPE and Bruch's membrane (Fu *et al.* 2007). TIMP3 mutations in SFD also result in accumulation of TIMP3 protein, however EFEMP1 expression in eyes from SFD patients has not been examined. As TIMP3 and EFEMP1 are binding partners (Klenotic *et al.* 2004), it might be expected that accumulations of TIMP3 in SFD would also lead to EFEMP1 accumulation, providing a common link between all three diseases. This assumes that SFD mutant forms of TIMP3 still bind EFEMP1.

The hypothesis of this chapter is that SFD-TIMP3 mutants retain their ability to bind to EFEMP1 resulting in TIMP3/EFEMP1 protein complexes that may contribute to SFD as well as ML. The initial aim of this chapter, therefore, was to investigate the interaction between EFEMP1 and TIMP3 using the HaloTag pull-down assay.

6.2 Methods

6.2.1 Plasmid construct preparation

Plasmid constructs used for the EFEMP1-TIMP3 protein pull down assays were already created in my supervisor's laboratory from previous projects. Plasmid constructs (listed in Table 6.1, Appendix 2) were used to transform α-gold competent cells to prepare highly pure maxi prep DNA (sections 2.2.1.3 and 2.2.1.4).

Table 6.1: Plasmid construct used for EFEMP1-TIMP3 pull-down.

No	First pull-down plasmid constructs	Purpose
1	pHTC-EFEMP1-HaloTag (wild type).	These vectors have *EFEMP1* fused to HaloTag at the C-terminus, facilitating their binding to HaloTag resin.
2	pHTC-EFEMP1-HaloTag (mutant).	
3	pcDNA3-TIMP3 (wild type).	Vectors contain *TIMP3* (WT or S181C) producing proteins without a tag as targets for the EFEMP1 fusion proteins.
4	pcDNA3-S181C (TIMP3 mutant).	
No	**Second pull-down plasmid constructs**	**Purpose**
1	pcDNA3-SS-HaloTag.	A vector containing HaloTag alone but with a chymotrypsinogen signal sequence to enable secretion - for use as a negative control in pull-down assay to guarantee that the HaloTag or resin do not interact to any other untagged proteins.
2	pcDNA3-SS-HaloTag-EFEMP1 (wild type).	Vectors contain HaloTag with chymotrypsinogen signal peptide followed by the *EFEMP1* (WT or Mutant) sequence at the C-terminus.
3	pcDNA3-SS-HaloTag-EFEMP1 (R345W mutant).	
4	pcDNA3-TIMP3-V5-KDEL (wild type).	TIMP3 proteins with C-terminal V5 Tag to make them easily detectable and KDEL endoplasmic reticulum (ER) retrieval sequence, used to prevent TIMP3 being secreted and binding to the ECM.
5	pcDNA3-S181C-V5-KDEL (TIMP3 mutant).	

6.2.2 EFEMP1 and TIMP3 HaloTag pull-down assay

6.2.2.1 Transfection of HEK293T cells and cell lysate preparation

HEK293T cells were transfected in 6-well plates as explained in section 2.2.3.6 with the plasmid combinations shown in table 6.2. The transfection of mammalian cells was divided into three groups including control vector, wild type EFEMP1 and mutant EFEMP1 (R345W). However, the first pull-down transfection was performed using COS-7 cells and incubated for 48 hours, whereas the second pull down transfection used HEK293T cells for 24 hours. This shorter period following transfection was previously found to be optimal for constructs bearing the KDEL sequence (see below) that was exploited in the second experiment.

Following transfection of the COS-7 cells or HEK293T cells, they were harvested and stored at -80°C followed by cell lysate preparation as described in section 2.2.3.6.

Both EFEMP1 and TIMP3 localise to the ECM where TIMP3, in particular, binds very tightly. This means that most of the expressed TIMP3 will be found in that location. However denaturing conditions, necessary to remove TIMP3 from the ECM, would almost certainly disrupt any interaction between TIMP3 and EFEMP1. KDEL is a four amino acid signal sequence found on the C-terminus of soluble ER resident proteins, such as chaperones, that prevents them being lost by secretion. KDEL receptors are found in vesicular tubular clusters and the Golgi apparatus (secretory structures downstream of the ER) and these bind KDEL bearing proteins, sending them back to the ER via COPI-coated vesicles (Ellgaard and Helenius 2003). Previous work in my supervisor's laboratory (unpublished observations) had shown that appending the KDEL sequence to the C-terminus of TIMP3 caused it to be processed correctly (e.g. glycosylation and disulphide bond formation, including formation of SFD dimers) but caused most of the protein to be retained inside the cell. In this location the TIMP3 would be in a soluble form, still able to bind normally associated proteins, but in a form that could be extracted without using denaturing conditions.

Table 6.2: HEK293T cells transfection for EFEMP1-TIMP3 pull-down.

Group	First pull-down transfection	
1	pHTC-EFEMP1-HaloTag (wild type)	pcDNA3-TIMP3 (wild type)
		pcDNA3-S181C (mutant)
2	pHTC-EFEMP1-HaloTag (R345W mutant)	pcDNA3-TIMP3 (wild type)
		pcDNA3-S181C (mutant)
Group	**Second pull-down transfection**	
1	Control vector pcDNA3-SS-HaloTag	pcDNA3-TIMP3-V5-KDEL (wild type)
		pcDNA3-S181C-V5-KDEL (mutant)
2	pcDNA3-SS-HaloTag-EFEMP1 (wild type)	pcDNA3-TIMP3-V5-KDEL (wild type)
		pcDNA3-S181C-V5-KDEL (mutant)
3	pcDNA3-SS-HaloTag-EFEMP1- (R345W mutant)	pcDNA3-TIMP3-V5-KDEL (wild type)
		pcDNA3-S181C-V5-KDEL (mutant)

6.2.2.2 Protein pull-down protocol and Western blotting

EFEMP1-TIMP3 protein pull-down was performed as described in section 2.2.3.6.2. Cell lysates, pull-down supernatant and pull-down eluate (10µl of each) were analysed by SDS-PAGE and western blotting (section 2.2.3.3). To detect TIMP3-KDEL-V5 proteins, the membranes were blocked in 5% blocking buffer and immunoblotting against V5 Epitope Tag monoclonal antibody at 4℃ overnight. This was followed by 4 washes in TBST wash buffer and then 1-hour incubation in goat anti-mouse HRP conjugated secondary antibody. To check the expression of EFEMP1-HaloTag protein, the membranes were re-probed with anti-HaloTag monoclonal primary antibody and then goat anti-mouse HRP conjugated secondary antibody.

6.3 Results

6.3.1 Western blotting of EFEMP1-TIMP3 pull-down

Initial pull-down experiments were performed using COS-7 cells transfected with pHTC-EFEMP1-HaloTag (wild type or mutant) and pcDNA3-TIMP3 (wild type or S181C mutant) (Table 6.2). Western blot analysis of both cell lysates and pull-down eluates failed to detect any TIMP3 proteins at the expected sizes (24 and 48kDa for wild-type and mutant TIMP3 respectively - Figure 6.1). The band at approximately 58kDa, present in all samples, is due to non-specific binding of the anti-TIMP3 antibody to a cellular protein. As alluded to earlier, this probably reflects the fact that most of the TIMP3 expressed was localised to the ECM and the non-denaturing lysis buffer used to solubilise the cells for the pull down experiments would be unlikely to remove this. However an additional confounding factor may be the fact that the C-terminal domain of EFEMP1 was shown to be responsible for TIMP3 binding (Klenotic *et al.* 2004) and the relatively large HaloTag protein (approximately 35kDa), present on the C-terminus, may interfere with this interaction.

In order to attempt to circumvent the former issue the ER retention signal, KDEL, was appended to the C-terminus of the TIMP3 proteins, as discussed earlier. While the HaloTag protein can be fused to the N-terminus of proteins in the pHTN vector (equivalent to pHTC but with a multiple cloning site on the C-terminal end of HaloTag), the HaloTag sequence lacks a signal sequence and so fusion proteins are directed into the cytosol. To remedy this, a new vector had been created in our laboratory in which the human chymotrypsinogen signal peptide (MAFLWLLSCWALLGTTFG) was appended to the N-terminus of the HaloTag protein, with a multiple cloning site at the C-terminal end (pcDNA3-SS-HaloTag). The revised pull-down experiments, therefore, utilised pcDNA3-SS-HaloTag-EFEMP1 (wild type or R345W mutant) and pcDNA3-TIMP3-V5-KDEL (wild type or S181C mutant).

Following these changes TIMP3 protein, in both wild type and SFD mutant forms, was clearly detectable in the cell lysate and also in the eluate from the HaloTag binding resin (Figure 6.2A). The non-reduced blot of S181C TIMP3 (Figure 6.2C) confirmed that the mutant was expressed and pulled down in the dimeric form (bands at approximately 44 and 48kDa, corresponding to unglycosylated and glycosylated dimer). Figure 6.2A also confirms that R345W EFEMP1 retains its ability to bind TIMP3.

Re-probing the membrane with anti-HaloTag antibody (Figure 6.2B) clearly showed high-level expression of the HaloTag-EFEMP1 fusion protein at the expected size (approximately

90kDa) in the cell lysate. Following pull-down, analysis of the supernatant showed that the vast majority bound to the HaloTag resin. No HaloTag-EFEMP1 was detectable in the resin eluate, confirming the fact that the binding of HaloTag to the haloalkane on the resin is irreversible. While pull down of TIMP3 was not as great as might be expected with this high level of expression of EFEMP1 (much of the TIMP3 remained in the supernatant), it did appear to be specific in that the HaloTag only control, did not result in pull-down of any TIMP3 (Figure 6.2D). Again, re-probing with anti-HaloTag antibody (Figure 6.2E) confirmed expression of the HaloTag protein at the expected size (approximately 35kDa), although in this case there was a small amount of HaloTag protein in the eluate.

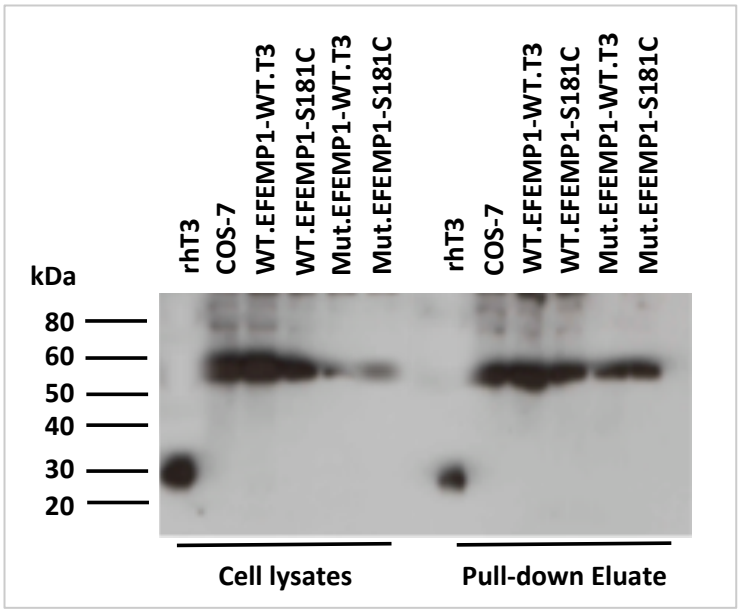

Figure 6.1: Western blotting analysis of first EFEMP1-TIMP3 pull-down.

COS-7 cells were transfected with pHTC-EFEMP1-HaloTag (wild type or mutant) and pcDNA3-TIMP3 (wild type or S181C mutant) and used for pull-down followed by western blotting. The membrane was probed with anti-TIMP3 first loop primary antibody to detect TIMP3 protein expression in cell lysates and pull-down eluate. rhT3: recombinant TIMP3, WT: wild type and Mut: mutant.

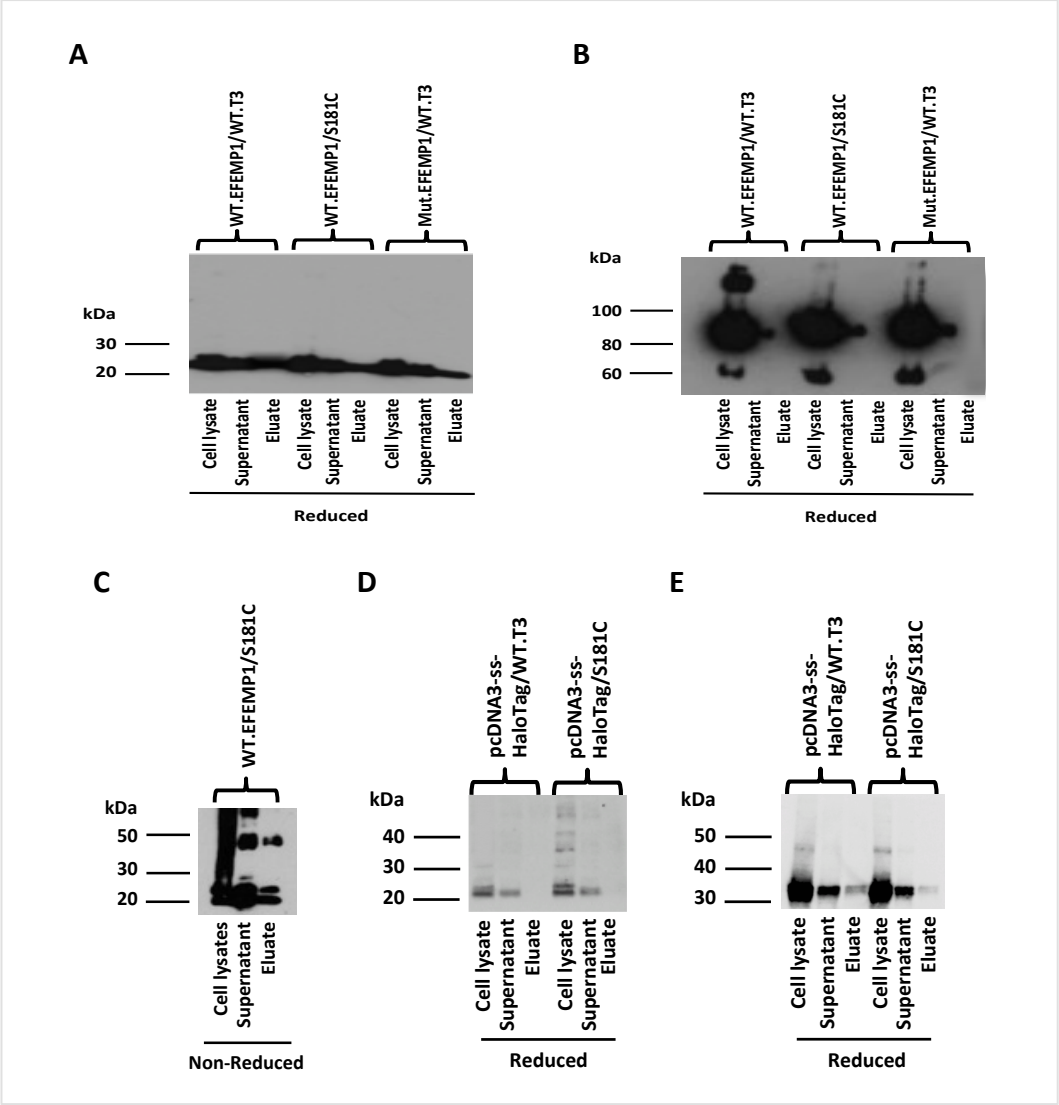

Figure 6.2: Western blotting of the second EFEMP1-TIMP3 pull-down experiment.

Western blotting of EFEMP1-TIMP3 pull-down in HEK293T cells transfected with pcDNA3-SS-HaloTag-EFEMP1 (wild type or mutant) (A, B & C) or pcDNA3-SS-HaloTag (D & E) together with pcDNA3-TIMP3-KDEL-V5 (wild type or S181C mutant). (A), (C) & (D) the membranes were initially probed with anti-V5 Epitope Tag antibody to detect the TIMP3 protein expression (reduced and non-reduced, respectively), and then (B) & (E) stripped and probed with monoclonal anti-HaloTag antibody to show EFEMP1 expression. WT: wild type and Mut: mutant.

6.4 Discussion

The data shown here, using N-terminally HaloTagged EFEMP1, indicate that both wild type and S181C mutated forms of TIMP3 are able to bind EFEMP1 in the pull-down assay although, as this is not a quantitative assay, differences in binding affinity cannot be ruled out. This being the case, it is likely that the high level expression of TIMP3 in SFD eyes will also be accompanied by deposition of EFEMP1, raising the possibility that TIMP3/EFEMP1 complexes play a role in ML, SFD and AMD. These complexes alone may be sufficient to interfere with traffic of nutrients across Bruch's membrane but accumulation of TIMP3 would also likely interfere with clearance of other proteins from the RPE by MMPs and deposition of additional proteins. As EFEMP1 has been shown to bind complement factor H (CFH), these complexes may also contain CFH protein. If this sequesters this protein, impairing its ability to regulate complement activation, it might explain the inflammatory aspect of these diseases.

If this were the case, however, it would not entirely explain the phenotypic differences between these diseases, with ML resembling dry AMD and SFD resembling wet AMD. However in ML the proposed protein complexes would contain normal TIMP3, which inhibits VEGFR2. In contrast we have shown the SFD mutant forms of TIMP3 have an impaired ability to inhibit VEGFR2. This could explain why SFD, but not ML, is characterized by choroidal neovascularisation. If in AMD these protein complexes are the result of oxidation/AGE formation, then TIMP3 may be partially functional with respect to VEGFR2 inhibition, with increasing cross-linking with time leading to an ever-diminishing ability to inhibit VEGFR2 and a gradual progression from dry to wet AMD. The unique honeycomb patterning of drusen found in ML may reflect the fact that the R345W mutation impairs protein secretion and result in accumulation of mutant protein in the endoplasmic reticulum, possibly together with TIMP3, triggering the unfolded protein response (Roybal *et al.* 2005). Overloading the unfolded protein response can induce apoptosis (Fribley *et al.* 2009). It is possible that this initial accumulation within the cell affects the pattern of deposition of the protein complexes in ML. In contrast SFD mutations do not impair TIMP3 secretion (unpublished observations from our laboratory) and so accumulation of TIMP3 in Bruch's is likely to be diffuse. This is also likely to be the case in AMD where any cross-linking occurs extracellulary.

Taken together, these data further support a potential common mechanism in the etiology of ML, SFD and AMD.

Chapter 7: The effect of SFD-TIMP3 on RAGE activation

7.1 Introduction

As mentioned in the introduction, there are numerous phenotypic similarities between SFD and AMD, including thickening in Bruch's membrane, drusen, photoreceptor dysfunction, RPE disruption and sub-retinal neovascularisation (Saksens *et al.* 2014). However AMD is a multifactorial disorder, not directly associated with mutations in the TIMP-3 sequence. Nevertheless these similarities, together with the observation that abnormally high concentrations of TIMP-3 are present in the retina in both diseases, suggests a potential role for TIMP3 in AMD and a link between these two degenerative eye diseases.

We have now demonstrated that all known SFD mutations result in TIMP3 oligomerisation. Moreover our laboratory has previously shown that this impairs turnover of the mutant proteins, which retain their ability to inhibit MMPs (Langton *et al.* 2005), potentially resulting in decreased ECM turnover. The questions remain as to what mechanism(s) could give rise to TIMP3 accumulation in AMD and whether such accumulation in both SFD and AMD has effects other than disruption of normal proteolysis.

In fact protein cross-linking is a well-established consequence of ageing and can result from oxidation, usually as a result of the generation of reactive oxygen intermediates (ROI) from a number of processes such as chronic inflammation and ultraviolet (UV) light exposure or through the formation of age-related glycation end products (AGEs), and advanced lipoxidation end products (ALEs) which result from glucose or lipid based modification of proteins (and other macromolecules), respectively (Glenn and Stitt 2009). Accumulation of AGEs has a detrimental effect on the retina, at least in part, due to activation of AGEs receptor (RAGE) that is a cell surface pattern recognition receptor and found to play an important role in a number of degenerative diseases such as AMD.

RAGE appears to be activated by ligand-induced dimerisation leading to activation of multiple protein kinases; for instance, Janus kinase (JAK), MAPKs, signal transducer and activator transcriptions (STATs) and activation of NF-$_K$B pathway (Zong *et al.* 2010, Hermani *et al.* 2006, Yeh *et al.* 2001, Lander *et al.* 1997, Yan *et al.* 1994). This activation associates RAGE with a variety of inflammation-related cell responses including migration, apoptosis and pro-inflammatory gene expression (Yan *et al.* 2009, Zong *et al.* 2010).

For AMD one possibility is that the age-related formation of advanced glycation end products (AGEs) results in TIMP3 cross-linking which could produce a toxic form of the protein analogous to that produced in SFD, and affect its interaction with for example TACE or VEGFR2. Conversely, it is also possible that the toxicity of SFD-TIMP-3 is due to the fact that it mimics AGE products and binds to AGE receptors.

The hypothesis of this chapter was that SFD-TIMP3 transcripts activate RAGE through direct binding and therefore the initial aim was to investigate the effect of SFD-TIMP3 on RAGE signalling. To test this hypothesis, the effect of SFD-TIMP3 on RAGE activation was examined by using human embryonic kidney 293T (HEK293T) cells transfected transiently with NF-$_{\kappa}$B-luciferase reporter constructs, as these cells were previously transfected with a similar reporter gene and demonstrated by Zong *et al.* (2010) to have activated NF-$_{\kappa}$B pathway in response to RAGE-ligand binding.

7.2 Methods

7.2.1 Vectors

A number of firefly luciferase reporter vectors including pGL3-Basic, pGL3-Control, pGL3-IL8-Luc, pGL4-Luc2P/NF-$_K$B and pNF-$_K$B, were prepared using maxiprep kits (sections 2.2.1.3, 2.2.1.4 & 2.2.1.5) and transfected either alone, in conjunction with the standard Luciferase Reporter assay or together with the *Renilla* luciferase control vector, pTK-green *Renilla* Luc vector (pTK-*Ren*) in conjunction with the Dual Luciferase reporter assay (Table 7.1, Appendix 3). The firefly pGL3-Basic, pGL3-Control and pGL4-luc/NF-$_K$B were purchased from Promega, whereas pGL3-IL8-Luc, and pTK-Renilla were a kind gift from Dr François Guesdon, University of Sheffield. Also, SFD-TIMP3 constructs encompassing WT.T3, E139X and S181C were also available in our lab in the pcDNA3 vector and prepared using a Maxiprep kit for mammalian cells transfection.

Table 7.1: Luciferase reporter DNA plasmids.

Plasmid	Luciferase gene	Specificity	Reason for usage
pTK-Green Renilla Luc	*Renilla* luciferase	Constitutively active thymidine kinase (TK) promoter.	Control Renilla co-transfection vector.
pNF-$_K$B-Luc	*Firefly luciferase*	Contains 4 tandem copies of the NF-$_K$B transcription factor binding site fused to a TATA-like promoter (PTAL) region from the Herpes simplex virus thymidine kinase (HSV-TK) promoter	NF-$_K$B reporter
pGL3-Basic	Modified firefly luciferase *(Luc+)*	Lacks eukaryotic promoter and enhancer sequences.	Negative control vector.
pGL3-Control	*Luc+*	Contains constitutively active SV40 promoter and enhancer sequences.	Positive control vector
pGL3-IL8-Luc	*Luc+*	Contains enhancer sequences and human IL-8 promoter sequence.	NF-$_K$B reporter
pGL4-Luc2p/NF-$_K$B	Alternatively modified (for increased expression) firefly luciferase *Luc2P*	Contains SV40 promoter and enhancer sequences and five copies of the NF-$_K$B response element. Also has hygromycin resistance cassette for selection of stable transfectants.	NF-$_K$B reporter

7.2.2 Transfection of mammalian cells

7.2.2.1 Transfection of ARPE19 cells with TIMP3 constructs

To examine the effect of TIMP3 on RAGE activation, ARPE19 cells were stably transfected with WT.T3, E139X and S181C in pcDNA3 using *Trans*IT-LT transfection reagent (section 2.2.2.9). WT.T3, E139X and S181C in pcDNA3 vector were already available in our lab (section 7.3.1). Cells were seeded into 6-well plates at a density of $15x10^4$ cells per well in complete growth medium and grown overnight until cells became 50-70% confluent.

Transfection was performed at 6:1 transfection ratio (*Trans*IT-LT1: DNA) and 48 hours post-transfection cells were trypsinised and seeded into T25 flask containing complete growth media and 50µl of Geneticin (500µg/ml). Cells were allowed to reach the desired confluence level before preparing 10cm plates for examining protein expression.

7.2.2.2 Transfection of HEK293T cells with luciferase reporter vectors

HEK293T cells were transfected transiently with the desired luciferase reporter vectors in 6-well plates or 24-well plates for the dual luciferase reporter assay system (section 2.2.3.4.1) or luciferase assay system (section 2.2.3.4.2), respectively.

7.2.3 ARPE19-ECM preparation for the dual luciferase assay

In order to prepare ARPE19-ECM for the dual luciferase reporter assay, un-transfected ARPE19 cells or ARPE19 cells stably transfected with WT.T3, E139X or S181C were grown to 80-90% confluence in T75 flasks, removed and counted (section 2.2.2.5) then seeded into 10cm tissue culture dishes ($1x10^6$ per plate) to check TIMP3 protein expression by western blotting or 24-well plates ($32x10^3$ per well) to be used in dual luciferase reporter assay. Cells were maintained for 10 days in complete growth medium without or with selection antibiotic for un-transfected and transfected cells, respectively.

The cells were then removed from the tissue culture dishes to analyse ECM protein expression using hypotonic buffers described in 2.2.3.1.2. Similarly ARPE19 cells were removed from the 24-well plate surface to prepare ECM for the dual luciferase reporter assay by incubating in 20mM NH_4OH for 5 minutes as described in section 2.2.3.1.3.

7.2.4 RAGE induction in mammalian cells

10cm tissue culture dishes were coated with RAGE ligands including S100B (10µg/ml) and AGE-BSA (200µg/ml) prepared in 0.05M bicarbonate buffer and incubated at 4°C for 24 hours. Then, un-transfected HEK293T were seeded into either un-coated or coated plates at $1x10^6$/plate and maintain for 2 days in 2% FBS-starving growth media. After the treatment period, cells were lysed in RIPA lysis buffer (see section 2.2.3.1.1) and cell lysates were stored at -80°C until analysed by SDS-PAGE and western blotting.

7.2.5 RAGE and TIMP3 expressions by western blotting

To examine RAGE expression in HEK293T cells and TIMP3 in ARPE19-ECM, SDS-PAGE and western blotting were performed (section 2.2.3.3). Polyclonal rabbit RAGE antibody was used to detect RAGE at dilution of 1:2000, and primary polyclonal rabbit anti-TIMP3-N-terminal antibody (first loop) was used to identify TIMP3 at 1:3000. Subsequently, the secondary antibody was swine horseradish peroxidase-conjugated anti-rabbit antibody at 1:10000 used for both primary antibodies. The PVDF membrane was developed using chemiluminescent substrate (section 2.2.3.3.5).

7.2.6 Luciferase assays

7.2.6.1 Dual Luciferase reporter assay system with RAGE ligands and ARPE19-ECM treatments

To examine the effect of wild type or SFD-mutant TIMP3 on RAGE signalling pathways, dual luciferase reporter assay was performed using ECM prepared from un-transfected and TIMP3-constructs transfected as explained in section 2.2.3.7.1.

7.2.6.1.1 Co-transfection of HEK293T cells

HEK293T cells were transfected with four luciferase reporter vectors accompanied by *Renilla* luciferase control vector (2.2.3.7.1).

7.2.6.2 Luciferase assay system

Luciferase assay system kit was applied according to manufacturer's instruction to study the effect of wild type and mutants TIMP3 on AGE receptor and to confirm data from the dual luciferase reporter assay (see section 2.2.3.4.2).

7.3 Results

7.3.1 Dual luciferase assay

Initially experiments were carried out using the dual luciferase reporter assay (section 2.2.3.7.1) as this is supposed to give more reliable results in transient transfection experiments than the firefly luciferase assay alone as any differences in transfection efficiency between cells are controlled by measuring the ratio of firefly luciferase from the reporter to constitutively expressed *Renilla* luciferase. Extracellular matrix from ARPE19 cell expressing wild type- or SFD- TIMP3 was used as the source of TIMP3 proteins and HEK293T cells, known to express RAGE, were transfected with the reporter constructs.

7.3.1.1 Expression of RAGE in HEK293T

Prior to measuring RAGE activation, the expression of RAGE by HEK293T cells was examined on both untreated cells and cells treated with different RAGE ligands or ARPE19 ECM containing TIMP3 proteins, to ensure any changes in activation that might be observed were not in fact due to changes in receptor expression.

In order to examine RAGE expression in HEK293T cells, they were seeded onto tissue culture petri dishes coated with RAGE-ligands S100B (10µg/ml) or AGE-BSA (200µg/ml) or ECM from ARPE19 transfected with WT.T3, E139X and S181C. At 2 days, cells were lysed in RIPA lysis buffer and then subjected to western blotting.

Western blotting analysis of whole cell lysates extracted from HEK293T cells revealed the presence of immune reactive protein species at approximately 55kDa, the expected size of glycosylated RAGE, in all un-treated and ligand treated cells in non-reduced gels (Figure 7.1A). In comparison with RAGE-ligand treatment, HEK293T cells treated with ARPE19-ECM showed similar bands at 55kDa. The expression of wild type and mutant TIMP3 in the ECM of ARPE19 cells was also confirmed using TIMP3 antibody in Figure 7.1B, although expression of S181C, appeared to be much stronger than E139X.

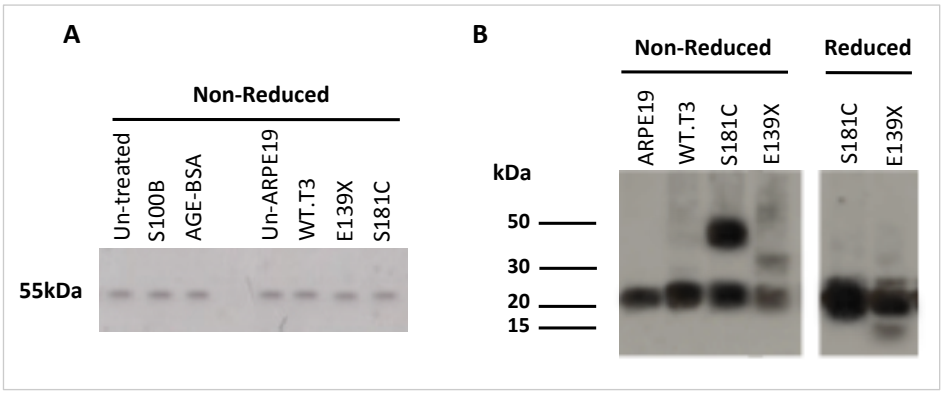

Figure 7.1: RAGE expression in mammalian cells.

(A) Western blotting analysis of RAGE expression in HEK293T cells showed a species at approximately 55kDa using polyclonal RAGE antibody. (B) Western blotting of ECM from ARPE19 cells transfected with WT.T3, E139X and S181C confirmed the expression of wild type TIMP3 protein and SFD-TIMP3 dimers.

7.3.1.2 Dual luciferase reporter assay system

To investigate the activation of NF-$_K$B in HEK293T cells treated with RAGE ligands or WT- and SFD-TIMP3, the dual luciferase reporter assay was initially optimised to determine which particular reporter vector gave the best response, to ascertain the optimal transfection ratio (experimental vector: co-reporter vector) and to determine the optimal incubation time with the RAGE ligands. Two different reporter vectors were initially tested pGL3-IL8-Luc and pNF-$_K$B-Luc together with two control vectors pGL3-Basic and pGL3-Control (Table 7.1). RAGE-ligands S100B and AGE-BSA were used at 10µg/ml as reported by Howes *et al.* (2004) and Zong *et al.* (2010).

The dual luciferase reporter assay was performed by transfecting HEK293T cells with each of the four reporter vectors together with the control *Renilla*-luc vector (at 4:1 transfection ratio of experimental vector: co-reporter vector) and then 24hrs post transfection cells were treated with S100B for 12-48 hours. Little, if any induction in response to S100B was seen with the pNF-$_K$B-Luc reporter but the pGL3-IL8-Luc gave a clear response at 24hrs post-induction. Surprisingly the pGL3-Control vector also showed an apparent increase in induction in response to S100B and it is possible that this is due to NF-$_K$B binding sequences in the SV40 enhancer present in this vector (Figure 7.2). For this reason the pGL3-IL8-Luc vector was chosen for further optimisation experiments.

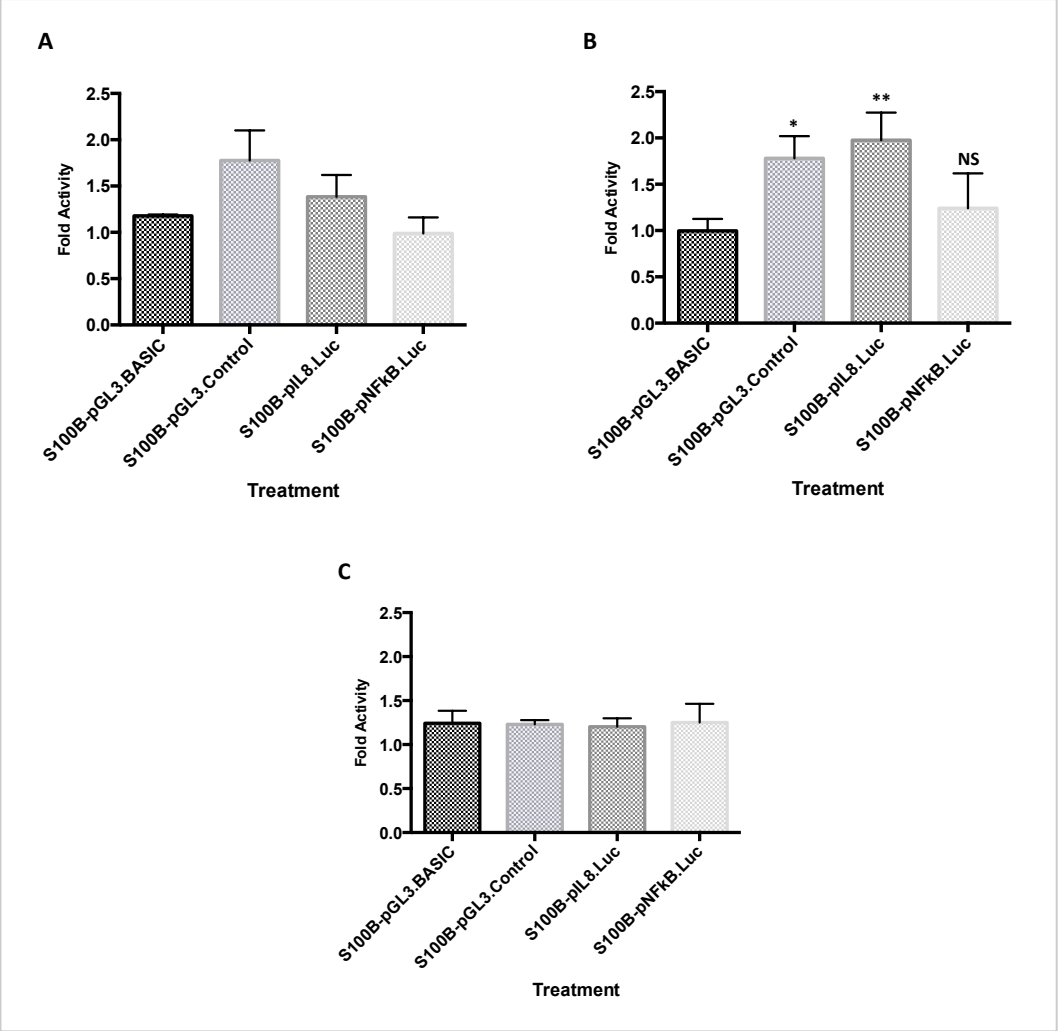

Figure 7.2: Optimisation of dual luciferase reporter assay parameters. Optimisation of dual luciferase reporter assay parameters.

*Transfected HEK293T cells treated with S100B for (A) 12hrs, (B) 24hrs & (C) 48hrs. Fold activity was calculated as the ratio of firefly to renilla and then normalised to the untreated vector transfected cells. *: P= 0.0211; **: P= 0.0082; NS: not significant. Data are as means ± S.E of two experiments and analysed using one-way ANOVA.*

In the following experiments, transfection of HEK293T cells was performed, using pGL3-IL8-luc, with *Renilla-luc* vector, at two transfection ratios (experimental vector: co-reporter vector) encompassing 4:1 and 40:1. At 24 hours post-transfection, transfected cells were treated with S100B (10µg/ml) or AGE-BSA (200µg/ml) for 12-48 hours (Figures 7.3 and 7.4).

This showed that a ratio of 40:1 firefly:*Renilla* gave a much higher induction than for 4:1 in response to S100B at 12 hours treatment, giving a 3.5 fold induction (Figure 7.4).

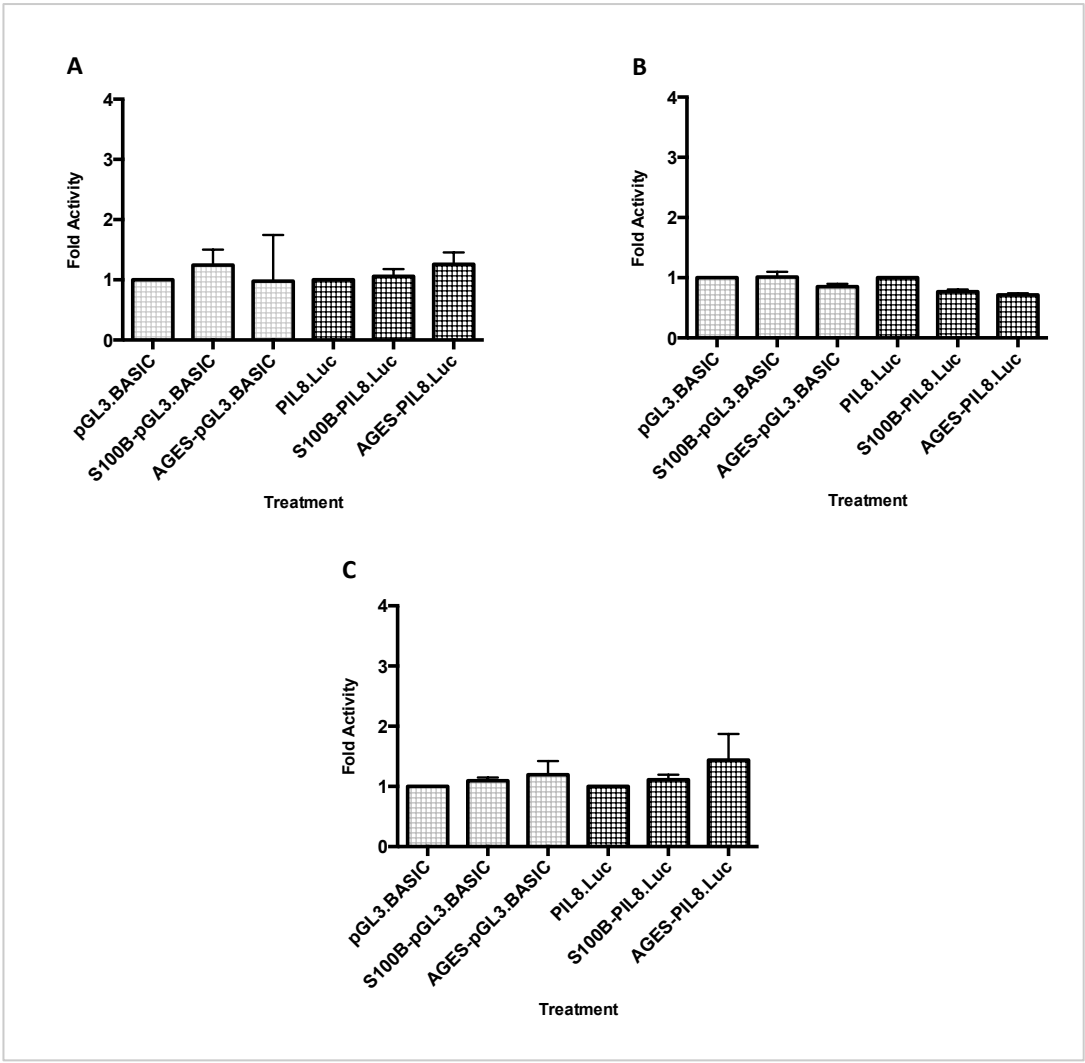

Figure 7.3: Dual luciferase reporter assay (4:1 transfection ratio).

HEK293T cells were transfected with reporter vectors at 4:1 transfection ratio (experimental vector: co-reporter vector) and then 24 hours post-transfection cells were seeded onto wells coated with S100B (10µg/ml) or AGES-BSA (200µg/ml). Representation of RAGE-ligands treated HEK293T cells for (A) 12 hrs, (B) 24hrs & (C) 48 hrs. Fold activity was initially calculated as the ratio of firefly to renilla and then the ratio of ligand treated to untreated vector transfected cells. Data of two experiments are shown as means ± S.E and analysed using one-way ANOVA.

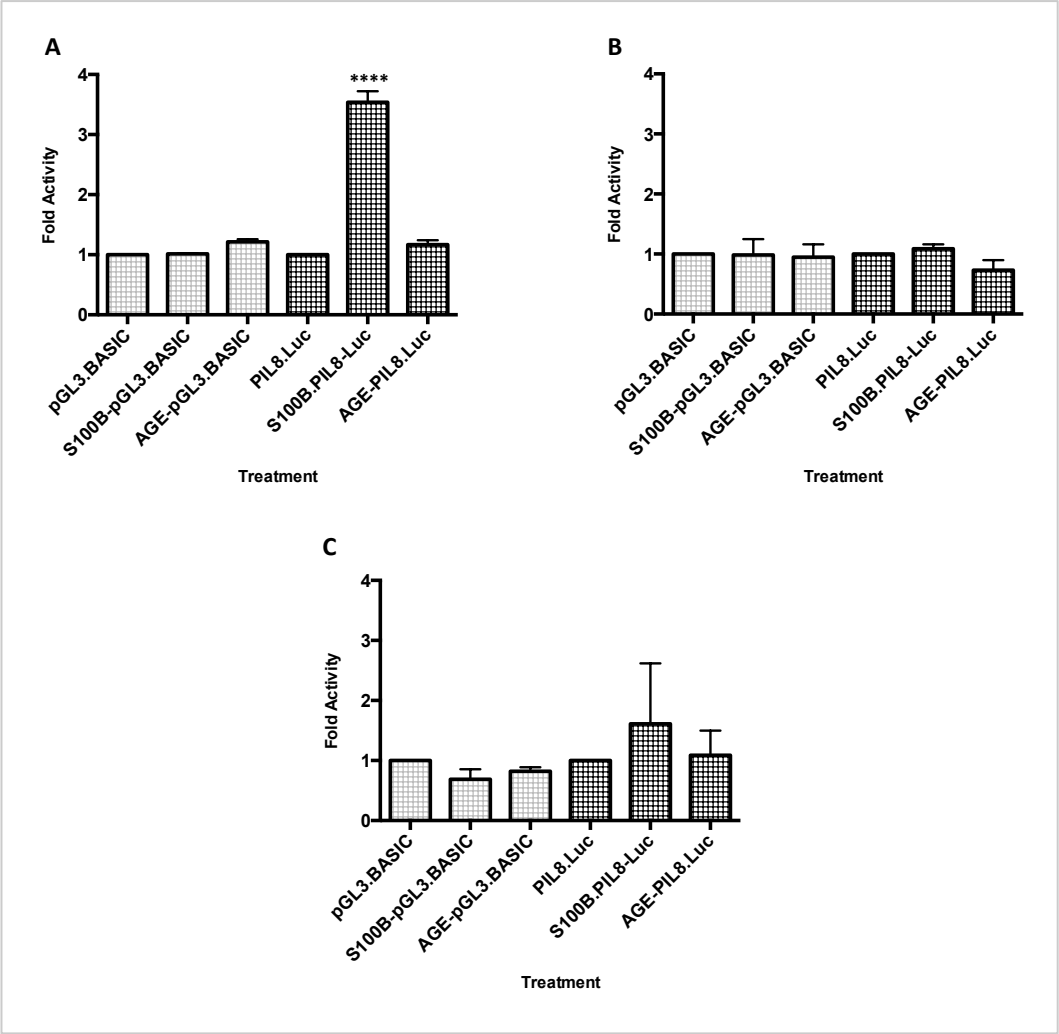

Figure 7.4: Dual luciferase reporter assay (40:1 transfection ratio).

*HEK293T cells were transiently transfected with reporter vectors and then seeded onto wells coated with S100B (10µg/ml) and AGES-BSA (200µg/ml) 24 hours post-transfection. Demonstration of RAGE-ligands treated HEK293T cells for (A) 12 hrs, (B) 24hrs & (C) 48 hrs. Fold activity was initially calculated as the ratio of firefly to renilla and then the ratio of ligand treated to untreated transfected cells. **** Comparison between pGL3-IL8-luc untreated and RAGE-ligands treated cells. Data are as means ± S.E of two replicate experiments and analysed using one-way ANOVA. (**** P Value <0.0001)*

Following this optimisation, experiments were performed using the ECM from TIMP3 and SFD-TIMP3 transfected ARPE19 cells using the pGL3-IL8-Luc vector: pTK-Luc at a ratio of 40:1 and measuring luciferase activity after 12 hours (Figure 7.5). This showed that ARPE19 cell matrix alone induced a strong luciferase response in the HEK293T cells, which was not significantly changed in response to matrix containing WT-TIMP3. However there did appear to be a significant increase ~1.5 fold in the luciferase response for matrix containing the S181C SFD mutant protein. However this result was put into some doubt by the fact that the E139X mutant gave a much lower response than either untransfected or WT-TIMP3 transfected cell ECM.

These data are difficult to explain but may be a combination of the facts that ARPE19 ECM will contain many factors that could induce an NF-$_K$B response through RAGE or other receptors that couple to NF-$_K$B. Moreover the IL8 promoter sequence contains additional transcription factor binding sites that may respond to other stimuli. Lastly Figure 7.1 shows that E139X was poorly expressed, relative to the endogenous TIMP3 or the S181C mutant.

As a result of this it was decided to carry out a simplified luciferase reporter assay in which pcDNA3-TIMP3/SFD-TIMP3 vectors were co-transfected into HEK293T cells together with a new reporter vector, pGL4-Luc2P/NF-$_K$B that contains five tandem copies of the NF-$_K$B response sequence upstream of Luc2P, a luciferase enzyme codon optimised to give high expression in mammalian cells. As the pcDNA3 vector contains the SV40 origin or replication this should give high level, transient expression of the TIMP sequences in these cells.

Additionally it was decided to also co-transfect the cells with a vector containing RAGE (pcDNA3-RAGE) to ensure that responses were not limited by the endogenous expression level of RAGE in HEK293T cells.

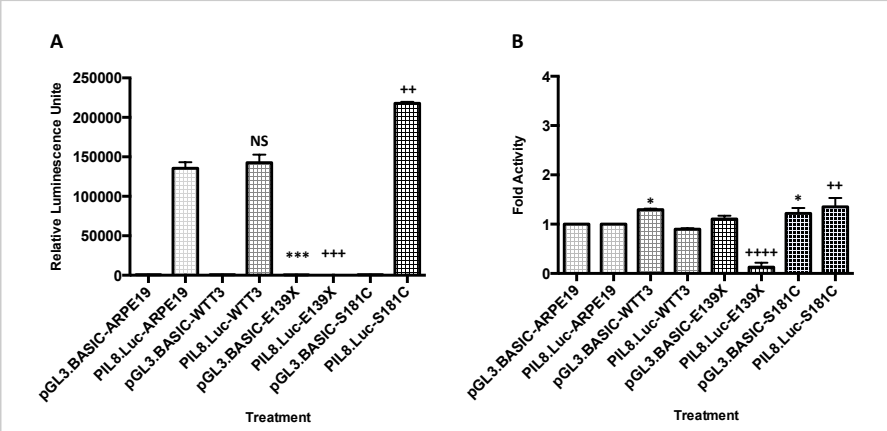

C

RLU P value	WT.T3	E139X	S181C
pGL3. Basic ARPE19 vs (*)	0.0859	0.0003	0.9321
PIL8.Luc ARPE19 vs (+)	0.1817	0.0003	0.0028

Fold activity P value	WT.T3	E139X	S181C
pGL3. Basic ARPE19 vs (*)	0.0127	0.8014	0.0943
PIL8.Luc ARPE19 vs (+)	0.8194	<0.0001	0.0026

Figure 7.5: Dual luciferase reporter assay (40:1 transfection ratio, ARPE19 ECM treatment).

*HEK293T cells transiently transfected with reporter vectors were seeded onto ARPE19-ECM, prepared using NH_4OH, 12 hours post-transfection. (A) & (B) Demonstration of 12hrs ARPE19-ECM treated HEK293T cells. (C) The Table shows the p value of cells treated with WT/SFD-TIMP3 ECM relative to un-transfected ARPE19-ECM. **** Comparison between pGL3-Basic ARPE19-ECM, and WT.T3/SFD-TIMP3-ECM. $^{++++}$ Comparison between pGL3-IL8-luc ARPE19-ECM and other pGL3-IL8-luc WT/SFD-TIMP3 ECM treated including E139X and S181C. Data of a single experiment are shown as means ± S.E and analysed using one-way ANOVA.*

7.3.2 Co-transfection of TIMP3/SFD-TIMP3, RAGE and pGL4-luc2p/NF-$_K$B using the Luciferase assay system

In order to investigate the effect of RAGE ligands or WT- and SFD- TIMP3 in NF-$_K$B transcriptional activity, luciferase assay system was performed using HEK293T cell transfected with triple DNAs including pGL4-luc2P/NF-$_K$B, RAGE and SFD-TIMP3.

7.3.2.1 RAGE expression in HEK293T cells

The expression of RAGE and SFD-TIMP3 in transfected HEK293T was initially examined prior to proceeding with the luciferase assay. To examine the expression of RAGE and dimeric TIMP3 in SFD-TIMP3 transfected HEK293T, cells were transfected with pGL4-luc2P/NF-$_K$B, RAGE and SFD-TIMP3 constructs including E139X, S181C and SplT3.Mutant (section 2.2.3.7.2). 48 hours post transfection, cell lysates were prepared to check the expression of RAGE, whereas, for TIMP3, cells were removed using hypotonic buffers and then ECM was extracted using 2X SDS sample buffer. Both samples, cell lysates and ECM, were subjected to western blotting (section 7.3.5).

Un-transfected HEK293T cell produced a basal level of RAGE under normal condition at 55kDa; conversely, transfected HEK293T cells showed a strong expression at 55kDa. The positive control is the extracellular domain of RAGE fused to Human IgG1 Fc domain and ran at the expected size of 80-90kDa (Figure 7.6A).

Western blotting analysis of ECM extracted from HEK293T cells demonstrated that TIMP3 species were expressed at 20- and 30- kDa in all un-transfected and TIMP3-transfected cells in non-reduced gel, corresponding to the previously reported un-glycosylated and glycosylated protein, respectively (Figure 7.6B). Also, ECM from SFD-TIMP3 transfected cells showed additional higher molecular weight protein species in non-reduced gels; for instance, S181C-TIMP3 expressed a protein at ~48kDa, E139X-TIMP3 expressed a protein at 30kDa and SplT3.Mut expressed two species at ~15 and 30 kDa. Upon reduction, the dimeric-TIMP3 bands reduced to 24kDa, 15kDa and 15kDa for S181C, E139X and SplT3.Mut, respectively. This confirmed that SFD-TIMP3 mutants expressed in HEK293T cells at 48 hours post transfection; enabling the possibility of performing luciferase assays

using HEK293T cells transiently transfected with triple DNA encompassing pGL4-luc2P/NF-$_K$B, RAGE and SFD-TIMP3 constructs.

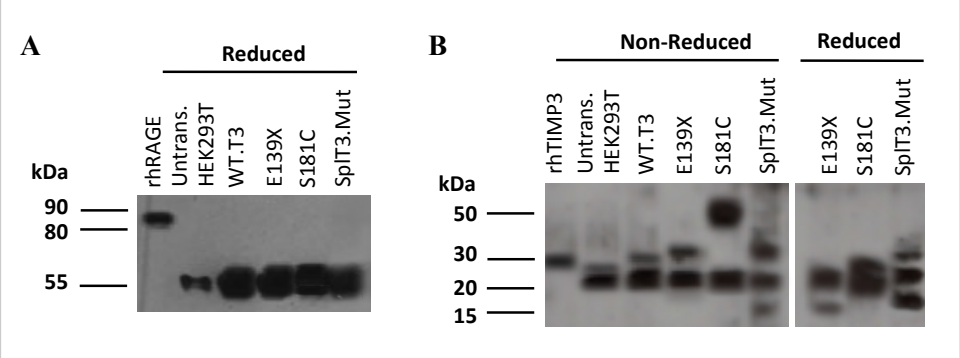

Figure 7.6: Western blotting HEK293T cell transfected with luciferase reporter vector, RAGE and SFD-TIMP3.

HEK293T cells were transfected with pGL4.Luc/NF-$_K$B, RAGE and TIMP3 constructs including WT.T3, E139X, S181C and SpIT3.Mutant. (A) RAGE expression in cell lysates using polyclonal RAGE antibody. (B) Expression of TIMP3 protein in the ECM using polyclonal anti-TIMP3.

7.3.2.2 Luciferase assay

Following the western blotting analysis of HEK293T cells transfected with triple DNAs that confirmed the expression of both RAGE and TIMP3, the luciferase assay was performed using those HEK293T cells transfected with three DNA vectors: pGL4-Luc2P/NF-$_{K}$B, RAGE and TIMP3 constructs including (WT.T3, E139X, S181C and SplT3.M) (see section 2.2.3.4.2).

While cells transfected with WT-TIMP3 showed some induction of luciferase activity this was significantly increased in cells transfected with all of the SFD-TIMP3 mutants (approximately 2-3 fold increase, relative to WT-TIMP3, p>0.0001) (Figure 7.7 C & D), indicating that SFD-mutant forms of TIMP3 may indeed activate RAGE.

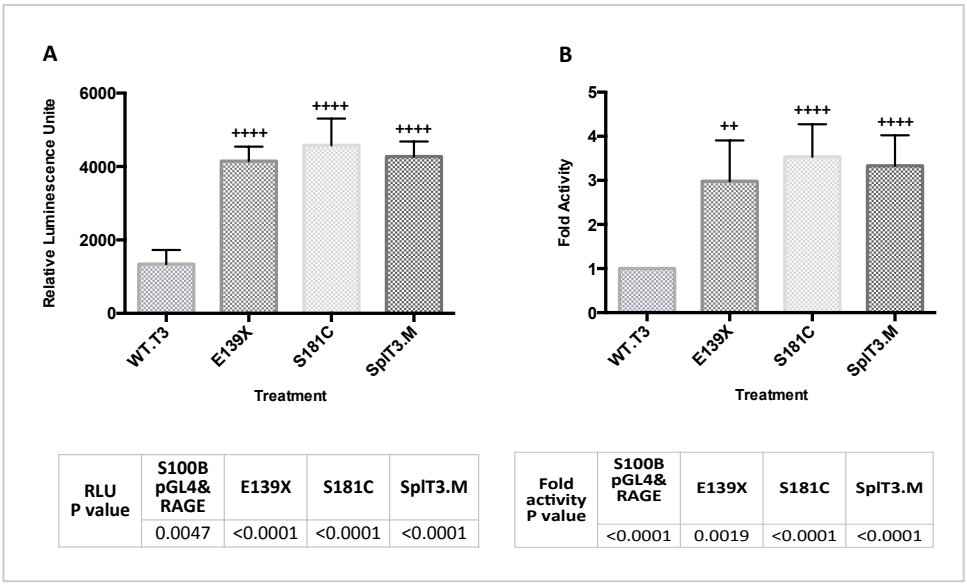

RLU P value	S100B pGL4& RAGE	E139X	S181C	SplT3.M
	0.0047	<0.0001	<0.0001	<0.0001

Fold activity P value	S100B pGL4& RAGE	E139X	S181C	SplT3.M
	<0.0001	0.0019	<0.0001	<0.0001

Figure 7.7: Luciferase assay of HEK293T cells transfected with reporter vectors and SFD-TIMP3.

HEK293T cells were transiently transfected with luciferase reporter vector, RAGE and SFD-TIMP3 in 24 well plate and, 24 hours post-transfection, incubated for another 24 hours. (A) & (B) Relative luminescence unit (RLU) and fold activity, respectively. ($^{++++}$ Comparison between SFD-TIMP3 and WT.T3 transfected cells). Fold activity was calculated as the ratio of SFD-transfected to WT.T3-transfected cells. Data of a three replicate experiments are shown as means ± S.E and analysed using one-way ANOVA.

7.4 Discussion

Advanced glycation end products receptor (RAGE) is a cell surface pattern recognition receptor that is widely expressed in a diversity of cell types; for instance, smooth muscle cells, cardiac myocytes, endothelium and neural tissue (Brett *et al.*, 1993). RAGE binds to multiple ligands that include amphoterin high mobility group box-1 (Hofmann *et al.*, 1999), Mac-1 (Chavakis *et al.* 2003), amyloid-β (Yan and Sage 1999) and S100 protein (Ghavami *et al.* 2008). Structurally, RAGE belongs to the immunoglobulin superfamily and consists of five domains including N-terminal signal peptide, V-type immunoglobulin- like, C-type immunoglobulin- like, a single trans-membrane and C-terminal intracellular cytoplasmic tail per (Neeper *et al.* 1992, Koch *et al.* 2010). The cytoplasmic domain is considered as a fundamental domain for RAGE-mediated cell signalling.

Previous binding studies showed that RAGE ligands including S100B and Amyloid-β function as oligomers that trigger RAGE activation through receptor dimerisation on the plasma membrane. RAGE dimerisation is believed to be responsible for recognising AGE-modified protein. (Chaney *et al.* 2005, Ostendorp *et al.* 2007, Xie *et al.* 2008, Zong *et al.* 2010)

It is well established that S100B occurs in dimer and tetramer forms and that S100B tetramer has higher binding affinity toward RAGE than the dimer form. S100B tetramer was observed to promoted cell survival and cause a strong cell growth, suggesting that such oligomer induces RAGE activation via receptor dimerisation at the V domain (Ostendorp *et al.* 2007).

All examined SFD-TIMP3 mutants have been shown to form dimers therefore the hypothesis here was that SFD-TIM3 dimers could mimic RAGE-ligands through direct binding to the receptor resulting in activation of RAGE signalling pathways. Western blotting confirmed RAGE expression on HEK293T cells and also that this expression was not affected by the various test ligands.

A considerable amount of time was spent in attempting to optimise the dual luciferase reporter assay as a means of assessing RAGE induction. While this appeared relatively successful for exogenously added RAGE ligands, S100B and AGE-BSA, treating the reporter cells with ECM from untransfected and TIMP3/SFD-TIMP3 transfected ARPE19 cells was somewhat inconclusive with untransfected and WT-TIMP3 transfected ARPE19 ECM

showing similarly high levels of induction and S181C TIMP3 an apparently significantly increased induction, relative to WT-TIMP3 but E139X TIMP3 showing very poor induction relative to even untransfected ARPE19 cells. Western blotting had indicated that the level of expression of E139X TIMP3 was somewhat lower than S181C TIMP3 but this would not seem to be sufficient to explain the differences seen. As alluded to earlier, it is possible that the level of TIMP3/SFD-TIMP3 expressed in the ARPE19 ECM is relatively low compared to the many other proteins that might be present there that could potentially induce an NFκB response, and this may have been exacerbated by using the IL8 promoter sequence that will respond to transcription factors in addition to NFκB.

In order to try and circumvent these issues the pcDNA3-TIMP/SFD-TIMP3 vectors were directly transfected into the ARPE19 cells, together with RAGE and a new reporter vector, pGL4-Luc2P/NF-$_{K}$B, that was expected to give higher expression of the modified luciferase gene and only in response to NF-$_{K}$B. While only preliminary, this seemed to produce much more consistent results, with all three SFD-mutant forms of TIMP3 tested giving a consistent 3-4 fold stronger induction of the NFκB reporter than the normal molecule.

However these experiments do not prove that the NFκB response is due to RAGE activation, it is possible that this is due to a different mechanism altogether. One way to confirm this would be to knock-down the expression of RAGE using small interfering RNA (siRNA) molecules and see if the SFD-induced NFκB response is supressed. Nevertheless the data presented here indicate that, unlike the wild-type molecule, SFD-TIMP3 has a proinflammatory effect on cells, which could contribute to the SFD phenotype.

Chapter 8: General Discussion

8.1 Introduction

As has already been mentioned, TIMP3 is unique among the TIMP family in being extremely highly conserved across species and this probably reflects the fact that it has such wide-ranging binding partners and functional activities. Not only it does inhibit all MMPs it also inhibits several members of the adamalysin family, and such plays wide ranging roles in regulating inflammation and cell matrix turnover. Moreover TIMP3 has unique characteristics that are independent of its ability to inhibit proteinases, including VEGFR2 inhibition, EFEMP1 binding and tight association with glycosaminoglycans in the ECM. These latter properties may be particularly important in the eye where TIMP3 is constitutively expressed by the retinal pigment epithelial and choroidal endothelial cells and is a constituent of Bruch's membrane.

These facts go some way towards explaining why mutations in the TIMP3 gene are associated with an inherited ocular disease, Sorsby's fundus dystrophy. Although the literature has enriched our understanding of the biochemical properties of wild type TIMP3, a definitive answer as to how SFD-TIMP3 mutations give rise to a disease with an exclusively ocular pathology remains uncertain, and this has been the focus of this thesis. Moreover, there are a number of clues that suggest TIMP3 plays a role in other retinopathies, such as Malattia Leventinese and age-related macular degeneration. AMD, in particular, is likely to have an ever increasing impact on quality of life and economic cost to health services as the elderly population increases and so establishing a common mechanism underpinning these diseases, if indeed one exists, has great potential for the development of new therapeutic strategies to alleviate these currently incurable conditions.

8.2 SFD-TIMP3 dimerisation

This project initially aimed to strengthen our hypothesis that TIMP3 dimerisation is a common characteristic of all SFD mutants and essential for SFD pathogenesis. Although most of the SFD mutations have been assessed in our laboratory, this project has examined five previously identified mutations where the effects on dimerisation were unknown. These included the recently described C-terminal mutations Y128C, Y154C and Y159C, and the novel mutations in the N-domain, S15C, and at the intron4/exon5 splice site.

This project has now demonstrated that all of these diverse mutations result in dimeric TIMP3 protein, providing overwhelming evidence that dimerisation is a prerequisite for SFD.

This would suggest that dimerisation of TIMP3 results in a protein with novel properties that could play a toxic role in the disease. Previous work in our laboratory by Langton *et al.* (2005) demonstrated that TIMP3 dimers and multimers show impaired turnover, relative to the wild-type molecule, likely explaining the increased TIMP3 protein deposition in the eye of SFD individuals observed by Fariss *et al.* (1998).

As the majority of data indicate that mutant TIMP3 retains its ability to inhibit MMPs, it is possible that this increased deposition of a potent proteinase inhibitor in Bruch's is sufficient to explain the SFD phenotype as decreased proteolysis might account for thickening of Bruch's membrane which could in turn lead to hypoxia, the release of VEGF and subsequently choroidal neovascularisation. However, if mutant TIMP3 retains its ability to inhibit VEGFR2, as reported by Fogarasi *et al.* (2008), it is difficult to explain why the high level of TIMP3 in the eyes of these patients does not inhibit this process.

Moreover, it is easily conceivable that other types of mutation in TIMP3 could impair its clearance from Bruch's yet all result in dimerisation. This lends support to the hypothesis that dimerisation of TIMP3 has a very specific effect on its function. This may be through increased avidity for cell surface proteins, such as TACE, or enabling TIMP3 to cross-link and potentially activate receptors.

8.3 The physiological functions of SFD-TIMP3 mutants

A number of possibilities have been explored in this thesis with varying degrees of success. It has previously been observed that very high concentrations of TIMP3 induce apoptosis in various cell types, and that SFD mutant forms appear more toxic (Baker *et al.*, 1999; Majid *et al.*, 2002). However here we explored whether lower concentrations of SFD-TIMP3, expressed *in situ* in the ECM of RPE cells, may make them more susceptible to other pro-apoptotic ligands.

This did indeed appear to be the case as the apoptosis assay data presented in Chapter 4 provides evidence for SFD-TIMP3 increasing the sensitivity of ARPE19 cells to Fas-induced apoptosis with all examined mutations including E139X, S156C, H158R and S181C demonstrating increased apoptosis relative to wild-type TIMP3. This may be particularly relevant in the retina as the concentrations of TIMP3 found to be directly pro-apoptotic *in*

vitro may not be reached *in vivo*, but may still be important in combination with other pro-apoptotic ligands that may be found there.

The pro-apoptotic effects of TIMP3 have been ascribed to its ability to inhibit sheddases, particularly TACE, and it is possible that dimerisation increases the avidity of TIMP3 for this protein on the cell surface. This possibility was made all the more intriguing by the report that TIMP3 stabilises TACE in an inactive *dimeric* form, with activation resulting in dissociation of TIMP3 and an active TACE monomer (Xu *et al.* 2012). While the pull-down assay, using C-terminally HaloTagged TIMP3, failed to confirm any increased association of the mutants with TACE following PMA-induced activation, this was probably more a result of limitations of the assay and it is possible that the relatively large HaloTag (approximately 30kDa) impaired the binding of the fusion protein to TACE.

An additional or alternative possibility, however, is that TIMP3 dimers/multimers are recognised by the pattern recognition receptor RAGE, activation of which is known to induce apoptosis in these cells (Howes *et al.* 2004). The data presented in Chapter 7 demonstrated that SFD-TIMP3 mutants appeared to have a pro-inflammatory effect in the HEK293 NF-$_{\mathbf{K}}$B reporter assay. While this effect was also seen with known RAGE ligands, unfortunately time did not allow for direct confirmation that the effect of SFD-TIMP3 was mediated by RAGE rather than other pro-inflammatory mechanisms.

Another intriguing possibility was that dimerisation of TIMP3 may actually convert the molecule into a VEGFR2 agonist, activating the receptor in the same way as the dimeric ligand and potentially explaining the choroidal neovascularisation that is characteristic of the disease in most patients. However, binding to VEGFR2 is mediated via the C-terminal domain of TIMP3 (Qi *et al.* 2003) and so this possibility can almost certainly be excluded for the E139X mutant that lacks all but fifteen amino acids of the C-terminal domain and also for the splice site mutation, which we show in Chapter 3, appears to result in TIMP3 proteins totally lacking this domain. Despite this, both of these mutations still give rise to dimers and these patients still exhibit CNV.

It had previously been reported that SFD mutant forms of TIMP3 induce increased expression of VEGFR2 on the surface of porcine aortic endothelial cells, potentially explaining why the increased level of TIMP3 expressed in Bruch's membrane of SFD patient retinas does not prevent the characteristic neovascularisation (Qi *et al.* 2009). However here we did not find any increase in VEGFR2 on the surface of HUVEC incubated on ECM

containing SFD-mutant forms of TIMP3. Nevertheless, this matrix showed reduced ability to inhibit invasion of HUVEC relative to the same matrix containing wild-type TIMP3. As virtually all mutations affect the C-domain of TIMP3, the most likely explanation for this is that dimerisation about this domain masks the VEGFR2 binding site of TIMP3. The S15C mutation in the N-domain is clearly an exception, yet these patients still exhibit CNV (Schoenberger and Agarwal 2012). However, S15C does lie in close proximity to the C-domain of TIMP3 (Figure 1.14) so it is possible that dimerisation about this residue still masks VEGFR2 binding. This also explains the contradiction between this data and that described by Fogarasi *et al.* (2008), who found that S156C-TIMP3 expressed in bacteria retained its ability to inhibit VEGFR2, as that protein was not dimeric.

Previous studies have shown EFEMP1 to be a binding partner of TIMP3 (Klenotic *et al.* 2004). The pull-down assay data in Chapter 6 demonstrated that mutation of either molecule did not inhibit this interaction so that accumulation of one protein, caused by mutation, may cause a similar accumulation of its binding partner. Such protein complexes may prevent trafficking of nutrients across Bruch's membrane and hence lead to deposition of other protein molecules seen in SFD and ML. As EFEMP1 binds to complement factor H (CFH), deposition of TIMP3-EFEMP1 complexes are likely to be accompanied by CFH, potentially sequestering this molecule, preventing its ability to regulate complement activation.

8.4 A common pathogenesis mechanism linking SFD, AMD and ML

Whereas SFD and ML are very rare, AMD is the leading cause of central vision loss in the elderly population in industrialised nations, and prevalence increases exponentially with age (Owen *et al.* 2012, Saksens *et al.* 2014); therefore there is a pressing need for a better understanding of the molecular aetiology of this disease.

Multiple factors seem to link AMD, SFD and ML including phenotypic similarities, the accumulation of TIMP3 and EFEMP1 and the fact that EFEMP1 is a binding partner for complement factor H, polymorphisms in which are the biggest known risk factor for AMD. While accumulation of TIMP3 or EFEMP1 in SFD and ML, respectively, are caused by specific mutations, age-related protein modifications, such as oxidation and AGE formation may play a role in this accumulation in AMD. Accumulation of TIMP3, by whatever mechanism, is likely to inhibit clearance of damaged proteins from Bruch's membrane, impairing nutrient transport. If this process also results in sequestration of CFH (Wyatt *et al.*

2013), it is likely to create a low-grade pro-inflammatory environment, which again is symptomatic of all three diseases.

There are of course phenotypic differences between these diseases, with SFD bearing much more similarity to wet AMD and ML to dry AMD. ML also shows a unique mosaic pattern of drusen formation. While these differences may be indicative of a different mechanism, they could also be explained by the differences in initiating agent. Mutations in EFEMP1 initially cause intracellular accumulation of the molecule, potentially also affecting the distribution of associated proteins which may then be released as the tissue atrophies. The differences in CNV between ML and SFD could well relate to the fact that, in contrast to SFD, any TIMP3 accumulating in ML will still be a functional VEGFR2 inhibitor.

Additionally, accumulation of these protein complexes may trigger activation of RAGE and other pattern recognition receptors, which can increase release of VEGF (Roybal *et al.* 2005) and trigger apoptosis (Howes *et al.* 2004). Accumulation of mutant EFEMP1 in the endoplasmic reticulum also leads to increase VEGF expression by RPE (Roybal *et al.* 2005).

8.5 Therapeutic implications

As described earlier in section 1.8, a number of approaches have been used to treat AMD, SFD and ML; however the vast majority target the damage caused by choroidal neovascularization. While recent drugs targeting VEGF, such as ranibizumab, have been a great success in this respect, they only limit this damage and do not address the geographic atrophy that also characterizes these diseases and results in slower but inevitable vision loss. As outlined in section 1.8, recent breakthroughs in gene editing have made gene therapy a more realistic possibility for treating both genetic and age-related retinopathies, and the eye is probably the most treatable tissue in the body in this respect. However, gene therapy has largely failed to live up to expectations over several decades and other treatment options are urgently needed to help alleviate the predicted increased burden AMD is set to inflict on society.

The data presented in this thesis strengthen the potential connection between ML, SFD and AMD. If, as postulated, accumulation of TIMP3, EFEMP1 and CFH complexes are an important factor in disease pathology, then this suggests that targeting these complexes with

drugs that prevent their association and/or trigger their dissociation, may be an important new therapeutic target that would have the potential to address both geographic atrophy and CNV.

8.6 Limitation of the project

The many different functional/molecular targets examined in this project meant that that much of the data is still quite provisional and needs further work to draw definitive conclusions. Work was hampered by the time taken to successfully establish the many different assays required. However, because TIMP3 is such a multi-functional molecule and it was unknown which, if any, of these functions might be affected by dimerisation, it was thought necessary to take a wide approach. Nevertheless, it has highlighted a number of areas that are ripe for further investigation, particularly where this may lead to the development of new therapeutic strategies.

Work on TIMP3 is greatly hampered by the difficulty in producing significant quantities of purified protein, and this is even more problematic for the mutant forms. This is at least partly due to relatively low levels of expression, the protein being highly basic and also strongly localising to the ECM. SFD-TIMP3 expressed in bacteria fails to dimerise (Fogarasi *et al.* 2008), and as this is almost certainly a prerequisite for disease, bacterial expression is not an option. For this reason, all the work described here was on proteins expressed *in situ*. While this is a much better reflection of the *in vivo* situation, it makes it much more difficult to clearly establish the molecular mechanisms involved. Moreover, all cell types examined express TIMP3 endogenously to some extent, which can further complicate results.

There have also been reports that SFD-mutant forms fail to dimerise in some mammalian cells, which would further complicate purification of the relevant molecule. For example, (Qi *et al.* 2009) reported that S156C TIMP3 overexpressed in ARPE19 cells was monomeric and (Lin *et al.* 2006) showed that H158R expressed in HEK293 did not dimerise. However we have shown that both of these proteins form dimers in ARPE19 cells (Langton *et al.* 2005, Mujamammi 2013). In the case of H158R, it seems the discrepancy is due to the relative low levels of expression achieved by those authors, although in our hands dimerisation was less pronounced and this may well explain the relatively late age of onset of the disease in these patients. In the case of the S156C mutant in ARPE19 cells this could be explained by the fact that the TIMP3 was being detected by using a C-terminal FLAG tag (Qi *et al.*, 2009). It is

quite possible that dimerisation about the C-domain sterically inhibits recognition of the FLAG epitope by the antibody.

8.7 Future work

Although this project has made some progress in understanding the molecular mechanism of SFD and indicated possible links to AMD, more precise data are required that will require production of significant quantities of purified recombinant proteins. As outlined above, this is technically challenging.

It is also obviously important to be able to determine whether multimeric TIMP3 produced as a result of ageing shares similar properties to SFD-TIMP3. As we have shown here (section 2.1.9), it is possible to create AGE-modified proteins *in vitro* but this does require very high concentrations of pure protein and this could only likely be achieved by expression in bacteria.

To date production of recombinant TIMP3 in bacteria has required refolding of the protein which is produced in an insoluble form. This may be suitable for AGE-modification but it does seem to preclude dimer formation of SFD-TIMP3 (Fogarasi *et al.* 2008). Functional dimeric VEGF has, however, been successfully purified from *E.coli* inclusion bodies (Scrofani *et al.* 2000) and so it may still be possible under appropriate conditions.

Production of TIMP3, fused to a protein know to be soluble in bacteria, such as glutathione-S-transferase or maltose binding protein, may help in this respect, although the redox potential inside bacteria is not favourable for disulphide bond formation. Fusion proteins do, however, also have other potential disadvantages with respect to TIMP3 as addition of even a single amino acid residue at the N-terminus of the molecule abrogates its MMP-inhibitory activity (Langton *et al.* 2005) and cleavage of most N-terminal fusion proteins leaves behind additional amino acids. Even if MMP-dependent functions are not being examined, this prevents assessment of correct folding by this means. The alternative of fusion at the C-terminus would likely inhibit dimerisation of SFD-TIMP3. The small ubiquitin-related modifier (SUMO) fusion system offers some advantages in this respect as it is fused to the N-terminus of the protein of interest and easily removed by SUMO protease to generate native protein without leaving any additional residues (Butt *et al.* 2005) and we have begun to explore this possibility in our laboratory.

While mammalian cell expression is the obvious alternative, and has been achieved for TIMP3 (Apte *et al.* 1995), protein yields are very low, probably as a result of binding of TIMP3 to glycoproteins on the cell surface and there are currently no reports of successful purification of SFD-TIMP3 from these cells.

Another possibility that is being explored in our laboratory is the use of biolayer-interferometry (Abdiche *et al.* 2008), using a BLItz machine produced by ForteBio. This enables kinetic analysis of protein interactions in very small volumes. Moreover, provided one of the proteins is available in purified form for immobilisation onto the chip, it is possible to get kinetic data from proteins expressed in a cell lysate. We have successfully detected binding of TIMP3 to immobilised VEGFR2-Fc fusion protein by this method (unpublished observations).

8.8 Conclusions

The original hypotheses of this project were:

1. That all TIMP3 mutations found in Sorsby's fundus dystrophy result in TIMP3 dimerisation
2. These TIMP3 dimers have a toxic effect on cells and trigger similar responses to those seen in age-related macular degeneration

The first of these has been successfully addressed and demonstrates that TIMP3 dimers are almost certainly the toxic agent responsible for SFD.

We have also found that these mutant forms of the molecule can trigger an inflammatory response and increase the susceptibility of retinal pigment epithelial cells to apoptotic death, both of which are features of age-related macular degeneration. Additionally, mutation does not appear to impair the interaction between TIMP3 and EFEMP1 and accumulation of these proteins, is a common feature of SFD, ML and AMD. All of this is circumstantial evidence that TIMP3 plays a role in the pathogenesis of AMD, and while it has been shown that TIMP3 multimers are indeed observed in AMD (Crabb *et al.* 2002), this does not prove they are a causative agent. However it is tempting to speculate that, if TIMP3 multimers cause SFD, then their presence in a phenotypically similar disease is unlikely to be coincidental. If this is indeed the case, it may lead the way for new therapeutic strategies in the treatment of this currently intractable disease.

Bibliography

ABBASZADE, I., LIU, R. Q., YANG, F., ROSENFELD, S. A., ROSS, O. H., LINK, J. R., ELLIS, D. M., TORTORELLA, M. D., PRATTA, M. A., HOLLIS, J. M., WYNN, R., DUKE, J. L., GEORGE, H. J., HILLMAN, M. C., JR., MURPHY, K., WISWALL, B. H., COPELAND, R. A., DECICCO, C. P., BRUCKNER, R., NAGASE, H., ITOH, Y., NEWTON, R. C., MAGOLDA, R. L., TRZASKOS, J. M., BURN, T. C. & *ET AL.* 1999. Cloning and characterization of ADAMTS11, an aggrecanase from the ADAMTS family. *J Biol Chem,* 274**,** 23443-50.

ABDICHE, Y., MALASHOCK, D., PINKERTON, A. & PONS, J. 2008. Determining kinetics and affinities of protein interactions using a parallel real-time label-free biosensor, the Octet. *Anal Biochem,* 377**,** 209-17.

AHONEN, M., POUKKULA, M., BAKER, A. H., KASHIWAGI, M., NAGASE, H., ERIKSSON, J. E. & KAHARI, V. M. 2003. Tissue inhibitor of metalloproteinases-3 induces apoptosis in melanoma cells by stabilization of death receptors. *Oncogene*, 22, 2121-34.

ALBIG, A. R., NEIL, J. R. & SCHIEMANN, W. P. 2006. Fibulins 3 and 5 antagonize tumor angiogenesis in vivo. *Cancer Res,* 66**,** 2621-9.

ALCAZAR, O., COUSINS, S. W., STRIKER, G. E. & MARIN-CASTANO, M. E. 2009. (Pro)renin receptor is expressed in human retinal pigment epithelium and participates in extracellular matrix remodeling. *Exp Eye Res,* 89**,** 638-47.

ALEXANDER, B. L., ALI, R. R., ALTON, E. W., BAINBRIDGE, J. W., BRAUN, S., CHENG, S. H., FLOTTE, T. R., GASPAR, H. B., GREZ, M., GRIESENBACH, U., KAPLITT, M. G., OTT, M. G., SEGER, R., SIMONS, M., THRASHER, A. J., THRASHER, A. Z. & YLA-HERTTUALA, S. 2007. Progress and prospects: gene therapy clinical trials (part 1). *Gene Ther,* 14**,** 1439-47.

ALEXANDER, P., THOMSON, H. A., LUFF, A. J. & LOTERY, A. J. 2015. Retinal pigment epithelium transplantation: concepts, challenges, and future prospects. *Eye (Lond),* 29**,** 992-1002.

ALMINE, J. F., BAX, D. V., MITHIEUX, S. M., NIVISON-SMITH, L., RNJAK, J., WATERHOUSE, A., WISE, S. G. & WEISS, A. S. 2010. Elastin-based materials. *Chem Soc Rev,* 39**,** 3371-9.

ALSAFFAR, FA. 2011. MSc Thesis: The role of a splice site mutation of TIMP3 in the inherited eye disease Sorsby's Fundus Dystrophy. *The University of Sheffield*. United Kingdom.

AMOUR, A., KNIGHT, C. G., WEBSTER, A., SLOCOMBE, P. M., STEPHENS, P. E., KNAUPER, V., DOCHERTY, A. J. & MURPHY, G. 2000. The in vitro activity of ADAM-10 is inhibited by TIMP-1 and TIMP-3. *FEBS Lett,* 473**,** 275-9.

AMOUR, A., SLOCOMBE, P. M., WEBSTER, A., BUTLER, M., KNIGHT, C. G., SMITH, B. J., STEPHENS, P. E., SHELLEY, C., HUTTON, M., KNAUPER, V., DOCHERTY, A. J. & MURPHY, G. 1998. TNF-alpha converting enzyme (TACE) is inhibited by TIMP-3. *FEBS Lett*, 435, 39-44.

APTE, S. S., MATTEI, M. G. & OLSEN, B. R. 1994. Cloning of the cDNA encoding human tissue inhibitor of metalloproteinases-3 (TIMP-3) and mapping of the TIMP3 gene to chromosome 22. *Genomics*, 19, 86-90.

APTE, S. S., OLSEN, B. R. & MURPHY, G. 1995. The gene structure of tissue inhibitor of metalloproteinases (TIMP)-3 and its inhibitory activities define the distinct TIMP gene family. *J Biol Chem,* 270**,** 14313-8.

BAILEY, T. A., ALEXANDER, R. A., DUBOVY, S. R., LUTHERT, P. J. & CHONG, N. H. 2001. Measurement of TIMP-3 expression and Bruch's membrane thickness in human macula. *Exp Eye Res*, 73, 851-8.

BAKER, A. H., GEORGE, S. J., ZALTSMAN, A. B., MURPHY, G. & NEWBY, A. C. 1999. Inhibition of invasion and induction of apoptotic cell death of cancer cell lines by overexpression of TIMP-3. *Br J Cancer,* 79**,** 1347-55.

BALASKAS, K., HOVAN, M., MAHMOOD, S. & BISHOP, P. 2013. Ranibizumab for the management of Sorsby fundus dystrophy. *Eye (Lond)*. 27, 101-2.

BARASCH, J., YANG, J., QIAO, J., TEMPST, P., ERDJUMENT-BROMAGE, H., LEUNG, W. & OLIVER, J. A. 1999. Tissue inhibitor of metalloproteinase-2 stimulates mesenchymal growth and regulates epithelial branching during morphogenesis of the rat metanephros. *J Clin Invest,* 103**,** 1299-307.

BARLEON, B., SIEMEISTER, G., MARTINY-BARON, G., WEINDEL, K., HERZOG, C. & MARME, D. 1997. Vascular endothelial growth factor up-regulates its receptor fms-like tyrosine kinase 1 (FLT-1) and a soluble variant of FLT-1 in human vascular endothelial cells. *Cancer Res,* 57**,** 5421-5.

BAUER, E. A., STRICKLIN, G. P., JEFFREY, J. J. & EISEN, A. Z. 1975. Collagenase production by human skin fibroblasts. *Biochem Biophys Res Commun*, 64, 232-40.

BENNETT, J., CHUNG, D. C. & MAGUIRE, A. 2012. Gene delivery to the retina: from mouse to man. *Methods Enzymol,* 507**,** 255-74.

BERTAUX, B., HORNEBECK, W., EISEN, A. Z. & DUBERTRET, L. 1991. Growth stimulation of human keratinocytes by tissue inhibitor of metalloproteinases. *J Invest Dermatol,* 97**,** 679-85.

BODE, W., GOMIS-RUTH, F. X. & STOCKLER, W. 1993. Astacins, serralysins, snake venom and matrix metalloproteinases exhibit identical zinc-binding environments (HEXXHXXGXXH and Met-turn) and topologies and should be grouped into a common family, the 'metzincins'. *FEBS Lett,* 331**,** 134-40.

BOND, M., MURPHY, G., BENNETT, M. R., NEWBY, A. C. & BAKER, A. H. 2002. Tissue inhibitor of metalloproteinase-3 induces a Fas-associated death domain-dependent type II apoptotic pathway. *J Biol Chem*, 277, 13787-95.

BONNANS, C., CHOU, J. & WERB, Z. 2014. Remodelling the extracellular matrix in development and disease. *Nat Rev Mol Cell Biol,* 15**,** 786-801.

BOOIJ, J. C., BAAS, D. C., BEISEKEEVA, J., GORGELS, T. G. & BERGEN, A. A. 2010. The dynamic nature of Bruch's membrane. *Prog Retin Eye Res,* 29**,** 1-18.

BORRAS, T. 2003. Recent developments in ocular gene therapy. *Exp Eye Res,* 76**,** 643-52.

BRETT, J., SCHMIDT, A. M., YAN, S. D., ZOU, Y. S., WEIDMAN, E., PINSKY, D., NOWYGROD, R., NEEPER, M., PRZYSIECKI, C., SHAW, A. & *ET AL.* 1993. Survey of the distribution of a newly characterized receptor for advanced glycation end products in tissues. *Am J Pathol,* 143**,** 1699-712.

BREW, K. & NAGASE, H. 2010. The tissue inhibitors of metalloproteinases (TIMPs): an ancient family with structural and functional diversity. *Biochim Biophys Acta*, 1803, 55-71.

BROGI, E., SCHATTEMAN, G., WU, T., KIM, E. A., VARTICOVSKI, L., KEYT, B. & ISNER, J. M. 1996. Hypoxia-induced paracrine regulation of vascular endothelial growth factor receptor expression. *J Clin Invest,* 97**,** 469-76.

BUCHHOLZ, D. E., HIKITA, S. T., ROWLAND, T. J., FRIEDRICH, A. M., HINMAN, C. R., JOHNSON, L. V. & CLEGG, D. O. 2009. Derivation of functional retinal pigmented epithelium from induced pluripotent stem cells. *Stem Cells,* 27**,** 2427-34.

BURKE, M. A., HUTTER, D., RESHAMWALA, R. P. & KNEPPER, J. E. 2003. Cathepsin L plays an active role in involution of the mouse mammary gland. *Dev Dyn,* 227**,** 315-22.

BUTT, T. R., EDAVETTAL, S. C., HALL, J. P. & MATTERN, M. R. 2005. SUMO fusion technology for difficult-to-express proteins. *Protein Expr Purif,* 43**,** 1-9.

BYLSMA, G. W. & GUYMER, R. H. 2005. Treatment of age-related macular degeneration. *Clin Exp Optom,* 88**,** 322-34.

CAL, S. & LOPEZ-OTIN, C. 2015. ADAMTS proteases and cancer. *Matrix Biol,* 44-46**,** 77-85.

CARMELIET, P., MOONS, L., LIJNEN, R., BAES, M., LEMAITRE, V., TIPPING, P., DREW, A., EECKHOUT, Y., SHAPIRO, S., LUPU, F. & COLLEN, D. 1997. Urokinase-generated plasmin activates matrix metalloproteinases during aneurysm formation. *Nat Genet,* 17**,** 439-44.

CAWSTON, T. E. & YOUNG, D. A. 2010. Proteinases involved in matrix turnover during cartilage and bone breakdown. *Cell Tissue Res,* 339**,** 221-35.

CHAKRAVARTHY, U., HARDING, S. P., ROGERS, C. A., DOWNES, S. M., LOTERY, A. J., CULLIFORD, L. A. & REEVES, B. C. 2013. Alternative treatments to inhibit VEGF in age-related choroidal neovascularisation: 2-year findings of the IVAN randomised controlled trial. *Lancet,* 382**,** 1258-67.

CHANEY, M. O., STINE, W. B., KOKJOHN, T. A., KUO, Y. M., ESH, C., RAHMAN, A., LUEHRS, D. C., SCHMIDT, A. M., STERN, D., YAN, S. D. & ROHER, A. E. 2005. RAGE and amyloid beta interactions: atomic force microscopy and molecular modeling. *Biochim Biophys Acta,* 1741**,** 199-205.

CHAUM, E. & HATTON, M. P. 2002. Gene therapy for genetic and acquired retinal diseases. *Surv Ophthalmol,* 47**,** 449-69.

CHAVAKIS, T., BIERHAUS, A., AL-FAKHRI, N., SCHNEIDER, D., WITTE, S., LINN, T., NAGASHIMA, M., MORSER, J., ARNOLD, B., PREISSNER, K. T. & NAWROTH, P. P. 2003. The pattern recognition receptor (RAGE) is a counterreceptor for leukocyte integrins: a novel pathway for inflammatory cell recruitment. *J Exp Med,* 198**,** 1507-15.

CHEN, Y. Y., BROWN, N. J., JONES, R., LEWIS, C. E., MUJAMAMMI, A. H., MUTHANA, M., SEED, M. P. & BARKER, M. D. 2014. A peptide derived from TIMP-3 inhibits multiple angiogenic growth factor receptors and tumour growth and inflammatory arthritis in mice. *Angiogenesis,* 17**,** 207-19.

CHEUNG, C. M. & WONG, T. Y. 2013. Treatment of age-related macular degeneration. *Lancet,* 382**,** 1230-2.

CHEW, E. Y., CLEMONS, T. E., AGRON, E., SPERDUTO, R. D., SANGIOVANNI, J. P., KURINIJ, N. & DAVIS, M. D. 2013. Long-term effects of vitamins C and E, beta-carotene, and zinc on age-related macular degeneration: AREDS report no. 35. *Ophthalmology,* 120**,** 1604-11.e4.

CHO, M. S., KIM, S. J., KU, S. Y., PARK, J. H., LEE, H., YOO, D. H., PARK, U. C., SONG, S. A., CHOI, Y. M. & YU, H. G. 2012. Generation of retinal pigment epithelial cells from human embryonic stem cell-derived spherical neural masses. *Stem Cell Res,* 9**,** 101-9.

CHUA, C. C., HAMDY, R. C. & CHUA, B. H. 1998. Upregulation of vascular endothelial growth factor by H2O2 in rat heart endothelial cells. *Free Radic Biol Med,* 25**,** 891-7.

CHUAH, Y. K., BASIR, R., TALIB, H., TIE, T. H. & NORDIN, N. 2013. Receptor for advanced glycation end products and its involvement in inflammatory diseases. *Int J Inflam,* 2013**,** 403460.

CHUONG, C., KATZ, J., PAULEY, K. M., BULOSAN, M. & CHA, S. 2009. RAGE expression and NF-kappaB activation attenuated by extracellular domain of RAGE in human salivary gland cell line. *J Cell Physiol,* 221**,** 430-4.

CRABB, J. W. 2014. The proteomics of drusen. *Cold Spring Harb Perspect Med,* 4**,** a017194.

CRABB, J. W., MIYAGI, M., GU, X., SHADRACH, K., WEST, K. A., SAKAGUCHI, H., KAMEI, M., HASAN, A., YAN, L., RAYBORN, M. E., SALOMON, R. G. & HOLLYFIELD, J. G. 2002. Drusen proteome analysis: an approach to the etiology of age-related macular degeneration. *Proc Natl Acad Sci U S A*, 99, 14682-7.

CUADRADO, E., ROSELL, A., BORRELL-PAGES, M., GARCIA-BONILLA, L., HERNANDEZ-GUILLAMON, M., ORTEGA-AZNAR, A. & MONTANER, J. 2009. Matrix metalloproteinase-13 is activated and is found in the nucleus of neural cells after cerebral ischemia. *J Cereb Blood Flow Metab,* 29**,** 398-410.

CURCIO, C. & JOHNSON, M. 2012. Structure, function, and pathology of Bruch's membrane. *Elastic,* 146.152, 210-213.

CZYZ, J. & WOBUS, A. 2001. Embryonic stem cell differentiation: the role of extracellular factors. *Differentiation,* 68**,** 167-74.

D'ALESSIO, A., MOCCIA, F., LI, J. H., MICERA, A. & KYRIAKIDES, T. R. 2015. Angiogenesis and Vasculogenesis in Health and Disease. *Biomed Res Int,* 2015**,** 126582.

DAAMEN, W. F., HAFMANS, T., VEERKAMP, J. H. & VAN KUPPEVELT, T. H. 2001. Comparison of five procedures for the purification of insoluble elastin. *Biomaterials,* 22**,** 1997-2005.

DAAMEN, W. F., VEERKAMP, J. H., VAN HEST, J. C. & VAN KUPPEVELT, T. H. 2007. Elastin as a biomaterial for tissue engineering. *Biomaterials,* 28**,** 4378-98.

DANTAS, M. A., SLAKTER, J. S., NEGRAO, S., FONSECA, R. A., KAGA, T. & YANNUZZI, L. A. 2002. Photodynamic therapy with verteporfin in mallatia leventinese. *Ophthalmology,* 109**,** 296-301.

DAWSON, D. W., VOLPERT, O. V., GILLIS, P., CRAWFORD, S. E., XU, H., BENEDICT, W. & BOUCK, N. P. 1999. Pigment epithelium-derived factor: a potent inhibitor of angiogenesis. *Science,* 285**,** 245-8.

DE CLERCK, Y., SZPIRER, C., ALY, M. S., CASSIMAN, J. J., EECKHOUT, Y. & ROUSSEAU, G. 1992. The gene for tissue inhibitor of metalloproteinases-2 is localized on human chromosome arm 17q25. *Genomics*, 14, 782-4.

DE LA PAZ, M. A., PERICAK-VANCE, M. A., LENNON, F., HAINES, J. L. & SEDDON, J. M. 1997. Exclusion of TIMP3 as a candidate locus in age-related macular degeneration. *Invest Ophthalmol Vis Sci,* 38**,** 1060-5.

DE VEGA, S., IWAMOTO, T. & YAMADA, Y. 2009. Fibulins: multiple roles in matrix structures and tissue functions. *Cell Mol Life Sci,* 66**,** 1890-902.

DELLA, N. G., CAMPOCHIARO, P. A. & ZACK, D. J. 1996. Localization of TIMP-3 mRNA expression to the retinal pigment epithelium. *Invest Ophthalmol Vis Sci,* 37**,** 1921-4.

DENTCHEV, T., MILAM, A. H., LEE, V. M., TROJANOWSKI, J. Q. & DUNAIEF, J. L. 2003. Amyloid-beta is found in drusen from some age-related macular degeneration retinas, but not in drusen from normal retinas. *Mol Vis,* 9**,** 184-90.

DING, J. D., JOHNSON, L. V., HERRMANN, R., FARSIU, S., SMITH, S. G., GROELLE, M., MACE, B. E., SULLIVAN, P., JAMISON, J. A., KELLY, U., HARRABI, O., BOLLINI, S. S., DILLEY, J., KOBAYASHI, D., KUANG, B., LI, W., PONS, J., LIN, J. C. & BOWES RICKMAN, C. 2011. Anti-amyloid therapy protects against retinal pigmented epithelium damage and vision loss in a model of age-related macular degeneration. *Proc Natl Acad Sci U S A,* 108**,** E279-87.

DREYMUELLER, D., UHLIG, S. & LUDWIG, A. 2015. ADAM-family metalloproteinases in lung inflammation: potential therapeutic targets. *Am J Physiol Lung Cell Mol Physiol,* 308**,** L325-43.

DUBAIL, J. & APTE, S. S. 2015. Insights on ADAMTS proteases and ADAMTS-like proteins from mammalian genetics. *Matrix Biol,* 44-46**,** 24-37.

EBRAHEM, Q., QI, J. H., SUGIMOTO, M., ALI, M., SEARS, J. E., CUTLER, A., KHOKHA, R., VASANJI, A. & ANAND-APTE, B. 2011. Increased neovascularization in mice lacking tissue inhibitor of metalloproteinases-3. *Invest Ophthalmol Vis Sci*, 52, 6117-23.

EDWARDS, A. O., RITTER, R., 3RD, ABEL, K. J., MANNING, A., PANHUYSEN, C. & FARRER, L. A. 2005. Complement factor H polymorphism and age-related macular degeneration. *Science*, 308, 421-4.

EHLERMANN, J., WEBER, S., PFISTERER, P. & SCHORLE, H. 2003. Cloning, expression and characterization of the murine Efemp1, a gene mutated in Doyne-Honeycomb retinal dystrophy. *Gene Expr Patterns,* 3**,** 441-7.

ELLGAARD, L. & HELENIUS, A. 2003. Quality control in the endoplasmic reticulum. *Nat Rev Mol Cell Biol,* 4**,** 181-91.

ENDRES, K., ANDERS, A., KOJRO, E., GILBERT, S., FAHRENHOLZ, F. & POSTINA, R. 2003. Tumor necrosis factor-alpha converting enzyme is processed by proprotein-convertases to its mature form which is degraded upon phorbol ester stimulation. *Eur J Biochem,* 270**,** 2386-93.

FANJUL-FERNANDEZ, M., FOLGUERAS, A. R., CABRERA, S. & LOPEZ-OTIN, C. 2010. Matrix metalloproteinases: evolution, gene regulation and functional analysis in mouse models. *Biochim Biophys Acta,* 1803**,** 3-19.

FARISS, R. N., APTE, S. S., LUTHERT, P. J., BIRD, A. C. & MILAM, A. H. 1998. Accumulation of tissue inhibitor of metalloproteinases-3 in human eyes with Sorsby's fundus dystrophy or retinitis pigmentosa. *Br J Ophthalmol,* 82**,** 1329-34.

FATA, J. E., LECO, K. J., VOURA, E. B., YU, H. Y., WATERHOUSE, P., MURPHY, G., MOOREHEAD, R. A. & KHOKHA, R. 2001. Accelerated apoptosis in the Timp-3-deficient mammary gland. *J Clin Invest,* 108**,** 831-41.

FELBOR, U., DOEPNER, D., SCHNEIDER, U., ZRENNER, E. & WEBER, B. H. 1997a. Evaluation of the gene encoding the tissue inhibitor of metalloproteinases-3 in various maculopathies. *Invest Ophthalmol Vis Sci,* 38**,** 1054-9.

FELBOR, U., STOHR, H., AMANN, T., SCHONHERR, U., APFELSTEDT-SYLLA, E. & WEBER, B. H. 1996. A second independent Tyr168Cys mutation in the tissue inhibitor of metalloproteinases-3 (TIMP3) in Sorsby's fundus dystrophy. *J Med Genet,* 33**,** 233-6.

FELBOR, U., STOHR, H., AMANN, T., SCHONHERR, U. & WEBER, B. H. 1995. A novel Ser156Cys mutation in the tissue inhibitor of metalloproteinases-3 (TIMP3) in Sorsby's fundus dystrophy with unusual clinical features. *Hum Mol Genet,* 4**,** 2415-6.

FELBOR, U., SUVANTO, E. A., FORSIUS, H. R., ERIKSSON, A. W. & WEBER, B. H. 1997b. Autosomal recessive Sorsby fundus dystrophy revisited: molecular evidence for dominant inheritance. *Am J Hum Genet,* 60**,** 57-62.

FERRARA, N. 1995. The role of vascular endothelial growth factor in pathological angiogenesis. *Breast Cancer Res Treat,* 36**,** 127-37.

FERRARA, N. & HENZEL, W. J. 1989. Pituitary follicular cells secrete a novel heparin-binding growth factor specific for vascular endothelial cells. *Biochem Biophys Res Commun,* 161**,** 851-8.

FERRIS, F. L., 3RD, WILKINSON, C. P., BIRD, A., CHAKRAVARTHY, U., CHEW, E., CSAKY, K. & SADDA, S. R. 2013. Clinical classification of age-related macular degeneration. *Ophthalmology,* 120**,** 844-51.

FISCHER, S. J. & WERB W. (1995). The catabolism of extracellular matrix components. Extracellular matrix: A practical approach. M. A. Haralson and J. R. Hassel. Oxford, IRL press. 151: 261-287.

FOGARASI, M., JANSSEN, A., WEBER, B. H. & STOHR, H. 2008. Molecular dissection of TIMP3 mutation S156C associated with Sorsby fundus dystrophy. *Matrix Biol*, 27, 381-92.

FRANTZ, C., STEWART, K. M. & WEAVER, V. M. 2010. The extracellular matrix at a glance. *J Cell Sci,* 123**,** 4195-200.

FRIBLEY, A., ZHANG, K. & KAUFMAN, R. J. 2009. Regulation of apoptosis by the unfolded protein response. *Methods Mol Biol,* 559**,** 191-204.

FU, L., GARLAND, D., YANG, Z., SHUKLA, D., RAJENDRAN, A., PEARSON, E., STONE, E. M., ZHANG, K. & PIERCE, E. A. 2007. The R345W mutation in EFEMP1 is pathogenic and causes AMD-like deposits in mice. *Hum Mol Genet*, 16, 2411-22.

FUH, G., LI, B., CROWLEY, C., CUNNINGHAM, B. & WELLS, J. A. 1998. Requirements for binding and signaling of the kinase domain receptor for vascular endothelial growth factor. *J Biol Chem,* 273**,** 11197-204.

FUNG, A. T., STOHR, H., WEBER, B. H., HOLZ, F. G. & YANNUZZI, L. A. 2013. Atypical sorsby fundus dystrophy with a novel tyr159cys timp-3 mutation. *Retin Cases Brief Rep,* 7**,** 71-4.

GAGGAR, A., HECTOR, A., BRATCHER, P. E., MALL, M. A., GRIESE, M. & HARTL, D. 2011. The role of matrix metalloproteinases in cystic fibrosis lung disease. *Eur Respir J,* 38**,** 721-7.

GANDHI, N. S. & MANCERA, R. L. 2008. The structure of glycosaminoglycans and their interactions with proteins. *Chem Biol Drug Des,* 72**,** 455-82.

GHAVAMI, S., RASHEDI, I., DATTILO, B. M., ESHRAGHI, M., CHAZIN, W. J., HASHEMI, M., WESSELBORG, S., KERKHOFF, C. & LOS, M. 2008. S100A8/A9 at low concentration promotes tumor cell growth via RAGE ligation and MAP kinase-dependent pathway. *J Leukoc Biol,* 83**,** 1484-92.

GIALELI, C., THEOCHARIS, A. D. & KARAMANOS, N. K. 2011. Roles of matrix metalloproteinases in cancer progression and their pharmacological targeting. *Febs j,* 278**,** 16-27.

GIEBELER, N. & ZIGRINO, P. 2016. A Disintegrin and Metalloprotease (ADAM): Historical Overview of Their Functions. *Toxins (Basel),* 8, 122.

GILPIN, B. J., LOECHEL, F., MATTEI, M. G., ENGVALL, E., ALBRECHTSEN, R. & WEWER, U. M. 1998. A novel, secreted form of human ADAM 12 (meltrin alpha) provokes myogenesis in vivo. *J Biol Chem,* 273**,** 157-66.

GLENN, J. V. & STITT, A. W. 2009. The role of advanced glycation end products in retinal ageing and disease. *Biochim Biophys Acta*, 1790, 1109-16.

GLIEM, M., MULLER, P. L., MANGOLD, E., HOLZ, F. G., BOLZ, H. J., STOHR, H., WEBER, B. H. & CHARBEL ISSA, P. 2015. Sorsby Fundus Dystrophy: Novel Mutations, Novel Phenotypic Characteristics, and Treatment Outcomes. *Invest Ophthalmol Vis Sci,* 56**,** 2664-76.

GOTTSCHALL, P. E. & HOWELL, M. D. 2015. ADAMTS expression and function in central nervous system injury and disorders. *Matrix Biol,* 44-46**,** 70-6.

GOURIER, H. C. & CHONG, N. V. 2015. Can Novel Treatment of Age-Related Macular Degeneration Be Developed by Better Understanding of Sorsby's Fundus Dystrophy. *J Clin Med,* 4**,** 874-83.

GREEN, K. A. & LUND, L. R. 2005. ECM degrading proteases and tissue remodelling in the mammary gland. *Bioessays,* 27**,** 894-903.

GREGORY-EVANS, K. 2000. What is Sorsby's fundus dystrophy? *Br J Ophthalmol,* 84**,** 679-80.

GRUNEWALD, F. S., PROTA, A. E., GIESE, A. & BALLMER-HOFER, K. 2010. Structure-function analysis of VEGF receptor activation and the role of coreceptors in angiogenic signaling. *Biochim Biophys Acta*, 1804, 567-80.

GUENETTE, R. S., MOOIBROEK, M., WONG, K., WONG, P. & TENNISWOOD, M. 1994. Cathepsin B, a cysteine protease implicated in metastatic progression, is also expressed during regression of the rat prostate and mammary glands. *Eur J Biochem,* 226**,** 311-21.

GUILAK, F., COHEN, D. M., ESTES, B. T., GIMBLE, J. M., LIEDTKE, W. & CHEN, C. S. 2009. Control of stem cell fate by physical interactions with the extracellular matrix. *Cell Stem Cell,* 5**,** 17-26.

GURURAJAN, R., GRENET, J., LAHTI, J. M. & KIDD, V. J. 1998. Isolation and characterization of two novel metalloproteinase genes linked to the Cdc2L locus on human chromosome 1p36.3. *Genomics,* 52**,** 101-6.

HAINES, J. L., HAUSER, M. A., SCHMIDT, S., SCOTT, W. K., OLSON, L. M., GALLINS, P., SPENCER, K. L., KWAN, S. Y., NOUREDDINE, M., GILBERT, J. R., SCHNETZ-BOUTAUD, N., AGARWAL, A., POSTEL, E. A. & PERICAK-VANCE, M. A. 2005. Complement factor H variant increases the risk of age-related macular degeneration. *Science,* 308**,** 419-21.

HAMZE, A. B., WEI, S., BAHUDHANAPATI, H., KOTA, S., ACHARYA, K. R. & BREW, K. 2007. Constraining specificity in the N-domain of tissue inhibitor of metalloproteinases-1; gelatinase-selective inhibitors. *Protein Sci.,* 16, 1905-13.

HARPER, S. J. & BATES, D. O. 2008. VEGF-A splicing: the key to anti-angiogenic therapeutics? *Nat Rev Cancer,* 8**,** 880-7.

HARRIS, S., CRAZE, M., NEWTON, J., FISHER, M., SHIMA, D. T., TOZER, G. M. & KANTHOU, C. 2012. Do anti-angiogenic VEGF (VEGFxxxb) isoforms exist? A cautionary tale. *PLoS One,* 7**,** e35231.

HAYAKAWA, T. 1994. Tissue inhibitors of metalloproteinases and their cell growth-promoting activity. *Cell Struct Funct,* 19**,** 109-14.

HAYAKAWA, T., YAMASHITA, K., OHUCHI, E. & SHINAGAWA, A. 1994. Cell growth-promoting activity of tissue inhibitor of metalloproteinases-2 (TIMP-2). *J Cell Sci,* 107 (Pt 9)**,** 2373-9.

HERMANI, A., DE SERVI, B., MEDUNJANIN, S., TESSIER, P. A. & MAYER, D. 2006. S100A8 and S100A9 activate MAP kinase and NF-kappaB signaling pathways and trigger translocation of RAGE in human prostate cancer cells. *Exp Cell Res,* 312**,** 184-97.

HOEGY, S. E., OH, H. R., CORCORAN, M. L. & STETLER-STEVENSON, W. G. 2001. Tissue inhibitor of metalloproteinases-2 (TIMP-2) suppresses TKR-growth factor signaling independent of metalloproteinase inhibition. *J Biol Chem*, 276, 3203-14.

HOFMANN, M. A., DRURY, S., FU, C., QU, W., TAGUCHI, A., LU, Y., AVILA, C., KAMBHAM, N., BIERHAUS, A., NAWROTH, P., NEURATH, M. F., SLATTERY, T., BEACH, D., MCCLARY, J., NAGASHIMA, M., MORSER, J., STERN, D. & SCHMIDT, A. M. 1999. RAGE mediates a novel proinflammatory axis: a central cell surface receptor for S100/calgranulin polypeptides. *Cell,* 97**,** 889-901.

HOJILLA, C. V., JACKSON, H. W. & KHOKHA, R. 2011. TIMP3 regulates mammary epithelial apoptosis with immune cell recruitment through differential TNF dependence. *PLoS One*, 6, e26718.

HOTODA, N., KOIKE, H., SASAGAWA, N. & ISHIURA, S. 2002. A secreted form of human ADAM9 has an alpha-secretase activity for APP. *Biochem Biophys Res Commun,* 293**,** 800-5.

HOWES, K. A., LIU, Y., DUNAIEF, J. L., MILAM, A., FREDERICK, J. M., MARKS, A. & BAEHR, W. 2004. Receptor for advanced glycation end products and age-related macular degeneration. *Invest Ophthalmol Vis Sci*, 45, 3713-20.

HUANG, K. & WU, L. D. 2008. Aggrecanase and aggrecan degradation in osteoarthritis: a review. *J Int Med Res,* 36**,** 1149-60.

HUBERT, T., GRIMAL, S., CARROLL, P. & FICHARD-CARROLL, A. 2009. Collagens in the developing and diseased nervous system. *Cell Mol Life Sci,* 66**,** 1223-38.

HUBMACHER, D. & APTE, S. S. 2013. The biology of the extracellular matrix: novel insights. *Curr Opin Rheumatol,* 25**,** 65-70.

HULLEMAN, J. D. & KELLY, J. W. 2015. Genetic ablation of N-linked glycosylation reveals two key folding pathways for R345W fibulin-3, a secreted protein associated with retinal degeneration. *Faseb j,* 29**,** 565-75.

HURSKAINEN, T. L., HIROHATA, S., SELDIN, M. F. & APTE, S. S. 1999. ADAM-TS5, ADAM-TS6, and ADAM-TS7, novel members of a new family of zinc metalloproteases. General features and genomic distribution of the ADAM-TS family. *J Biol Chem,* 274**,** 25555-63.

HUTTUNEN, H. J., FAGES, C. & RAUVALA, H. 1999. Receptor for advanced glycation end products (RAGE)-mediated neurite outgrowth and activation of NF-kappaB require the cytoplasmic domain of the receptor but different downstream signaling pathways. *J Biol Chem,* 274**,** 19919-24.

IOZZO, R. V. 1998. Matrix proteoglycans: from molecular design to cellular function. *Annu Rev Biochem,* 67**,** 609-52.

ISASHIKI, Y., TABATA, Y., KAMIMURA, K. & OHBA, N. 1999. Sorsby's fundus dystrophy in two Japanese families with unusual clinical features. *Jpn J Ophthalmol*, 43, 472-80.

JACOBSON, S. G., CIDECIYAN, A. V., BENNETT, J., KINGSLEY, R. M., SHEFFIELD, V. C. & STONE, E. M. 2002. Novel mutation in the TIMP3 gene causes Sorsby fundus dystrophy. *Arch Ophthalmol*, 120, 376-9.

JACOBSON, S. G., CIDECIYAN, A. V., RATNAKARAM, R., HEON, E., SCHWARTZ, S. B., ROMAN, A. J., PEDEN, M. C., ALEMAN, T. S., BOYE, S. L., SUMAROKA, A., CONLON, T. J., CALCEDO, R., PANG, J. J., ERGER, K. E., OLIVARES, M. B., MULLINS, C. L., SWIDER, M., KAUSHAL, S., FEUER, W. J., IANNACCONE, A., FISHMAN, G. A., STONE, E. M., BYRNE, B. J. & HAUSWIRTH, W. W. 2012. Gene therapy for leber congenital amaurosis caused by RPE65 mutations: safety and efficacy in 15 children and adults followed up to 3 years. *Arch Ophthalmol,* 130**,** 9-24.

JACOBSON, S. G., CIDECIYAN, A. V., REGUNATH, G., RODRIGUEZ, F. J., VANDENBURGH, K., SHEFFIELD, V. C. & STONE, E. M. 1995. Night blindness in Sorsby's fundus dystrophy reversed by vitamin A. *Nat Genet,* 11**,** 27-32.

JAFFE, G. J., ELIOTT, D., WELLS, J. A., PRENNER, J. L., PAPP, A. & PATEL, S. 2016. A Phase 1 Study of Intravitreous E10030 in Combination with Ranibizumab in Neovascular Age-Related Macular Degeneration. *Ophthalmology,* 123**,** 78-85.

JANSSEN, A., HOELLENRIEGEL, J., FOGARASI, M., SCHREWE, H., SEELIGER, M., TAMM, E., OHLMANN, A., MAY, C. A., WEBER, B. H. & STOHR, H. 2008. Abnormal vessel formation in the choroid of mice lacking tissue inhibitor of metalloprotease-3. Invest *Ophthalmol Vis Sci*, 49, 2812-22.

JOHNSON, L. V., LEITNER, W. P., RIVEST, A. J., STAPLES, M. K., RADEKE, M. J. & ANDERSON, D. H. 2002. The Alzheimer's A beta -peptide is deposited at sites of complement activation in pathologic deposits associated with aging and age-related macular degeneration. *Proc Natl Acad Sci U S A,* 99**,** 11830-5.

KAMEI, M. & HOLLYFIELD, J. G. 1999. TIMP-3 in Bruch's membrane: changes during aging and in age-related macular degeneration. *Invest Ophthalmol Vis Sci,* 40**,** 2367-75.

KASSIRI, Z., OUDIT, G. Y., SANCHEZ, O., DAWOOD, F., MOHAMMED, F. F., NUTTALL, R. K., EDWARDS, D. R., LIU, P. P., BACKX, P. H. & KHOKHA, R. 2005. Combination of tumor necrosis factor-alpha ablation and matrix metalloproteinase inhibition prevents heart failure after pressure overload in tissue inhibitor of metalloproteinase-3 knock-out mice. *Circ Res*, 97, 380-90.

KAUR, I., RATHI, S. & CHAKRABARTI, S. 2010. Variations in TIMP3 are associated with age-related macular degeneration. *Proc Natl Acad Sci U S A*, 107, E112-3.

KECK, P. J., HAUSER, S. D., KRIVI, G., SANZO, K., WARREN, T., FEDER, J. & CONNOLLY, D. T. 1989. Vascular permeability factor, an endothelial cell mitogen related to PDGF. *Science,* 246**,** 1309-12.

KEELEY, F. W., BELLINGHAM, C. M. & WOODHOUSE, K. A. 2002. Elastin as a self-organizing biomaterial: use of recombinantly expressed human elastin polypeptides as a model for investigations of structure and self-assembly of elastin. *Philos Trans R Soc Lond B Biol Sci,* 357**,** 185-9.

KELLEY, L. A. & STERNBERG, M. J. 2009. Protein structure prediction on the Web: a case study using the Phyre server. *Nat Protoc,* 4**,** 363-71.

KELWICK, R., DESANLIS, I., WHEELER, G. N. & EDWARDS, D. R. 2015. The ADAMTS (A Disintegrin and Metalloproteinase with Thrombospondin motifs) family. *Genome Biol,* 16**,** 113.

KESSENBROCK, K., PLAKS, V. & WERB, Z. 2010. Matrix metalloproteinases: regulators of the tumor microenvironment. *Cell,* 141**,** 52-67.

KHOKHA, R., MURTHY, A. & WEISS, A. 2013. Metalloproteinases and their natural inhibitors in inflammation and immunity. *Nat Rev Immunol,* 13**,** 649-65.

KIM, S. H., TURNBULL, J. & GUIMOND, S. 2011. Extracellular matrix and cell signalling: the dynamic cooperation of integrin, proteoglycan and growth factor receptor. *J Endocrinol,* 209**,** 139-51.

KLEINMAN, H. K., PHILP, D. & HOFFMAN, M. P. 2003. Role of the extracellular matrix in morphogenesis. *Curr Opin Biotechnol,* 14**,** 526-32.

KLENOTIC, P. A., MUNIER, F. L., MARMORSTEIN, L. Y. & ANAND-APTE, B. 2004. Tissue inhibitor of metalloproteinases-3 (TIMP-3) is a binding partner of epithelial growth factor-containing fibulin-like extracellular matrix protein 1 (EFEMP1). Implications for macular degenerations. *J Biol Chem*, 279, 30469-73.

KOCH, M., CHITAYAT, S., DATTILO, B. M., SCHIEFNER, A., DIEZ, J., CHAZIN, W. J. & FRITZ, G. 2010. Structural basis for ligand recognition and activation of RAGE. *Structure,* 18**,** 1342-52.

KOLB, H. 1995. Simple Anatomy of the Retina. *In:* KOLB, H., FERNANDEZ, E. & NELSON, R. (eds.) *Webvision: The Organization of the Retina and Visual System.* Salt Lake City (UT): University of Utah Health Sciences Center.

KUMAR, S., RAO, N. & GE, R. 2012. Emerging Roles of ADAMTSs in Angiogenesis and Cancer. *Cancers (Basel),* 4**,** 1252-99.

LAMALICE, L., LE BOEUF, F. & HUOT, J. 2007. Endothelial cell migration during angiogenesis. *Circ Res,* 100**,** 782-94.

LANDER, H. M., TAURAS, J. M., OGISTE, J. S., HORI, O., MOSS, R. A. & SCHMIDT, A. M. 1997. Activation of the receptor for advanced glycation end products triggers a p21(ras)-dependent mitogen-activated protein kinase pathway regulated by oxidant stress. *J Biol Chem,* 272**,** 17810-4.

LANGTON, K. P., BARKER, M. D. & MCKIE, N. 1998. Localization of the functional domains of human tissue inhibitor of metalloproteinases-3 and the effects of a Sorsby's fundus dystrophy mutation. *J Biol Chem,* 273**,** 16778-81.

LANGTON, K. P., MCKIE, N., CURTIS, A., GOODSHIP, J. A., BOND, P. M., BARKER, M. D. & CLARKE, M. 2000. A novel tissue inhibitor of metalloproteinases-3 mutation reveals a common molecular phenotype in Sorsby's fundus dystrophy. *J Biol Chem*, 275, 27027-31.

LANGTON, K. P., MCKIE, N., SMITH, B. M., BROWN, N. J. & BARKER, M. D. 2005. Sorsby's fundus dystrophy mutations impair turnover of TIMP-3 by retinal pigment epithelial cells. *Hum Mol Genet*, 14, 3579-86.

LECLERC, E., FRITZ, G., WEIBEL, M., HEIZMANN, C. W. & GALICHET, A. 2007. S100B and S100A6 differentially modulate cell survival by interacting with distinct RAGE (receptor for advanced glycation end products) immunoglobulin domains. *J Biol Chem,* 282**,** 31317-31.

LECO, K. J., KHOKHA, R., PAVLOFF, N., HAWKES, S. P. & EDWARDS, D. R. 1994. Tissue inhibitor of metalloproteinases-3 (TIMP-3) is an extracellular matrix-associated protein with a distinctive pattern of expression in mouse cells and tissues. *J Biol Chem,* 269**,** 9352-60.

LECO, K. J., WATERHOUSE, P., SANCHEZ, O. H., GOWING, K. L., POOLE, A. R., WAKEHAM, A., MAK, T. W. & KHOKHA, R. 2001. Spontaneous air space enlargement in the lungs of mice lacking tissue inhibitor of metalloproteinases-3 (TIMP-3). *J Clin Invest,* 108**,** 817-29.

LEE, M. H., ATKINSON, S. & MURPHY, G. 2007. Identification of the extracellular matrix (ECM) binding motifs of tissue inhibitor of metalloproteinases (TIMP)-3 and effective transfer to TIMP-1. *J Biol Chem*, 282, 6887-98.

LEPPANEN, V. M., PROTA, A. E., JELTSCH, M., ANISIMOV, A., KALKKINEN, N., STRANDIN, T., LANKINEN, H., GOLDMAN, A., BALLMER-HOFER, K. & ALITALO, K. 2010. Structural determinants of growth factor binding and specificity by VEGF receptor 2. *Proc Natl Acad Sci U S A,* 107**,** 2425-30.

LEVY, G. G., NICHOLS, W. C., LIAN, E. C., FOROUD, T., MCCLINTICK, J. N., MCGEE, B. M., YANG, A. Y., SIEMIENIAK, D. R., STARK, K. R., GRUPPO, R., SARODE, R., SHURIN, S. B., CHANDRASEKARAN, V., STABLER, S. P., SABIO, H., BOUHASSIRA, E. E., UPSHAW, J. D., JR., GINSBURG, D. & TSAI, H. M. 2001. Mutations in a member of the ADAMTS gene family cause thrombotic thrombocytopenic purpura. *Nature,* 413**,** 488-94.

LI, Z., CLARKE, M. P., BARKER, M. D. & MCKIE, N. 2005. TIMP3 mutation in Sorsby's fundus dystrophy: molecular insights. *Expert Rev Mol Med*, 7, 1-15.

LILIENSIEK, B., WEIGAND, M. A., BIERHAUS, A., NICKLAS, W., KASPER, M., HOFER, S., PLACHKY, J., GRONE, H. J., KURSCHUS, F. C., SCHMIDT, A. M., YAN, S. D., MARTIN, E., SCHLEICHER, E., STERN, D. M., HAMMERLING, G. G., NAWROTH, P. P. & ARNOLD, B. 2004. Receptor for advanced glycation end products (RAGE) regulates sepsis but not the adaptive immune response. *J Clin Invest,* 113**,** 1641-50.

LIMB, G. A., MATTER, K., MURPHY, G., CAMBREY, A. D., BISHOP, P. N., MORRIS, G. E. & KHAW, P. T. 2005. Matrix metalloproteinase-1 associates with intracellular organelles and confers resistance to lamin A/C degradation during apoptosis. *Am J Pathol,* 166**,** 1555-63.

LIN, R. J., BLUMENKRANZ, M. S., BINKLEY, J., WU, K. & VOLLRATH, D. 2006. A novel His158Arg mutation in TIMP3 causes a late-onset form of Sorsby fundus dystrophy. *Am J Ophthalmol*, 142, 839-48.

LIN, Z., WANG, Z., LI, G., LI, B., XIE, W. & XIANG, D. 2016. Fibulin-3 may improve vascular health through inhibition of MMP-2/9 and oxidative stress in spontaneously hypertensive rats. *Mol Med Rep,* 13**,** 3805-12.

LU, P., TAKAI, K., WEAVER, V. M. & WERB, Z. 2011. Extracellular matrix degradation and remodeling in development and disease. *Cold Spring Harb Perspect Biol,* 3, a005058.

LUO, D., MARI, B., STOLL, I. & ANGLARD, P. 2002. Alternative splicing and promoter usage generates an intracellular stromelysin 3 isoform directly translated as an active matrix metalloproteinase. *J Biol Chem,* 277**,** 25527-36.

MA, W., LEE, S. E., GUO, J., QU, W., HUDSON, B. I., SCHMIDT, A. M. & BARILE, G. R. 2007. RAGE ligand upregulation of VEGF secretion in ARPE-19 cells. *Invest Ophthalmol Vis Sci*, 48, 1355-61.

MAC GABHANN, F. & POPEL, A. S. 2007. Dimerization of VEGF receptors and implications for signal transduction: a computational study. *Biophys Chem*, 128, 125-39.

MAJID, M. A., SMITH, V. A., EASTY, D. L., BAKER, A. H. & NEWBY, A. C. 2002. Adenovirus mediated gene delivery of tissue inhibitor of metalloproteinases-3 induces death in retinal pigment epithelial cells. *Br J Ophthalmol,* 86**,** 97-101.

MARMORSTEIN, L. Y., MUNIER, F. L., ARSENIJEVIC, Y., SCHORDERET, D. F., MCLAUGHLIN, P. J., CHUNG, D., TRABOULSI, E. & MARMORSTEIN, A. D. 2002. Aberrant accumulation of EFEMP1 underlies drusen formation in Malattia Leventinese and age-related macular degeneration. *Proc Natl Acad Sci U S A*, 99, 13067-72.

MATA, N. L., LICHTER, J. B., VOGEL, R., HAN, Y., BUI, T. V. & SINGERMAN, L. J. 2013. Investigation of oral fenretinide for treatment of geographic atrophy in age-related macular degeneration. *Retina,* 33**,** 498-507.

MCLAUGHLIN, P. J., BAKALL, B., CHOI, J., LIU, Z., SASAKI, T., DAVIS, E. C., MARMORSTEIN, A. D. & MARMORSTEIN, L. Y. 2007. Lack of fibulin-3 causes early aging and herniation, but not macular degeneration in mice. *Hum Mol Genet*, 16, 3059-70.

MILLINGTON-WARD, S., CHADDERTON, N., O'REILLY, M., PALFI, A., GOLDMANN, T., KILTY, C., HUMPHRIES, M., WOLFRUM, U., BENNETT, J., HUMPHRIES, P., KENNA, P. F. & FARRAR, G. J. 2011. Suppression and replacement gene therapy for autosomal dominant disease in a murine model of dominant retinitis pigmentosa. *Mol Ther,* 19**,** 642-9.

MOHAMMED, F. F., SMOOKLER, D. S., TAYLOR, S. E., FINGLETON, B., KASSIRI, Z., SANCHEZ, O. H., ENGLISH, J. L., MATRISIAN, L. M., AU, B., YEH, W. C. & KHOKHA, R. 2004. Abnormal TNF activity in Timp3-/- mice leads to chronic hepatic inflammation and failure of liver regeneration. Nat Genet, 36, 969-77.

MOTT, J. D. & WERB, Z. 2004. Regulation of matrix biology by matrix metalloproteinases. *Curr Opin Cell Biol,* 16**,** 558-64.

MOUW, J. K., OU, G. & WEAVER, V. M. 2014. Extracellular matrix assembly: a multiscale deconstruction. *Nat Rev Mol Cell Biol,* 15**,** 771-85.

MUJAMAMMI, AH. 2013. PhD Thesis: Characterisation and Therapeutic Targeting of TIMP3 in Sorsby's Fundus Dystrophy. *The University of Sheffield*. United Kingdom.

NAGASE, H., VISSE, R. & MURPHY, G. 2006. Structure and function of matrix metalloproteinases and TIMPs. *Cardiovasc Res*, 69, 562-73.

NAGASE, H. & WOESSNER, J. F., JR. 1999. Matrix metalloproteinases. *J Biol Chem,* 274**,** 21491-4.

NAGY, J. A., DVORAK, A. M. & DVORAK, H. F. 2007. VEGF-A and the induction of pathological angiogenesis. *Annu Rev Pathol,* 2**,** 251-75.

NAIK, R., MUKHOPADHYAY, A. & GANGULI, M. 2009. Gene delivery to the retina: focus on non-viral approaches. *Drug Discov Today,* 14**,** 306-15.

NEEPER, M., SCHMIDT, A. M., BRETT, J., YAN, S. D., WANG, F., PAN, Y. C., ELLISTON, K., STERN, D. & SHAW, A. 1992. Cloning and expression of a cell surface receptor for advanced glycosylation end products of proteins. *J Biol Chem,* 267**,** 14998-5004.

NITA, M., STRZALKA-MROZIK, B., GRZYBOWSKI, A., MAZUREK, U. & ROMANIUK, W. 2014. Age-related macular degeneration and changes in the extracellular matrix. *Med Sci Monit,* 20**,** 1003-16.

OLSON, T. M., HIROHATA, S., YE, J., LECO, K., SELDIN, M. F. & APTE, S. S. 1998. Cloning of the human tissue inhibitor of metalloproteinase-4 gene (TIMP4) and localization of the TIMP4 and Timp4 genes to human chromosome 3p25 and mouse chromosome 6, respectively. *Genomics*, 51, 148-51.

OSTENDORP, T., LECLERC, E., GALICHET, A., KOCH, M., DEMLING, N., WEIGLE, B., HEIZMANN, C. W., KRONECK, P. M. & FRITZ, G. 2007. Structural and functional insights into RAGE activation by multimeric S100B. *Embo j,* 26**,** 3868-78.

OWEN, C. G., JARRAR, Z., WORMALD, R., COOK, D. G., FLETCHER, A. E. & RUDNICKA, A. R. 2012. The estimated prevalence and incidence of late stage age related macular degeneration in the UK. *Br J Ophthalmol,* 96**,** 752-6.

PAGE-MCCAW, A., EWALD, A. J. & WERB, Z. 2007. Matrix metalloproteinases and the regulation of tissue remodelling. *Nat Rev Mol Cell Biol,* 8**,** 221-33.

PANT, K., ADLAKHA, N. & MITTAL, A. 2010. Multi class classification approach for classification of ADAMs, MMPs and their subclasses. *IACSIT*, 2 (3), 1703-8236.

PARSONS, C. G., RUITENBERG, M., FREITAG, C. E., SROKA-SAIDI, K., RUSS, H. & RAMMES, G. 2015. MRZ-99030 - A novel modulator of Abeta aggregation: I - Mechanism of action (MoA) underlying the potential neuroprotective treatment of Alzheimer's disease, glaucoma and age-related macular degeneration (AMD). *Neuropharmacology,* 92**,** 158-69.

PATAN, S. 2000. Vasculogenesis and angiogenesis as mechanisms of vascular network formation, growth and remodeling. *J Neurooncol,* 50**,** 1-15.

PAVLOFF, N., STASKUS, P. W., KISHNANI, N. S. & HAWKES, S. P. 1992. A new inhibitor of metalloproteinases from chicken: ChIMP-3. A third member of the TIMP family. *J Biol Chem,* 267**,** 17321-6.

PENN, J. S., MADAN, A., CALDWELL, R. B., BARTOLI, M., CALDWELL, R. W. & HARTNETT, M. E. 2008. Vascular endothelial growth factor in eye disease. *Prog Retin Eye Res*, 27, 331-71.

PERRIMON, N. & BERNFIELD, M. 2001. Cellular functions of proteoglycans--an overview. *Semin Cell Dev Biol,* 12**,** 65-7.

PORTER, S., CLARK, I. M., KEVORKIAN, L. & EDWARDS, D. R. 2005. The ADAMTS metalloproteinases. *Biochem J,* 386**,** 15-27.

PRAGER, F., MICHELS, S., GEITZENAUER, W. & SCHMIDT-ERFURTH, U. 2007. Choroidal neovascularization secondary to Sorsby fundus dystrophy treated with systemic bevacizumab (Avastin). *Acta Ophthalmol Scand*, 85, 904-6.

QI, J. H. & ANAND-APTE, B. 2015. Tissue inhibitor of metalloproteinase-3 (TIMP3) promotes endothelial apoptosis via a caspase-independent mechanism. *Apoptosis,* 20**,** 523-34.

QI, J. H., DAI, G., LUTHERT, P., CHAURASIA, S., HOLLYFIELD, J., WEBER, B. H., STOHR, H. & ANAND-APTE, B. 2009. S156C mutation in tissue inhibitor of metalloproteinases-3 induces increased angiogenesis. *J Biol Chem*, 284, 19927-36.

QI, J. H., EBRAHEM, Q., ALI, M., CUTLER, A., BELL, B., PRAYSON, N., SEARS, J., KNAUPER, V., MURPHY, G. & ANAND-APTE, B. 2013. Tissue inhibitor of metalloproteinases-3 peptides inhibit angiogenesis and choroidal neovascularization in mice. *PLoS One,* 8**,** e55667.

QI, J. H., EBRAHEM, Q., MOORE, N., MURPHY, G., CLAESSON-WELSH, L., BOND, M., BAKER, A. & ANAND-APTE, B. 2003. A novel function for tissue inhibitor of metalloproteinases-3 (TIMP3): inhibition of angiogenesis by blockage of VEGF binding to VEGF receptor-2. *Nat Med*, 9, 407-15.

QUERQUES, G., GUIGUI, B., LEVEZIEL, N., QUERQUES, L., BANDELLO, F. & SOUIED, E. H. 2013. Multimodal morphological and functional characterization of Malattia Leventinese. *Graefes Arch Clin Exp Ophthalmol,* 251**,** 705-14.

RAHIMI, N. 2006. Vascular endothelial growth factor receptors: molecular mechanisms of activation and therapeutic potentials. *Exp Eye Res,* 83**,** 1005-16.

RAKOCZY, E. P., LAI, C. M., MAGNO, A. L., WIKSTROM, M. E., FRENCH, M. A., PIERCE, C. M., SCHWARTZ, S. D., BLUMENKRANZ, M. S., CHALBERG, T. W., DEGLI-ESPOSTI, M. A. & CONSTABLE, I. J. 2015. Gene therapy with recombinant adeno-associated vectors for neovascular age-related macular degeneration: 1 year follow-up of a phase 1 randomised clinical trial. *Lancet,* 386**,** 2395-403.

REISS, K. & SAFTIG, P. 2009. The "a disintegrin and metalloprotease" (ADAM) family of sheddases: physiological and cellular functions. *Semin Cell Dev Biol,* 20**,** 126-37.

RISAU, W., SARIOLA, H., ZERWES, H. G., SASSE, J., EKBLOM, P., KEMLER, R. & DOETSCHMAN, T. 1988. Vasculogenesis and angiogenesis in embryonic-stem-cell-derived embryoid bodies. *Development,* 102**,** 471-8.

ROCKS, N., PAULISSEN, G., EL HOUR, M., QUESADA, F., CRAHAY, C., GUEDERS, M., FOIDART, J. M., NOEL, A. & CATALDO, D. 2008. Emerging roles of ADAM and ADAMTS metalloproteinases in cancer. *Biochimie,* 90**,** 369-79.

ROWE, R. G. & WEISS, S. J. 2008. Breaching the basement membrane: who, when and how? *Trends Cell Biol,* 18**,** 560-74.

ROYBAL, C. N., MARMORSTEIN, L. Y., VANDER JAGT, D. L. & ABCOUWER, S. F. 2005. Aberrant accumulation of fibulin-3 in the endoplasmic reticulum leads to activation of the unfolded protein response and VEGF expression. *Invest Ophthalmol Vis Sci*, 46, 3973-9.

RUIZ, A., BRETT, P. & BOK, D. 1996. TIMP-3 is expressed in the human retinal pigment epithelium. *Biochem Biophys Res Commun*, 226, 467-74.

RUOSLAHTI, E., HAYMAN, E. G. & PIERSCHBACHER, M. D. 1985. Extracellular matrices and cell adhesion. *Arteriosclerosis,* 5**,** 581-94.

SAIHAN, Z., LI, Z., RICE, J., RANA, N. A., RAMSDEN, S., SCHLOTTMANN, P. G., JENKINS, S. A., BLYTH, C., BLACK, G. C., MCKIE, N. & WEBSTER, A. R. 2009. Clinical and biochemical effects of the E139K missense mutation in the TIMP3 gene, associated with Sorsby fundus dystrophy. *Mol Vis*, 15, 1218-30.

SAKSENS, N. T., FLECKENSTEIN, M., SCHMITZ-VALCKENBERG, S., HOLZ, F. G., DEN HOLLANDER, A. I., KEUNEN, J. E., BOON, C. J. & HOYNG, C. B. 2014. Macular dystrophies mimicking age-related macular degeneration. *Prog Retin Eye Res,* 39**,** 23-57.

SASAHIRA, T., AKAMA, Y., FUJII, K. & KUNIYASU, H. 2005. Expression of receptor for advanced glycation end products and HMGB1/amphoterin in colorectal adenomas. *Virchows Arch,* 446**,** 411-5.

SAVIC, N. & SCHWANK, G. 2016. Advances in therapeutic CRISPR/Cas9 genome editing. *Transl Res,* 168**,** 15-21.

SCHMIDT, A. M., VIANNA, M., GERLACH, M., BRETT, J., RYAN, J., KAO, J., ESPOSITO, C., HEGARTY, H., HURLEY, W., CLAUSS, M. & *ET AL.* 1992. Isolation and characterization of two binding proteins for advanced glycosylation end products from bovine lung which are present on the endothelial cell surface. *J Biol Chem,* 267**,** 14987-97.

SCHOENBERGER, S. D. & AGARWAL, A. 2013. A novel mutation at the N-terminal domain of the TIMP3 gene in Sorsby fundus dystrophy. *Retina*, 33, 429-35.

SCHWARTZ, S. D., TAN, G., HOSSEINI, H. & NAGIEL, A. 2016. Subretinal Transplantation of Embryonic Stem Cell-Derived Retinal Pigment Epithelium for the

Treatment of Macular Degeneration: An Assessment at 4 Years. *Invest Ophthalmol Vis Sci,* 57**,** ORSFc1-9.

SCROFANI, S. D., FABRI, L. J., XU, P., MACCARONE, P. & NASH, A. D. 2000. Purification and refolding of vascular endothelial growth factor-B. *Protein Sci,* 9**,** 2018-25.

SEANDEL, M., NOACK-KUNNMANN, K., ZHU, D., AIMES, R. T. & QUIGLEY, J. P. 2001. Growth factor-induced angiogenesis in vivo requires specific cleavage of fibrillar type I collagen. *Blood,* 97**,** 2323-32.

SENGER, D. R., GALLI, S. J., DVORAK, A. M., PERRUZZI, C. A., HARVEY, V. S. & DVORAK, H. F. 1983. Tumor cells secrete a vascular permeability factor that promotes accumulation of ascites fluid. *Science,* 219**,** 983-5.

SEO, D. W., LI, H., GUEDEZ, L., WINGFIELD, P. T., DIAZ, T., SALLOUM, R., WEI, B. Y. & STETLER-STEVENSON, W. G. 2003. TIMP-2 mediated inhibition of angiogenesis: an MMP-independent mechanism. *Cell*, 114, 171-80.

SHIOMI, T., LEMAITRE, V., D'ARMIENTO, J. & OKADA, Y. 2010. Matrix metalloproteinases, a disintegrin and metalloproteinases, and a disintegrin and metalloproteinases with thrombospondin motifs in non-neoplastic diseases. *Pathol Int*, 60, 477-96.

SIVAPRASAD, S., WEBSTER, A. R., EGAN, C. A., BIRD, A. C. & TUFAIL, A. 2008. Clinical course and treatment outcomes of Sorsby fundus dystrophy. *Am J Ophthalmol*, 146, 228-234.

SMITH, N. R., BAKER, D., JAMES, N. H., RATCLIFFE, K., JENKINS, M., ASHTON, S. E., SPROAT, G., SWANN, R., GRAY, N., RYAN, A., JURGENSMEIER, J. M. & WOMACK, C. 2010. Vascular endothelial growth factor receptors VEGFR-2 and VEGFR-3 are localized primarily to the vasculature in human primary solid cancers. *Clin Cancer Res,* 16**,** 3548-61.

SOHN, E. H., PATEL, P. J., MACLAREN, R. E., ADATIA, F. A., PAL, B., WEBSTER, A. R. & TUFAIL, A. 2011. Responsiveness of choroidal neovascular membranes in patients with R345W mutation in fibulin 3 (Doyne honeycomb retinal dystrophy) to anti-vascular endothelial growth factor therapy. *Arch Ophthalmol,* 129**,** 1626-8.

SOLOMON, S. D., LINDSLEY, K. B., KRZYSTOLIK, M. G., VEDULA, S. S. & HAWKINS, B. S. 2016. Intravitreal Bevacizumab Versus Ranibizumab for Treatment of Neovascular Age-Related Macular Degeneration: Findings from a Cochrane Systematic Review. *Ophthalmology,* 123**,** 70-77.e1.

SORSBY, A. & MASON, M. E. 1949. A fundus dystrophy with unusual features. *Br J Ophthalmol,* 33**,** 67-97.

SPARROW, J. R., UEDA, K. & ZHOU, J. 2012. Complement dysregulation in AMD: RPE-Bruch's membrane-choroid. *Mol Aspects Med,* 33**,** 436-45.

STETLER-STEVENSON, W. G., BERSCH, N. & GOLDE, D. W. 1992. Tissue inhibitor of metalloproteinase-2 (TIMP-2) has erythroid-potentiating activity. *FEBS Lett*, 296, 231-4.

STOCKER, W., GRAMS, F., BAUMANN, U., REINEMER, P., GOMIS-RUTH, F. X., MCKAY, D. B. & BODE, W. 1995. The metzincins--topological and sequential relations between the astacins, adamalysins, serralysins, and matrixins (collagenases) define a superfamily of zinc-peptidases. *Protein Sci,* 4**,** 823-40.

STOHR, H., ROOMP, K., FELBOR, U. & WEBER, B. H. 1995. Genomic organization of the human tissue inhibitor of metalloproteinases-3 (TIMP3). *Genome Res,* 5**,** 483-7.

STONE, E. M., LOTERY, A. J., MUNIER, F. L., HEON, E., PIGUET, B., GUYMER, R. H., VANDENBURGH, K., COUSIN, P., NISHIMURA, D., SWIDERSKI, R. E., SILVESTRI, G., MACKEY, D. A., HAGEMAN, G. S., BIRD, A. C., SHEFFIELD, V. C. & SCHORDERET, D. F. 1999. A single EFEMP1 mutation associated with both Malattia Leventinese and Doyne. *Nat Genet,* 22**,** 199-202.

STUPACK, D. G. & CHERESH, D. A. 2002. ECM remodeling regulates angiogenesis: endothelial integrins look for new ligands. *Sci STKE,* 2002**,** pe7.

TABATA, Y., ISASHIKI, Y., KAMIMURA, K., NAKAO, K. & OHBA, N. 1998. A novel splice site mutation in the tissue inhibitor of the metalloproteinases-3 gene in Sorsby's fundus dystrophy with unusual clinical features. *Hum Genet,* 103**,** 179-82.

TAKEUCHI, T., HAYASHI, T., BEDELL, M., ZHANG, K., YAMADA, H. & TSUNEOKA, H. 2010. A novel haplotype with the R345W mutation in the EFEMP1 gene

associated with autosomal dominant drusen in a Japanese family. *Invest Ophthalmol Vis Sci,* 51**,** 1643-50.

TALLANT, C., MARRERO, A. & GOMIS-RUTH, F. X. 2010. Matrix metalloproteinases: fold and function of their catalytic domains. *Biochim Biophys Acta,* 1803**,** 20-8.

TANIGUCHI, N., KAWAHARA, K., YONE, K., HASHIGUCHI, T., YAMAKUCHI, M., GOTO, M., INOUE, K., YAMADA, S., IJIRI, K., MATSUNAGA, S., NAKAJIMA, T., KOMIYA, S. & MARUYAMA, I. 2003. High mobility group box chromosomal protein 1 plays a role in the pathogenesis of rheumatoid arthritis as a novel cytokine. *Arthritis Rheum,* 48**,** 971-81.

TAUBE, M. E., LIU, X. W., FRIDMAN, R. & KIM, H. R. 2006. TIMP-1 regulation of cell cycle in human breast epithelial cells via stabilization of p27(KIP1) protein. *Oncogene*, 25, 3041-8.

THEOCHARIS, A. D., SKANDALIS, S. S., TZANAKAKIS, G. N. & KARAMANOS, N. K. 2010. Proteoglycans in health and disease: novel roles for proteoglycans in malignancy and their pharmacological targeting. *Febs j,* 277**,** 3904-23.

TIMPL, R., SASAKI, T., KOSTKA, G. & CHU, M. L. 2003. Fibulins: a versatile family of extracellular matrix proteins. *Nat Rev Mol Cell Biol*, 4, 479-89.

TORTORELLA, M. D., BURN, T. C., PRATTA, M. A., ABBASZADE, I., HOLLIS, J. M., LIU, R., ROSENFELD, S. A., COPELAND, R. A., DECICCO, C. P., WYNN, R., ROCKWELL, A., YANG, F., DUKE, J. L., SOLOMON, K., GEORGE, H., BRUCKNER, R., NAGASE, H., ITOH, Y., ELLIS, D. M., ROSS, H., WISWALL, B. H., MURPHY, K., HILLMAN, M. C., JR., HOLLIS, G. F., NEWTON, R. C., MAGOLDA, R. L., TRZASKOS, J. M. & ARNER, E. C. 1999. Purification and cloning of aggrecanase-1: a member of the ADAMTS family of proteins. *Science,* 284**,** 1664-6.

VAN GOOR, H., MELENHORST, W. B., TURNER, A. J. & HOLGATE, S. T. 2009. Adamalysins in biology and disease. *J Pathol,* 219**,** 277-86.

VAN ZOELEN, M. A., VAN DER SLUIJS, K. F., ACHOUITI, A., FLORQUIN, S., BRAUN-PATER, J. M., YANG, H., NAWROTH, P. P., TRACEY, K. J., BIERHAUS, A. & VAN DER POLL, T. 2009. Receptor for advanced glycation end products is detrimental during influenza A virus pneumonia. *Virology,* 391**,** 265-73.

VELASCO, C. R., COLLIEC-JOUAULT, S., REDINI, F., HEYMANN, D. & PADRINES, M. 2010. Proteoglycans on bone tumor development. *Drug Discov Today,* 15**,** 553-60.

VRHOVSKI, B. & WEISS, A. S. 1998. Biochemistry of tropoelastin. *Eur J Biochem,* 258**,** 1-18.

WANG, L., LI, S. & JUNGALWALA, F. B. 2008. Receptor for advanced glycation end products (RAGE) mediates neuronal differentiation and neurite outgrowth. *J Neurosci Res,* 86**,** 1254-66.

WANG, W. M., GE, G., LIM, N. H., NAGASE, H. & GREENSPAN, D. S. 2006. TIMP-3 inhibits the procollagen N-proteinase ADAMTS-2. *Biochem J*, 398, 515-9.

WAYNE, G. J., DENG, S. J., AMOUR, A., BORMAN, S., MATICO, R., CARTER, H. L. & MURPHY, G. 2007. TIMP-3 inhibition of ADAMTS-4 (Aggrecanase-1) is modulated by interactions between aggrecan and the C-terminal domain of ADAMTS-4. *J Biol Chem*, 282, 20991-8.

WEBER, B. H., LIN, B., WHITE, K., KOHLER, K., SOBOLEVA, G., HERTERICH, S., SEELIGER, M. W., JAISSLE, G. B., GRIMM, C., REME, C., WENZEL, A., ASAN, E. & SCHREWE, H. 2002. A mouse model for Sorsby fundus dystrophy. *Invest Ophthalmol Vis Sci,* 43**,** 2732-40.

WEBER, B. H., VOGT, G., PRUETT, R. C., STOHR, H. & FELBOR, U. 1994. Mutations in the tissue inhibitor of metalloproteinases-3 (TIMP3) in patients with Sorsby's fundus dystrophy. *Nat Genet,* 8**,** 352-6.

WENDT, T. M., TANJI, N., GUO, J., KISLINGER, T. R., QU, W., LU, Y., BUCCIARELLI, L. G., RONG, L. L., MOSER, B., MARKOWITZ, G. S., STEIN, G., BIERHAUS, A., LILIENSIEK, B., ARNOLD, B., NAWROTH, P. P., STERN, D. M., D'AGATI, V. D. & SCHMIDT, A. M. 2003. RAGE drives the development of glomerulosclerosis and implicates podocyte activation in the pathogenesis of diabetic nephropathy. *Am J Pathol,* 162**,** 1123-37.

WICK, M., HARONEN, R., MUMBERG, D., BURGER, C., OLSEN, B. R., BUDARF, M. L., APTE, S. S. & MULLER, R. 1995. Structure of the human TIMP-3 gene and its cell cycle-regulated promoter. *Biochem J,* 311 (Pt 2)**,** 549-54.

WILLARD, H. F., DURFY, S. J., MAHTANI, M. M., DORKINS, H., DAVIES, K. E. & WILLIAMS, B. R. 1989. Regional localization of the TIMP gene on the human X chromosome. Extension of a conserved synteny and linkage group on proximal Xp. *Hum Genet,* 81**,** 234-8.

WISNIEWSKA, M., GOETTIG, P., MASKOS, K., BELOUSKI, E., WINTERS, D., HECHT, R., BLACK, R. & BODE, W. 2008. Structural determinants of the ADAM inhibition by TIMP-3: crystal structure of the TACE-N-TIMP-3 complex. *J Mol Biol,* 381**,** 1307-19.

WONG, S. C., FONG, K. C., LEE, N., GREGORY-EVANS, K. & GREGORY-EVANS, C. Y. 2003. Successful photodynamic therapy for subretinal neovascularisation due to Sorsby's fundus dystrophy: 1 year follow up. *Br J Ophthalmol,* 87**,** 796-7.

WOOLLEY, D. E., GLANVILLE, R. W., CROSSLEY, M. J. & EVANSON, J. M. 1975. Purification of rheumatoid synovial collagenase and its action on soluble and insoluble collagen. *Eur J Biochem,* 54**,** 611-22.

WYATT, M. K., TSAI, J. Y., MISHRA, S., CAMPOS, M., JAWORSKI, C., FARISS, R. N., BERNSTEIN, S. L. & WISTOW, G. 2013. Interaction of complement factor h and fibulin3 in age-related macular degeneration. *PLoS One,* 8**,** e68088.

XIE, J., REVERDATTO, S., FROLOV, A., HOFFMANN, R., BURZ, D. S. & SHEKHTMAN, A. 2008. Structural basis for pattern recognition by the receptor for advanced glycation end products (RAGE). *J Biol Chem,* 283**,** 27255-69.

XU, C., INOKUMA, M. S., DENHAM, J., GOLDS, K., KUNDU, P., GOLD, J. D. & CARPENTER, M. K. 2001. Feeder-free growth of undifferentiated human embryonic stem cells. *Nat Biotechnol,* 19**,** 971-4.

XU, P., LIU, J., SAKAKI-YUMOTO, M. & DERYNCK, R. 2012. TACE activation by MAPK-mediated regulation of cell surface dimerization and. *Sci Signal,* 5**,** ra34.

YAMAMOTO, K., MURPHY, G. & TROEBERG, L. 2015. Extracellular regulation of metalloproteinases. *Matrix Biol,* 44-46**,** 255-63.

YAN, Q. & SAGE, E. H. 1999. SPARC, a matricellular glycoprotein with important biological functions. *J Histochem Cytochem,* 47**,** 1495-506.

YAN, S. D., SCHMIDT, A. M., ANDERSON, G. M., ZHANG, J., BRETT, J., ZOU, Y. S., PINSKY, D. & STERN, D. 1994. Enhanced cellular oxidant stress by the interaction of advanced glycation end products with their receptors/binding proteins. *J Biol Chem,* 269**,** 9889-97.

YAN, S. F., RAMASAMY, R. & SCHMIDT, A. M. 2009. The receptor for advanced glycation endproducts (RAGE) and cardiovascular disease. *Expert Rev Mol Med,* 11**,** e9.

YEH, C. H., STURGIS, L., HAIDACHER, J., ZHANG, X. N., SHERWOOD, S. J., BJERCKE, R. J., JUHASZ, O., CROW, M. T., TILTON, R. G. & DENNER, L. 2001. Requirement for p38 and p44/p42 mitogen-activated protein kinases in RAGE-mediated nuclear factor-kappaB transcriptional activation and cytokine secretion. *Diabetes,* 50**,** 1495-504.

YEHOSHUA, Z., DE AMORIM GARCIA FILHO, C. A., NUNES, R. P., GREGORI, G., PENHA, F. M., MOSHFEGHI, A. A., ZHANG, K., SADDA, S., FEUER, W. & ROSENFELD, P. J. 2014. Systemic complement inhibition with eculizumab for geographic atrophy in age-related macular degeneration: the COMPLETE study. *Ophthalmology,* 121**,** 693-701.

YOO, S. Y. & KWON, S. M. 2013. Angiogenesis and its therapeutic opportunities. *Mediators Inflamm,* 2013**,** 127170.

YU, W. H., YU, S., MENG, Q., BREW, K. & WOESSNER, J. F., JR. 2000. TIMP-3 binds to sulfated glycosaminoglycans of the extracellular matrix. *J Biol Chem*, 275, 31226-32.

YUAN, X., GU, X., CRABB, J. S., YUE, X., SHADRACH, K., HOLLYFIELD, J. G. & CRABB, J. W. 2010. Quantitative proteomics: comparison of the macular Bruch membrane/choroid complex from age-related macular degeneration and normal eyes. *Mol Cell Proteomics,* 9**,** 1031-46.

ZAREPARSI, S., BRANHAM, K. E., LI, M., SHAH, S., KLEIN, R. J., OTT, J., HOH, J., ABECASIS, G. R. & SWAROOP, A. 2005. Strong association of the Y402H variant in complement factor H at 1q32 with susceptibility to age-related macular degeneration. *Am J Hum Genet,* 77**,** 149-53.

ZHANG, T., XIE, X., CAO, G., JIANG, H., WU, S., SU, Z., ZHANG, K. & LU, F. 2014. Malattia leventinese/Doyne honeycomb retinal dystrophy in a chinese family with mutation of the EFEMP1 gene. *Retina,* 34**,** 2462-71.

ZHANG, Y. & MARMORSTEIN, L. Y. 2010. Focus on molecules: fibulin-3 (EFEMP1). *Exp Eye Res*, 90, 374-5.

ZONG, H., MADDEN, A., WARD, M., MOONEY, M. H., ELLIOTT, C. T. & STITT, A. W. 2010. Homodimerization is essential for the receptor for advanced glycation end products (RAGE)-mediated signal transduction. *J Biol Chem,* 285**,** 23137-46.

Appendix

1. Preparation of buffers and solutions

AGE-BSA solution

AGE-modified albumin was prepared according to Zong *et al.* (2010) by mixing 50mg/ml BSA and 0.5M D-glucose in PBS (pH 7.4). The solution was sterilised using 0.2μm pore filter and incubated at 37°C for 2 months. Subsequently the solution was dialysed against 0.2M sodium phosphate buffer (pH 7.4) followed by passing through endotoxin removing column (Detoxi-Gel, Pierce). Aliquots were made and AGEs protein concentration was quantified by BCA protein assay.

Ammonium hydroxide (NH_4OH) Solution

To prepare 20mM ammonium hydroxide solution, 70μl of NH_4OH stock solution was mixed with 50ml water in a fume hood. Then, the diluted NH_4OH solution was sterilised using a 0.2μm pore filter inside a tissue culture class II safety cabinet.

Ammonium persulfate (APS)

100mg of ammonium persulfate was dissolved in 1ml water to prepare 10% APS solution.

Antibiotics for bacterial culture

Carbenicillin or kanamycin was used for selection of transformed bacteria depending on the selection marker present in the plasmid. Carbenicillin (disodium salt) stock solution, at 100mg/ml, was prepared in 70% ethanol and stored at -20°C. Kanamycin stock, prepared at 50mg/ml in water, was sterilised using a 0.2μm pore filter and divided into aliquots that were stored at -20°C.

Antibiotics for mammalian tissue culture

Hygromycin B or Geneticin (G-418 sulfate) were used to select stably transfected mammalian cells, depending on the resistance gene present in the vector. Geneticin stock solution was prepared at 50mg/ml in DPBS then sterilised by filtration and stored at 4°C. Hygromycin B was purchased as a sterile stock solution in PBS at 50mg/ml and kept at 4°C according to manufacturer's storage instructions.

Blocking buffer

5% blocking buffer was prepared by dissolving 2.5mg skimmed milk powder in 50ml of 1X TBST buffer.

Bovine serum albumin (BSA)

Stock BSA solution was prepared at a concentrations of 2mg/ml and stored in 1ml aliquots at -20°C.

Bromophenol blue dye

Bromophenol blue stock solution comprised 1% (w/v) bromophenol blue and 10% (v/v) glycerol in water.

5-bromo-4-chloro-3-indolyl-β-D-galactoside (X-gal)

20mg X-gal was dissolved in 1ml dimethylformamide to give a 2% w/v stock solution and stored at -20°C.

CAPS buffer (N-cyclohexyl-3-aminopropanesulfonic acid)

A 10X CAPS stock solution was prepared by dissolving 22.1g of CAPS powder in 800ml of water. The pH was adjusted to 11 using 1M NaOH and the total volume was completed to 1000ml with water, which was kept at 4°C. To prepare 1X CAPs buffer, 100ml of 10X CAPs stock solution was mixed with 100ml methanol and 800ml water.

Carbonate-Bicarbonate buffer

50mM carbonate-bicarbonate buffer (pH 9.2) was prepared by mixing 4ml of 0.2M sodium carbonate solution with 46ml of 0.2M sodium bicarbonate solution and 150ml water.

Cell Tracker dye

The cell tracker green CMFDA fluorescent dye (5-chloromethylfluorescien diacetate) was stored at -20°C and prepared according to the manufacturer's instructions. The dye was warmed to room temperature, briefly centrifuged then dissolved in DMSO at a concentration of 10mM. For labelling cells this stock was diluted in serum free medium to give a final concentration of 2.5μM.

Diethylpyrocarbonate (DEPC)-treated water (RNA extraction)

RNase free water was prepared by adding 0.1% DEPC and mixing vigorously before leaving to stand for 1 hour at room temperature prior to autoclave. The sterilised stock solution was stored at room temperature.

Hypotonic lysis buffers

Three hypotonic buffers were prepared including Hypo, NP-40 and deoxycholate buffers. Whereas Hypo-buffer was prepared by mixing 10mM Tris-HCl and CaCl2 in water, NP-40 buffer prepared by dissolving 0.25% NP-40 in Hypo-buffer. Deoxycholate buffer was made of 50mM Tris-HCl (pH 7.5), 0.1% sodium deoxycholate and water.

IPTG (Isopropylthio-β-D-galactoside)

0.5g IPTG was dissolved in 1ml water to give a 20% stock solution that was distributed in aliquots and kept at -20°C.

LB Broth

LB broth was prepared from LB High Salt granules (25g/litre water) as instructed by the manufacturer. The solution was sterilised by autoclaving and then stored at room temperature.

LB agar plates

LB agar plates were prepared from LB Agar High Salt granules (35g/ litre water) followed by autoclaving. Autoclaved LB agar was allowed to cool in a 50°C water bath and subsequently antibiotics such as carbenicillin (100mg/ml) or kanamycin (50mg/ml) were added. The agar was aseptically poured into 10cm petri dishes (approximately 15ml/plate). Plates were allowed to stand at room temperature for 1 hour to completely set and then stored at 4°C.

Lysis Buffers

Two lysis buffers were prepared including RIPA lysis buffer and single detergent lysis buffer. **RIPA lysis buffer** (**r**adio**i**mmuno**p**recipitation **a**ssay), consisted of 50mM Tris-HCL (pH 8), 150mM NaCl, 1% Triton X-100, 0.1% SDS, 2mM EDTA, 50 mM NaF, 0.5% Na-deoxycholate and 1 protease inhibitor tablet. The final volume of RIPA buffer was made up to 10ml and aliquots were prepared and stored at -20°C. **Single detergent lysis buffer,** a stock solution (total volume 10ml) consisted of 10mM Tris-HCl (pH 8), 1% Triton X-100, 1 protease inhibitor tablet and water, prepared in aliquots (1ml each) and stored at -20°C.

6X Orange G (DNA loading dye)

The stock dye was prepared by mixing 100mg orange G, 15ml glycerol and 35ml water. Aliquots were made and stored at 4°C.

4% Paraformaldehyde (PFA) fixation solution

1.2g PFA was dissolved in pre-warmed 30ml DPBS on a magnetic stirrer inside a fume hood. After cooling to room temperature the pH was adjusted to 7. The prepared stock solution was stored at 4°C and could be used for 1 week.

Phosphate buffer saline (PBS)

1 PBS tablet was dissolved in 100ml water to give a solution containing 137mM sodium chloride, 10mM phosphate buffer and 2.7mM potassium (pH 7.3-7.5).

Recombinant human TIMP3 (rhTIMP3)

A stock solution of 5ng/µl was prepared by dissolving 10µg rhTIMP3 in 2ml sterile water and storing at -20°C.

S100B

1mg S100B was dissolved in 1ml autoclaved water and subsequently aliquots were prepared (100µl each) and stored at -20°C.

SDS sample buffer

4X SDS and 2X SDS sample buffers were prepared for western blotting. To prepare 4X SDS sample buffer, 1g of SDS was dissolved in 2.5ml of 0.5M Tris-HCl (pH 6.8) and 4ml glycerol and then the total volume was made up to 10ml with water. Similarly 2X SDS sample buffer was made by mixing 4ml 10% SDS, 2ml glycerol and 2.5ml 0.5M Tris-HCl (pH 6.8), and

then 4mg bromophenol blue dye was dissolved in the mixture whose final volume was completed to 10ml with water.

Sodium phosphate buffer

A 0.2M stock buffer (pH 7.4) was prepared by dissolving 5.93g $NaH_2PO_4.H_2O$ and 23g $NaHPO_4$ in 800ml water. The final volume was completed to 1000ml with water and the buffer was stored for up to 1 month at 4°C.

Starving medium

Two different starving growth media were prepared including 0.5% FBS supplemented EBM2 and 2% FBS supplemented DMEM/DMEM F12 and used for HUVEC and HEK293T/ARPE19, respectively.

Stripping buffer

The buffer comprised of 2% SDS, 100mM 2-mercaptoethanol and 6.28mM Tri-HCl (pH 6.7).

50X Tris-acetate-ethylenediaminetetraacetic acid (TAE) buffer

A stock TAE buffer was prepared at concentration of 50X by dissolving 242g Tris base in 600ml water and 100ml 0.5M EDTA and 57.1ml glacial acetic acid. The volume was completed up to 1000ml with water and then stored at room temperature. Subsequently, 1X TAE buffer was prepared by mixing 20ml of 50x TAE with 980ml water.

Tris buffered saline with Tween-20 (TBST)

To prepare 1X TBST, a stock solution of 20X TBST was initially prepared by dissolving 6.05g Tris base and 43.8g NaCl in water. Then, the pH was adjusted to 8 and the final volume was completed to 250ml. Subsequently, 1X TBST was made by diluting 25ml of 20X TBST in 475ml water and adding 500µl Tween-20.

Vascular endothelial growth factor (VEGF)

A 100µg/ml stock was prepared inside a class II safety cabinet by dissolving 10µg VEGF in 100µl DPBS. The protein was then stored in 5µl aliquots at -20°C.

Water-saturated butanol

Butanol was saturated with water by vigorously shaking 50ml butanol and 50ml water.

2. Composition of the resolving and stacking gels for SDS-PAGE.

Ingredients	10% resolving gel	4% Stacking gel
dH_2O (ml)	4.85	6.36
1.5 M Resolving gel buffer (ml)	2.5	-
0.5 M Stacking gel buffer (ml)	-	2.52
4% Acrylamide/Bisarylamide (ml)	2.5	1
10% SDS (µl)	100	100
10% APS (µl)	50	50
TEMED (µl)	5	5

3. TIMP3 splice mutant full gene sequence

- Sequence: T3 exons + intron 4 splice mutant + cloning sites
  Range: 1 to 5429

```
                        >NotI
                          |
          >SalI   >EcoRV  |   >HindIII
            |       |     |      |
           10       |20   |     30        40        50        60
GCCGCCGCCGTCGACGATATCGCGGCCGCAAGCTTGCCACCATGACCCCTTGGCTCGGGC
CGGCGGCGGCAGCTGCTATAGCGCCGGCGTTCGAACGGTGGTACTGGGGAACCGAGCCCG
                  ______>
                  ______>

           70        80        90       100       110       120
TCATCGTGCTCCTGGGCAGCTGGAGCCTGGGGGACTGGGGCGCCGAGGCGTGCACATGCT
AGTAGCACGAGGACCCGTCGACCTCGGACCCCCTGACCCCGCGGCTCCGCACGTGTACGA

       130       140       150       160       170       180
CGCCCAGCCACCCCCAGGACGCCTTCTGCAACTCCGACATCGTGATCCGGGCCAAGGTGG
GCGGGTCGGTGGGGGTCCTGCGGAAGACGTTGAGGCTGTAGCACTAGGCCCGGTTCCACC

       190       200       210       220       230       240
TGGGGAAGAAGCTGGTAAAGGAGGGGCCCTTCGGCACGCTGGTCTACACCATCAAGCAGA
ACCCCTTCTTCGACCATTTCCTCCCCGGGAAGCCGTGCGACCAGATGTGGTAGTTCGTCT

       250       260       270       280       290       300
TGAAGATGTACCGAGGCTTCACCAAGATGCCCCATGTGCAGTACATCCATACGGAGGCTT
ACTTCTACATGGCTCCGAAGTGGTTCTACGGGGTACACGTCATGTAGGTATGCCTCCGAA

       310       320       330       340       350       360
CCGAGAGTCTCTGTGGCCTTAAGCTGGAGGTCAACAAGTACCAGTACCTGCTGACAGGTC
GGCTCTCAGAGACACCGGAATTCGACCTCCAGTTGTTCATGGTCATGGACGACTGTCCAG

       370       380       390       400       410       420
GCGTCTATGATGGCAAGATGTACACGGGGCTGTGCAACTTCGTGGAGAGGTGGGACCAGC
CGCAGATACTACCGTTCTACATGTGCCCCGACACGTTGAAGCACCTCTCCACCCTGGTCG

       430       440       450       460       470       480
TCACCCTCTCCCAGCGCAAGGGGCTGAACTATCGGTATCACCTGGGTTGTAACTGCAAGG
AGTGGGAGAGGGTCGCGTTCCCCGACTTGATAGCCATAGTGGACCCAACATTGACGTTCC

       490       500       510       520       530       540
TAAGCTCTGGGGTCACTGGGGGAAGGAGGGGAGGTGCTGACTTGCAGCCCTAGAAACATC
ATTCGAGACCCCAGTGACCCCCTTCCTCCCCTCCACGACTGAACGTCGGGATCTTTGTAG

       550       560       570       580       590       600
AGCTCCCAATGCACTGGGTGCCAGGCCCTCGGCTGGGAAGGGTATGCATGTGTTAGGCCA
TCGAGGGTTACGTGACCCACGGTCCGGGAGCCGACCCTTCCCATACGTACACAATCCGGT

       610       620       630       640       650       660
GGGCAGAGGGGCAGGTCTGAGCAGATATAGTAAGGATTGTTGCCCCAGGTGGGGCAGTGA
CCCGTCTCCCCGTCCAGACTCGTCTATATCATTCCTAACAACGGGGTCCACCCCGTCACT

       670       680       690       700       710       720
```

```
GGAAGGCAGGGAAGGAAGAATGCCTTTCTGCTGTAATCGGCTGCCTCCATGATGACCACT
CCTTCCGTCCCTTCCTTCTTACGGAAAGACGACATTAGCCGACGGAGGTACTACTGGTGA

       730        740        750        760        770        780
TGGAAGCTGCTGGGGCATGAGGGCTCTTGAGTCCCTGGCCCCACCTGGCAGTTCAAGGCT
ACCTTCGACGACCCCGTACTCCCGAGAACTCAGGGACCGGGGTGGACCGTCAAGTTCCGA

       >BamHI
         |
       790        800        810        820        830        840
GGAGGTATAGGATCCTGACACTGGCAGGTTCTCCCAAGTGGTTTCAAGTGGGCTCACCCT
CCTCCATATCCTAGGACTGTGACCGTCCAAGAGGGTTCACCAAAGTTCACCCGAGTGGGA

       850        860        870        880        890        900
GGTAGCTGACTCATCGCTAACCCCACCCCAGGTAGGCAAATGGGCCCAGGACTGCAGAGA
CCATCGACTGAGTAGCGATTGGGGTGGGGTCCATCCGTTTACCCGGGTCCTGACGTCTCT

       910        920        930        940        950        960
CCAGATGCTACAGAAGGTCTCTCTTTACCAGGCCCATCCCCCTGACCCAAGTATAGGGCC
GGTCTACGATGTCTTCCAGAGAGAAATGGTCCGGGTAGGGGGACTGGGTTCATATCCCGG

       970        980        990       1000       1010       1020
AAGGTGCAGCCTGCCTGCTGTGGGAGGAAGTTGGGCCATTCTCTCACTTCATCTTCAAAA
TTCCACGTCGGACGGACGACACCCTCCTTCAACCCGGTAAGAGAGTGAAGTAGAAGTTTT

      1030       1040       1050       1060       1070       1080
CAGTCCTGTGTGGTTTTAATTACTATGATCTCCATTCTGCAGATGAGAGCTCAGAGAACT
GTCAGGACACACCAAAATTAATGATACTAGAGGTAAGACGTCTACTCTCGAGTCTCTTGA

      1090       1100       1110       1120       1130       1140
TAAGTAACTAGCCCTAGGTCCCACAGTTCACTGAATCTGGTTTCCAACCTAGGGCAGCTA
ATTCATTGATCGGGATCCAGGGTGTCAAGTGACTTAGACCAAAGGTTGGATCCCGTCGAT

      1150       1160       1170       1180       1190       1200
GACTCCAAAGTTTATGCTCTAACCTTTCTAATTCCTCGATTCCCTAAAACAACTGAGATC
CTGAGGTTTCAAATACGAGATTGGAAAGATTAAGGAGCTAAGGGATTTTGTTGACTCTAG

      1210       1220       1230       1240       1250       1260
TCCCACCTGAGACGAAAAAGTCCTCTCAGTAGTCTAATTCTGCTACTTACTGGCTGTGTG
AGGGTGGACTCTGCTTTTTCAGGAGAGTCATCAGATTAAGACGATGAATGACCGACACAC

      1270       1280       1290       1300       1310       1320
ACCTGCAGCAAGTTACTTAACCTCTCAGAGCCTCCTAAAACTGTGATAAGAATTAAAGAG
TGGACGTCGTTCAATGAATTGGAGAGTCTCGGAGGATTTTGACACTATTCTTAATTTCTC

      1330       1340       1350       1360       1370       1380
AATAATATCAAAGCACTTATCAGAATGTCTGTTAGACAGCAGATGCTCAAGCTAGTGCTA
TTATTATAGTTTCGTGAATAGTCTTACAGACAATCTGTCGTCTACGAGTTCGATCACGAT

      1390       1400       1410       1420       1430       1440
TTTATATTATGATCACTGAGGGACTGATGTGGCTAGGCTTCCCATGCAGTGGCCCCAGGG
AAATATAATACTAGTGACTCCCTGACTACACCGATCCGAAGGGTACGTCACCGGGGTCCC

      1450       1460       1470       1480       1490       1500
tctgaatccaggctcggtagcctcaggcctgggcataccatggcagagtccatcaactgc
agacttaggtccgagccatcggagtccggacccgtatggtaccgtctcaggtagttgacg

      1510       1520       1530       1540       1550       1560
tgcctgttatctaattgcaagATCAAGTCCTGCTACTACCTGCCTTGCTTTGTGACTTCC
acggacaatagattaacgttcTAGTTCAGGACGATGATGGACGGAACGAAACACTGAAGG
```

```
      1570      1580      1590      1600      1610      1620
AAGAACGAGTGTCTCTGGACCGACATGCTCTCCAATTTCGGTTACCCTGGCTACCAGTCC
TTCTTGCTCACAGAGACCTGGCTGTACGAGAGGTTAAAGCCAATGGGACCGATGGTCAGG

                                                >KpnI
                                                  |
      1630      1640      1650      1660      1670      1680
AAACACTACGCCTGCATCCGGCAGAAGGGCGGCTACTGCAGCTGGTACCGAGGATGGGCC
TTTGTGATGCGGACGTAGGCCGTCTTCCCGCCGATGACGTCGACCATGGCTCCTACCCGG

      1690      1700      1710      1720      1730      1740
CCCCCGGATAAAAGCATCATCAATGCCACAGACCCCTGAGCGCCAGACCCTGCCCCACCT
GGGGGCCTATTTTCGTAGTAGTTACGGTGTCTGGGGACTCGCGGTCTGGGACGGGGTGGA

      1750      1760      1770      1780      1790      1800
CACTTCCCTCCCTTCCCGCTGAGCTTCCCTTGGACACTAACTCTTCCCAGATGATGACAA
GTGAAGGGAGGGAAGGGCGACTCGAAGGGAACCTGTGATTGAGAAGGGTCTACTACTGTT

      1810      1820      1830      1840      1850      1860
TGAAATTAGTGCCTGTTTTCTTGCAAATTTAGCACTTGGAACATTTAAAGAAAGGTCTAT
ACTTTAATCACGGACAAAAGAACGTTTAAATCGTGAACCTTGTAAATTTCTTTCCAGATA

      1870      1880      1890      1900      1910      1920
GCTGTCATATGGGGTTTATTGGGAACTATCCTCCTGGCCCCACCCTGCCCCTTCTTTTTG
CGACAGTATACCCCAAATAACCCTTGATAGGAGGACCGGGGGTGGGACGGGGAAGAAAAAC

      1930      1940      1950      1960      1970      1980
GTTTTGACATCATTCATTTCCACCTGGGAATTTCTGGTGCCATGCCAGAAAGAATGAGGA
CAAAACTGTAGTAAGTAAAGGTGGACCCTTAAAGACCACGGTACGGTCTTTCTTACTCCT

      1990      2000      2010      2020      2030      2040
ACCTGTATTCCTCTTCTTCGTGATAATATAATCTCTATTTTTTTAGGAAAACAAAAATGA
TGGACATAAGGAGAAGAAGCACTATTATATTAGAGATAAAAAAATCCTTTTGTTTTTACT

      2050      2060      2070      2080      2090      2100
AAAACTACTCCATTTGAGGATTGTAATTCCCACCCCTCTTGCTTCTTCCCCACCTCACCA
TTTTGATGAGGTAAACTCCTAACATTAAGGGTGGGGAGAACGAAGAAGGGGTGGAGTGGT

      2110      2120      2130      2140      2150      2160
TCTCCCAGACCCTCTTCCCTTTGCCCTTCTCCTCCAATACATAAAGGACACAGACAAGGA
AGAGGGTCTGGGAGAAGGGAAACGGGAAGAGGAGGTTATGTATTTCCTGTGTCTGTTCCT

      2170      2180      2190      2200      2210      2220
ACTTGCTGAAAGGCCAACCATTTCAGGATCAGTCAAAGGCAGCAAGCAGATAGACTCAAG
TGAACGACTTTCCGGTTGGTAAAGTCCTAGTCAGTTTCCGTCGTTCGTCTATCTGAGTTC

      2230      2240      2250      2260      2270      2280
GTGTGTGAAAGATGTTATACACCAGGAGCTGCCACTGCATGTCCCAACCAGACTGTGTCT
CACACACTTTCTACAATATGTGGTCCTCGACGGTGACGTACAGGGTTGGTCTGACACAGA

      2290      2300      2310      2320      2330      2340
GTCTGTGTCTGCATGTAAGAGTGAGGGAGGGAAGGAAGGAACTACAAGAGAGTCGGAGAT
CAGACACAGACGTACATTCTCACTCCCTCCCTTCCTTCCTTGATGTTCTCTCAGCCTCTA

      2350      2360      2370      2380      2390      2400
GATGCAGCACACACACAATTCCCCAGCCCAGTGATGCTTGTGTTGACCAGATGTTCCTGA
CTACGTCGTGTGTGTGTTAAGGGGTCGGGTCACTACGAACACAACTGGTCTACAAGGACT
```

```
      2410      2420      2430      2440      2450      2460
GTCTGGAGCAAGCACCCAGGCCAGAATAACAGAGCTTTCTTAGTTGGTGAAGACTTAAAC
CAGACCTCGTTCGTGGGTCCGGTCTTATTGTCTCGAAAGAATCAACCACTTCTGAATTTG


      2470      2480      2490      2500      2510      2520
ATCTGCCTGAGGTCAGGAGGCAATTTGCCTGCCTTGTACAAAAGCTCAGGTGAAAGACTG
TAGACGGACTCCAGTCCTCCGTTAAACGGACGGAACATGTTTTCGAGTCCACTTTCTGAC

      2530      2540      2550      2560      2570      2580
AGATGAATGTCTTTCCTCTCCCTGCCTCCCACCAGACTTCCTCCTGGAAAACGCTTTGGT
TCTACTTACAGAAAGGAGAGGGACGGAGGGTGGTCTGAAGGAGGACCTTTTGCGAAACCA

      2590      2600      2610      2620      2630      2640
AGATTTGGCCAGGAGCTTTCTTTTATGTAAATTGGATAAATACACACACCATACACTATC
TCTAAACCGGTCCTCGAAAGAAAATACATTTAACCTATTTATGTGTGTGGTATGTGATAG

      2650      2660      2670      2680      2690      2700
CACAGATATAGCCAAGTAGATTTGGGTAGAGGATACTATTTCCAGAATAGTGTTTAGCTC
GTGTCTATATCGGTTCATCTAAACCCATCTCCTATGATAAAGGTCTTATCACAAATCGAG

      2710      2720      2730      2740      2750      2760
ACCTAGGGGGATATGTTTGTATACACATTTGCATATACCCACATGGGGACATAAGCTAAT
TGGATCCCCCTATACAAACATATGTGTAAACGTATATGGGTGTACCCCTGTATTCGATTA

              >EcoRI
                |
      2770      2780      2790      2800      2810      2820
TTTTTTACAGGACACAGAATTCTGTTCAATGCTGTTAAATATGCCAATAGTTTAATCTCT
AAAAAATGTCCTGTGTCTTAAGACAAGTTACGACAATTTATACGGTTATCAAATTAGAGA

      2830      2840      2850      2860      2870      2880
TCTATTTTGTTGTCGTTGCTTGTTTGAAGAAAATCATGACATTCCAAGTTGACATTTTTT
AGATAAAACAACAGCAACGAACAAACTTCTTTTAGTACTGTAAGGTTCAACTGTAAAAAA

      2890      2900      2910      2920      2930      2940
TTTCATTTTAATTAAAATTTGAAATTCTGAACACCGTCAGCACCCTCTCTTCCCTATCAT
AAAGTAAAATTAATTTTAAACTTTAAGACTTGTGGCAGTCGTGGGAGAGAAGGGATAGTA

      2950      2960      2970      2980      2990      3000
GGGTCATCTGACCCCTGTCCGTCTCCTTGTCCCTGCTTCATGTTTGGGGGCCTTTCTTTA
CCCAGTAGACTGGGGACAGGCAGAGGAACAGGGACGAAGTACAAACCCCCGGAAAGAAAT

      3010      3020      3030      3040      3050      3060
ACTGCCTTCCTGGCTTAGCTCAGATGGCAGATGAGAGTGTAGTCAAGGGCCTGGGCACAG
TGACGGAAGGACCGAATCGAGTCTACCGTCTACTCTCACATCAGTTCCCGGACCCGTGTC

      3070      3080      3090      3100      3110      3120
GAGGGAGAGCTGCAGAGTGTCCTGCCTGCCTTGGCTGGAGGGACACCTCTCCTGGGTGTG
CTCCCTCTCGACGTCTCACAGGACGGACGGAACCGACCTCCCTGTGGAGAGGACCCACAC

      3130      3140      3150      3160      3170      3180
GAGACAGCTTGGTTCCCTTTCCCTAGCTCCCTGGTGGGTGAATGCCACCTCCTGAGATCC
CTCTGTCGAACCAAGGGAAAGGGATCGAGGGACCACCCACTTACGGTGGAGGACTCTAGG

      3190      3200      3210      3220      3230      3240
TCACCTCTTGGAATTAAAATTGTTGGTCACTGGGGAAAGCCTGAGTTTGCAACCAGTTGT
AGTGGAGAACCTTAATTTTAACAACCAGTGACCCCTTTCGGACTCAAACGTTGGTCAACA
```

```
      3250       3260       3270       3280       3290       3300
AGGGTTTCTGTTGTGTTTTTTTTTTTTTTTTTGAAATAAAACTATAATATAAATTCTCCT
TCCCAAAGACAACACAAAAAAAAAAAAAAAAACTTTATTTTGATATTATATTTAAGAGGA

      3310       3320       3330       3340       3350       3360
ATTAAATAAAATTATTTTAAGTTTTAGTGTCAAAAGTGAGATGCTGAGAGTAGGTGATAA
TAATTTATTTTAATAAAATTCAAAATCACAGTTTTCACTCTACGACTCTCATCCACTATT

      3370       3380       3390       3400       3410       3420
TGTATATTTTACAGAGTGGGGGTTGGCAGGATGGTGACATTGAACATGATTGCTCTCTGT
ACATATAAAATGTCTCACCCCCAACCGTCCTACCACTGTAACTTGTACTAACGAGAGACA

      3430       3440       3450       3460       3470       3480
CTCTTTTTTCAGCTTATGGGTATTTATCTTCTATTAGTATTTGTATCTTCAGTTCATTCC
GAGAAAAAAGTCGAATACCCATAAATAGAAGATAATCATAAACATAGAAGTCAAGTAAGG

      3490       3500       3510       3520       3530       3540
ACTTTAGGAAACAGAGCTGCCAATTGAAACAGAAGAAGAAAAAAAAAAAAAAGCAGCAGAC
TGAAATCCTTTGTCTCGACGGTTAACTTTGTCTTCTTCTTTTTTTTTTTTTCGTCGTCTG

      3550       3560       3570       3580       3590       3600
AACACACTGTAGAGTCTTGCACACACACAAGTGCCCAGGCAAGGTGCTTGGCAGAACCGC
TTGTGTGACATCTCAGAACGTGTGTGTGTTCACGGGTCCGTTCCACGAACCGTCTTGGCG

      3610       3620       3630       3640       3650       3660
AGAGTGGGAAGAGAGTACCGGCATCGGGTTTCCTTGGGATCAATTTCATTACCGTGTACC
TCTCACCCTTCTCTCATGGCCGTAGCCCAAAGGAACCCTAGTTAAAGTAATGGCACATGG

      3670       3680       3690       3700       3710       3720
TTTCCCATTGTGGTCATGCCATTTGGCAGGGGGAGAATGGGAGGCTTGGCCTTCTTTGTG
AAAGGGTAACACCAGTACGGTAAACCGTCCCCCTCTTACCCTCCGAACCGGAAGAAACAC

      3730       3740       3750       3760       3770       3780
AGGCAGTGTGAGCAGAAGCTGATGCCAGCATGTCACTGGTTTTGAAGGGATGAGCCCAGA
TCCGTCACACTCGTCTTCGACTACGGTCGTACAGTGACCAAAACTTCCCTACTCGGGTCT

      3790       3800       3810       3820       3830       3840
CTTGATGTTTTGGGATTGTCCTTATTTTAACCTCAAGGTCTCGCATGGTGGGGCCCCTGA
GAACTACAAAACCCTAACAGGAATAAAATTGGAGTTCCAGAGCGTACCACCCCGGGGACT

      3850       3860       3870       3880       3890       3900
CCAACCTACACAAGTTCCCTCCCACAAGTGGACATCAGTGTCTTCTCTGTGAGGCATCTG
GGTTGGATGTGTTCAAGGGAGGGTGTTCACCTGTAGTCACAGAAGAGACACTCCGTAGAC

      3910       3920       3930       3940       3950       3960
GCCATTCGCACTCCCTGGTGTGGTCAGCCTCTCTCACACAAGGAGGAACTTGGGTGAAGG
CGGTAAGCGTGAGGGACCACACCAGTCGGAGAGAGTGTGTTCCTCCTTGAACCCACTTCC

      3970       3980       3990       4000       4010       4020
CTGAGTGTGAGGCACCTGAAGTTTCCCTGCGGAGTCGATAAATTAGCAGAACCACATCCC
GACTCACACTCCGTGGACTTCAAAGGGACGCCTCAGCTATTTAATCGTCTTGGTGTAGGG

      4030       4040       4050       4060       4070       4080
CATCTGTTAGGCCTTGGTGAGGAGGCCCTGGGCAAAGAAGGGTCTTTCGCAAAGCGATGT
GTAGACAATCCGGAACCACTCCTCCGGGACCCGTTTCTTCCCAGAAAGCGTTTCGCTACA

      4090       4100       4110       4120       4130       4140
CAGAGGGCGGTTTTGAGCTTTCTATAAGCTATAGCTTTGTTTATTTCACCCGTTCACTTA
GTCTCCCGCCAAAACTCGAAAGATATTCGATATCGAAACAAATAAAGTGGGCAAGTGAAT
```

```
      4150      4160      4170      4180      4190      4200
CTGTATAATTTAAAATCATTTATGTAGCTGAGACACTTCTGTATTTCAATCATATCATGA
GACATATTAAATTTTAGTAAATACATCGACTCTGTGAAGACATAAAGTTAGTATAGTACT

      4210      4220      4230      4240      4250      4260
ACATTTTATTTTGCTAAATCTTGTGTCATGTGTAGGCTGTAATATGTGTACATTGTGTTT
TGTAAAATAAAACGATTTAGAACACAGTACACATCCGACATTATACACATGTAACACAAA

      4270      4280      4290      4300      4310      4320
AAGAGAAAAATGAAACCCACATGCCGCCATTTTCCTGAATCAAATTCTGCAGTGGAATGG
TTCTCTTTTTACTTTGGGTGTACGGCGGTAAAAGGACTTAGTTTAAGACGTCACCTTACC

      4330      4340      4350      4360      4370      4380
AGAGGAAAATACTTCTAGGCAAGCAGCTAGACTGGTGAATTGGGGGAAATAGAAGGAACT
TCTCCTTTTATGAAGATCCGTTCGTCGATCTGACCACTTAACCCCCTTTATCTTCCTTGA

      4390      4400      4410      4420      4430      4440
AGTAACTGAGACTCCTCCAGCCTCCTCCCTATTGGAATCCCAATGGCTCCTGGAGTAGGA
TCATTGACTCTGAGGAGGTCGGAGGAGGGATAACCTTAGGGTTACCGAGGACCTCATCCT

      4450      4460      4470      4480      4490      4500
AAAAAGTTTAAACTACATTCATGTTCTTGTTCTGTGTCACTCGGCCCTGGGTAGTCTACC
TTTTTCAAATTTGATGTAAGTACAAGAACAAGACACAGTGAGCCGGGACCCATCAGATGG

      4510      4520      4530      4540      4550      4560
ATTTACTTCACCCCAAGTCCTGCTGCCCATCCAGTTGGGAAGCCATGATTTTCCTAAGAA
TAAATGAAGTGGGGTTCAGGACGACGGGTAGGTCAACCCTTCGGTACTAAAAGGATTCTT

      4570      4580      4590      4600      4610      4620
TCCAGGGCCATGGGAGATACAATTCCAAGTTCTCGCTTCCTCCTTTGGGCATCTCTTCTG
AGGTCCCGGTACCCTCTATGTTAAGGTTCAAGAGCGAAGGAGGAAACCCGTAGAGAAGAC

      4630      4640      4650      4660      4670      4680
CCTCCCAATCAAGGAAGCTCCATGCTCAGGCTCTCAGCTCTCGGGCCAGTGCTCTGCTCT
GGAGGGTTAGTTCCTTCGAGGTACGAGTCCGAGAGTCGAGAGCCCGGTCACGAGACGAGA

      4690      4700      4710      4720      4730      4740
GTCCAGGGTAGGTAATACTGGGAGACTCCTGTCTTTTACCCTCCCCTCGTTCCAGACCTG
CAGGTCCCATCCATTATGACCCTCTGAGGACAGAAAATGGGAGGGGAGCAAGGTCTGGAC

      4750      4760      4770      4780      4790      4800
CCTCATGGTGGCAACATGGTTCTTGAACAATTAAAGAAACAAATGACTTTTTGGAATAGC
GGAGTACCACCGTTGTACCAAGAACTTGTTAATTTCTTTGTTTACTGAAAAACCTTATCG

      4810      4820      4830      4840      4850      4860
CCTGTCTAGGGCAAACTGTGGCCCCCAGGAGACACTACCCTTCCATGCCCCAGACCTCTG
GGACAGATCCCGTTTGACACCGGGGGTCCTCTGTGATGGGAAGGTACGGGGTCTGGAGAC

      4870      4880      4890      4900      4910      4920
TCTTGCATGTGACAATTGACAATCTGGACTACCCCAAGATGGCACCCAAGTGTTTGGCTT
AGAACGTACACTGTTAACTGTTAGACCTGATGGGGTTCTACCGTGGGTTCACAAACCGAA

      4930      4940      4950      4960      4970      4980
CTGGCTACCTAAGGTTAACATGTCACTAGAGTATTTTTATGAGAGACAAACATTATAAAA
GACCGATGGATTCCAATTGTACAGTGATCTCATAAAAATACTCTCTGTTTGTAATATTTT

      4990      5000      5010      5020      5030      5040
ATCTGATGGCAAAAGCAAAACAAAATGGAAAGTAGGGGAGGTGGATGTGACAACAACTTC
TAGACTACCGTTTTCGTTTTGTTTTACCTTTCATCCCCTCCACCTACACTGTTGTTGAAG
```

```
      5050      5060      5070      5080      5090      5100
CAAATTGGCTCTTTGGAGGCGAGAGGAAGGGGAGAACTTGGAGAATAGTTTTTGCTTTGG
GTTTAACCGAGAAACCTCCGCTCTCCTTCCCCTCTTGAACCTCTTATCAAAAACGAAACC

      5110      5120      5130      5140      5150      5160
GGGTAGAGGCTTCTTAGATTCTCCCAGCATCCGCCTTTCCCTTTAGCCAGTCTGCTGTCC
CCCATCTCCGAAGAATCTAAGAGGGTCGTAGGCGGAAAGGGAAATCGGTCAGACGACAGG

                                                  >XbaI
                                                    |
      5170      5180      5190      5200      5210      5220
TGAAACCCAGAAGTGATGGAGAGAAACCAACAAGAGATCTCGAACCCTGTCTAGAAGGAA
ACTTTGGGTCTTCACTACCTCTCTTTGGTTGTTCTCTAGAGCTTGGGACAGATCTTCCTT

      5230      5240      5250      5260      5270      5280
TGTATTTGTTGCTAAATTTCGTAGCACTGTTTACAGTTTTCCTCCATGTTATTTATGAAT
ACATAAACAACGATTTAAAGCATCGTGACAAATGTCAAAAGGAGGTACAATAAATACTTA

      5290      5300      5310      5320      5330      5340
TTTATATTCCGTGAATGTATATTGTCTTGTAATGTTGCATAATGTTCACTTTTTATAGTG
AAATATAAGGCACTTACATATAACAGAACATTACAACGTATTACAAGTGAAAAATATCAC

                                              >XhoI   >NotI
                                                 |      |
      5350      5360      5370      5380      |5390  |   5400
TGTCCTTTATTCTAAACAGTAAAGTGGTTTTATTTCTATCACACACTCGAGGCGGCCGCG
ACAGGAAATAAGATTTGTCATTTCACCAAAATAAAGATAGTGTGTGAGCTCCGCCGGCGC

>EcoRV          >AgeI
  |               |
  |    5410      5420
ATATCGGGCCCGCCGCCACCGGTGCCGCC
TATAGCCCGGGCGGCGGTGGCCACGGCGG
```

Green = RT/reverse PCR primer sequence (minus restriction site)

4. Pull-down vectors

4.1 pHTC vector map

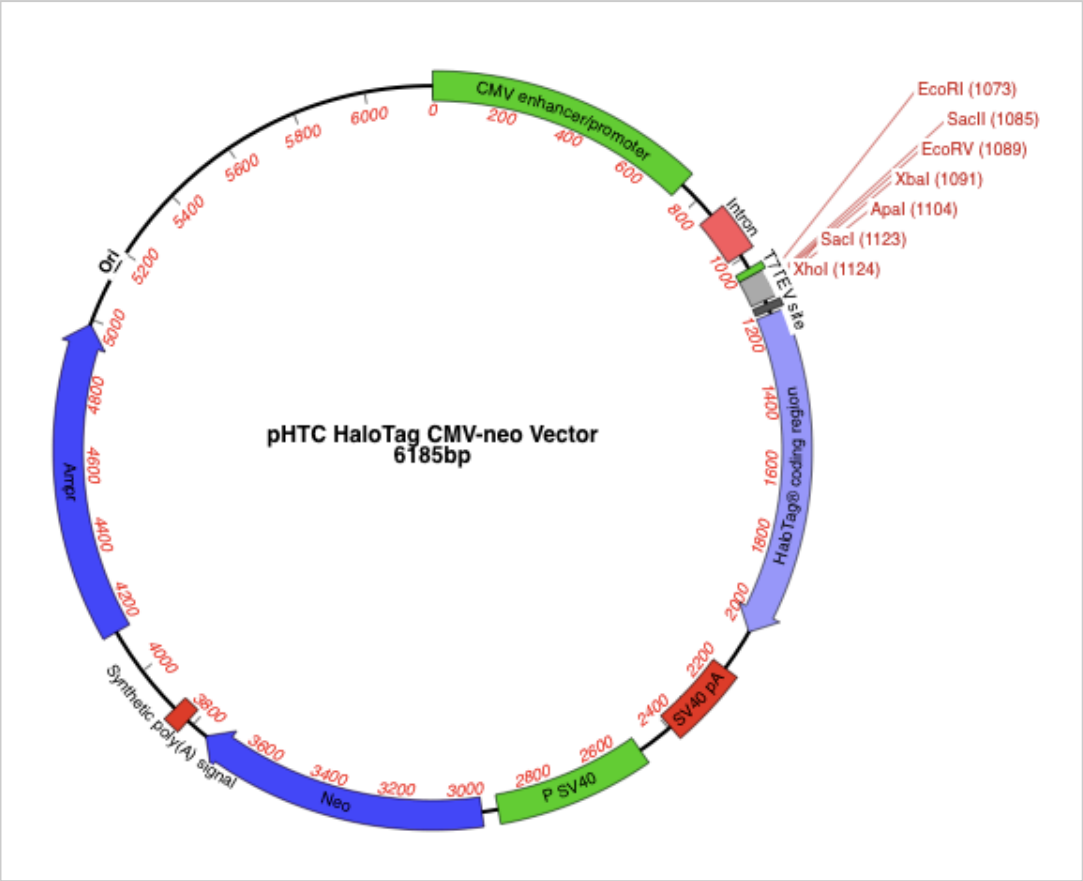

4.2 pHTC-EFEMP1-HaloTag

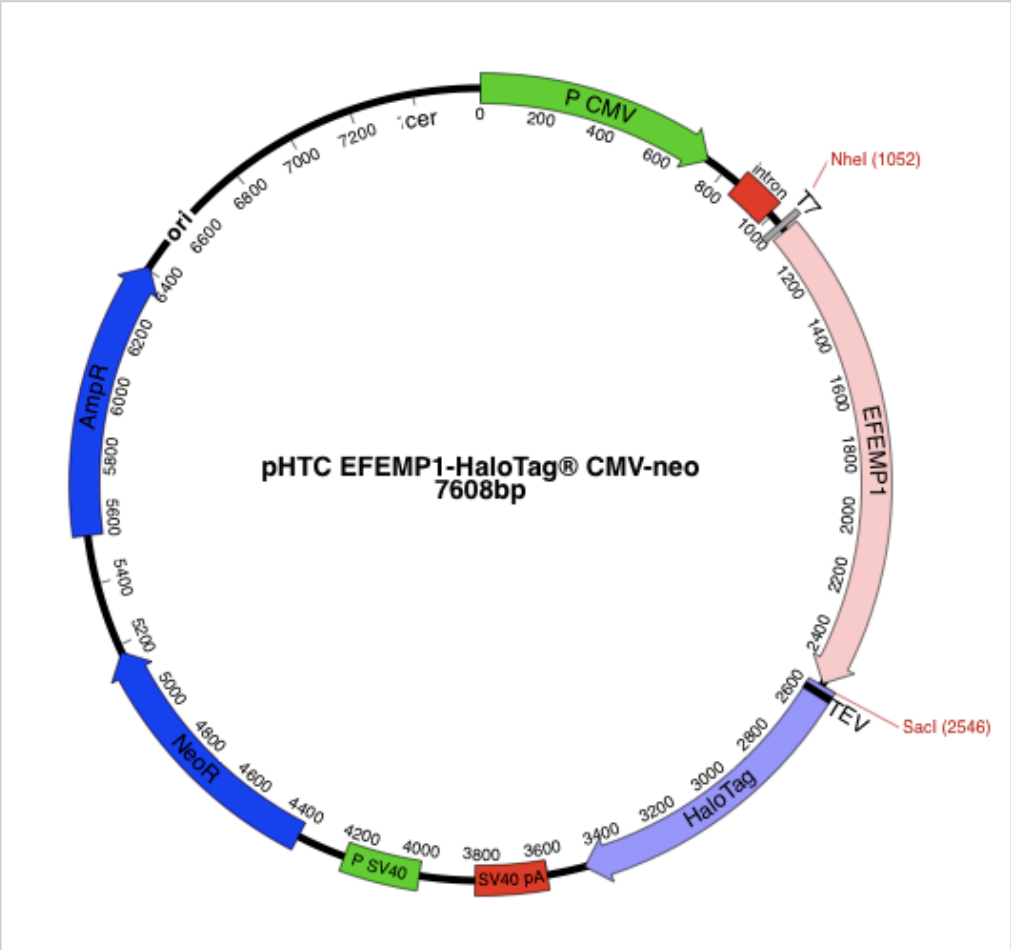

4.3 pHTC-TIMP3-HaloTag

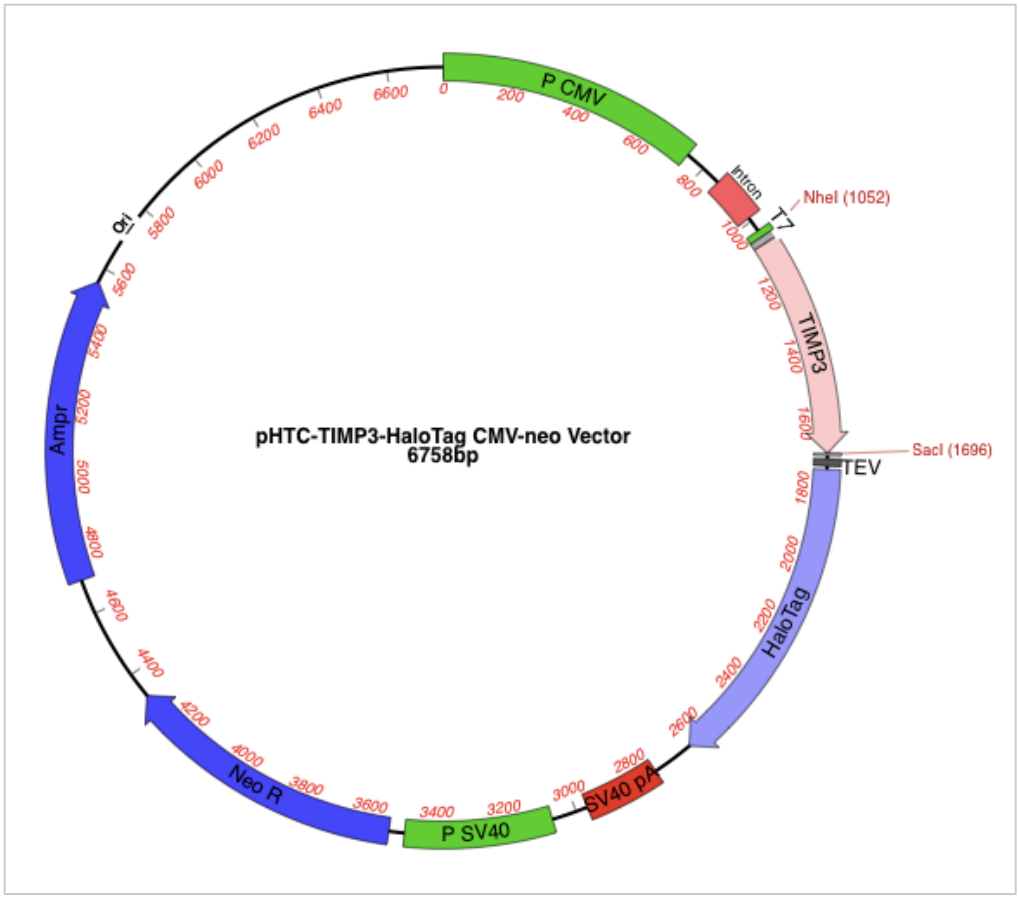

4.4 pcDNA3-TIMP3 vector map

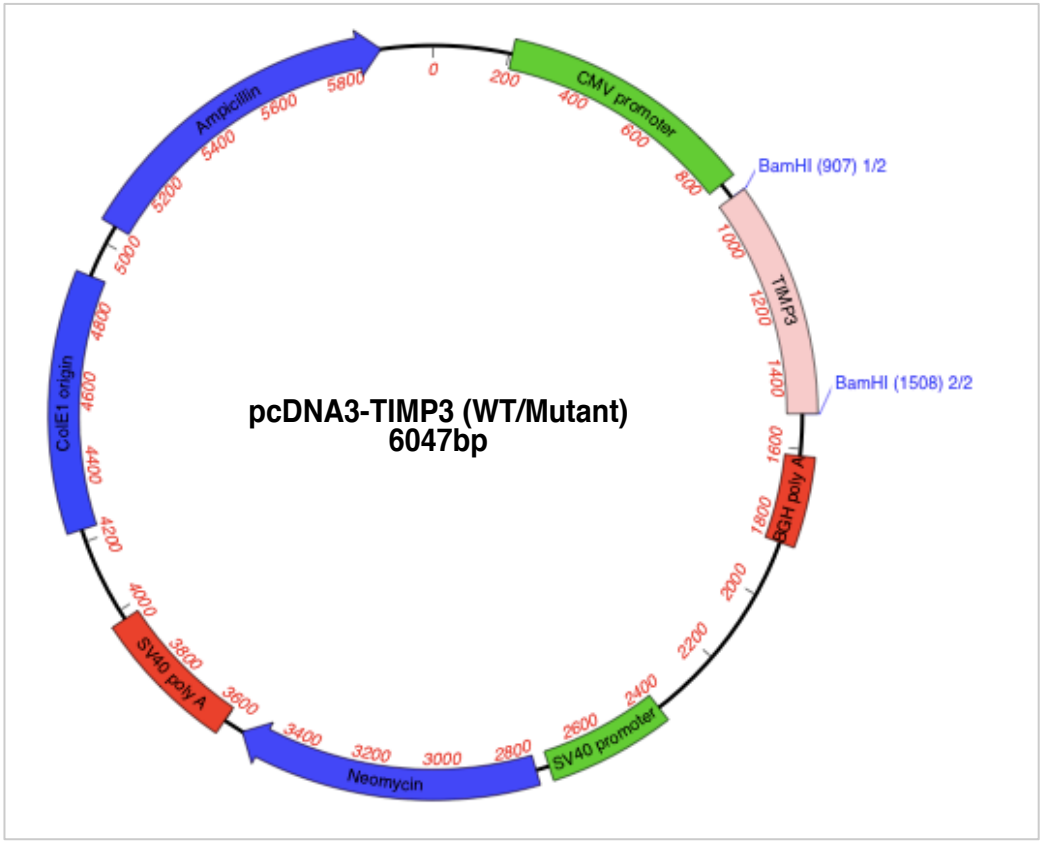

4.5 pcDNA3-SS-HaloTag vector map

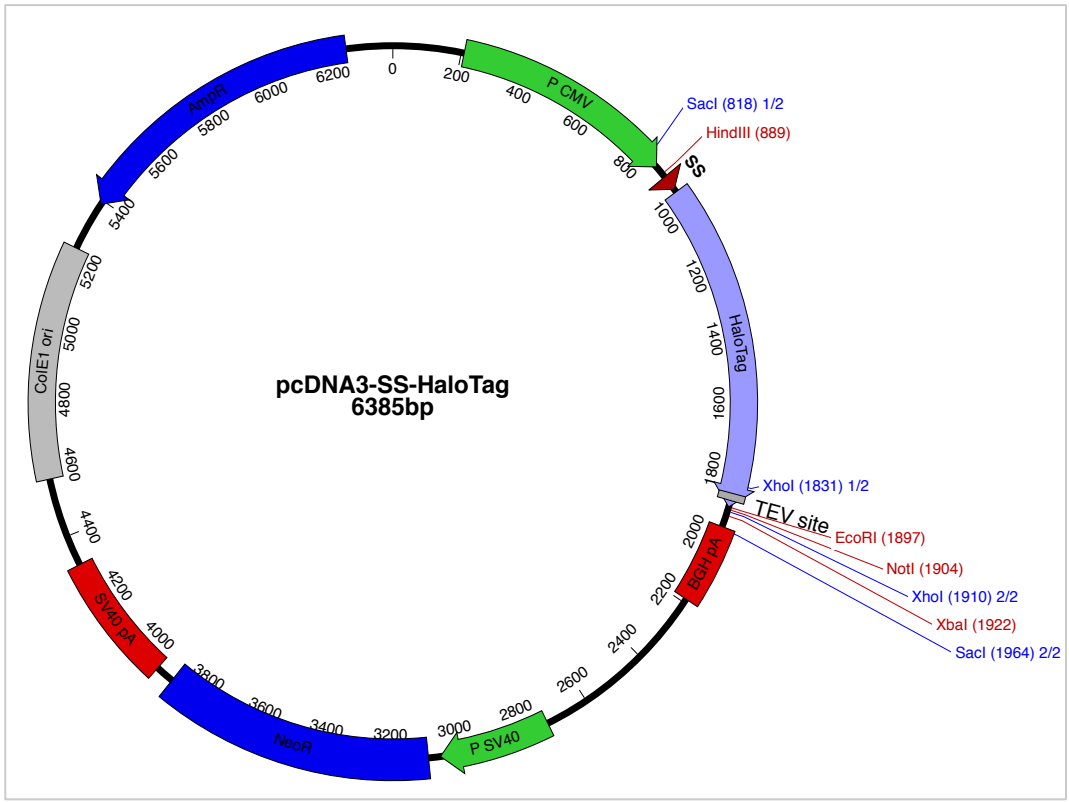

4.6 pcDNA3-SS-HaloTag-EFEMP1 vector map

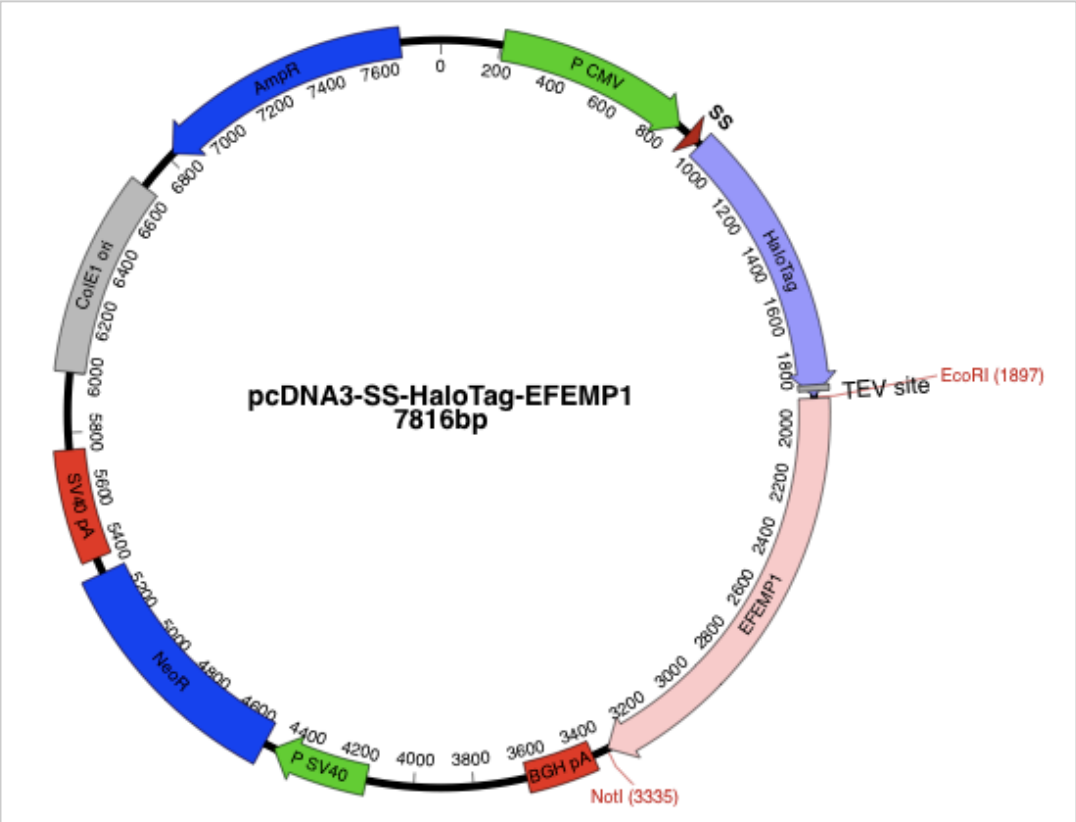

5. Luciferase reporter vectors

5.1 pTK-green Renilla luciferase vector map

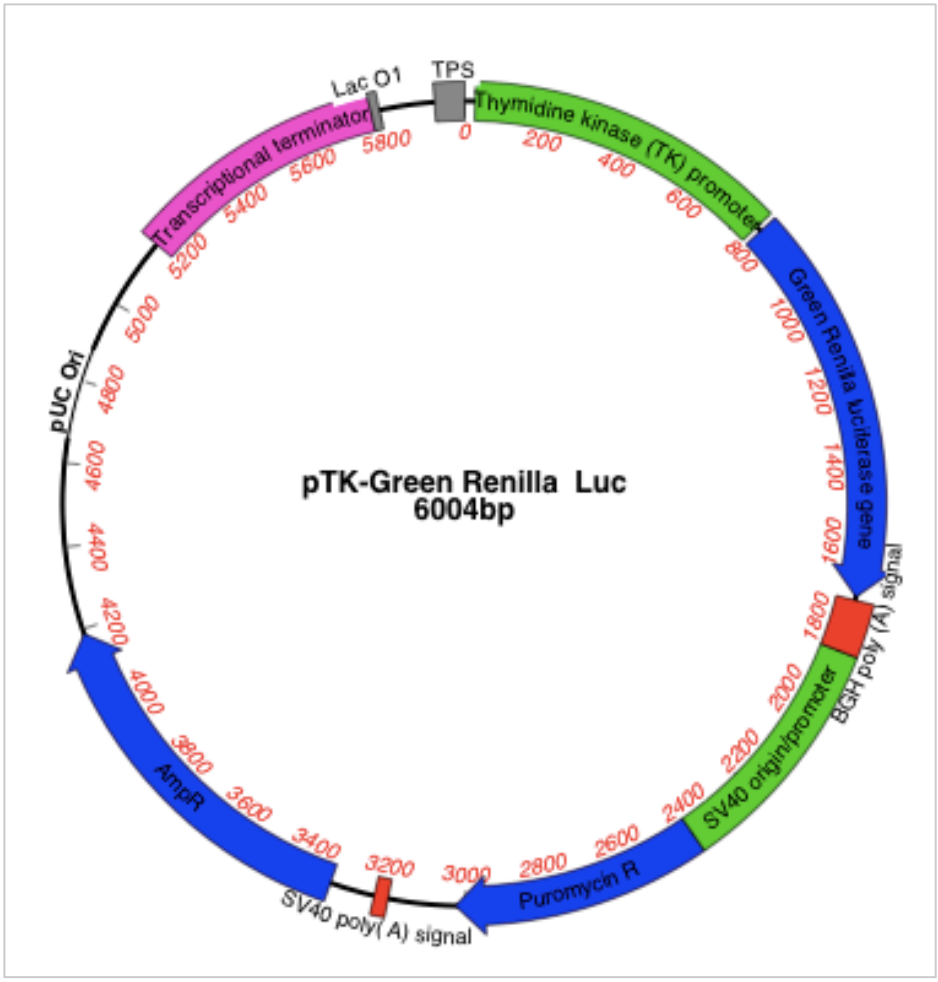

5.2 pGL3-Basic vector map

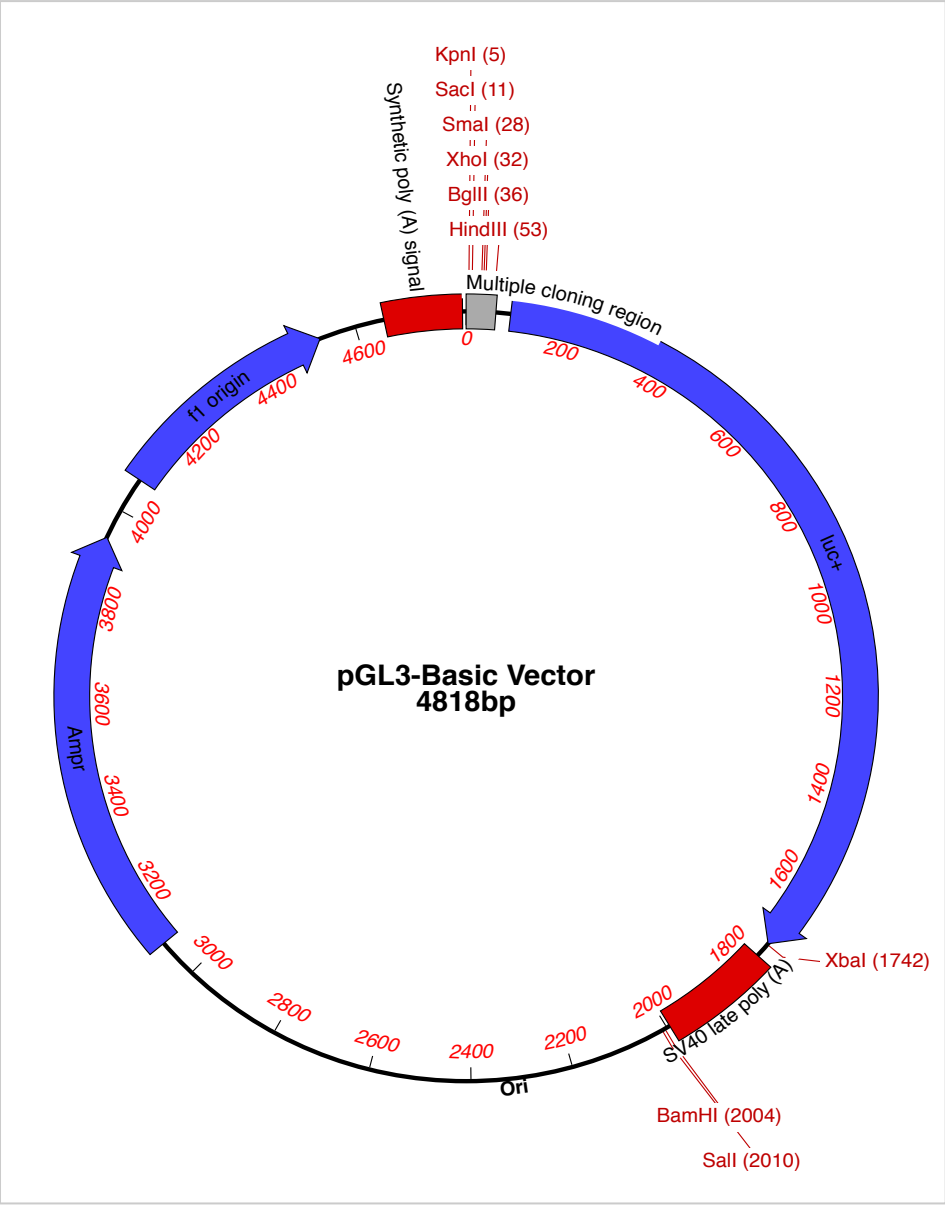

5.3 pGL3-control vector map

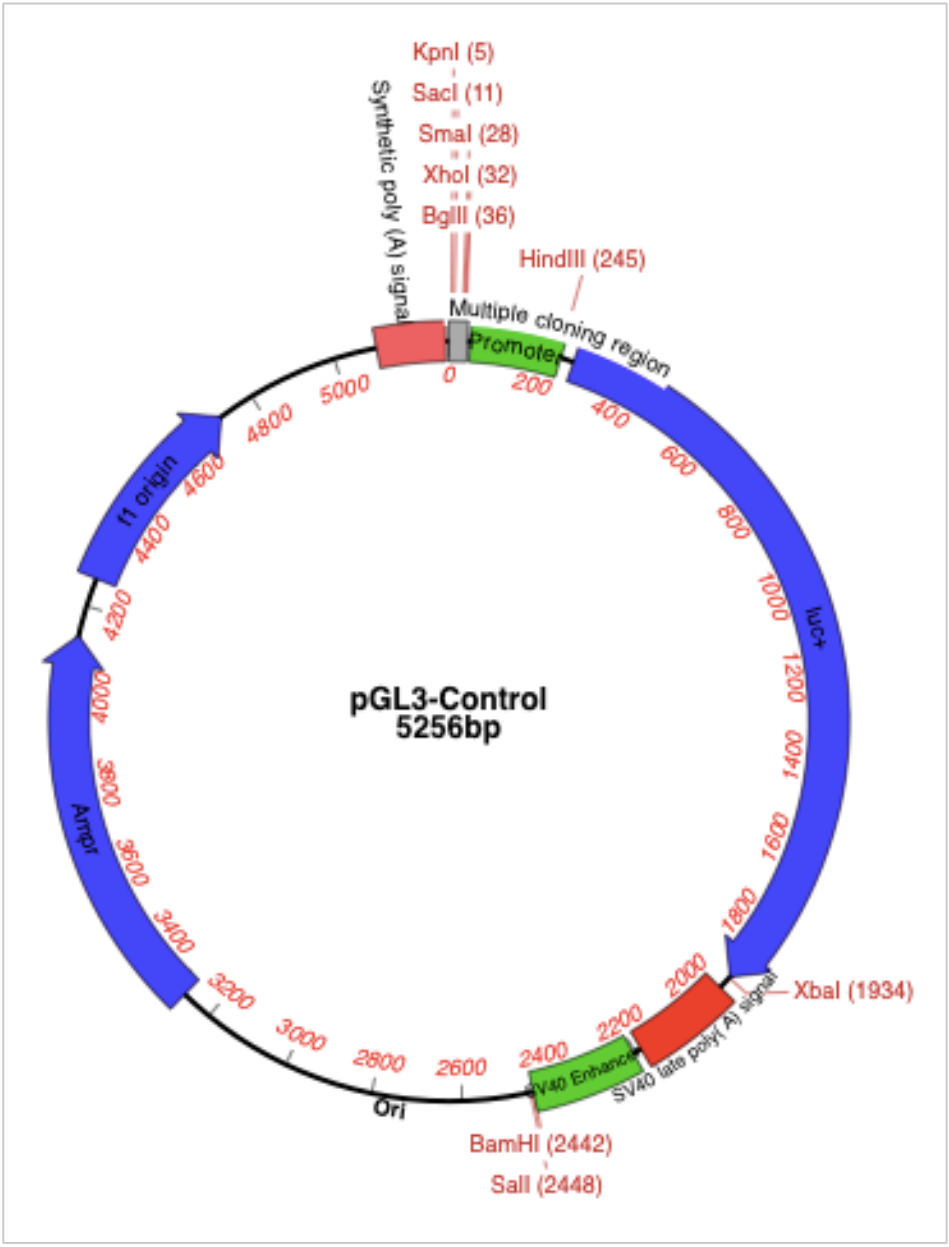

5.4 pGL4-luc2p/NF_KB vector map